

CONSTRUCTION AND LOAD TESTS OF A SEGMENTAL

PRECAST BOX GIRDER BRIDGE MODEL

APPROVED BY SUPERVISORY COMMITTEE:

John E. Breen  
W. H. Breen

C. Philip Johnson

James J. Jura  
Daniel J. Foubert

CONSTRUCTION AND LOAD TESTS OF A SEGMENTAL  
PRECAST BOX GIRDER BRIDGE MODEL

by

SATOSHI KASHIMA, B.S.C.E., M.S. C.E.

DISSERTATION

Presented to the Faculty of the Graduate School of

The University of Texas at Austin

in Partial Fulfillment

of the Requirements

for the Degree of

DOCTOR OF PHILOSOPHY

THE UNIVERSITY OF TEXAS AT AUSTIN

January 1974

TO

My Parents and Brother

## A C K N O W L E D G M E N T S

The research described herein was conducted as a research program at The University of Texas Center for Highway Research sponsored by the Texas Highway Department and Federal Highway Administration.

The author would like to thank the members of his supervising committee, Dr. John E. Breen, chairman, Dr. Ned H. Burns, Dr. James O. Jirsa, Dr. David W. Fowler and Dr. C. Philip Johnson. Particular thanks are extended to Dr. Breen for his consultation, suggestions and encouragement throughout this study.

The author wishes to express his gratitude to Professor Phil M. Ferguson who helped the author enter this University and with whom he had the opportunity to work during the first year.

Many thanks are extended to Mr. George E. Moden who made the necessary tools and equipment for construction and loading tests of the model bridge, Mrs. Maxine R. DeButts for her encouragement throughout this study and extreme help in making the final report, and Mr. Jerry Crane who had responsibility for operating the electrical instruments and modified the data reduction program SPEED, which was originally developed at the National Bureau of Standard, to run for CDC system in the University.

The author wishes to record his sincere thanks to Messrs. David Alexander, Harman F. Ramsey and James E. Moore for their devoted help throughout the study of the model bridge, Mr. John E. DeButts for his devoted help in construction and testing of the model bridge, and Mr. Terry Newman who drew all figures for this report.

For their assistance and friendship throughout the completion of this study many thanks are extended to the following: Dr. Nicolae Bodor who gave valuable suggestions about the epoxy resin and concrete;



Mr. Lawrence G. Griffis who was very responsible in casting the concrete segments and worked for a half of construction of the model bridge; Mr. Ronald D. Sullivan who helped in writing this report.

Thanks are also due to: Mr. John T. Wall who worked with casting of segments and piers, and a part of construction; Mr. Thomas Gallaway who worked for the anchorage test of the model prior to casting the model segments; Messrs. Gorham W. Hinckley, Gary D. Iselt and James E. Motlock who helped throughout the model study; Messrs. S. Ali Mirza and Tom Word who helped to assemble the cages for the model segments; Messrs. Aristides Karabinis, Michael Warren, Barry Miller, James S. Ford and Russell W. Barr who helped throughout construction; Messrs. George Hadnot, Alford Bleeker and Gordon Derr who helped in testing of the model bridge; John Furlong and Bruce Phillips who helped a part of the construction.

The University of Texas at Austin  
June 1973

## A B S T R A C T

The cantilever construction of the first segmental precast prestressed concrete box girder bridge in the United States has been recently completed on the John F. Kennedy Memorial Causeway, Corpus Christi, Texas. The segments were precast, transported to the site, and erected by the balanced cantilever method of post-tensioned construction, using epoxy resin as a jointing material.

In order to check the applicability and accuracy of the design criteria, analytical methods, construction techniques, and the shear performance of the epoxy joints, an accurate one-sixth scale model of the three-span continuous bridge was built at the Civil Engineering Structures Research Laboratory of The University of Texas Balcones Research Center.

This study documents the construction and load testing of the bridge. Experimental results are compared with analytical values for the various stages of construction, service loadings, ultimate proof loadings, and final failure tests. During the cantilever construction and under service level loadings after completion, experimental results generally agreed with the computerized theoretical analyses. Because of the general absence of warping, a beam theory analysis reasonably predicted behavior of the bridge during the cantilever construction and under uniform service level loading. However, the folded plate theory analysis was required to predict distribution for nonuniform loadings and transverse moment distribution for wheel loadings. Ultimate load theories correctly indicated the load capacity of the structure, when all loading and structural configurations were considered.

The model bridge carried the ultimate proof loads [1.35 dead load + 2.25 (live load + impact load)] specified by Bureau of Public Roads' criteria for all critical conditions. During tests to failure, the epoxy

joints performed very well and there was no evidence of epoxy separation at the joints. The theoretical calculation for the failure load agreed very well with the experimental results and indicated the necessity for change in the conventional procedure for computing ultimate design load for this type of bridge. Since the structural configuration changes from a simple cantilever to a continuous beam during construction of the bridge, the ultimate design load for the completed bridge should be specified as follows:

$$U = U_1 + U_2$$

$$U_1 = 1.15 \text{ DL} \text{ -- to be computed for a balanced cantilever}$$

$$U_2 = 0.20 \text{ DL} + 2.25 (\text{LL} + \text{IL}) + \text{SL} \text{ -- to be computed for the completed continuous structure}$$

where

DL = dead load

LL = live load

IL = impact load

SL = resultant reactions due to prestressing of positive tendons and seating forces at outer supports.

## T A B L E   O F   C O N T E N T S

	Page
ACKNOWLEDGMENTS.....	iv
ABSTRACT.....	vi
LIST OF TABLES.....	xii
LIST OF FIGURES.....	xiii
NOTATION.....	xx
 Chapter	
1 INTRODUCTION.....	1
1.1 General.....	1
1.2 Related Research in This Program.....	4
1.3 Objective and Scope of the Model Study.....	6
1.4 Summary of the Following Chapters.....	7
2 SCALE FACTORS FOR THE BRIDGE MODEL.....	9
2.1 Factors Affecting Scale Selection.....	9
2.2 Dimenstions of Prototype and Model Bridge.....	9
2.2.1 Longitudinal Dimensions.....	9
2.2.2 Transverse Dimensions.....	9
2.3 Choice of Materials.....	11
2.3.1 Concrete.....	11
2.3.2 Prestressing Steel.....	11
2.3.3 Reinforcing Bars.....	13
3 MATERIAL PROPERTIES.....	15
3.1 Concrete.....	15
3.1.1 Concrete Mix Design.....	15
3.1.2 Strength of Concrete.....	16
3.1.3 Modulus of Elasticity.....	17
3.1.4 Poisson's Ratio.....	18

Chapter		Page
3.2	Steel.....	18
	3.2.1 Prestressing Strands and Wire.....	18
	3.2.2 Reinforcing Wire.....	19
	3.2.3 Strength of Bolts at Main Piers.....	21
3.3	Epoxy Resin as a Jointing Material.....	21
	3.3.1 General.....	21
	3.3.2 Test Procedure and Test Results.....	22
	3.3.3 Selection of Epoxy Resin and Further Test..	31
4	SEGMENT DETAILS.....	34
4.1	Reinforcing Cage for Precast Segments.....	34
	4.1.1 Reinforcement.....	34
	4.1.2 Anchorages.....	39
	4.1.3 Tendon Duct.....	42
4.2	Forms.....	43
4.3	Strain Instrumentation in Cages.....	48
4.4	Casting Procedure.....	49
4.5	Curing of Segments.....	52
4.6	Surface Preparation of Segments.....	52
4.7	Compensation Dead Load for Model Bridge.....	53
4.8	Actual Properties of the Model Bridge.....	55
5	INSTRUMENTATION AND DATA REDUCTION.....	57
5.1	General.....	57
5.2	Load Cells and Pressure Gages.....	57
5.3	Strain Gage Instrumentation and Data Reduction.....	57
5.4	Surveyor's Level and Dial Gages.....	59
6	CONSTRUCTION DETAILS.....	61
6.1	Construction Procedure.....	61
	6.1.1 General.....	61
	6.1.2 Construction of Piers.....	61
	6.1.3 Erection of Pier Segments.....	64
	6.1.4 Erection of Segments during the Cantilever Stages.....	64

Chapter		Page
	6.1.5 Correction of Horizontal and Vertical Alignment.....	73
	6.1.6 Casting of the Closure Segment.....	77
	6.1.7 Prestressing of the Positive Tendons.....	78
	6.1.8 Grouting of Tendons.....	81
	6.1.9 Casting of the Midstrip Closure between the Two Box Units.....	85
6.2	Behavior of the Bridge during Construction.....	86
	6.2.1 Rotational Stiffness at the Main Pier.....	86
	6.2.2 Prestressing Force.....	91
	6.2.3 Deflections.....	94
	6.2.4 Strains.....	98
	6.2.5 Reaction at Outer Supports during Positive Tendon Operations.....	109
7	SERVICE AND DESIGN ULTIMATE LOAD TESTS.....	112
	7.1 General.....	112
	7.2 Test Procedures.....	113
	7.2.1 Simulation of Loading.....	113
	7.2.2 Loading System and Instrumentation.....	119
	7.3 Test Results and Interpretations.....	124
	7.3.1 General.....	124
	7.3.2 Service Loading.....	125
	7.3.3 Ultimate Design Loading Specified by BPR Criteria.....	138
	7.3.4 Study of Transverse Moment.....	157
8	LOADING TO FAILURE TEST.....	166
	8.1 General.....	166
	8.2 Failure Test of the Side Span.....	167
	8.2.1 General.....	167
	8.2.2 Test Results.....	167
	8.2.3 Determination of Side Span Live Load Capacity.....	176
	8.3 Failure in the Main Span.....	199

Chapter		Page
	8.3.1 General.....	199
	8.3.2 Test Results.....	200
	8.3.3 Determination of the Main Span Live Load Capacity.....	211
	8.4 Punching Shear Test.....	226
9	CONCLUSIONS AND RECOMMENDATIONS.....	229
	9.1 Conclusions.....	229
	9.1.1 Primary Conclusions.....	229
	9.1.2 Secondary Conclusions.....	230
	9.2 Recommendations.....	232
	9.2.1 Design Recommendations.....	232
	9.2.2 Construction Recommendations.....	233
<b>Appendix</b>		
A	PROTOTYPE BRIDGE PLANS.....	235
B	SPECIFICATION FOR EPOXY BONDING AGENT.....	246
	REFERENCES.....	248

L I S T O F T A B L E S

Table		Page
2.1	CHOICE OF STRANDS AND WIRE FOR THE MODEL BRIDGE.....	11
2.2	CHOICE OF REINFORCING BARS FOR THE MODEL BRIDGE.....	13
3.1	CONCRETE MIX DESIGN.....	15
3.2	COMPRESSIVE STRENGTH OF CONCRETE.....	16
3.3	SPLITTING TENSILE STRENGTH OF CONCRETE.....	16
3.4	MODULUS OF ELASTICITY OF CONCRETE.....	18
3.5	ULTIMATE STRENGTH OF PRESTRESSING STRANDS AND WIRE.....	19
3.6	MODULUS OF ELASTICITY OF WIRE AND STRANDS.....	19
3.7	TEST RESULTS OF REINFORCING WIRE OF PRECAST SEGMENTS.....	20
3.8	TENSILE STRENGTH OF BOLTS AT MAIN PIERS.....	21
3.9	FLEXURE TEST RESULTS OF EPOXIES (A) AND (B).....	25
3.10	FLEXURE TEST RESULTS.....	26
3.11	SHEAR TEST RESULTS.....	29
3.12	SHEAR TEST RESULTS OF EPOXIES (A) AND (B).....	30
3.13	POT LIFE BY CONSISTENCY TEST.....	31
4.1	DIMENSION OF BEARING PLATE FOR THE MODEL BRIDGE.....	39
4.2	<del>MATERIAL PROPERTIES AND SECTION PROPERTIES OF THE MODEL BRIDGE.....</del>	<del>56</del>
6.1	FRICITION LOSS TEST RESULTS.....	92
6.2	ELONGATION OF PRESTRESSING CABLES IN SEVERAL STAGES.....	93
6.3	DETAILS OF EACH STAGE OF CONSTRUCTION.....	99
6.4	REACTIONS AT OUTER SUPPORT DURING PRESTRESSING IN MAIN SPAN.....	110
7.1	CRITICAL LOADING CONDITIONS IN LONGITUDINAL DIRECTION...	112
7.2	MOMENT OR SHEAR FOR EACH LOADING CASE.....	118
7.3	COMPARISON OF EXPERIMENTAL AND THEORETICAL TRANSVERSE STRAINS.....	163
8.1	LF OF (LL + IL) FOR THE FIRST PLASTIC HINGE AT EACH JOINT.....	217
8.2	PUNCHING SHEAR TEST RESULTS.....	227



## LIST OF FIGURES

Figure		Page
1.1	Typical balanced cantilever construction.....	2
2.1	Longitudinal dimensions of bridge.....	10
2.2	Cross section of bridge.....	10
2.3	Details of prestressing strands and wire.....	12
2.4	Details of reinforcing bars in segment.....	14
3.1	Testing of reinforcing wire.....	20
3.2	Bending test specimen.....	23
3.3	Shear test specimen.....	27
3.4	Development of bond strength of epoxy resins.....	32
4.1	Individual mat composed cage.....	35
4.2	Cage for a segment.....	35
4.3	Details of reinforcing mats.....	36
4.4	Details of web reinforcement modification.....	38
4.5	Modification for the main pier segment.....	40
4.6	Details of anchorage and spiral reinforcement.....	41
4.7	Typical arrangement of tendon duct near anchorage.....	42
4.8	Tendon duct profiles in main span.....	44
4.9	Tendon duct profiles in side span.....	45
4.10	Details of tendon profile specified by the plans.....	46
4.11	General view of soffit forms.....	47
4.12	Details of forms for segment.....	47
4.13	General view of assembled forms.....	48
4.14	Position of strain gages in segment.....	50
4.15	Sequence of casting segments.....	51
4.16	Position of rams for separation of segment.....	52
4.17	Tools used for surface preparation.....	53
4.18	Compensating dead loads for the model bridge.....	54

Figure	Page
5.1 Strain gage instrumentation.....	58
5.2 VIDAR system and teletype.....	60
6.1 Reinforcement of the main pier.....	62
6.2 Connection of pier to the testing floor.....	63
6.3 Detail of support at main pier.....	63
6.4 General view of the pier segment on the main pier.....	65
6.5 Typical independent crane used for erection of segments..	66
6.6 Mechanical device for temporary joining.....	67
6.7 Typical structure supported crane used in some cases.....	67
6.8 Insertion of prestressing cable.....	69
6.9 Adjustment of level.....	70
6.10 Application of the epoxy resin on the joining surface....	70
6.11 General view of prestressing system for negative tendons.....	71
6.12 Details of prestressing system.....	72
6.13 Errors of horizontal alignment.....	73
6.14 Adjustment of horizontal alignment.....	75
6.15 Accumulation of joining error.....	76
6.16 Correction of the vertical alignment.....	77
6.17 Connection of tendon duct at the closure.....	79
6.18 Simulation of the closure.....	79
6.19 Setup for prestressing of positive tendons.....	80
6.20 Order of grouting for each tendon group.....	82
6.21 Examples of tendon arrangement.....	83
6.22 Connection of injection pipes and inlets of tendons.....	84
6.23 Deflection at unbalanced loading.....	86
6.24 Individual factors effecting the deflection.....	88
6.25 Suggested improvement for temporary support.....	90
6.26 Deflection predicted by SIMPLA2 for cantilever erection..	95
6.27 Typical measured deflection during cantilever erection...	95
6.28 Deflection relative to the center of 6th segment.....	96
6.29 Deflection at the center in main span during positive tendon operations.....	97

Figure	Page
6.30	Strains in M1 and S1 segments during balanced cantilever construction..... 100
6.31	Strains in M1 and S1 segments during erection of half segments..... 101
6.32	Strains in M1 segments during closure operation..... 102
6.33	Strains in the top slab of M1 segments during construction..... 103
6.34	Strains in the bottom slab of M1 segments during construction..... 104
6.35	Strains in the M6 and S6 segments at erection of the 6th segment..... 105
6.36	Strains in the M9 segment during closure operations..... 106
6.37	Strains in the top slab around the center of the main span..... 107
6.38	Strains in the bottom slab around the center of the main span..... 107
6.39	Calculation of end reaction due to positive tendons..... 110
7.1	Dimensions of full size and 1/6 scale model AASHO HS20-S16 truck..... 114
7.2	Scaled wheels and AASHO HS20-S16 truck..... 115
7.3	Application of concentrated loads above the webs (in each lane)..... 116
7.4	Lane loads and equivalent concentrated loads for four lanes with impact allowances..... 117
7.5	Application of lane load..... 120
7.6	Arrangement of rams, hoses, manifolds and pumps..... 121
7.7	Locations of dial gage readings..... 122
7.8	Load cell to measure the reaction at ultimate loading..... 123
7.9	Position of truck loading..... 125
7.10	Deflections for truck loadings (four lanes) in side span..... 126
7.11	Reactions at outer supports for truck loadings (four lanes) in side span..... 127
7.12	Longitudinal strains along SS7 and SS6 for truck loadings (four lanes) in side span..... 128
7.13	Deflections for lane loadings (four lanes) in main span..... 129

Figure	Page
7.14 Reactions at outer supports for lane loadings (four lanes) in main span.....	129
7.15 Longitudinal strains along NM9 for lane loadings (four lanes) in main span.....	130
7.16 Deflections for lane loadings (four lanes) in main and one side span.....	131
7.17 Reactions at outer supports for lane loadings in main and one side span.....	131
7.18 Longitudinal strains for lane loadings (four lanes) in main and one side span.....	132
7.19 Deflections for lane loadings (two lanes) in main span....	134
7.20 Longitudinal strains along NM9 for lane loadings (two lanes) in main span.....	135
7.21 Reactions at outer supports for lane loadings (two lanes) in main span.....	135
7.22 Deflections for lane loadings (two lanes) in main and one side span.....	136
7.23 Longitudinal strains for lane loadings (two lanes) in main and one side span.....	137
7.24 Reactions at outer supports for lane loadings (two lanes) in main and one side span.....	139
7.25 Concrete blocks for 0.35 DL.....	140
7.26 Deflections for 0.35 DL.....	141
7.27 Reactions at outer supports for 0.35 DL.....	141
7.28 Longitudinal strains along NM9, NM1 and NS1 for 0.35 DL.....	142
7.29 Deflections at SM10 for lane loadings (four lanes) in main span (design ultimate).....	144
7.30 Deflections for lane loadings (four lanes) in main span (design ultimate).....	145
7.31 Reactions at outer supports for lane loadings (four lanes) in main span (design ultimate).....	146
7.32 Longitudinal strains along NM9 for lane loadings (four lanes) in main span (design ultimate).....	146
7.33 Development of cracks for lane loadings (four lanes) in main span (design ultimate).....	148
7.34 Relation between the end reaction and cracking moment.....	150

Figure	Page
7.35 Deflections of SM10 for lane loadings (four lanes) in the main and one side span (design ultimate).....	150
7.36 Deflections for lane loadings (four lanes) in the main and one side span (design ultimate).....	151
7.37 Longitudinal strains at NM9 for lane loadings (four lanes) in the main and one side span (design ultimate).....	153
7.38 Longitudinal strains at NM1 for lane loadings (four lanes) in the main and one side span (design ultimate)....	153
7.39 Reactions at outer supports for lane loadings (four lanes) in the main and one side span (design ultimate)....	154
7.40 Development of cracks for lane loadings (four lanes) in the main and one side span (design ultimate).....	155
7.41 Arrangement of slip gage at the first joint.....	156
7.42 Position of truck loadings (design ultimate).....	158
7.43 Deflections at SS7 for truck loadings (four lanes) in side span (design ultimate).....	158
7.44 Deflections for truck loadings (four lanes) in side span (design ultimate).....	159
7.45 Longitudinal strains at SS7 for truck loadings (four lanes) in side span (design ultimate).....	160
7.46 Longitudinal strains at SS6 for truck loadings (four lanes) in side span (design ultimate).....	160
7.47 Reactions at outer supports for truck loadings (four lanes) in side span (design ultimate).....	161
7.48 Transverse strain at SS7R for truck loading (four lanes) in side span (design ultimate).....	161
7.49 Transverse slab moment (My) diagram for different loading cases by MUPDI.....	162
7.50 Typical strain readings in punching shear tests.....	165
8.1 Bridge failure loading.....	168
8.2 Truck loadings at 1.0 (LL + IL) for maximum positive moment in the side span.....	168
8.3 Deflections at the center of the SS7 segment in side span.....	169
8.4 Longitudinal strains at the center of the SS6L segment....	170
8.5 Longitudinal strains at the center of the SS7R segment....	170

Figure	Page
8.6	Development of cracks during loading..... 171
8.7	Longitudinal strains at the center of the SS1 segment..... 173
8.8	Reactions at the outer supports..... 174
8.9	Failure mechanism for truck loadings in the side span..... 175
8.10	Horizontal force on the top of the outer pier..... 176
8.11	Deflections along the center of the SS7 segment in side span..... 177
8.12	Transverse strains at the center of the SS7 segment..... 178
8.13	Forces and moments acting on the bridge for a typical cantilever stage..... 179
8.14	Horizontal forces and moments at completion of cantilever erection..... 181
8.15	Horizontal forces and moments due to prestressing in side span..... 182
8.16	Horizontal forces and moments due to prestressing in main span..... 183
8.17	Horizontal forces and moments at completion of all prestressing operations..... 185
8.18	Moment diagram for 0.35 DL ( $M_{E3}$ )..... 187
8.19	Moment diagram for truck loads in side span ( $M_{E4}$ )..... 187
8.20	Ultimate force at a certain section..... 188
8.21	Stress-strain curves of prestressing cables..... 190
8.22	Calculation of $T_i$ for different strain profiles..... 191
8.23	Calculation of ultimate internal moment..... 192
8.24	Calculation of ultimate internal moment at pier section..... 195
8.25	Plastic hinges and moment diagram..... 197
8.26	1.0 (LL + IL) loading for maximum shear at the NM pier..... 199
8.27	Reaction at outer supports during loading to failure..... 201
8.28	Longitudinal strains at SS7R and SS6L during loading to failure..... 201
8.29	Longitudinal strains at SS1 during loading to failure..... 202
8.30	Longitudinal strains at SMI during loading to failure..... 202

Figure	Page
8.31	Longitudinal strains at NS6 during loading to failure..... 203
8.32	Longitudinal strains at NM6 during loading to failure..... 203
8.33	Deflections at SM10 during loading to failure..... 204
8.34	Development of cracks around NM pier during loading to failure..... 206
8.35	Development of cracks around the center of main span during loading to failure..... 207
8.36	Typical crack around the joint (after failure)..... 208
8.37	Longitudinal strains at NM9 during loading to failure..... 209
8.38	Longitudinal strains at NM1 during loading to failure..... 210
8.39	Longitudinal strains at NS1 during loading to failure..... 210
8.40	General view of the bridge after failure..... 212
8.41	Deflections along the bridge during loading to failure.... 213
8.42	Moment diagram due to resultant force of prestressing and jacking force at end supports ( $M_{E2}$ )..... 214
8.43	Moment diagram for 0.35 DL for three different conditions ( $M_{E3}$ )..... 214
8.44	Moment diagram for 1.0 (LL + IL) for three different conditions ( $M_{E4}$ )..... 215
8.45	Failure loading at the center of the main span..... 221

## N O T A T I O N

$A$	= average area of cross sections of specimens [Chapter 3]; area of bolt [Chapter 6]
$A_p$	= area of prestressing cable
$A_v$	= area of web reinforcement placed perpendicular to the axis of the member
$a$	= depth of equivalent rectangular stress block
$b$	= average width of specimen [Chapter 3]; width of compression face of flexural member [Chapter 8]
$b'$	= minimum width of a flanged member
<hr/>	
$C$	= ultimate compressive force
$c$	= distance from extreme compression fiber to neutral axis
$d$	= average depth of specimen [Chapter 3]; distance from extreme compression fiber to centroid of prestressing force [Chapter 8]
$d_c$	= distance from plastic center to centroid of compressive force
<hr/>	
$d_p$	= distance from plastic center to centroid of negative tendon
$d_{t1}, d_{t2},$ $d_{t3}$	= distance from plastic center to centroid of each positive tendon
DL	= dead load
$E_c$	= modulus of elasticity of concrete
$E_s$	= modulus of elasticity of steel
$E_1$	= thickness of error in joint at bottom
$E_2$	= accumulated error in height at the distance $l_E$
$e$	= distance from centroid of prestressing cable to C.G.



$e_1, e_2$	= distance from centroid of each prestressing cable to C.G.
$f'_c$	= compressive strength of concrete
$F_{sp}$	= ratio of splitting tensile strength to the square root of compressive strength
$F_s$	= ultimate load of steel
$f'_s$	= ultimate strength of steel
$f_y$	= yield strength of reinforcement
$f_{cp}$	= permissible compressive concrete stress on bearing area under anchor plate of post-tensioning steel
$F$	= internal force
$F_I, F_{I1}, F_{I2}, F_{I3}$	= internal force due to prestressing cable
$^{\circ}F$	= fahrenheit degree
$f_{sp}$	= splitting tensile strength of concrete
$f_{pe}$	= compressive stress of concrete due to prestressing only at bottom fiber
$f_d$	= stress due to dead load at the extreme fiber of a section at which tensile stress is caused by applied load
$f_{pc}$	= compressive stress in concrete, after all prestress losses have occurred, at the centroid of the cross section resisting the applied load
$h$	= depth of segment
$h_p$	= height of pier
$I$	= moment of inertia [Chapter 6]; impact factor [Chapter 7]
$IL$	= impact load
$jd$	= distance between ultimate compressive force (C) and ultimate tensile force (T)
$l$	= span length
$l_E$	= distance from the joint with the erection errors

$l_c$	= length of bolt in compression side
$l_t$	= length of bolt in tension side
$l_p$	= length of prestressing cable
LL	= live load
LF	= load factor
M	= moment due to externally applied load
$M_p$	= moment due to prestressing force
$M_{cr}$	= net flexural cracking moment
$M_s$	= moment due to end reaction caused by prestressing of positive tendons and seating forces at outer supports
$M_{s1}$	= secondary moment due to prestressing of negative tendons
$M_{s2}$	= secondary moment due to prestressing positive tendons in main span
$M_{s3}$	= secondary moment due to prestressing of positive tendons in side span
$M_u$	= ultimate external moment
$M_{DL}$	= moment due to dead load
$M_{(LL+IL)}$	= moment due to (live + impact) load
$M_x$	= longitudinal slab moment per unit width
$M_y$	= transverse slab moment per unit width
$M_{01}, M_{02}$	= plastic moment
$M_E$	= external moment
$M_I$	= internal moment
$M_{E1}$	= moments due to weight of segment (1.0 DL)
$M_{E2}$	= moments due to resultant force of prestressing in main span and jacking force at outer supports (= $M_s$ )
$M_{E3}$	= moments due to 0.35 DL

$M_{E4}$	= moment due to live load
$M_{UI}$	= ultimate internal moment
$M_{I1}$	= moments due to negative tendons
$M_{I2}$	= moments due to positive tendons in side span
$M_{I3}$	= moments due to positive tendons in main span
$P$	= applied load [Chapters 3, 6, 7]; prestressing force [Chapters 6, 8]
$P_u$	= ultimate applied load indicated by the testing machine
$P_{ij}$	= prestressing force at a certain point
$P_{io}$	= prestressing force applied at the end
$P_1, P_2$	= prestressing force of each tendon
$RH$	= relative humidity
$\bar{s}$	= standard deviation
$s_1, s_2$	= force on the bolt
$SL$	= resultant reactions due to prestressing of positive tendons and seating forces at outer supports
$s$	= longitudinal spacing of web reinforcement
$T$	= ultimate tensile force
$T_1, T_2, T_3$	= tensile force of each prestressing cable
$U$	= ultimate design load
$V$	= shear force due to externally applied load
$V_p$	= equivalent vertical load of prestressing force
$V_c$	= shear carried by concrete
$V_{ci}$	= shear at diagonal cracking due to all loads, when such cracking is the result of combined shear and moment

$V_{cw}$	= shear force at diagonal cracking due to all loads, when such cracking is the result of excessive principal tensile stress in the web
$V_d$	= shear due to dead load
$V_u$	= shear due to specified ultimate load
$w$	= unit weight of concrete
$W$	= weight of truck
$W_b$	= section modulus at bottom
$W_T$	= section modulus at top
$X$	= load factor of (LL + IL)
$Y$	= reaction at support at complete collapse of the structure

$\alpha$	= angle change of tendon
$\phi$	= diameter [Chapter 2]; capacity reduction fraction [Chapter 8]
$\tau_u$	= ultimate shear strength
$\sigma_u$	= ultimate flexural strength
$\sigma_s$	= stress of prestressing cable
$\epsilon'_s$	= ultimate steel strain
$\epsilon_c$	= concrete strain
$\epsilon_{s1}, \epsilon_{s2}, \epsilon_{s3}$	= strain of each prestressing cable (positive tendon)
$\epsilon_p$	= strain at level of prestressing cable (negative tendon)
$\epsilon_s$	= steel strain
$\epsilon_{sp}$	= steel strain due to prestressing
$\epsilon_{sl}$	= steel strain due to external load
$\delta_1$	= deflection due to flexure of segment at cantilever end

- $\delta_2$  = deflection due to elongation of bolts at cantilever end
- $\delta_3$  = deflection due to bending of pier at cantilever end
- $\Delta_1, \Delta_2$  = elongation of bolts
- $\theta_2$  = angle change due to elongation of bolts
- $\theta_3$  = angle change of pier at the top due to bending of pier
- $\mu$  = Poisson's ratio [Chapter 4]; friction coefficient [Chapter 6]
- $\lambda$  = wobble coefficient

## CHAPTER 1

### INTRODUCTION

#### 1.1 General

Construction of longer span bridges is increasing in the United States to satisfy requirements of function, economics, safety, and aesthetics. Impetus was recently given by a special AASHTO Traffic Committee which called for elimination of piers normally placed adjacent to the outside shoulders of underpassing highways. This can be accomplished only with longer span overpass structures.<sup>10\*</sup>

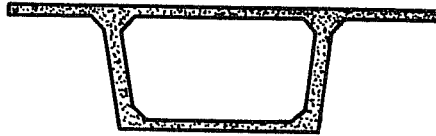
The full potential of prestressed concrete has not been developed by present U. S. bridge construction practices, such as wide use of pretensioned I-girder and composite slab systems. These systems have potential clear span limits in the 100 ft. to 120 ft. range. However, substantially longer span prestressed concrete bridges have been built in several countries by utilizing a precasting and cantilevering technique.<sup>26</sup> These are generally termed segmental precast prestressed concrete box girder bridges and are usually built in cantilever.

Precast segments (Fig. 1.1(a)) are cast and transported to the construction site. The precast segments are erected as balanced cantilevers from the pier segment which is usually rigidly connected to the pier either temporarily or permanently, as shown in Fig. 1.1(b). In some applications, temporary props are used to provide the cantilever moment capacity. Epoxy resin, mortar or concrete can be used as the jointing material between segments. In the early stages of the development of this technique, concrete was used as a jointing material. However, the French used the epoxy resin successfully as a jointing

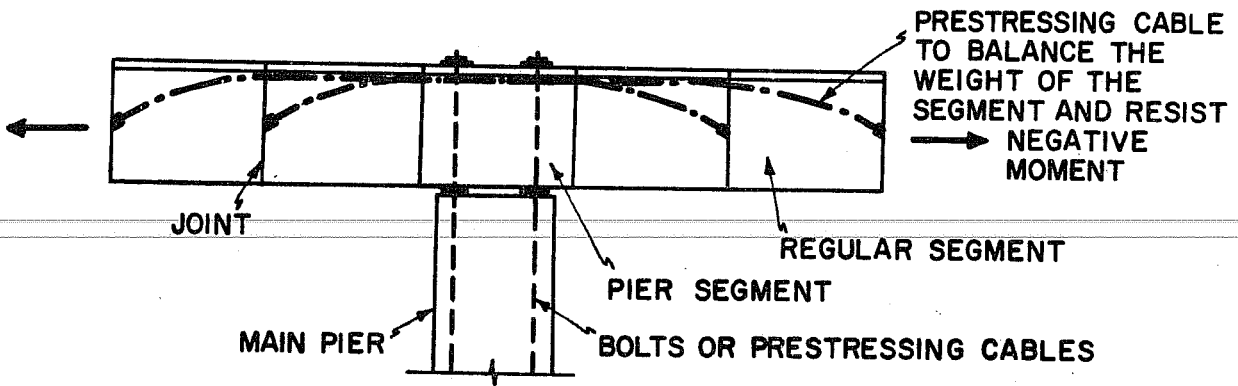
---

\* Superscript numbers refer to references in the Bibliography.

(a) TYPICAL CROSS SECTION OF BOX GIRDER



(b) CANTILEVER ERECTION OF PRECAST SEGMENTS



(c) COMPLETION OF CANTILEVER CONSTRUCTION

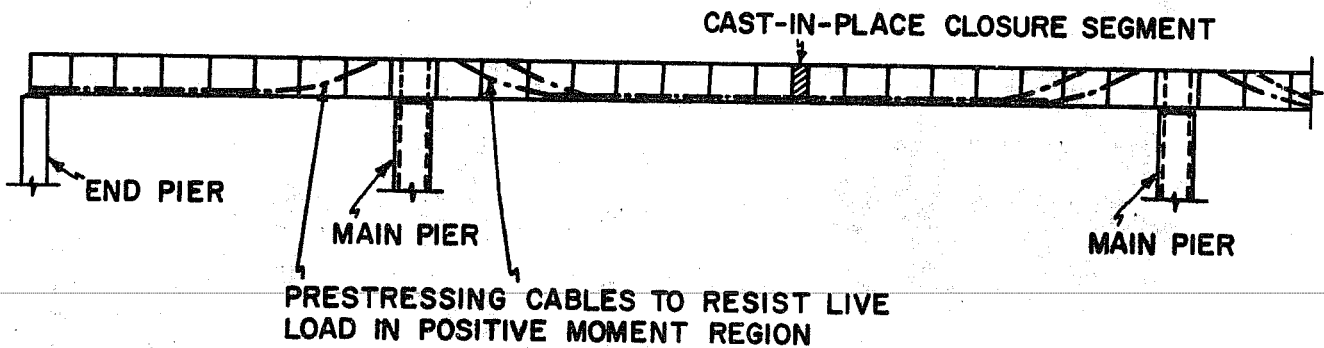


Fig. 1.1. Typical balanced cantilever construction

material in 1964.<sup>24</sup> Because of the rapid setting of the epoxy resin, this type of jointing can shorten the construction period appreciably. The negative tendons must provide for moment capacity for the full cantilever moment. The ends of the last cantilevered sections are located at either the center of the span or at the end supports, as shown in Fig. 1.1(c). The positive tendons in the end span are prestressed and the end segments are seated on their supports prior to or during stressing of prestressing cables in the main span positive moment region. At the center of the span, the gap between the two cantilever arms extending from the two piers is closed with cast-in-place concrete and then prestressing cables to resist live load in the positive moment region are inserted and stressed.

The use of these precasting and cantilevering techniques in a prestressed concrete box girder bridge has the following advantages:<sup>14, 24</sup>

- (1) Maintenance of navigational clearance during construction.
- (2) High quality control of segments and control of deflection.
- (3) Flexible choice of the segment length depending on the capacity of transportation and lifting equipment.
- (4) Simultaneous start of casting segments and construction of the piers.
- (5) Less erection time period at the site.
- (6) Efficient use of forms.

Beside the above advantages, long spans will minimize obstructions and will be more aesthetic in urban expressways. This type of bridge will save on maintenance costs by utilizing concrete in corrosive environments.

Because this type of bridge had never been built in the United States, a cooperative research project with the Texas Highway Department and the Federal Highway Administration to investigate the various problems associated with formulation of design procedures for long span precast prestressed concrete bridges of segmental construction was started at The University of Texas Center for Highway Research in 1968.<sup>9</sup>



The Texas Highway Department finalized and implemented a preliminary design developed as part of the project by The University of Texas researchers with an experimental structure which is part of the John F. Kennedy Memorial Causeway, Park Road 22, Corpus Christi, Texas. The requirement to maintain navigational clearance during construction and the highly corrosive environment on the Texas coast led to the choice of the precast prestressed concrete box girder bridge built in cantilever.

In order to study the applicability and accuracy of the design criteria, analytical methods, construction techniques, and shear performance of the epoxy resin joint, an accurate one-sixth scale model of the three span continuous bridge was built and tested at the Civil Engineering Structures Research Laboratory of The University of Texas' Balcones Research Center. This report mainly deals with construction and testing of the model.

## 1.2 Related Research in This Program

The followings are the related research which has been completed.

(1) State of the Art.<sup>17</sup> In the first year of the research program, many references from various countries were collected and a comprehensive literature survey was done by Lacey and Komura under the direction of Dr. Breen. The object of the literature survey was to investigate the technical problems in design and construction reported in available literatures and to study the applicability of the method with American standards of safety and economics.

(2) Design and Optimization.<sup>16</sup> Criteria were developed for design procedures and preliminary designs of several example structures were made by Lacey. The Texas Highway Department adopted this preliminary design for the United States' first segmentally constructed precast prestressed concrete box girder bridge, although a number of changes were made by Texas Highway Department designers, as the final plans and

details were developed. The bridge was largely designed by the Ultimate Strength Design method assuming beam theory as applicable. Stresses during construction and under service loads were also checked using Working Stress Design procedures and the beam method. Service load behavior of the completed structure was also checked by folded plate theory to determine the effect of warping. Optimal cross sections were also studied by unconstrained nonlinear programming, although the optimal cross section was not used in the final design.

(3) Theoretical Segmental Analysis.<sup>10</sup> Because the response of a box girder is sometimes much more complex than that assumed in the design procedure and no computer program to accurately analyze the structure during the cantilevering stages was available, a computer program utilizing the Finite Segment Method was developed by Brown. This program (SIMPLA2) can treat external load and longitudinal prestressing forces and determine effects in both the longitudinal and transverse directions.

(4) Experimental Study of Epoxy Resin.<sup>15</sup> Use of epoxy resins with concrete is very popular in the United States, as coating or patching material, etc. Although a guide<sup>4</sup> has been specified for the general use of epoxy resin with concrete, there was no specification for the specific use in jointing the segmental precast prestressed concrete box girder bridge. After a literature study<sup>26</sup> two epoxy resins which were available in 1969 were tested by the author for various conditions during and after construction of the bridge, such as the flexural and shear strength of the epoxy joint, and the pot life of the epoxy resin. Development of a Texas Highway Department tentative specification followed this study. Prior to the model bridge construction, six different epoxy resins were furnished and one of the epoxy resins which was closest to meeting the specification was selected from these test results.

(5) Field Study. This study consisted of instrumentation of the prototype bridge. Strain gages were mounted on the reinforcement in various segments and readings from these gages were taken at the time of cantilever erection. Structural behavior under actual service loads was

observed for various loading conditions upon completion of the prototype construction.

### 1.3 Objective and Scope of the Model Study

Tests of model structures are very powerful tools to check the adaptability or accuracy of design procedures and to verify analytical procedures.

In utilizing precast segments to build the bridge, continuity of the structure at the joints is a very important problem. Several concrete box girder bridge models were previously tested in various laboratories.<sup>29, 14, 11, 30</sup> All of the model bridges, except for a two-span (72 ft. long) four-cell reinforced concrete box girder model tested in California,<sup>29</sup> were precast prestressed microconcrete box segments joined with mortar. However, one of these, a PCA "Direct" model<sup>11</sup> (81 ft. long) maintained the continuity of reinforcement across all the joints. The 1/12th Mancunian Highway microconcrete model<sup>14</sup> (16 ft. 10 in. long) and 1/16th scale three cell box beam tested by Swann<sup>30</sup> proved the adequate strength of the mortar joint in failure tests.

Some other tests have been reported which focused on the investigation of the structural continuity of epoxy joints in the continuous slab [(1/4.64th scale, 50 ft. long) in France<sup>14</sup>]. An investigation of the shear capacity of the precast segment joined with epoxy resin has been reported in Japan.<sup>14</sup>

However, to the author's knowledge, no other precast prestressed concrete segmental bridge model joined with epoxy resin has accurately simulated the construction procedure and been loaded to failure. Since this three span precast prestressed concrete segmental twin box girder bridge, joined with epoxy resin, is a one-sixth scale "direct" model,<sup>1, 23</sup> it can simulate the behavior of the prototype both in the elastic and inelastic range. The objective and scope of this model study was to investigate the following:

- (1) Strain distribution due to prestressing during cantilever construction.
- (2) Behavior of the bridge under service level loading for the various loading conditions.
- (3) Comparison of analytical results of the beam theory and folded plate theory computer programs with the above experimental results.
- (4) Behavior of the bridge under the ultimate proof loading (1.35 DL + 2.25(LL + IL)) for the various loading conditions.
- (5) Determination of the flexural failure mechanism and the effect of the epoxy resin on the shear capacity of the bridge as well as the punching shear capacity of the top slab.
- (6) Applicability of the Ultimate Strength Design criteria proposed for this bridge.
- (7) Improvement of the design details in construction to minimize field problems prior to the prototype bridge construction.
- (8) Demonstration to the prospective contractors to assist in the visualization of the construction technique.

#### 1.4 Summary of the Following Chapters

Details of procedure used for reduction of scale in dimensions and materials are given in Chapter 2 and the test results of materials used for the model are discussed in Chapter 3. Details of the segments, casting procedures and preparation of segments for the model bridge are illustrated in Chapter 4.

Prior to discussing the actual construction and the loading tests, the instrumentation used in the model bridge tests and the procedures for data reduction are briefly explained in Chapter 5. Chapter 6 illustrates all construction procedures for the model bridge and discusses the behavior of the bridge during construction. After

completion of construction, a wide variety of service level loadings were first applied to the bridge and then various design ultimate loads specified by the 1969 Bureau of Public Roads criteria were applied to prove the safety of the structure. These tests are discussed in Chapter 7.

Finally, the bridge was loaded to failure and the behavior during loading is documented for the ultimate strength of the bridge and comparisons of the theoretical and experimental values are discussed in Chapter 8.

Chapter 9 gives the conclusions determined from the model study and recommendations for future design criteria and construction.

## C H A P T E R 2

### SCALE FACTORS FOR THE BRIDGE MODEL

#### 2.1 Factors Affecting Scale Selection

Selection of the scale factor for the model bridge was primarily governed by availability of materials and loading facilities. Consideration of dependability of results, costs, and construction times were additional important factors.

The 1/6-scale factor was dictated by availabilities of model materials (mainly prestressing cable).<sup>13</sup> All prestressing strands and reinforcing bars could be reduced very closely to required scale (max. 9% deviation). Although deformed bars for these small sizes are not available, bonding of the wire was not a critical problem in this study. After tentative selection of the 1/6-scale factor, testing facility and loading equipment availability were not found to be controlling factors.

#### 2.2 Dimensions of Prototype and Model Bridge

##### 2.2.1 Longitudinal Dimensions

Since a 200 ft. main span was needed in the prototype bridge, 100 ft. side spans were taken for balance (Fig. 2.1).

##### 2.2.2 Transverse Dimensions

Details of the transverse cross section are shown in Fig. 2.2.

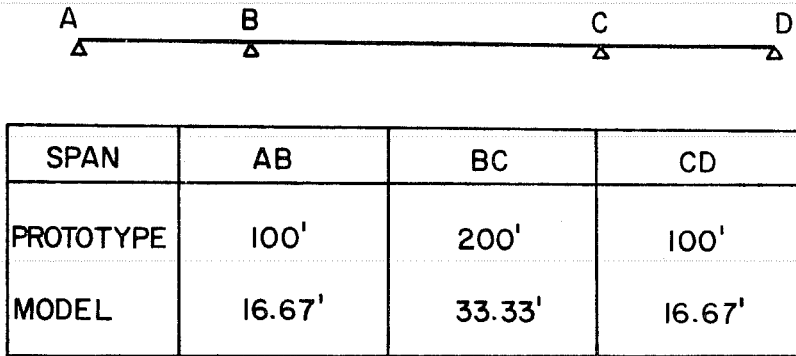
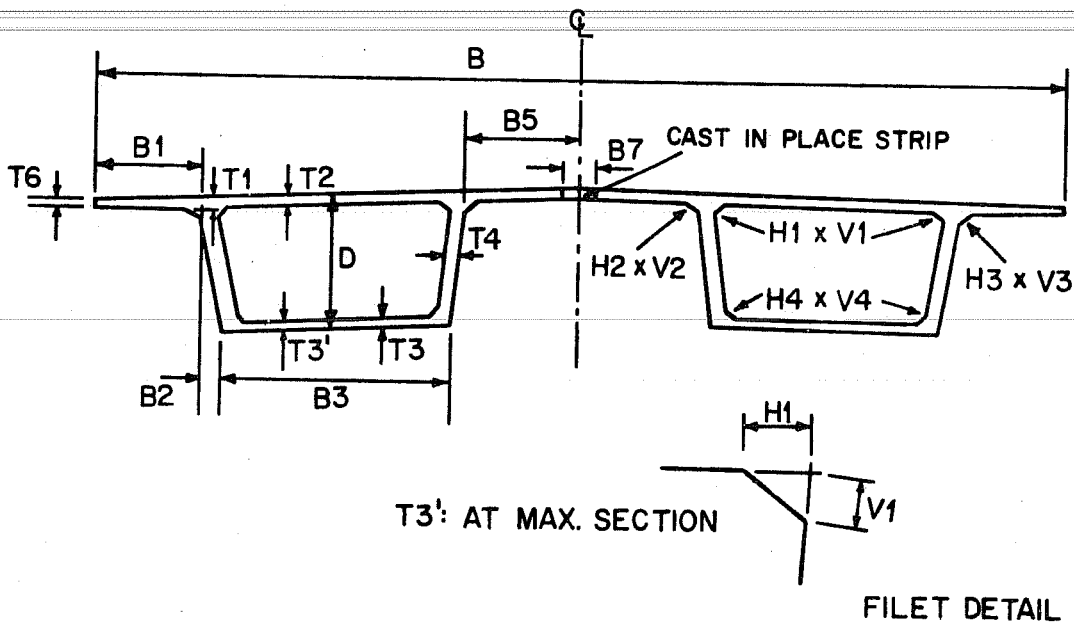


Fig. 2.1. Longitudinal dimensions of bridge



	B	B1	B2	B3	B5	B7	T1	T2	T3	T3'	T4	T6	D	H1	V1	H2	V2	H3	V3	H4	V4
PROTOTYPE	671"	71.5"	14"	156"	80"	24"	8"	7"	6"	10"	12"	6"	96"	8"	6"	8"	6"	8"	6"	4"	4"
MODEL	112"	11.9"	2.3"	26"	13.3"	4"	1.33"	1.17"	1"	1.67"	2"	1"	16"	1.33"	1"	1.33"	1"	1.33"	1"	0.67"	0.67"

Fig. 2.2. Cross section of bridge

## 2.3 Choice of Materials

### 2.3.1 Concrete

At The University of Texas, a 1/5.5 scaled microconcrete<sup>18</sup> (reduced aggregate which has a similar gradation to ordinary aggregate gradation) was frequently used for a number of model studies. Microconcrete is designed to have the same properties (in  $E_c$  and  $f'_c$ ) as the prototype concrete. It was decided to use this concrete after some trial mixes to get minimum  $f'_c = 6000$  psi. Details of the scaled microconcrete are described in Sec. 3.1.

### 2.3.2 Prestressing Steel

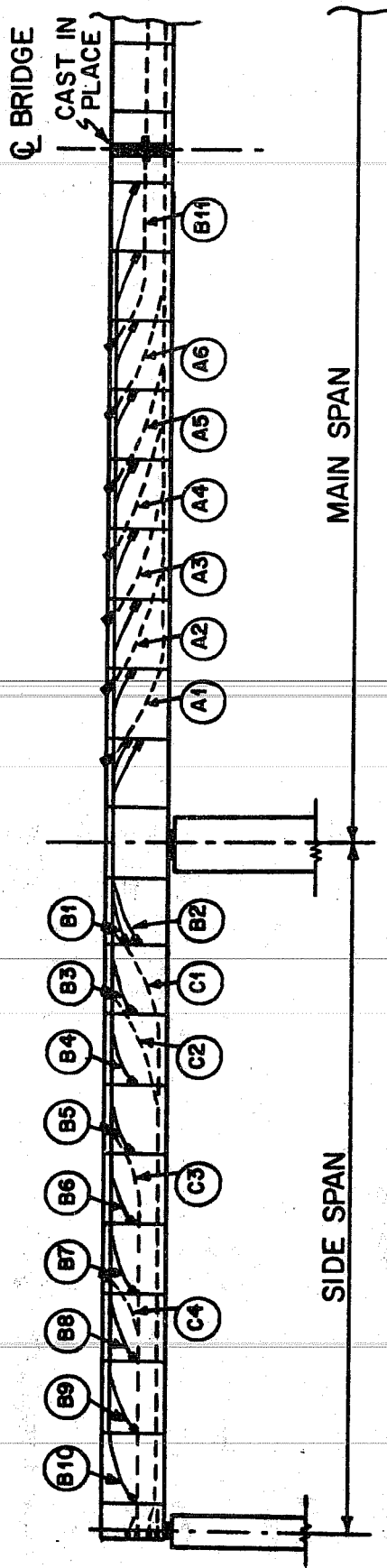
Four groups of strands were used for the prototype and the scale reduction for the model tendons is shown in Table 2.1. All strands were scaled down using breaking force values, so prestressing wire has to be used in some cases in order to have the same total breaking force. Therefore, the grades of steel for the prototype and the model were not the same in some cases. Fig. 2.3 shows the position of each tendon.

TABLE 2.1

CHOICE OF STRANDS AND WIRE FOR THE MODEL BRIDGE

Prototype		Model		
No. of 1/2" $\phi$ 270K Strands	Ultimate Strength (kip)	Required Ultimate Strength (kip)	Selected Wires or Strands	Strength of Selected Material (kip)
20	825	22.9	3/8 in. Strands	23.0
13	537	14.9	7 mm Wire	14.7
8	329	9.1	1/4 in. Strands	9.0
6	248	6.9	6 ga. Wire	7.2





	PROTOTYPE	MODEL
A1	8 STRANDS	1/4 IN. STRANDS
A2	8 STRANDS	1/4 IN. STRANDS
A3	8 STRANDS	1/4 IN. STRANDS
A4	8 STRANDS	1/4 IN. STRANDS
A5	8 STRANDS	1/4 IN. STRANDS
A6	8 STRANDS	1/4 IN. STRANDS
C1	6 STRANDS	6 GA. WIRE
C2	6 STRANDS	6 GA. WIRE
C3	6 STRANDS	6 GA. WIRE
C4	6 STRANDS	6 GA. WIRE

	PROTOTYPE *	MODEL
B1	13 STRANDS	7 MM. WIRE
B2	13 STRANDS	7 MM. WIRE
B3	20 STRANDS	3/8 IN. STRANDS
B4	20 STRANDS	3/8 IN. STRANDS
B5	13 STRANDS	7 MM. WIRE
B6	13 STRANDS	7 MM. WIRE
B7	13 STRANDS	7 MM. WIRE
B8	6 STRANDS	6 GA. WIRE
B9	6 STRANDS	6 GA. WIRE
B10	6 STRANDS	6 GA. WIRE
B11	6 STRANDS	6 GA. WIRE

\* AS ORIGINALLY DESIGNED

Fig. 2.3. Details of prestressing strands and wire

### 2.3.3 Reinforcing Bars

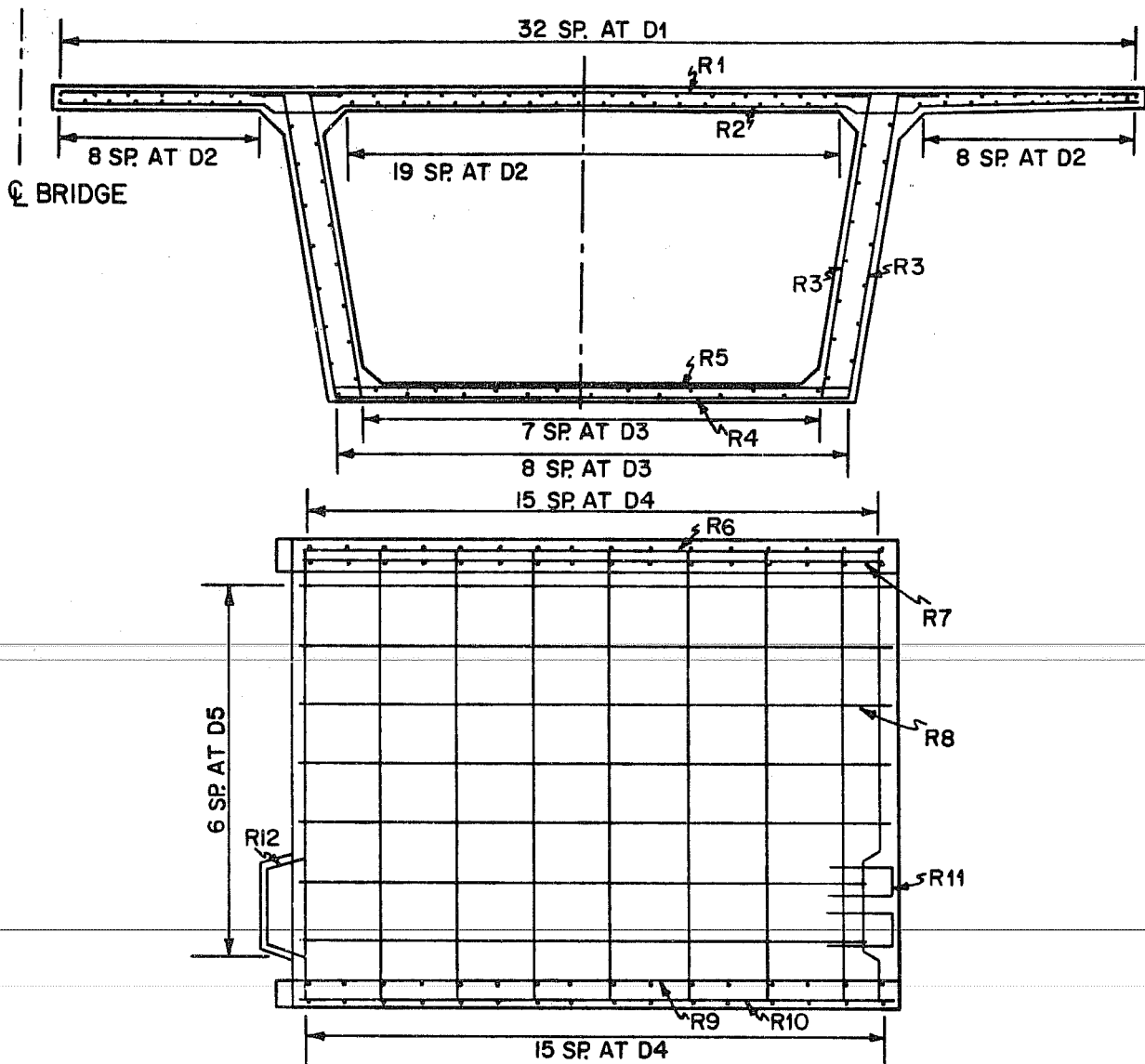
Three different reinforcing bar sizes were used in each segment and another bar size was used for the longitudinal cast-in-place joint. These bars were specified as Grade 60 in the prototype. The reduction to 1/6-scale for these bars is described in Table 2.2. Reinforcing bars used for the model were C-1018 wire. Wires for the model were not deformed, but bond strength of wire to microconcrete has been shown to be adequate in other tests.<sup>1</sup> Another problem with the wire for the model is the stress-strain characteristics, because yield strength varies between different size wires of the same quality. In order to obtain a distinct yield plateau in the wires to match the reinforcing bars of the prototype, wires for the cage were annealed by a commercial firm in a controlled temperature oven. Then the reinforcing cages were assembled. Details of the reinforcement are shown in Fig. 2.4.

TABLE 2.2

## CHOICE OF REINFORCING BARS FOR THE MODEL BRIDGE

Prototype		Model		
Bar	Area (sq. in.)	Required Area (sq. in.)	Chosen Wire	Area of Chosen Wire (sq. in.)
#8	0.79	0.0220	8 ga. Wire	0.0206
#6	0.44	0.0122	1/8 in. Wire	0.0122
#5	0.31	0.0086	12 ga. Wire	0.0087
#4	0.20	0.0056	14 ga. Wire	0.0050

Details of individual bars and some modifications (such as spirals and anchorages) are shown in Sec. 4.1.



REINFORCEMENT	PROTOTYPE	MODEL
R1	#8	8 GA. WIRE
R2	#8	8 GA. WIRE
R3	#8	8 GA. WIRE
R4	#4	14 GA. WIRE
R5	#4	14 GA. WIRE
R6	#4	14 GA. WIRE
R7	#6	1/8 IN. WIRE
R8	#4	14 GA. WIRE
R9	#4	14 GA. WIRE
R10	#4	14 GA. WIRE
R11	#4	14 GA. WIRE
R12	#3	16 GA. WIRE

SPACING	PROTOTYPE	MODEL
D1	10 IN.	1.67 IN.
D2	7 IN.	1.17 IN.
D3	18 IN.	3 IN.
D4	7 1/2 IN.	1.25 IN.
D5	12 IN.	2 IN.

Fig. 2.4. Details of reinforcing bars in segment

## CHAPTER 3

### MATERIAL PROPERTIES

#### 3.1 Concrete

##### 3.1.1 Concrete Mix Design

After several trial mixes, the following mix (Table 3.1) was used to cast a segment because mix design for 6000 psi concrete was not previously available. Consistency of microconcrete was judged by visual inspection. The workability of microconcrete mixes was good even though the mixes appeared somewhat dry and harsh. Concrete mix design of Table 3.1 is enough volume to cast a segment.

TABLE 3.1

#### CONCRETE MIX DESIGN (2.4 cu. ft.)

Design Strength	6000 psi
W/C (lb/lb)	51.6 %
Water	41.5 lbs.
Cement (Type III Portland Cement)	80.5 lbs.
TCM 154 (Aggregate)	61.2 lbs.
Ottawa Sand	70.9 lbs.
Blast Sand No. 1	65.4 lbs.
Blast Sand No. 2	18.9 lbs.
Colorado River Red Sand	18.9 lbs.
Airsene L (Retarder)	94.8 cc

### 3.1.2 Strength of Concrete

One or two cylinders (3 × 6 in. or 2 × 4 in.) were cast with each segment. Several cylinders were tested at the time of construction and the remainder were tested at the time of loading test. Compressive strength of the closure segment was tested one week after casting but prior to positive tendon operation. Test results are summarized in Table 3.2 and Table 3.3.

TABLE 3.2

#### COMPRESSIVE STRENGTH OF CONCRETE

Type of Cylinder	No. of Cylinders Tested	Average Compressive Strength (psi)	Standard Deviation ( $\bar{s}$ ) of Compressive Strength (psi)
3 × 6 in.	49	7090	523
2 × 4 in.	24	7430	810

TABLE 3.3

#### SPLITTING TENSILE STRENGTH OF CONCRETE

Type of Cylinder	No. of Cylinders Tested	Average Tensile Strength (psi)	Standard Deviation ( $\bar{s}$ ) of Tensile Strength (psi)
3 × 6 in.	35	597	31
2 × 4 in.	20	633	71

A universal hydraulic testing machine (max. 120 kip) was used for compression and splitting tensile tests of cylinders. Scaled loading heads and caps were necessary to minimize scatter of test results.<sup>1,25</sup>

For the compression test, cylinders were capped on both ends with sulphur capping compound in an approximately scaled capping device and tested by using scaled adjustable spherical load heads on the top of cylinders. For the splitting tensile test, loading bars and wooden strips were scaled down for each size of cylinders. Also the loading rate was reduced in appropriate scale because the loading rate would affect the strength of concrete.

There was no cylinder which had lower compressive strength than 6000 psi. The strengths of the 2 × 4 in. cylinders were slightly greater but showed higher variations than the 3 × 6 in. cylinders. The values obtained with the 3 × 6 in. cylinders are more reliable than those of the 2 × 4 in. cylinders because standard deviation for the 3 × 6 in. cylinders is much less than that for the 2 × 4 in. cylinders. Therefore the value for  $f'_c$  of 7090 psi and splitting tensile strength of 597 psi are used in later calculations.  $F_{sp}$  for the 3 × 6 in. cylinders is  $597/\sqrt{7090} = 7.09$ .

### 3.1.3 Modulus of Elasticity

Four - 0.4 in. paper strain gages were mounted vertically in series at the middle of the cylinders. The cylinders were preloaded to about 1/10 of the estimated failure load 2 or 3 times prior to taking any strain reading. The strain readings of all 4 gages were averaged and stress-strain curves were drawn to find  $E_c$ .  $E_c$  was determined by the slope of the chord up to about  $0.5f'_c$  (the secant modulus of elasticity).<sup>12</sup> Eight cylinders (3 × 6 in.) including one of closure were tested and the results are shown in Table 3.4. Although the value obtained with the 3 × 6 in. cylinder is used for later calculation,  $E_c$  of the 2 × 4 in. cylinders was also checked by the same procedure.

The ACI<sup>2</sup> formula gives  $E_c = w^{1.5} \times 33 \sqrt{f'_c}$ . Since the unit weight of microconcrete is 133 lb/cu.ft.,<sup>1,18</sup>  $E_c = 133^{1.5} \times \sqrt{7550} = 4.39 \times 10^6$  psi for  $f'_c = 7550$  psi.

TABLE 3.4  
MODULUS OF ELASTICITY OF CONCRETE

Type of Cylinder	No. of Cylinders Tested	Average $E_c$ (psi)	Standard Deviation (s) of $E_c$ (psi)	Average $f'_c$ (psi)
3 × 6 in.	8	$4.56 \times 10^6$	$0.37 \times 10^6$	7550
2 × 4 in.	2	$4.46 \times 10^6$	$0.24 \times 10^6$	7190

#### 3.1.4 Poisson's Ratio

Six - 0.4 in. paper strain gages were mounted vertically and horizontally in series at the middle of test cylinders. About 1/10 of the failure load was preloaded 2 or 3 times prior to taking any reading. Three vertical strain readings and three horizontal strain readings were averaged and Poisson's ratio was calculated. Three - 3 × 6 in. cylinders were tested to find Poisson's ratio. The average Poisson's ratio was 0.184 and standard deviation was 0.016.

### 3.2 Steel

#### 3.2.1 Prestressing Strands and Wire

##### 3.2.1.1 Ultimate Strength

Six to seven specimens of each size were tested and the results are as follows (Table 3.5).

##### 3.2.1.2 Modulus of Elasticity

Two strain gages (EA-06-125BT-120) were mounted on the opposite two faces of the wire and  $E_s$  was calculated from stress-strain curves. In an attempt to measure the modulus of strands, epoxy resin coatings were applied to get a smooth surface for strain gages. Two strain gages were then mounted using the same procedure as that for the wire.

But since strain was not measured successfully,  $E_s$  values for strands were taken from a reference.<sup>20</sup> These values are shown in Table 3.6.

TABLE 3.5  
ULTIMATE STRENGTH OF PRESTRESSING STRANDS AND WIRE

Type of Cable	No. of Specimens	Average $F'_s$ (kip)	Area (sq. in.)	Average $f'_s$ and $(\bar{s})$ (ksi)
6 ga. Wire	6	8.22	0.029	280 (13)
1/4 in. Strands	6	9.15	0.0356	257 (8)
7 mm Wire	6	15.3	0.0594	258 (8)
3/8 in. Strands	7	22.0	0.085	259 (4)

TABLE 3.6  
MODULUS OF ELASTICITY OF WIRE AND STRANDS

Type of Cable	No. of Specimens	Average $E_s$ and $(\bar{s})$ (psi)
6 ga. Wire	4	$30.9 \times 10^6$ ( $0.11 \times 10^6$ )
1/4 in. Strands	—	$27.0 \times 10^6$ (—)
7 mm Wire	5	$30.5 \times 10^6$ ( $0.17 \times 10^6$ )
3/8 in. Strands	—	$27.0 \times 10^6$ (—)

### 3.2.2 Reinforcing Wire

Samples of all reinforcing wire sizes used in the segments were tested without breaking the cross-connected wires at the intersection as shown in Fig. 3.1. Some difference in  $f_y$  and  $f'_s$  was noticed between



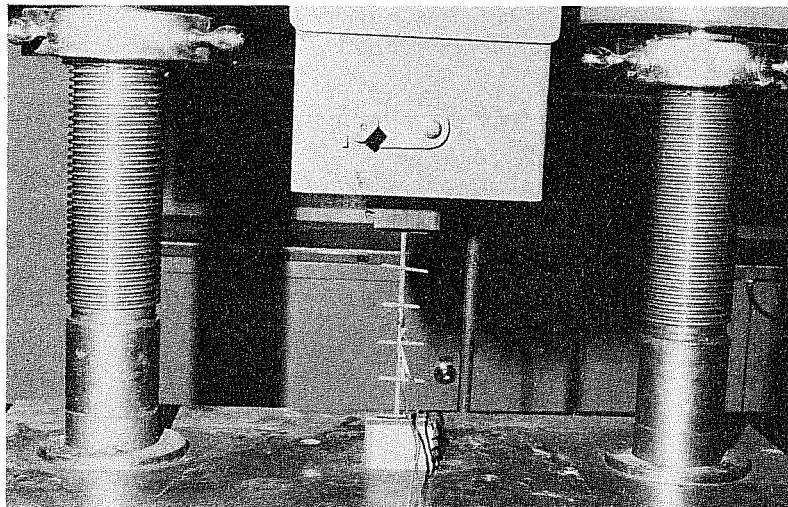


Fig. 3.1. Testing of reinforcing wire

sizes of wires and the smaller wire showed more variation than the larger wires. These results are shown in Table 3.7. All reinforcing wires of precast segments were above Grade 60. Twelve ga. wire which was used longitudinally at the midstrip closure had  $f_y = 45.1$  ksi ( $\bar{s} = 3.1$ ) and  $f'_s = 53.6$  ksi ( $\bar{s} = 1.8$ ).

TABLE 3.7

TEST RESULTS OF REINFORCING WIRE OF PRECAST SEGMENTS

Type of Wire	No. of Specimens	Average $f_y$ and ( $\bar{s}$ ) (ksi)	Average $f'_s$ and ( $\bar{s}$ ) (ksi)
8 ga. Wire	6	70.6 (3.4)	75.1 (4.2)
1/8 in. Wire	6	79.0 (4.3)	80.4 (3.0)
14 ga. Wire	15	72.2 (12.1)	74.6 (11.4)

### 3.2.3 Strength of Bolts at Main Piers

Texas Highway Department plans specify that twelve-3 in. diameter threaded rods were to be used for moment connections at the main piers during construction. For the model bridge, twelve-1/2 in. diameter high strength bolts were used at the main piers to hold segments temporarily during construction. Test results of those bolts are shown in Table 3.8. Experimental  $f'_s$  was in the range (60-100 ksi) specified by ASTM.

TABLE 3.8

TENSILE STRENGTH OF BOLTS AT MAIN PIERS

Type of Bolt	No. of Specimens	Average $f_y$ and (s) (ksi)	Average $f'_s$ and (s) (ksi)
1/2 in. diameter	3	75.1 (0.85)	78.8 (0.9)

### 3.3 Epoxy Resin as a Jointing Material

#### 3.3.1 General

The advantage of the epoxy resin as a jointing material as compared to concrete or mortar joints is its quick hardening. It may be possible to construct the precast segments with dry joints but it will be better to seal the joint against corrosion. Therefore a good epoxy resin is required to assure durability. Also it will be better to have a resin which is certainly as good as concrete in flexure and shear. At the region where maximum shear and maximum moment occur simultaneously, there is a possibility of direct shear failure as flexural cracks extend if segments are constructed with dry joints. The epoxy resin joints will increase the capacity of cracking moment at joints or shift the cracks to some other positions under overloading, if a good epoxy resin is used in stead of dry joint.

The use of epoxy resin to join precast segments is not well developed in the United States. It was felt necessary to study properties under various conditions in order to develop guideline specifications and provide a basis for selecting a suitable epoxy resin for jointing. Flexural and shear strength of hardened joined concrete specimens, pot life, tensile strength, ease of mixing and application, development of bond strength and color were tested for two epoxy resins which were available.<sup>15</sup> The specification of the Texas Highway Department (see Appendix B) was based on this study.

In the practical use of epoxy resin, the conditions which must be considered include: (1) some bond releasing agent has to be used on the surface of the old concrete segment prior to casting a new segment against it; (2) oil may be put on the end form at the time of casting; or (3) the precast segments may be wet at the time of construction. These conditions were considered in selecting the best epoxy resin for the model bridge construction.

Because of limited time and the large number of epoxy resins submitted for evaluation, the number of tests run was minimized. The effect of oil and moisture conditions was evaluated by flexure tests only since the effect of these variables on both flexural and shear strength had been shown to be essentially the same in the prior series. Also, monolithic concrete specimens were tested in order to compare their strength with joined specimens. Epoxy resins were mainly evaluated by comparing the flexural and shear strength of hardened joined concrete specimens, evaluating the pot life, and observing the ease of mixing and application.

### 3.3.2 Test Procedure and Test Results

#### 3.3.2.1 Flexure Tests

(a) Test procedure. Dimensions of the flexure test specimen are shown in Fig. 3.2. Segment (A) was cast first. The steel plate facing Segment (B) was removed one day after casting and a liquid bond breaking compound TBC (Thompson Bond Breaking Compound) was put on the surface, and

Segment (B) was cast against Segment (A). Although TBC does not contain any silicon or paraffin which might reduce the strength of the joint,<sup>26</sup> it was felt necessary to check the performance of TBC prior to the casting of the model segments. Desired compressive strength of concrete was 6500 - 7000 psi, which is equivalent to the compressive strength of the model and prototype concrete. One day after casting Segment (B), Segments (A) and (B) were separated easily without any damage.

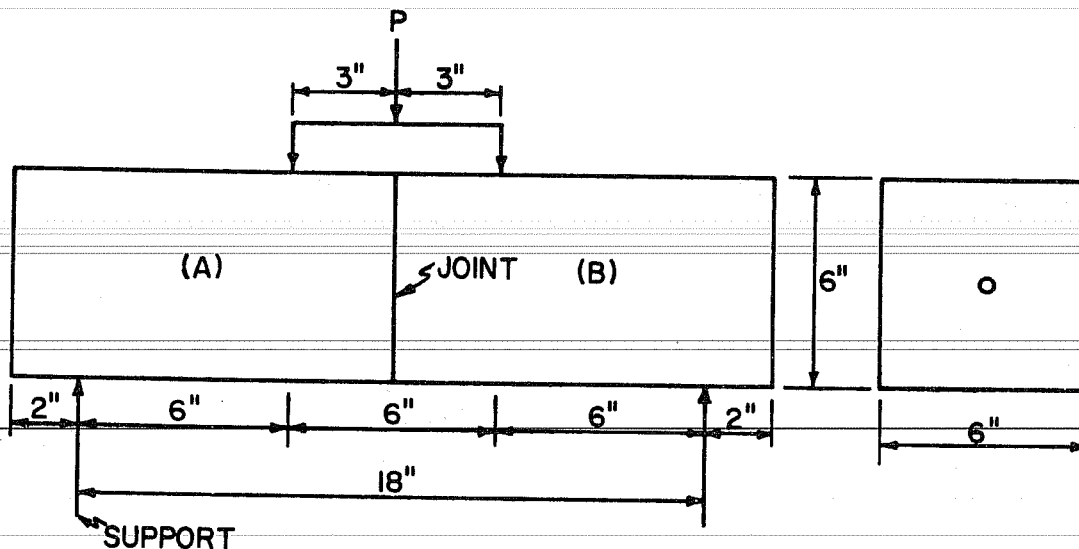


Fig. 3.2. Bending test specimen

After curing for one to two weeks, the joining surfaces were cleaned with a wire brush, washed with water or steam cleaned and wiped with acetone.

Epoxy resin was put on both matching faces and the specimen was prestressed using a bolt inserted in a concentric duct to produce 70 psi uniform compressive stress.

The joined specimens were cured at room temperature ( $85 \pm 5^{\circ}\text{F}$ ) for ten days prior to loading tests. The bolt which was used for stressing

was removed before applying the load and the load was applied until failure occurred. Figure 3.2 shows the loading setup.

(b) Test Results. For most of the epoxy resins three specimens were tested. These three specimens were usually tested under different conditions since variations in flexural strength were usually very small. These conditions were:

(1) Dry, No Oil. TBC was put on the form before casting Segment (A) in Fig. 3.2. TBC was also applied to the surface of the concrete of Segment (A) which was facing Segment (B) after removal of the plate. Segment (B) was then cast. Those specimens were dry at the time of jointing.

(2) Dry, Oil. Oil was put on the form surfaces before casting Segment (A). TBC was then applied to the concrete surface of Segment (A) which was facing Segment (B) after removal of the plate. Segment (B) was then cast. These specimens were then steam cleaned one to three days before jointing.

(3) Saturated, No Oil. TBC was put on the form before casting Segment (A) in Fig. 3.2. TBC was then applied to the concrete surface of Segment (A) which was facing Segment (B) after removal of plate. Segment (B) was then cast. Those specimens were put into a water bath for 24 hours and were removed one to two hours prior to jointing.

For the loading conditions and specimen dimensions used, the flexural strength was calculated by the equation:

$$\sigma_u = P_u \ell / bd^2$$

where

$\sigma_u$  = ultimate flexural strength (psi)

$P_u$  = ultimate applied load indicated by the testing machine (lbs.)

$\ell$  = span length (in.)

$b$  = average width of specimen (in.)

$d$  = average depth of specimen (in.)

Earlier flexure test results for Epoxy (A) and (B) are summarized in Table 3.9. The Texas Highway Department specified the minimum flexural strength of joined specimens as 90 percent of the monolithic specimen.

TABLE 3.9

## FLEXURE TEST RESULTS OF EPOXIES (A) AND (B)

Epoxy Resin	Condition of Specimen	Average Flexural Strength and (s) (psi)	Percentage of Strength of Monolithic Specimen (percent)
(A)	Dry, soap*	614 (44)	96.6
	Saturated, soap	403 (22)	63.4
	Monolithic	636 (18)	-----
(B)	Dry, soap	737 (60)	107
	Saturated, soap	80 (4)	11.6
	Monolithic	689 (44)	-----

\* Soap was used for bond breaking in place of TBC.

Test results for Epoxies (C) - (G) are summarized in Table 3.10. For the specimens which were dry at the time of jointing and where there was no form oil on the jointing surface, the ultimate flexural strength of all epoxy resin performed as well as the monolithic specimen. However, if there was any form oil on the jointing surface, the strength of Epoxies (C), (D), and (G) dropped significantly. Epoxies (C) and (D) were joined three days after steam cleaning and Epoxies (E), (F), and (G) were joined one day after steam cleaning. Additional specimens were tested using Epoxy (E) to investigate the effect of time after steam cleaning. Although specimens were joined using Epoxy (E) three days after steam cleaning, flexural strength was 759 psi and it was concluded

TABLE 3.10  
FLEXURE TEST RESULTS

Epoxy Resin	Conditions of Specimen	Flexural Strength (psi)	Type of Failure	Percentage of Strength of Monolithic Specimen (%)
	Dry, No Oil	766	Concrete Adjacent to Joint	105
(C)	Dry, Oil	625	Concrete Adjacent to Joint	86
	Saturated, No Oil	133	Epoxy Separation	18
	Dry, No Oil	800	Concrete Adjacent to Joint	110
(D)	Dry, Oil	500	Concrete Adjacent to Joint	69
	Saturated, No Oil	50	Epoxy Separation	7
	Dry, No. Oil	733	Concrete Adjacent to Joint	100
(E)	Dry, Oil	742	Concrete	102
	Saturated, No Oil	467	Concrete Adjacent to Joint	64
	Dry, No Oil	750	Concrete	103
(F)	Dry, Oil	758	Concrete	104
	Saturated, No Oil	175	Epoxy Separation	24
	Dry, No Oil	725	Concrete	99
(G)	Dry, Oil	221	Epoxy Separation	30
	Saturated, No Oil	183	Epoxy Separation	25
Compressive Strength of Cylinder:		6760 psi ( $\bar{s} = 842$ )		
Splitting Tensile Strength:		538 psi ( $\bar{s} = 73$ )		
Flexural Strength of Monolithic Specimen:		729 psi ( $\bar{s} = 43$ )		

that there will be no difference when joining one day or three days after cleaning with form oil exposed specimens.

For saturated specimens, joints were extremely weak, except with Epoxy (E) which showed about a 1/3 strength reduction under this extremely severe exposure condition. It was also concluded that TBC does not reduce the strength at the joint.

Because the flexural strength of concrete (flexural strength of the monolithic specimen) in Tables 3.9 and 3.10 was different, the values of the flexural strength of joined specimens cannot be compared directly. But the percentage of the strength of the monolithic specimen indicates the performance of each epoxy resin. It was concluded that only Epoxy (E) will perform as well as Epoxy (A) for flexure with the various surface conditions studied.

### 3.3.2.2 Shear Tests

(a) Test Procedure. Dimensions of the shear test specimen are shown in Fig. 3.3. Segments (A) were cast first. Steel plates facing Segment (B) were then removed one day after casting and TBC (details are in Sec. 3.3.2.1 (a)) was put on those surfaces, and Segment (B) was cast against Segment (A). Other details of joining were same as in Sec. 3.3.2.1 (a). Fig. 3.3 shows the loading setup for the shear tests.

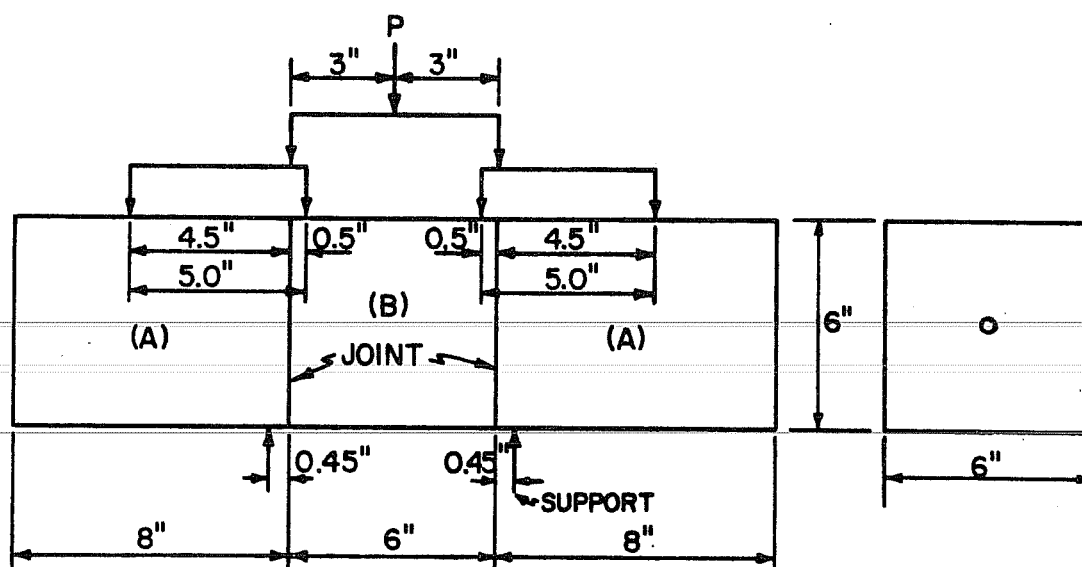


Fig. 3.3. Shear test specimen



(b) Test Results. For each epoxy resin, three specimens were tested for the same basic condition. All specimens were tested with no form oil application, and specimens were dry at the time of jointing. Test results are summarized in Table 3.11.

For the loading conditions and specimen dimensions used, the average shear strength was calculated by the equation:

$$\tau_u = V/bd = 0.45 P_u/bd = 0.45 P_u/A$$

where

$\tau_u$  = ultimate shear strength (psi)

V = shear force (lbs.)

$P_u$  = ultimate applied load indicated by the testing machine (lbs.)

b = average width of specimen (in.)

d = average depth of specimen (in.)

A = average area of cross section of specimen (sq. in.)

All of the epoxy resins except Epoxy (G) have enough shear strength for a jointing material, especially Epoxies (C) and (D) which nearly developed the equal strength of the monolithic specimens.

Shear test results of Epoxies (A) and (B), which had been tested previously, are summarized in Table 3.12. The Texas Highway Department specified the minimum shear strength of joined specimens as 70% of the monolithic specimen. Therefore Epoxies (C), (D), (E) and (F) passed the specification.

### 3.3.2.3 Pot Life of Epoxy Resins

Two different tests for pot life of epoxy resins are specified in ASTM D 1338-56<sup>5</sup> as

(1) Consistency Test

(2) Bond Strength Test.

Since the pot life of an epoxy resin is severely affected more by consistency or viscosity of the epoxy resin than bond strength,<sup>15</sup> pot life was measured

TABLE 3.11

## SHEAR TEST RESULTS

Epoxy Resin	Shear Strength (psi)	Type of Failure	Average Shear Strength and (s) (psi)	Percentage of Strength of Monolithic Specimen (%)
	806	Concrete Adjacent to Joint		
(C)	744	Concrete Adjacent to Joint	755 (31)	103
	---	Error in Jointing		
	744	Epoxy Separation		
(D)	680	Concrete Adjacent to Joint	727 (33)	97
	756	Concrete Adjacent to Joint		
	542	Epoxy Separation		
(E)	504	Concrete Adjacent to Joint	571 (69)	76
	666	Concrete Adjacent to Joint		
	530	Concrete Adjacent to Joint		
(F)	504	Epoxy Separation	608 (125)	81
	781	Concrete		
	340	Epoxy Separation		
(G)	378	Epoxy Separation	328 (47)	44
	265	Epoxy Separation		
Compressive Strength of Cylinder:			6760 psi	( $\bar{s}$ = 842)
Splitting Tensile Strength:			538 psi	( $\bar{s}$ = 73)
Shear Strength of Monolithic Specimen:			753 psi	( $\bar{s}$ = 103)

TABLE 3.12  
SHEAR TEST RESULTS OF EPOXIES (A) AND (B)

Epoxy Resin	Condition of Specimen	Average Shear Strength and (s) (psi)	Percentage of Strength of Monolithic Specimen (%)
(A)	Dry, Soap*	501 (30)	69.9
	Wet, Soap	240 (35)	33.5
	Monolithic	717 ( 9)	----
(B)	Dry, Soap	456 (43)	59.7
	Wet, Soap	92 (12)	12.0
	Monolithic	764 (42)	----

\* Soap was used for bond breaking in place of TBC.

by consistency tests specified by ASTM D 1338-56. Epoxy resin was put into a beaker, and consistency of it was checked by rotating a glass rod at certain intervals until regular rotation became impossible. Viscosity was judged by visual inspection.

Test results of pot life (at  $75 \pm 3^{\circ}\text{F}$ ) by consistency are shown in Table 3.13.

None of the epoxy resins except Epoxy (A) passed the 90 minute pot life Texas Highway Department specification, although temperature conditions of the test were slightly different. In a segmentally constructed model bridge, epoxy resin is usually put on the joining surface within 30 minutes of mixing, and stressing operations are usually completed within one hour after mixing. Since most of the epoxy resins have a longer pot life when the epoxy resin is spread in thin layers (because of less heat concentration), all epoxy resins except Epoxy (D) can be used without any problem.

TABLE 3.13  
 POT LIFE BY CONSISTENCY TEST

Epoxy	Pot Life (min.)
(A)	90
(B)	60
(C)	70
(D)	20
(E)	50
(F)	60
(G)	70
Texas Highway Dept. Specification	90 min. at 68°F

#### 3.3.2.4 Ease of Mixing and Application

All epoxy resins except Epoxy (D) were easy to mix because the viscosity of the resins and hardeners were almost the same.

After mixing the resin and hardener, there was no problem in applying the mixture to the surface of the concrete. All epoxy resins submitted had reasonable viscosity except Epoxy (E). However the manufacturer of Epoxy (E) changed the viscosity as required to meet reasonable limits.

#### 3.3.3 Selection of Epoxy Resin and Further Test

The prototype bridge was going to be constructed on the Texas coast and the segments transported by barge to the site. It was felt that the effect of moisture might be quite important. Therefore Epoxy (E) was selected as the best overall material for use in construction

of the model bridge. Development of bond strength of Epoxy (E) was tested by direct tension tests using bolts (1-3/4 in. diameter) as shown in Fig. 3.4.

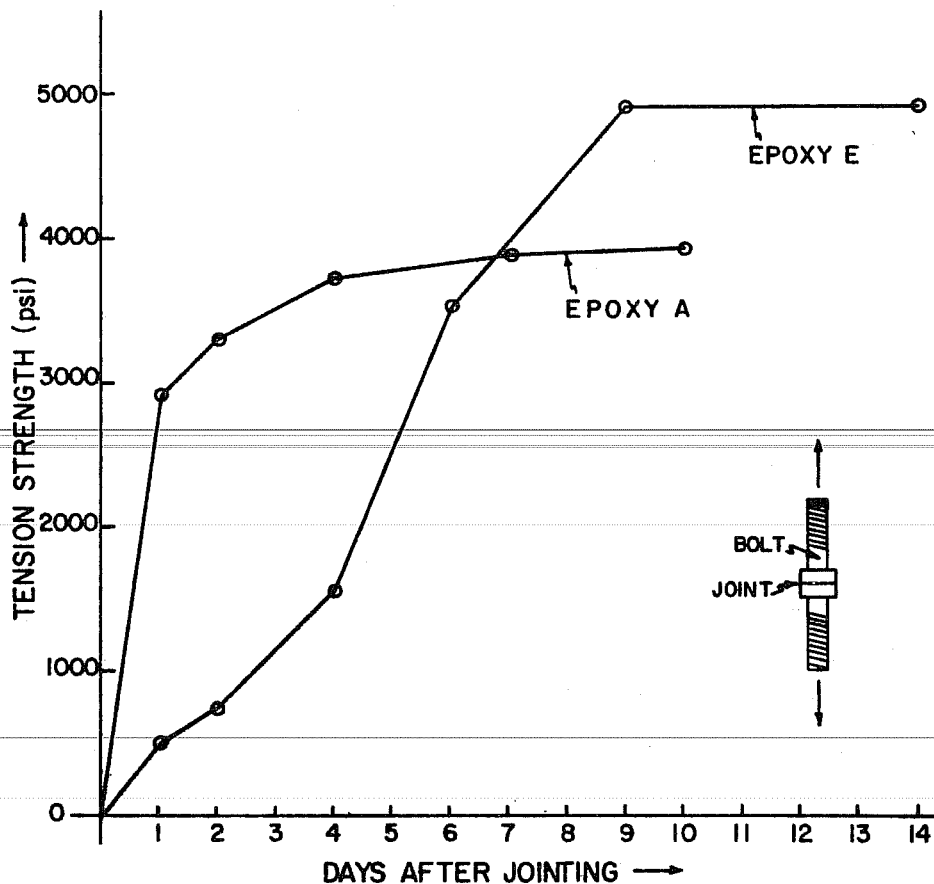


Fig. 3.4. Development of bond strength of epoxy resins

Development of strength may change depending on joining material. Development of the strength of Epoxy (E) was very slow compared to Epoxy (A) which was used in previous tests and was not available for use in the prototype or model selection. One of the desired benefits in using epoxy resin as a joining material for segmentally constructed precast prestressed

concrete bridges is its quick development of strength. This helps speed up construction time. Although there was no problem using Epoxy (E) for the model bridge construction, it is necessary to accelerate the development of strength when used in prototype bridge construction, to prevent slip at joints.

In Japan, most of the epoxy resins in use are capable of attaining the same strength whether wet or dry specimens are used.<sup>26</sup> As segmental construction is becoming more widespread in the United States, it is necessary to improve the quality of epoxy resins for strength under all conditions.

## CHAPTER 4

### SEGMENT DETAILS

#### 4.1 Reinforcing Cage for Precast Segments

##### 4.1.1 Reinforcement

As mentioned in Sec. 2.3.3, one of the basic problems in using wires is that the yield strength varies somewhat inversely with the size because the wire is cold drawn. In order to get a uniform yield strength for each wire, it would be ideal to anneal each size of wire separately and tie the individual wire into the proper shape. This would have taken excessive time to complete 84 segments. Therefore, the five different wire mats which were required for each segment were lightly spot-welded and were then annealed simultaneously by a commercial firm. These sets of wire mats were then cut as required and bent in proper length and shape as shown in Fig. 4.1. The two top mats were tied first, with spacers provided at eight points. The two bottom slab mats were then tied using the same procedure. Then, all mats of a segment were assembled as shown in Fig. 4.2, by using a jig. Details of each mat are shown in Fig. 4.3. Development length of web reinforcement (Fig. 4.3) spliced into the top slab was longer than that specified by the prototype plan, because plain bars were used in the model instead of deformed bars. The ACI Code<sup>2</sup> specifies that the minimum amount of lap for plain bars shall be twice that specified for deformed bars. The 84 cages required for the model were assembled using these procedures and stored. Since all mats were welded to close position tolerances, assembly of the mats into cages proceeded very smoothly.

Modification of the cages was required at the shear key and anchorage points. Those details are shown in Fig. 4.4. Whenever a

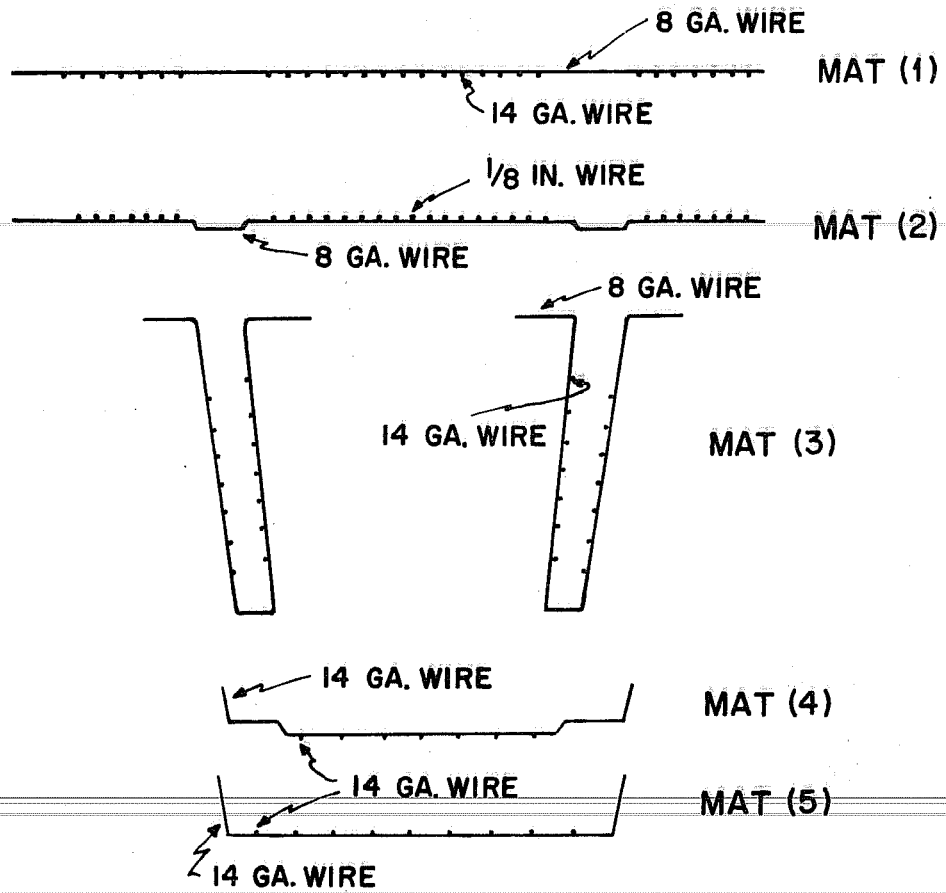


Fig. 4.1. Individual mat composed cage

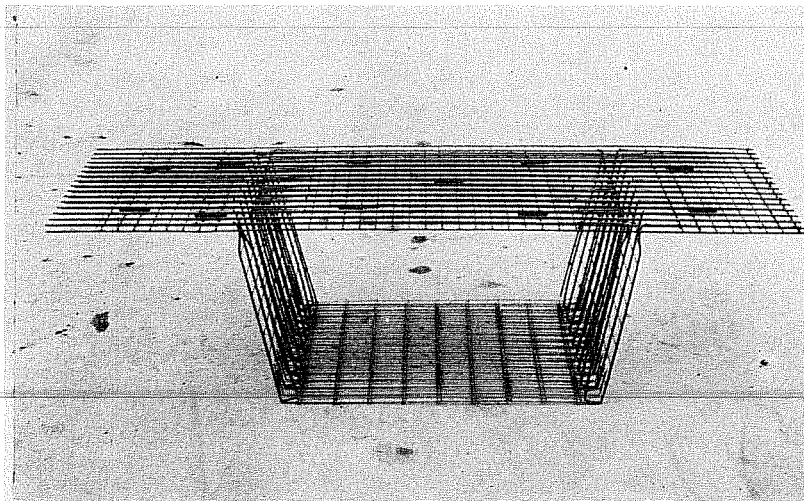
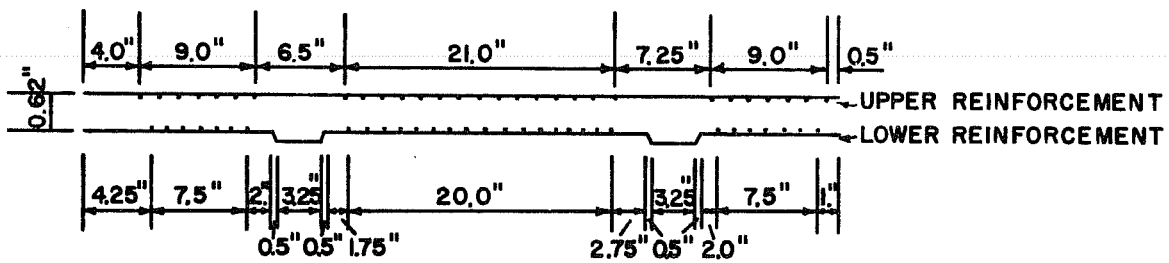
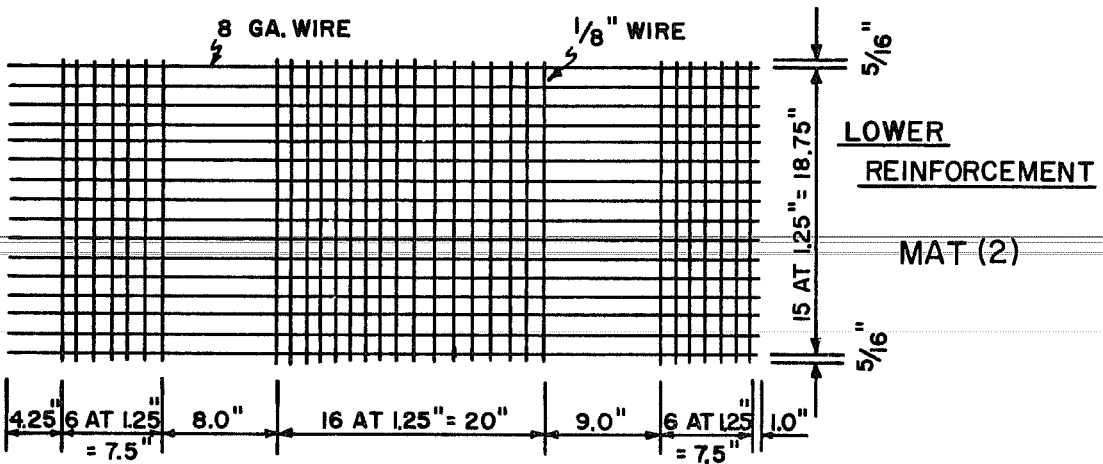
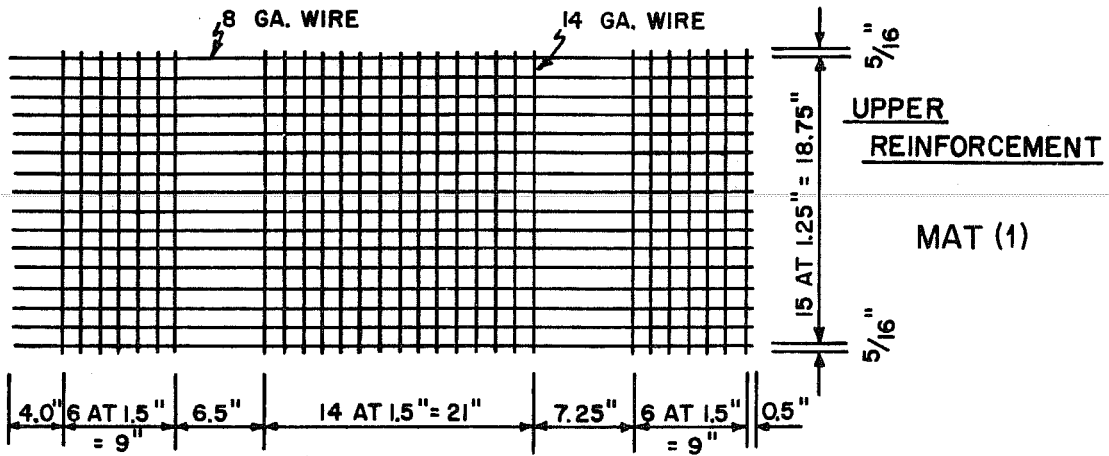


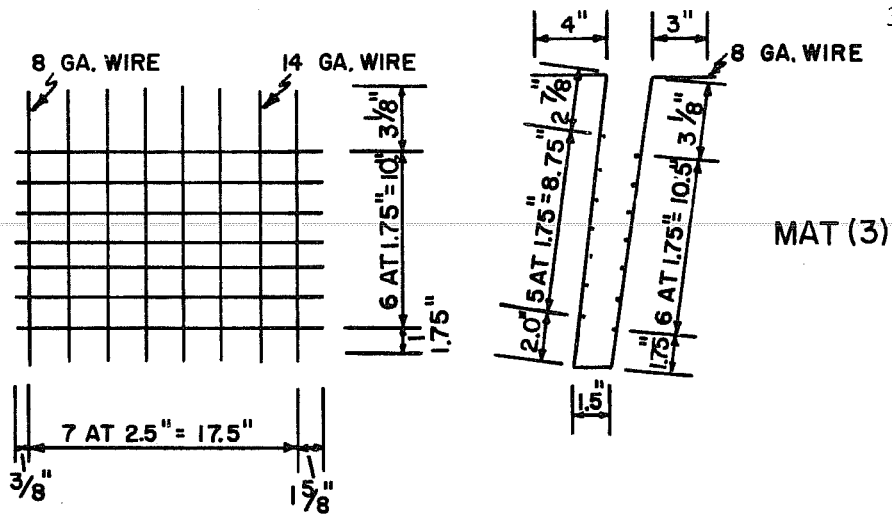
Fig. 4.2. Cage for a segment





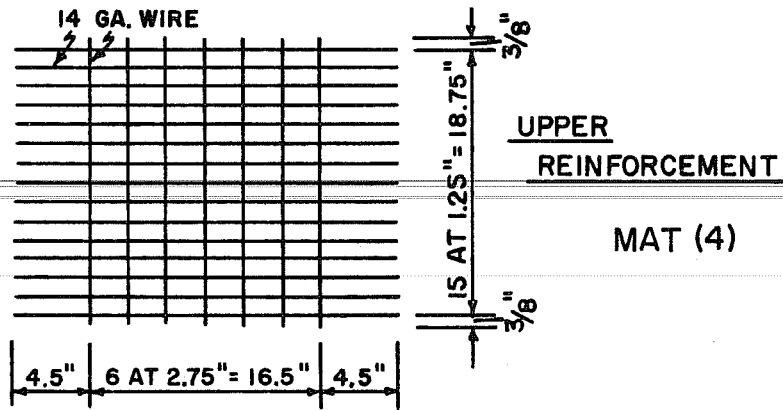
REINFORCEMENT IN TOP SLAB

Fig. 4.3. Details of reinforcing mats

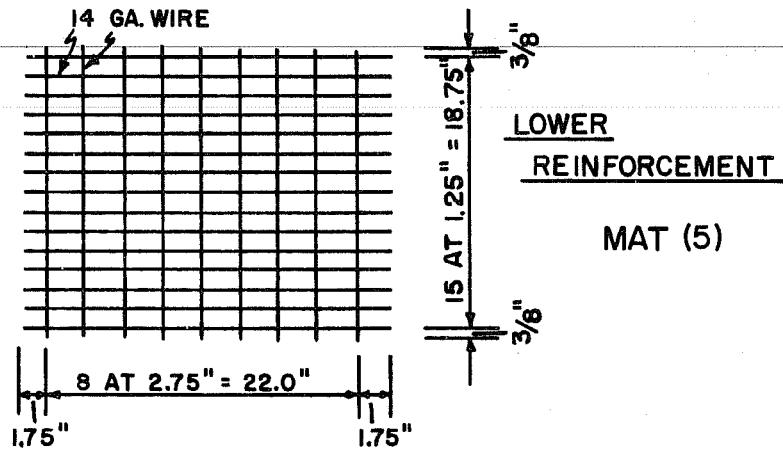


MAT (3)

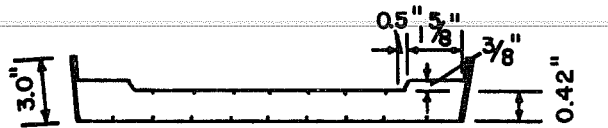
WEB REINFORCEMENT



MAT (4)

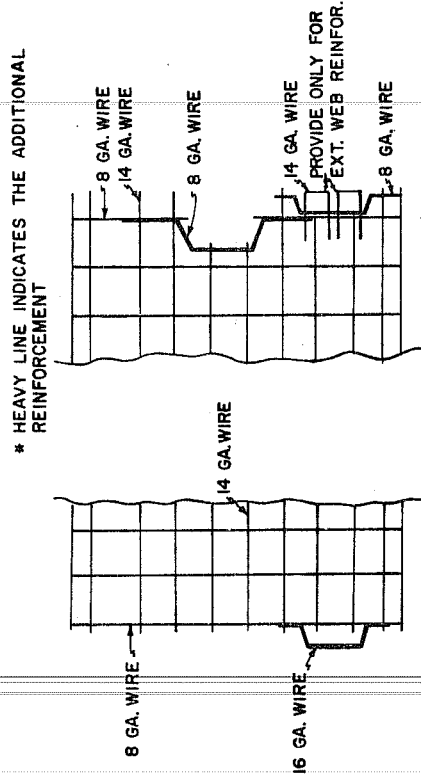


MAT (5)



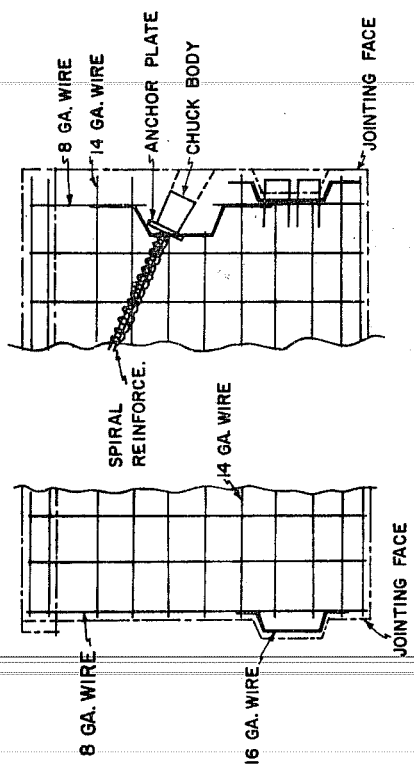
REINFORCEMENT IN BOTTOM SLAB

Fig. 4.3. Continued



STEP (1)-ORIGINAL CAGE

STEP (3)-ADD REINFORCEMENTS FOR SHEAR KEY AND ANCHORAGE



STEP (2)-CUT SOME REINFORCEMENT

STEP (4)-FINAL SET CHUCK BODY AND TENDON DUCT

Fig. 4.4. Details of web reinforcement modification

wire was cut, replacement bars were spliced in, or wires were rotated or rerouted as necessary. No bars called for on the plans were ever omitted.

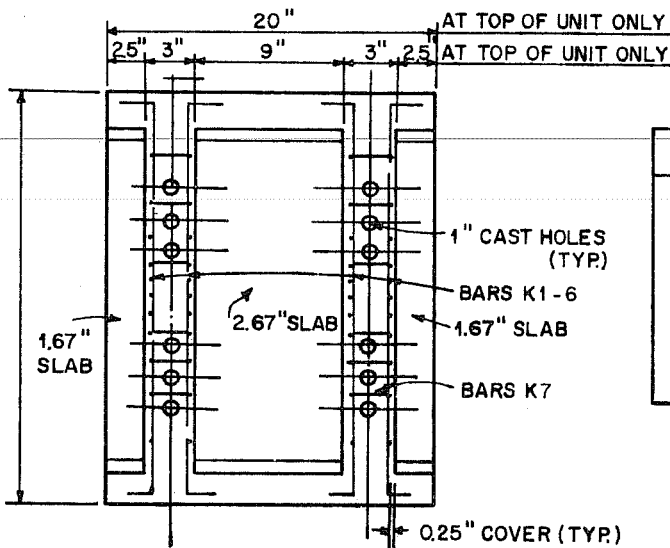
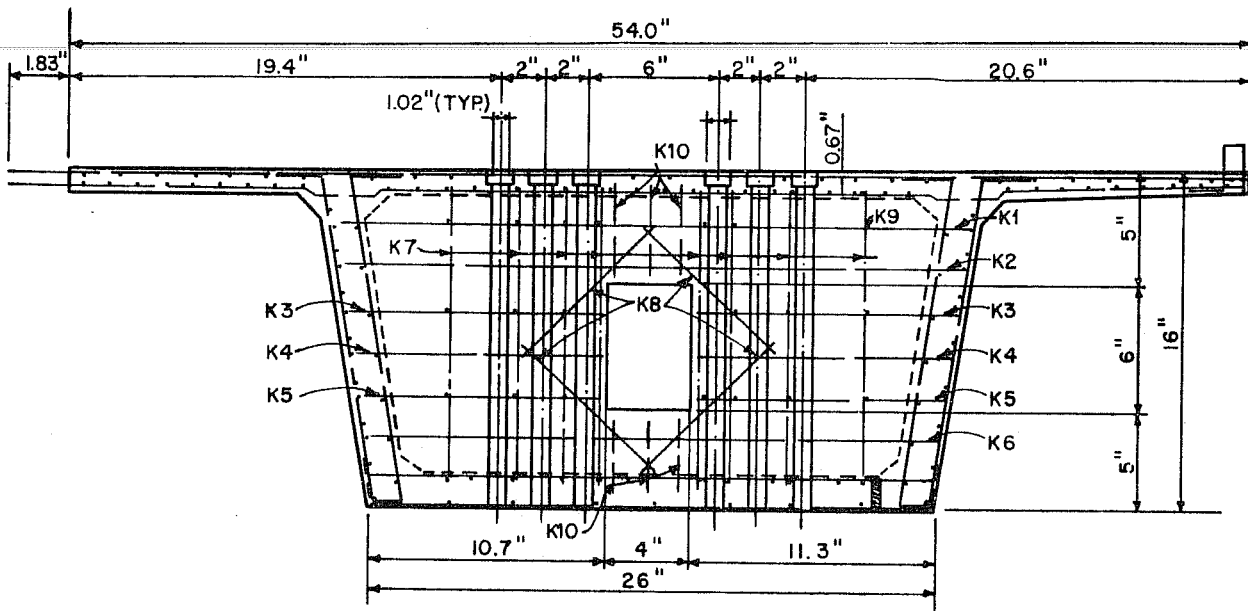
The reinforcement of the pier segments was modified according to the plans. Figure 4.5 shows the details as reduced for the model bridge.

#### 4.1.2 Anchorages

Since it was impossible to exactly scale the commercial tendons and anchorages used in the prototype, prestressing cables for the model were simply scaled by reducing the prestressing force and using an equivalent single cable. Therefore, normal strand chucks were selected as the basic anchorage device for the single cables. At the time of anchorage selection for the model, the prototype plans allowed the choice of bearing or wedge types of anchorage. For the model, the bearing type was chosen. The dimensions of the anchorage bearing plates were sized to satisfy the current ACI<sup>2</sup> and AASHTO<sup>6</sup> specification in a preparatory study.<sup>13</sup> The dimensions for the model are shown in Table 4.1. The commercial anchorage chuck was welded to the bearing plate as shown in Fig. 4.6. When double tendons were used at the first segments adjacent to the main piers, the area of the bearing plate was doubled and both commercial anchorages were welded to the same plate.

TABLE 4.1  
DIMENSION OF BEARING PLATE FOR THE MODEL BRIDGE

Cable	Bearing Plate (in. × in. × in.)	Bearing Stress at $0.8f'_s$ (psi)	Allowable $f_{cp}$ (psi)
3/8 in. Strands	1-1/2 × 1/4 × 3	4280	4390
7 mm Wire	1-1/2 × 1/4 × 2	4200	4410
1/4 in. Strands	1-1/2 × 1/4 × 1-1/2	3370	4390
6 ga. Wire	1-1/2 × 1/4 × 1-1/2	2700	4390



TYPE OF REINFORCING BAR	
K1, K2, K3	1/8 IN. WIRE
K4, K5	
K6, K8	
K7, K9, K10	12 GA. WIRE

TOP VIEW

Fig. 4.5. Modification for the main pier segment

\* (COMMERCIAL "SUPERIOR"  
SINGLE USE)

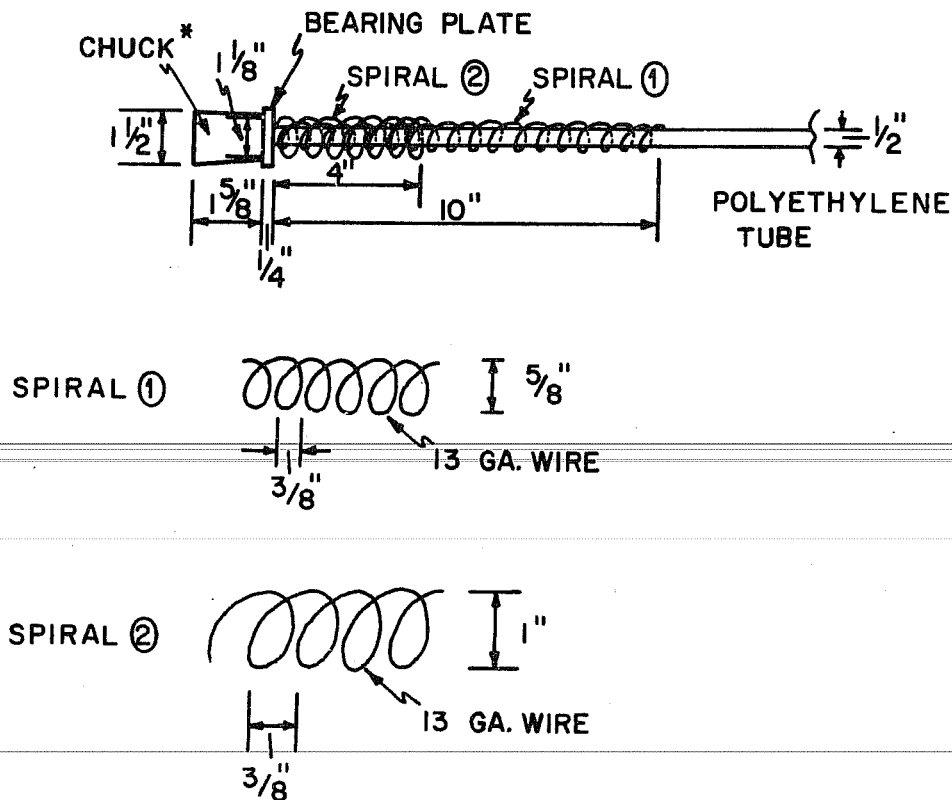


Fig. 4.6. Details of anchorage and spiral reinforcement

During preliminary tests, a tendency for splitting along the tendon was observed, which was restricted by use of a spiral. Even though the bearing plates for the model were correctly sized to be on the safe side and the curvature of tendon in the model was not as high as the one used in the preliminary tests, the use of the spiral was adopted as a guide line for better containment. Details of the spiral are shown in Fig. 4.6. Each duct and its spiral were always completely contained in the shear and transversed reinforcement cages.

### 4.1.3 Tendon Duct

Polyethelene tubes were used to form the ducts in the segments containing the duct anchorages, because of the large amount of curvature of the tendon duct in these sections. Steel tubes were used as duct formers in the other straight portions as shown in Fig. 4.7. Pipes for grouting holes were welded to steel pipe near the anchorage as shown in Fig. 4.7.

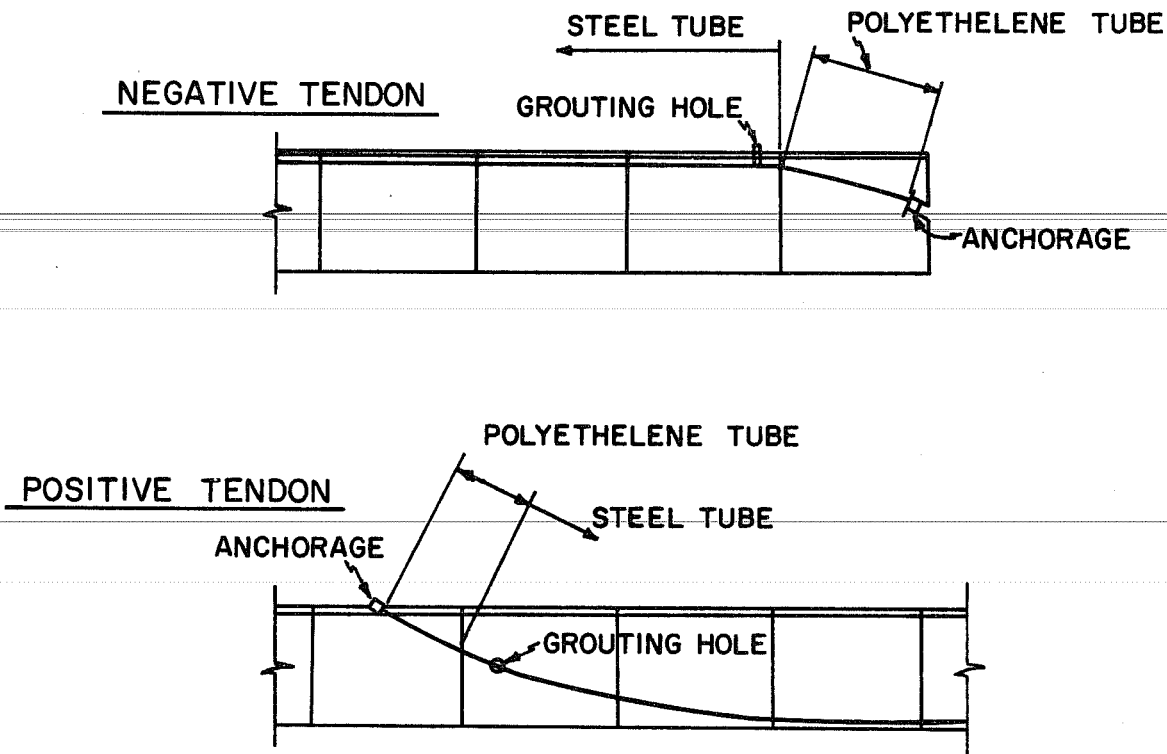


Fig. 4.7. Typical arrangement of tendon duct near anchorage

Two different sizes of ducts were used for each material, 7/16 in. diameter (I.D.) was used for 7 mm wire, 1/4 in. strands and 6 ga. wire and 9/16 in. diameter (I.D.) was used for the 3/8 in. strands.

Figures 4.8 and 4.9 show the profile of the tendon ducts in the main and side spans and Fig. 4.10 shows the detailed profiles of tendon ducts specified by the plans in the curved portions.

## 4.2 Forms

The accuracy of vertical and horizontal alignment of the segments is a very important factor to be considered at the time of casting. Also, it is very important to match the faces of precast segments exactly at the time of construction. Therefore, continuous soffit forms were used for the base form and segments were cast against the segment to which they were going to be joined at the time of construction. Two continuous soffit forms (half the length of the total span of the bridge) made of plywood (1/2 in. thick) were secured to the testing floor, as shown in Fig. 4.11. ~~These soffits were built straight (longitudinally) and level~~ within 1/16 in. accuracy.

Three materials (steel, plywood, and plexiglas) were considered for segment forms during the planning stage. Steel was abandoned at the beginning because of the high cost of construction. After several trial castings using plexiglas and plywood, stiffened plexiglas forms (1/4 in. thick) and plywood forms (1/2 in. thick) were used in combination, as shown in Fig. 4.12. Lacquer was coated on the surface of the plywood to simplify stripping and protect the surface for repeated use. Plywood is the cheapest material to use. However, it was realized that use of plexiglas was desirable for either the interior or exterior side forms in order to observe the flow of concrete in the webs so as to minimize honeycombing in congested areas around the anchorages. The bulkheads were made of plywood faced with plexiglas. These forms were set at the end of the segment and secured rigidly to the side forms with bolts. Figure 4.13 is a general view of the combined forms. All forms were stripped one day after casting. Bulkhead and outer sideforms were stripped first and then the inner top form [Form (3) in Fig. 4.12] was stripped by folding the joint at the center. Then the interior side forms were stripped. These forms were moved ahead as each segment was cast against the previous segment. Most segments were not separated



GRADUAL TRANSITION OF CURVATURE

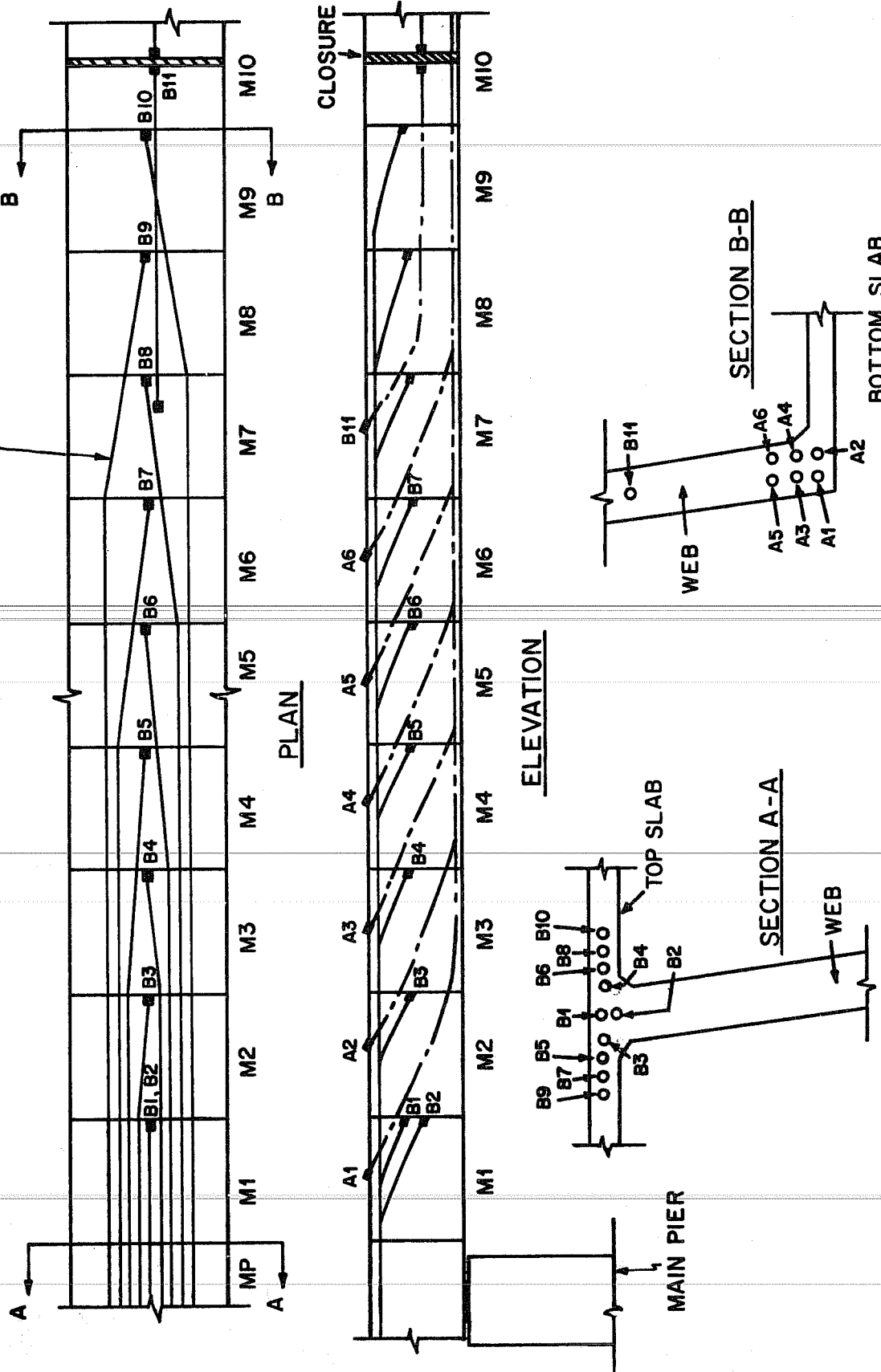


Fig. 4.8. Tendon duct profiles in main span

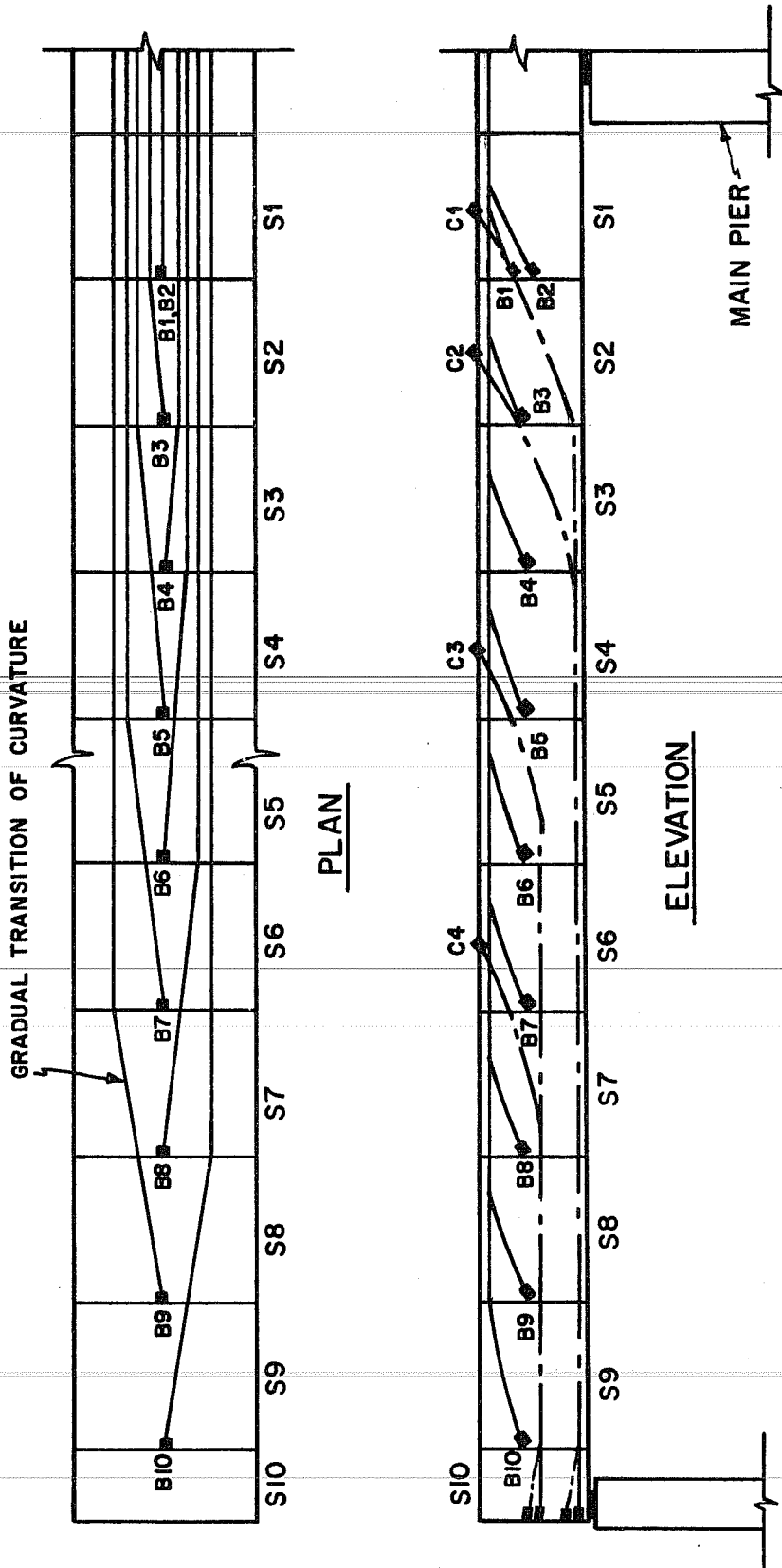


Fig. 4.9. Tendon duct profiles in side span

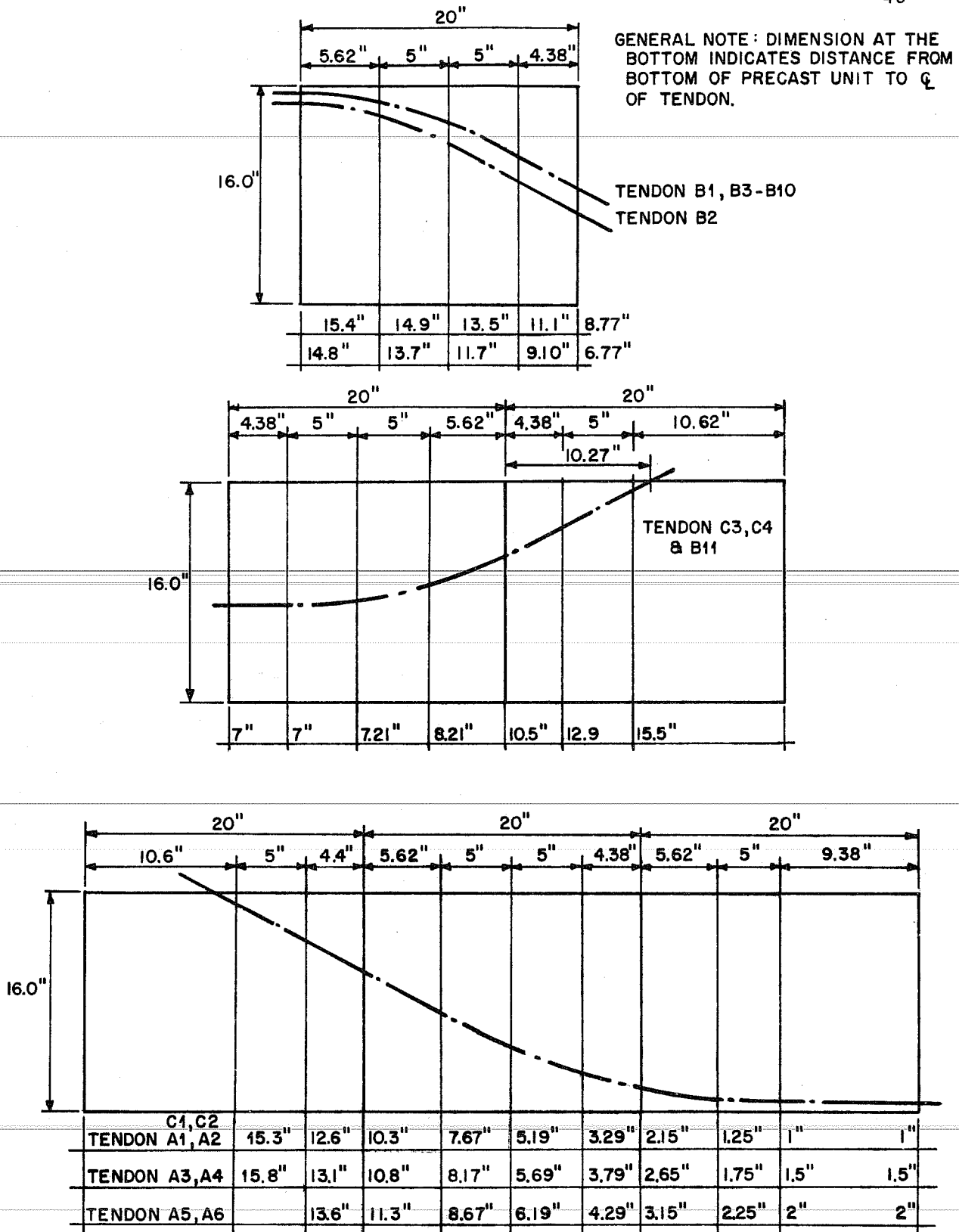


Fig. 4.10. Details of tendon profile specified by the plans

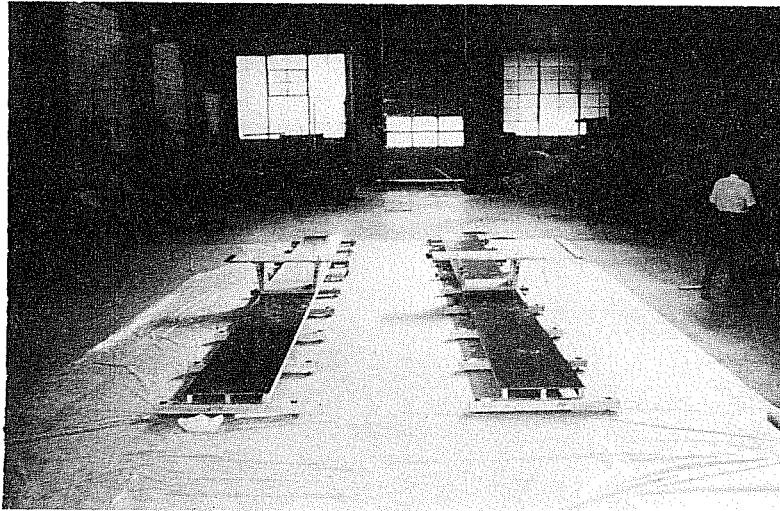


Fig. 4.11. General view of soffit forms

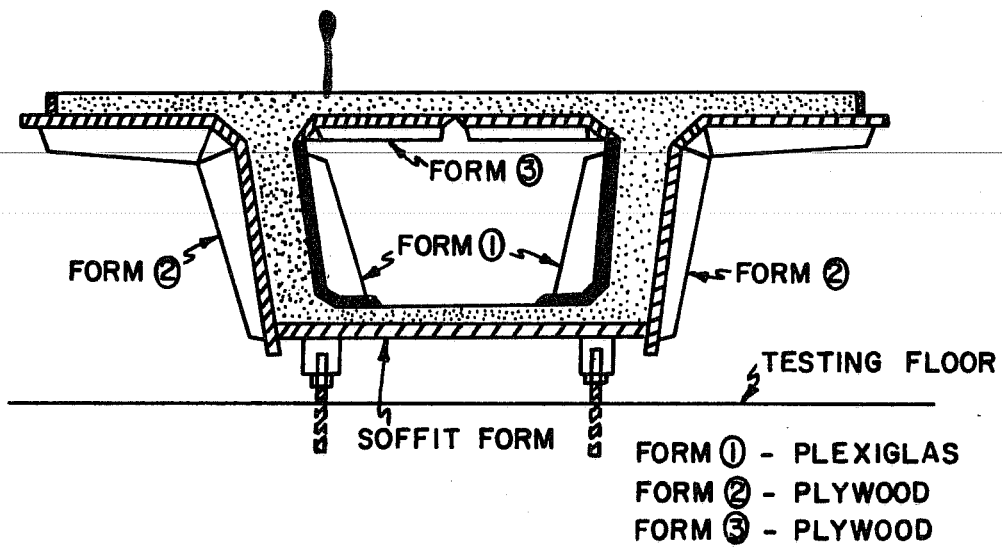


Fig. 4.12. Details of forms for segment

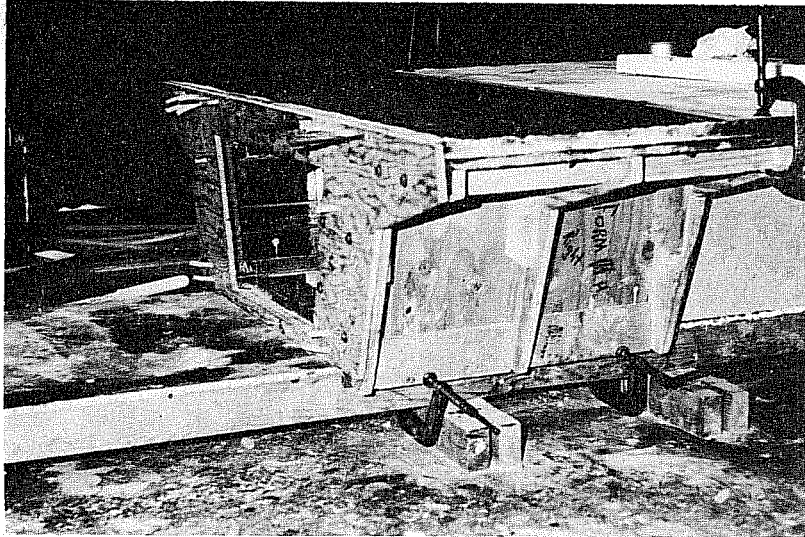


Fig. 4.13. General view of assembled forms

until all segments on the soffit were cast, in order to keep overall tolerances. A few segments were initially separated to check the effect of the bond-breaking compound.

#### 4.3 Strain Instrumentation in Cages

Since the main purpose of this study was to document the behavior of critical sections during various stages of construction as well as during the loading tests, strain gages were primarily placed in the first segments next to main piers and at the center of the main span.

Although it was possible to put strain gages directly on the wires of the cage, it was decided to put strain gages on separate 0.1 in.  $\phi$  - 10 in. lengths of wire and to connect these to the cages at certain positions because of the difficulty of protecting the gages during cage preparation and handling. This was done in order to save time and prevent damage to the gages during handling and casting. Strain gages were

positioned longitudinally underneath the top mat in the upper slab and on top of the bottom mat in the lower slab. Strain gages could not be successfully placed transversely on the cage to get the transverse behavior of the segments due to the difficulty of casting concrete in correct thickness. Paper gages were put transversely on the concrete surface of the segments at required positions before the loading tests.

Four types of gage installation patterns were used with the segments. The position of strain gages for each pattern and the instrumentation pattern used in each particular segment location is shown in Fig. 4.14.

#### 4.4 Casting Procedure

Usually 4 segments were cast per day, with 2 segments cast on each continuous soffit form. The order of casting for a continuous soffit form is shown in Fig. 4.15.

For the first segment, the two bulkheads were set at carefully determined distances. Subsequently the forms were moved ahead, and each segment was cast against the previously cast segment.

The preparation for casting segments after the first segments was as follows:

- (1) Remove all forms.
- (2) Clean the surface of previous segment and grind off the excess tendon duct. Also seal the anchorage holes of previous segment with styrofoam.
- (3) Clean all parts of forms and put on coating of lacquer.
- (4) Put bond breaking compound TBC (details in Sec. 3.3.2.1 (a)) on the outer face of the hardened segment one day before the next casting.
- (5) Set reinforcing cage on the soffit form adjacent to the previous segments.
- (6) Set chucks and polyethelene duct in curved portion, and set steel duct in straight portion.

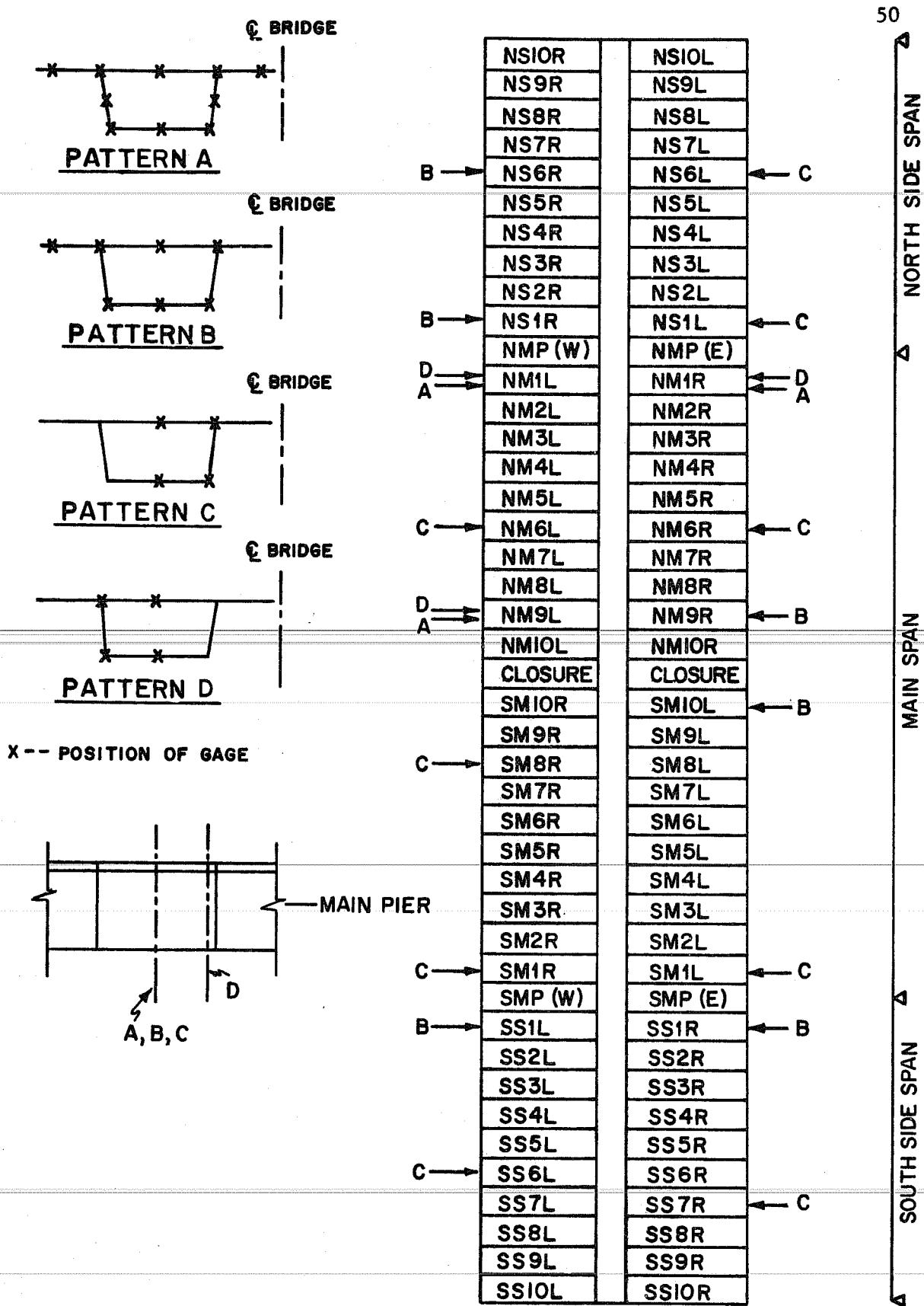


Fig. 4.14. Position of strain gages in segment

S10	S9	S8	S7	S6	S5	S4	S3	S2	S1	MP	M1	M2	M3	M4	M5	M6	M7	M8	M9	M10
10	9	8	7	6	5	4	3	2	1	11	1	2	3	4	5	6	7	8	9	10

Fig. 4.15. Sequence of casting segments

(7) Set bulkhead into position and adjust all tendons in the proper holes of the bulkhead. Tie the bulkhead to the bottom form.

(8) Put caulking compound along the joints of forms and set both inner and outer side forms into position. Set interior form for the top slab in position. All side forms have to be bolted to the bulkhead and soffit forms.

(9) Put polyethelene tube formers, used to hang dead load blocks, in the top and bottom slab, and place polyethelene tube formers in the bottom of webs for separation and temporary prestressing operation.

(10) Install bracing for interior side forms.

Web concrete was placed through the top of the web and filled from bottom to top and consolidated to eliminate any honeycomb effect. A vibrator was used carefully for this consolidation while the web was observed through the interior plexiglass form. Although many ways of vibrating the web concrete were tried, it was concluded that the most effective way was to vibrate directly on the cage of the top slab over the web. Before casting the web portion, blocks were set between the webs and the bottom slab to prevent the flow of concrete from the web portion to the bottom slab. The bottom slab was cast after completing the casting of the webs and then the blocks between the webs and bottom slab were removed. The top slab was cast last. After casting the entire portion, the top slab was coated with a membrane coating compound to prevent shrinkage cracks.

After completing all casting of 21 segments on a soffit form, each segment was separated by using four 4-ton rams. Figure 4.16 shows the position of rams. Although it would be possible to develop



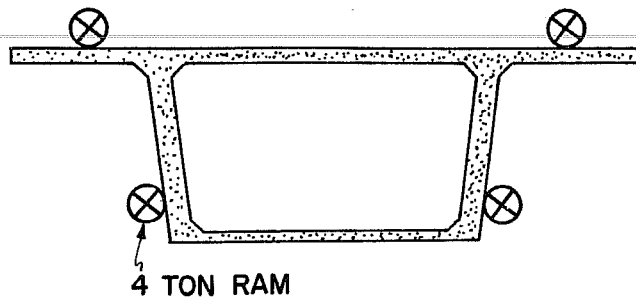


Fig. 4.16. Position of rams for separation of segment

the forces required to separate the segments by hand, rams were used. Equalization of ram forces minimized damage at the shear keys on the webs and the guide keys of the top and bottom slabs. In most cases, the force actually applied on each ram was less than 0.4 kips.

#### 4.5 Curing of Segments

Because the sequence used in casting and construction was the same, all segments except the pier segments were erected five to six months after casting. Pier segments were erected four months after casting. The segments were air cured in the laboratory and surface preparation was done at the same place. Segments were kept in the room (at  $75 \pm 3^{\circ}\text{F}$ ) until they were steam cleaned.

#### 4.6 Surface Preparation of Segments

Surface preparation of the joint faces is necessary to insure a good joint between segments. The order of surface preparation was as follows:

- (1) The segments were checked to make sure that the tendons did not extend beyond the joining surface of the segments.
- (2) Excess concrete and sealing material were taken out using a hand grinder (No. 4 in Fig. 4.17).
- (3) Grinding of the joint faces was accomplished using a small grinder connected to an electric drill (No. 3 in Fig. 4.17).

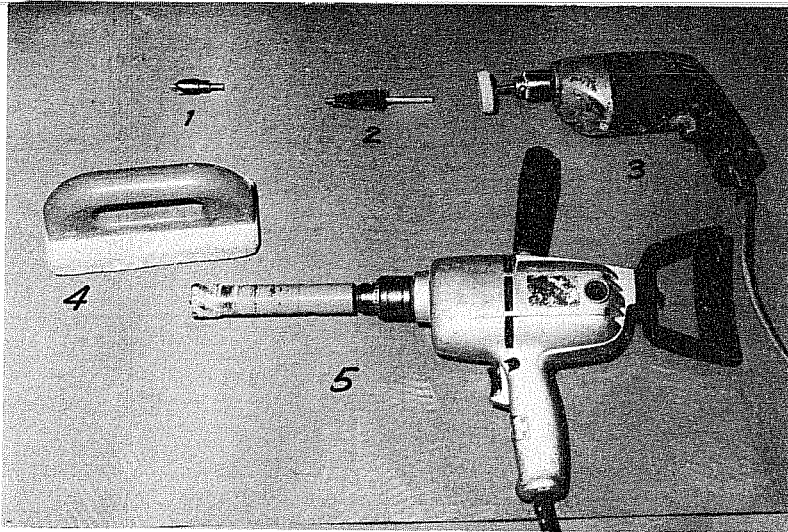


Fig. 4.17. Tools used for surface preparation

(4) The holes for the seating attachment at anchorage were enlarged by drilling using No. 5 shown in Fig. 4.17, if the jack seating attachment could not set on chuck body smoothly.

(5) Chucks were cleaned using a wire brush connected to an electric drill (No. 2 in Fig. 4.17).

(6) Segments were steam cleaned and rust was removed from chucks and steel ducts. Steam cleaning was used because it was found that form oil had been used on the bulkhead before casting for some of the first half of the segments. As shown in Sec. 3.3.2.1 (b), the effect of oil was eliminated by steam cleaning.

#### 4.7 Compensation Dead Load for Model Bridge

To satisfy similitude requirements, it is necessary that the density of a 1/6th scale model material be six times that of the prototype, in order to get the same dead load stress conditions as the prototype bridge.

Compensating dead loads have been added in various ways for model structures.<sup>1,11</sup> In this case, five times the weight of the model segment was added to the segments using concrete blocks as shown in Fig. 4.18.

All dead load blocks were distributed to represent the weight of each portion and to give reasonable transverse as well as longitudinal distribution. Two 140 lb. blocks were used for the top slab cantilever portions, 310 lb. blocks for the interior top slab and two 355 lb. blocks for the webs and bottom slab as shown in Fig. 4.18.

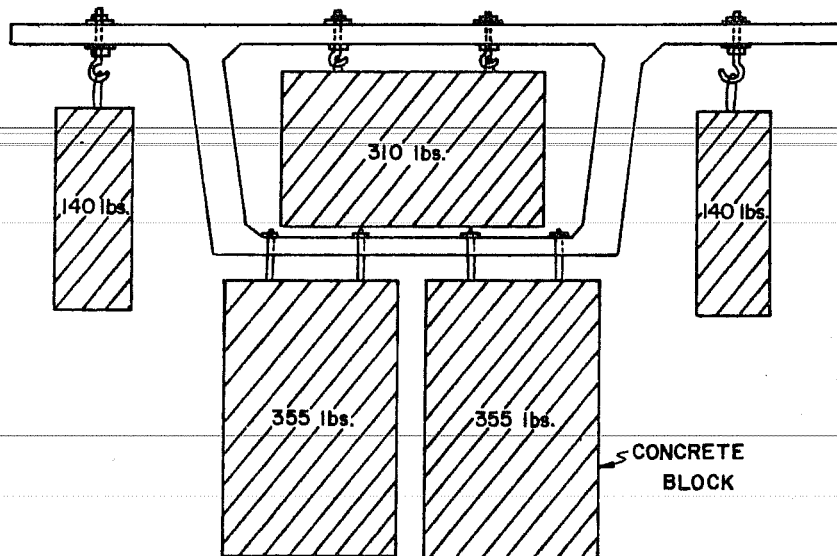


Fig. 4.18. Compensating dead loads for the model bridge

Four points were used to support the 310 and 355 lb. dead loads and two points were used for the 140 lb. blocks, since the additional dead weight could not be placed uniformly. The maximum weight on any loading point was less than 90 lbs., which closely simulate the uniform load.

Because of the heavier weight of the thicker slabs in the segments adjacent to the main piers, it was theoretically necessary to hang 70 lbs.



TABLE 4.2

MATERIAL PROPERTIES AND SECTION PROPERTIES OF THE MODEL BRIDGE

	HALF SECTION		FULL SECTION			
	MAX. SECT.	MIN. SECT.	MAX. SECT.	MIN. SECT.		
SECTION PROPERTIES OF BOX SECTION	AREA (IN. <sup>2</sup> )	179	165	363		
	DIST. FROM TOP TO CENTROID (IN.)	6.86	6.20	6.77		
	SECOND MOMENT OF AREA (IN. <sup>4</sup> )	6970	6060	14100		
	SECTION MODULUS AT TOP (IN. <sup>3</sup> )	1020	977	2090		
	SECTION MODULUS AT BOT. (IN. <sup>3</sup> )	752	611	1590		
PROPERTIES OF CONCRETE	$E_c = 4.56 \times 10^6 \text{ PSI } (\bar{s} = 0.37 \times 10^6 \text{ PSI})$ $f'_c = 7090 \text{ PSI } (\bar{s} = 523 \text{ PSI})$ $f'_{sp} = 597 \text{ PSI } (\bar{s} = 31 \text{ PSI})$ $u = 0.184 (\bar{s} = 0.016)$					
		REQUIRED	EXPERIMENTL.	EXPERIMENTL.		
		$0.6 F'_s$ (KIPS)	$F'_s$ (KIPS)	$f'_s$ (KSI)		
		A (IN. <sup>2</sup> )	$E_s$ (PSI)			
PROPERTIES OF PRESTRESSING CABLES	3/8 IN. STRANDS	13.75	22.1	0.085	259	$27.0 \times 10^6$
	7 MM. WIRE	8.94	15.3	0.0594	258	$30.5 \times 10^6$
	1/4 IN. STRANDS	5.46	9.16	0.0356	257	$27.0 \times 10^6$
	6 GA. WIRE	4.13	8.12	0.029	280	$30.9 \times 10^6$

## CHAPTER 5

### INSTRUMENTATION AND DATA REDUCTION

#### 5.1 General

Strain gages, dial gages, surveyor's level, load cells and pressure gages comprised the instrumentation used for the model study. Load cells and pressure gages were usually used to monitor forces for prestressing and loading. Details of these instruments are described in the following sections.

#### 5.2 Load Cells and Pressure Gages

Prestressing forces during construction and loads for the completed structure were applied by hydraulic rams connected to pumps by hoses. In addition to the calibrated hydraulic pressure gages, strain indicators connected to load cells indicated the amounts of forces applied. Primary control of forces was by the load cell indications. Pressure gages were used to approximately check the applied force because it was difficult to get accurate calibration of the pressure gages at the low range of loading.

#### 5.3 Strain Gage Instrumentation and Data Reduction

Two types of strain gages were used for the model bridge: Foil strain gages were used on the steel wires and paper gages were used on the surface of the concrete. Foil strain gages were mainly placed longitudinally in the cage (see Sec. 4.3) and paper gages transversely on the surface of the concrete.

Foil strain gages (1/4 in. long) were put on 0.1 in.  $\phi$   $\times$  10 in. long steel wire as shown in Fig. 5.1 (a). These strain gages were

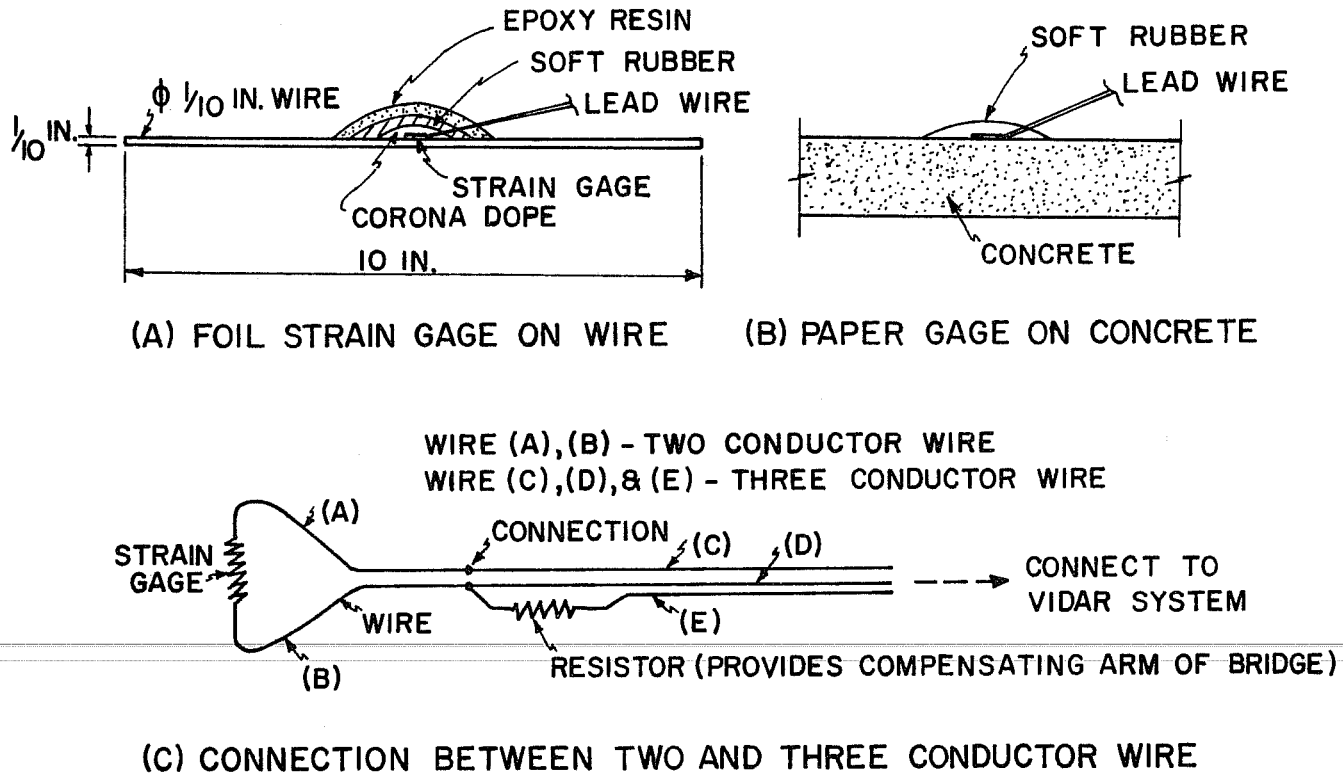


Fig. 5.1. Strain gage instrumentation

waterproofed and rarely failed even if they were kept in a segment more than one year. Paper gages (8/10 in. long) were put on the smooth surface of the concrete prior to loading tests (Fig. 5.1 (b)). Two short wires were connected to the strain gages in the segment. Then three conductor wires were connected to two conductor wires as shown in Fig. 5.1 (c). Because of the use of three conductor wires the affect of temperature change in wire was eliminated. These three conductor wires were connected to the VIDAR system.<sup>31</sup>

The VIDAR is a high grade digital volt meter which is able to read and range between 10 milivolt full scale (1 microvolt resolution) and 1000 volt full scale (100 milivolt resolution), and is connected to a high speed reed scanner. Output from the system can be either

teletype, punch paper tape or magnetic tape. Figure 5.2 shows the VIDAR system and teletype.

These outputs were put into permanent file in the computation center and were reduced by the data reduction program SPEED.<sup>8</sup> This was originally developed in the National Bureau of Standard and modified for the CDC system by the University. SPEED is composed of three segments for completion of data reduction. Those are described as follows:

PLOT 1: Coded data are converted to numbers with proper decimal point. This number has already taken into account variations in bridge voltage, temperature variations and multiplier (such as  $E_c$  to change from strain to stress) supplied by input.

Data are plotted by a line printer for each channel vs. one channel.

PLOT 2: Vector manipulation of data from PLOT 1 is done.

Data are plotted by line printer for any six channels vs. one independent channel.

PLOT 3: Data are plotted with CALCOMP plotter (i.e. film or paper). It can plot any 10 channels against one independent channel.

#### 5.4 Surveyor's Level and Dial Gages

A surveyor's level and dial gages were used to measure the deflection during construction and loading test. Accuracy of level reading was 0.01 in. and deflection errors of dial gage should be less than 0.0005 in.



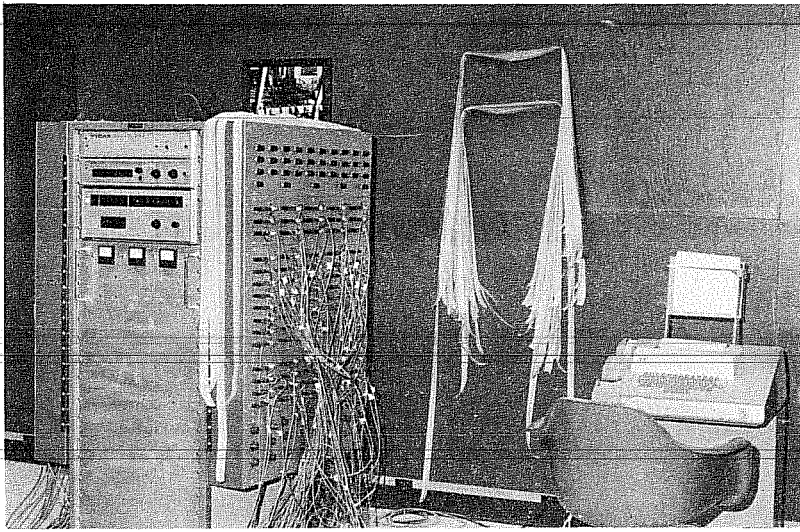


Fig. 5.2. VIDAR system and teletype

## CHAPTER 6

### CONSTRUCTION DETAILS

#### 6.1 Construction Procedure

##### 6.1.1 General

The following is an outline of the steps followed in the model bridge erection and closure:

- (1) Pier segments were temporarily fixed to the piers using bolts tightened to a predetermined torque.
- (2) The precast segments were sequentially erected using the cantilever construction scheme with epoxy joints.
- (3) Vertical and horizontal alignment was adjusted after completion of the erection of precast segments 1 through 9.
- (4) The outer pier segments (S10) were erected and the positive moment tendons in the side spans were prestressed.
- (5) The half segments (M10) in the main span were erected. The longitudinal reinforcement extending across the midspan gap from each of the half segments was joined and the concrete closure segment was cast.
- (6) The positive tendons in the main span were inserted and prestressed after 7 days of curing of the closure segment. The bolts used for the temporary fixing of the segments to the main piers were released during the positive tendon stressing operation.
- (7) The bridge was lowered to final position on neoprene pads on the piers.
- (8) The correct reactions were jacked into the outer piers.

##### 6.1.2 Construction of Piers

Because the pier height of the prototype bridge was 90 ft. and complete pier similitude was not a requirement of the study, the full

height of the pier was not scaled in the model. The reduced pier height for the model bridge was set at 55 in. to allow adequate space below the model for insertion of compensating dead load blocks. However the general cross section of the prototype piers (see Appendix A) was used at 1/6th-scale. Figure 6.1 shows the reinforcing bars for an inner pier model. The piers were carefully set in correct position prior to casting of concrete. In order to prevent overturning of the piers under unbalanced loading, I-beams were welded to the pier base and tied down to the testing floor using 1 in. diameter bolts as shown in Fig. 6.2.

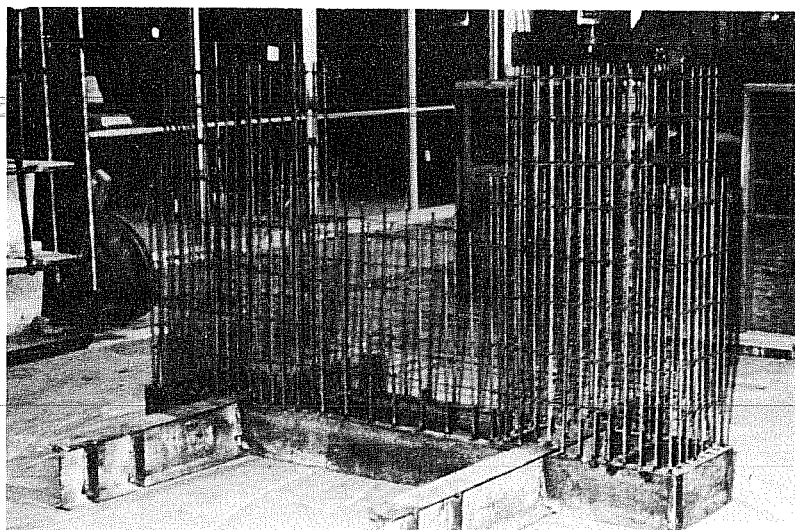


Fig. 6.1. Reinforcement of the main pier

The completed pier with the bolts for temporary connection of pier segments and the neoprene pads for final bearing is shown in Fig. 6.3. The bolts and neoprene pads were scaled down to 1/6th actual size. The diameter of the bolts in the model was 1/2 in. and the size of the neoprene pad was  $4\text{-}1/6 \times 7 \times 1/4$  in. Dimensions of the bearing plates used to restrain or support the pier segments at the top and bottom faces for each 6-bolt group were  $4 \times 6 \times 1/2$  in.

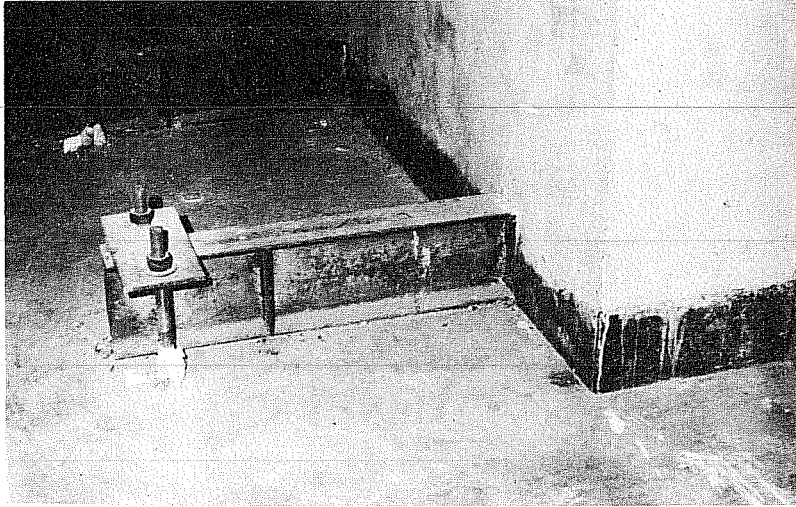


Fig. 6.2. Connection of pier to the testing floor

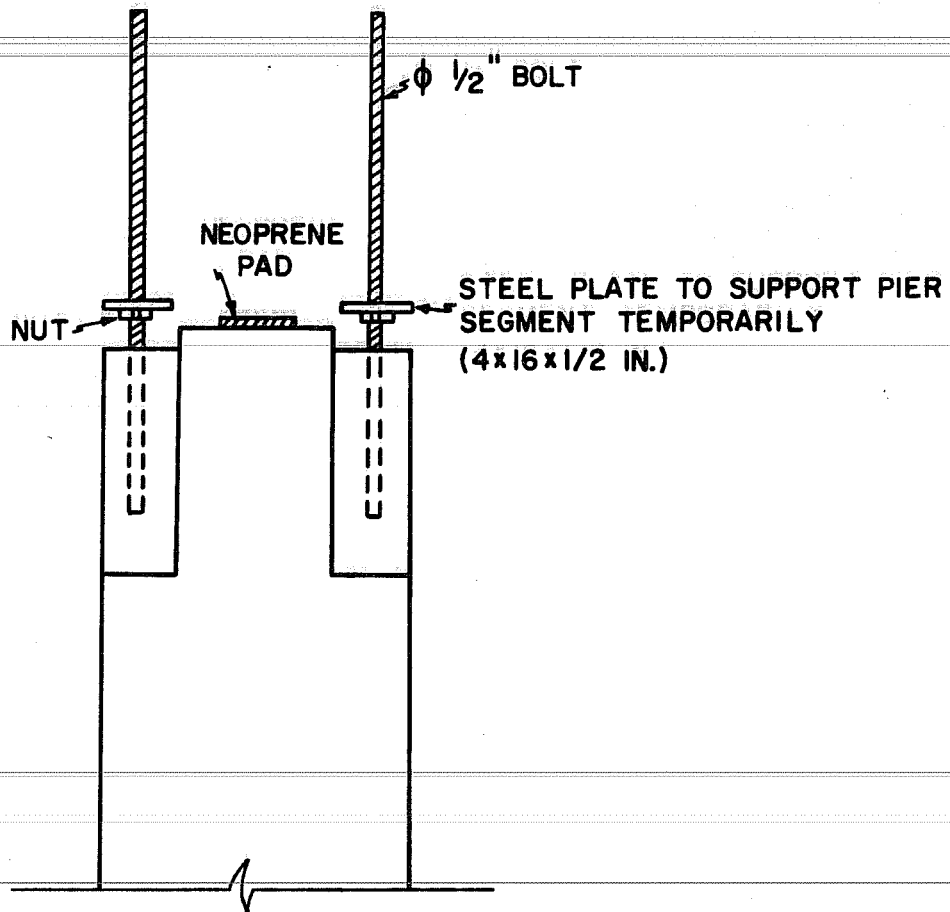


Fig. 6.3. Detail of support at main pier

### 6.1.3 Erection of Pier Segments

It is very important to set the horizontal and vertical alignment of the pier segments as correctly as possible in order to minimize adjustments of the two separate cantilever sections prior to the closure operation. Adjustment of the vertical alignment was made prior to setting the pier segment by turning the nuts under the steel plates as shown in Fig. 6.3. For erection of the first half of the box girder bridge, the horizontal alignment of the pier segments was judged by eye and was later considered inaccurate. In erection of the second half, the horizontal alignment of each pier segment was carefully adjusted using a positive reference line formed by a piano wire stretched between each pier segment. The mechanism for anchoring each pier segment consisted of 12-1/2 in. diameter bolts and 1/2 in. thick steel bearing plates. The pipes which formed vertical ducts in the pier segments to pass over the 1/2 in. diameter bolts had a 1 in. inner diameter, so that there was adequate play to allow adjustment of the horizontal alignment. After initial alignment of the pier segments, the anchor bolts were tensioned to approximately 1 kip each using a torque wrench. The gap between the segment and the neoprene pad on the main pier was set to 1/4 in. for the first half of the bridge. However, a gap of 3/4 in. had to be used for the second half to minimize later vertical adjustment in order to match the first half of the bridge. Figure 6.4 shows the general view of the pier segment on the pier.

### 6.1.4 Erection of Segments during the Cantilever Stages

#### 6.1.4.1 General

Possible erection methods for precast concrete cantilever construction over water may be classified as follows:<sup>24</sup>

- (1) Segments floated in on barges with barge-mounted crane erection.
- (2) Segments floated in on barges but erection using lifting equipment supported on the previously erected cantilever segments.
- (3) Transportation of segments on the structure itself with a large launching gantry used to place segments.

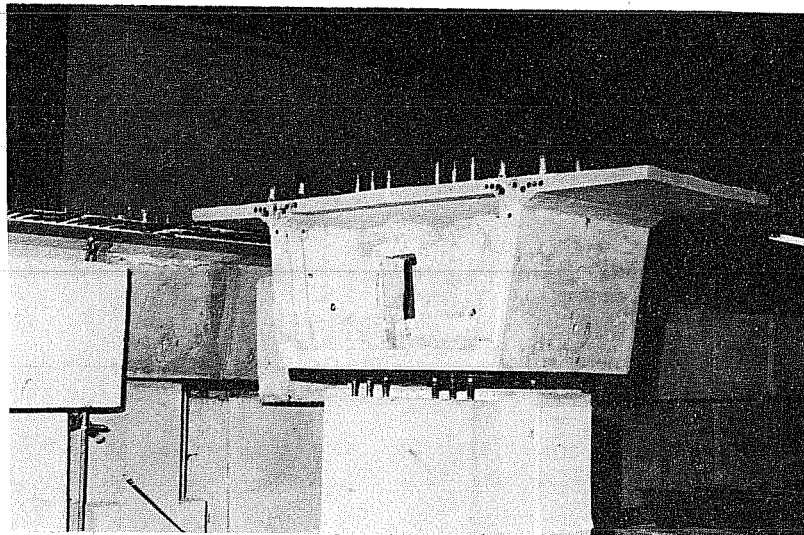
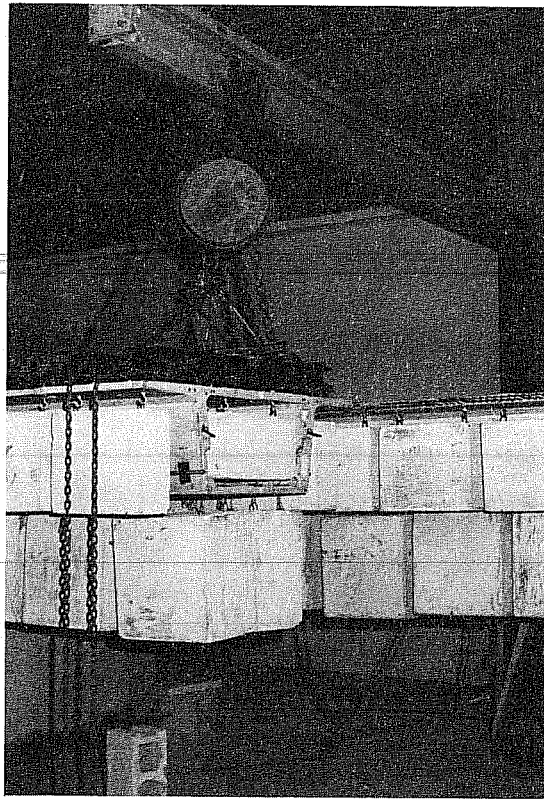


Fig. 6.4. General view of the pier segment on the main pier

The cost of erection equipment for method (3) was considered too expensive and not necessary for the prototype bridge. Erection methods (1) and (2) were both considered practical for this prototype. Since in the initial planning contractors would have an option for either method, both were simulated in the model bridge erection. During the majority of the model bridge erection, segments were lifted by various overhead cranes, as shown in Fig. 6.5. These cranes were not supported on previously erected segments. The units were connected temporarily by mechanical devices (Fig. 6.6) to ensure correct seating and were then prestressed. This mechanical device was intended to prevent any movement at the joint until stressing started and could not affect the prestressing force applied by the cables. However, in a number of cases, lifting equipment simulating light cranes supported on the previously erected cantilever structure was used (Fig. 6.7). The weight of a crane was about 370 lbs. (13.3 kips in the prototype).



**Fig. 6.5. Typical independent crane used for erection of segments**

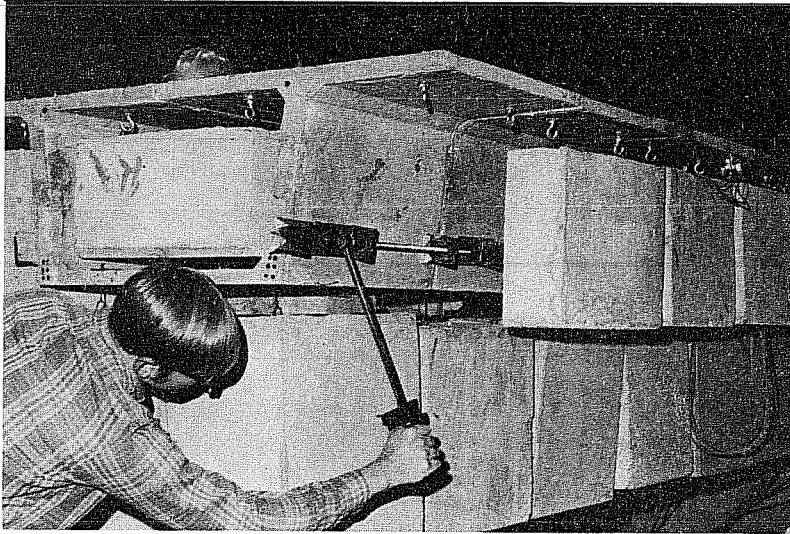


Fig. 6.6. Mechanical device for temporary joining

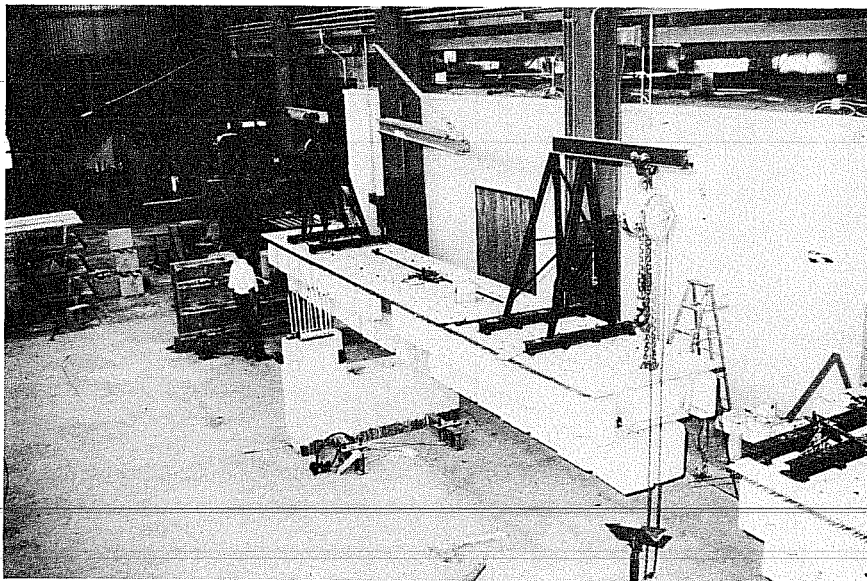


Fig. 6.7. Typical structure supported crane used in some cases



#### 6.1.4.2 Details of Segment Erection

Two segments were usually erected per day. However, it was not difficult to erect four segments per day with proper preparation and adequate labor availability. All erection work was done in the afternoon to minimize the effect of temperature change on instrumentation. Temperature and humidity during the time of erection varied between 75 - 90°F and 50 - 70% RH respectively.

Details of the erection procedure were as follows:

(1) Lead wires of any implanted strain gages in the unit to be erected were connected to the VIDAR system.

(2) Two wide flanges (4 × 4 × 50 in.) were connected to the bolts used to support the dead load blocks which pierced the top slab of each segment, as shown in Fig. 6.5.

(3) Preweighed epoxy resin and hardener sufficient for joining two segments was mixed.

(4) Prestressing wire or strands were inserted in the straight portion of the tendon ducts (Stage 1 in Fig. 6.8).

(5) Segment (A) was lifted, the height adjusted and leveled by turn buckles as shown in Fig. 6.9 (Stage 2 in Fig. 6.8).

(6) Segment (A) was separated after this adjustment. The joining surfaces were cleaned with acetone and the epoxy resin was spread on both joining surfaces as shown in Fig. 6.10.

(7) Segment (A) was clamped temporarily near the lower flange as shown in Fig. 6.6 and also at the top of the segments (Stage 3 in Fig. 6.8). The force applied on the mechanical clamping devices was approximately 1 kip each and was checked with a torque wrench. Lead wires connected to the prestressing cable were pulled South until the end of the prestressing wire at the far end reached the end of the straight portion. Lead wires were not necessary for the strands as they could be pushed through by hand.

(8) Same as (5) for Segment (B).

(9) Same as (6) for Segment (B).

(10) Segment (B) was joined temporarily. The lead wire was pulled North until the prestressing cable was extended just enough for seating (Stage 4 in Fig. 6.8).

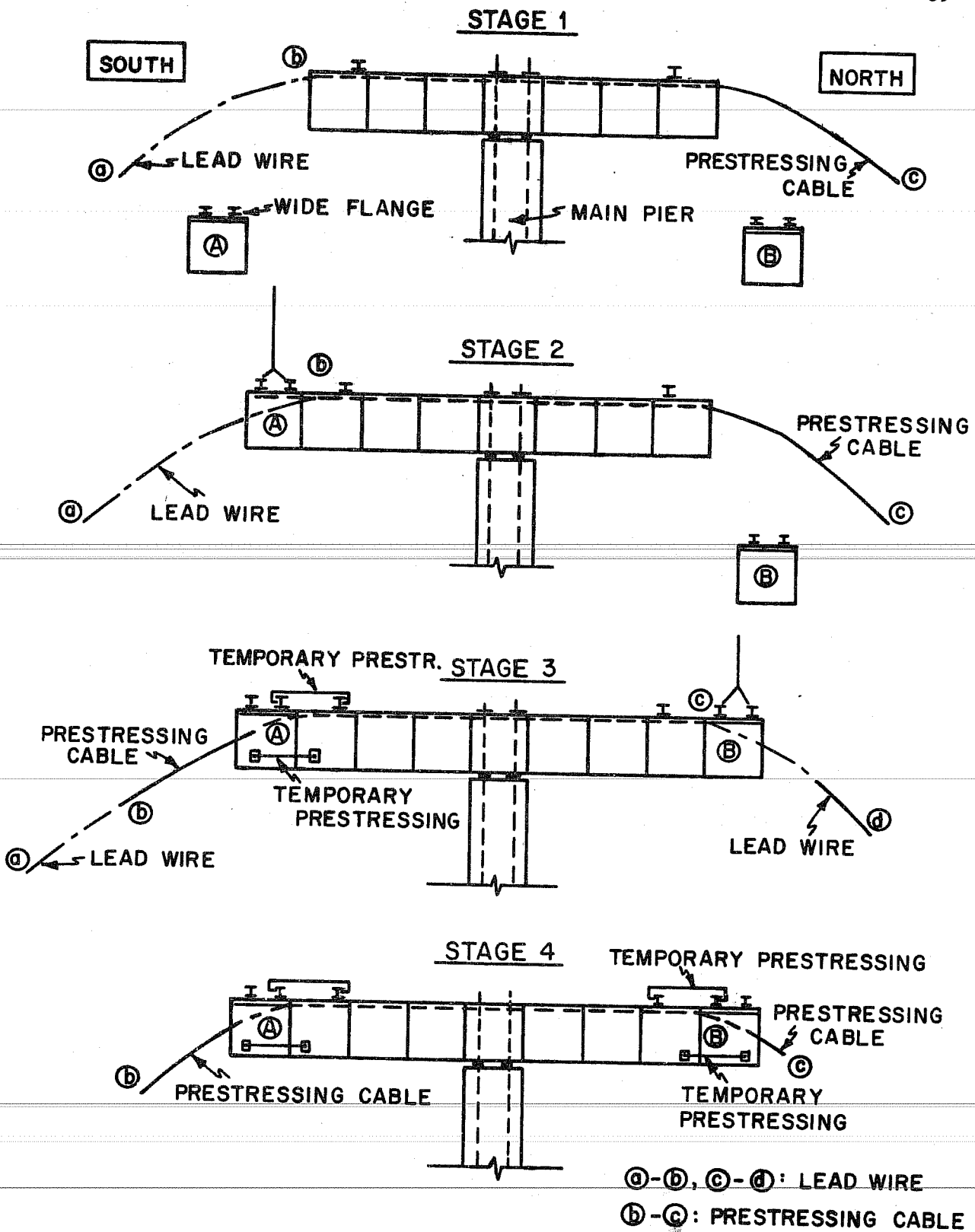


Fig. 6.8. Insertion of prestressing cable

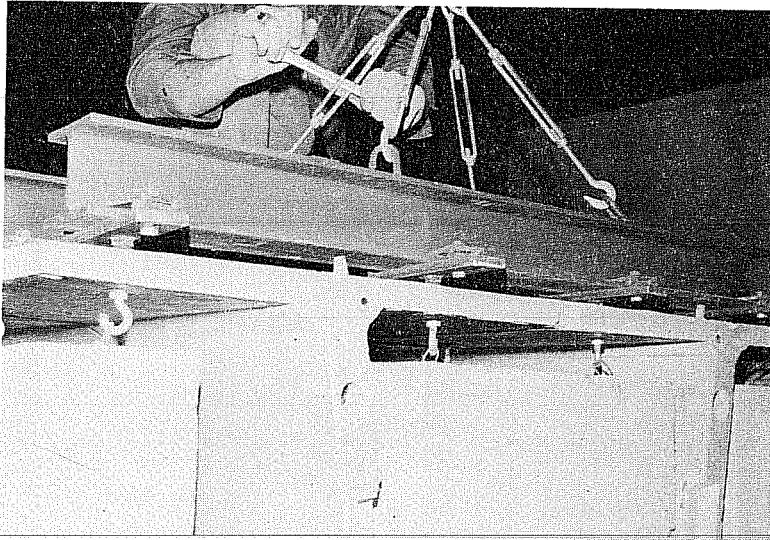


Fig. 6.9. Adjustment of level

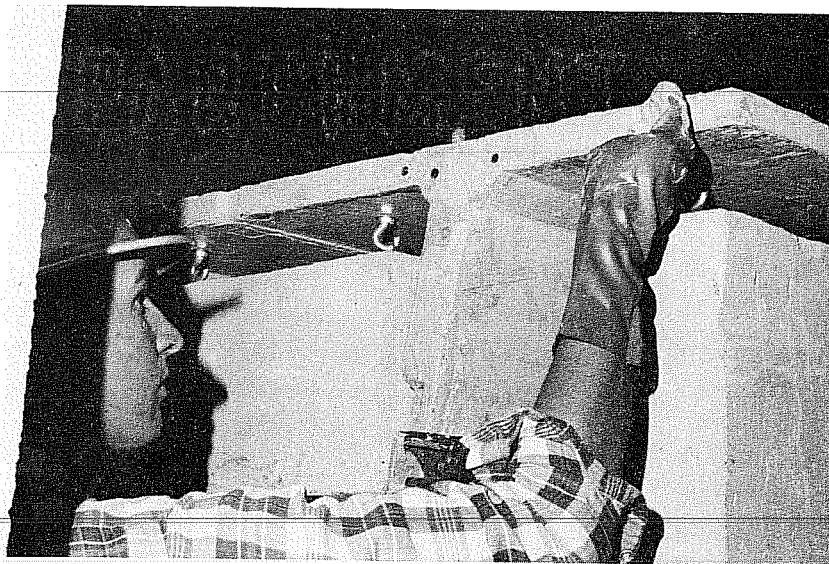


Fig. 6.10. Application of the epoxy resin on the joining surface

(11) The prestressing equipment was set on one end (Fig. 6.11). Details of the prestressing system are shown in Fig. 6.12. Prestressing force was applied using 30 ton hydraulic rams. The amount of force applied was controlled by a load cell. In addition, the prestressing force applied was checked approximately with a pump pressure gage. Elongation of the prestressing tendon was measured using a steel tape.

(12) A prestressing force of  $0.8f'_g$  was applied in order to overcome the friction loss and then was dropped to  $0.65f'_g$  for seating. The addition of  $0.05f'_g$  to the specified  $0.60f'_g$  was to compensate for seating loss, as found in the preliminary tests. Although the prestressing operations must be performed at both ends in the prototype, prestressing force was applied only from one end for the model because of the shorter work involved. However, prestressing operations were done alternatively at each end. Friction loss tests were performed at various stages, as reported in Sec. 6.2.2.

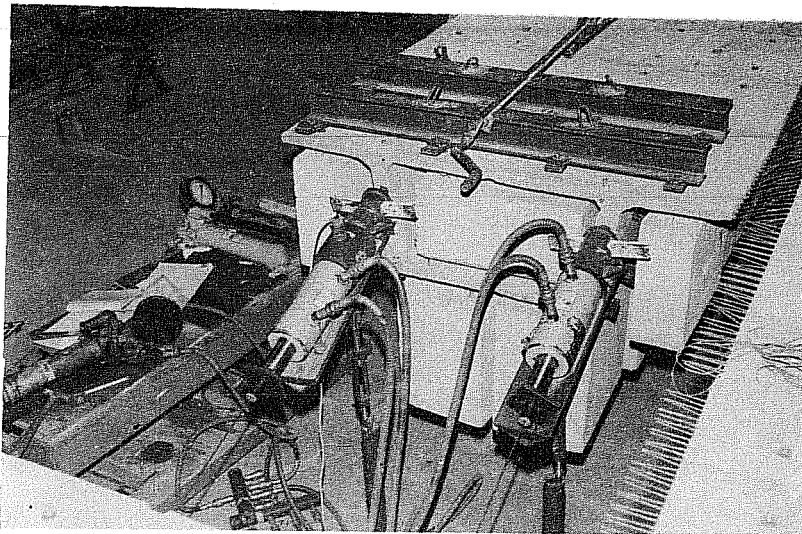
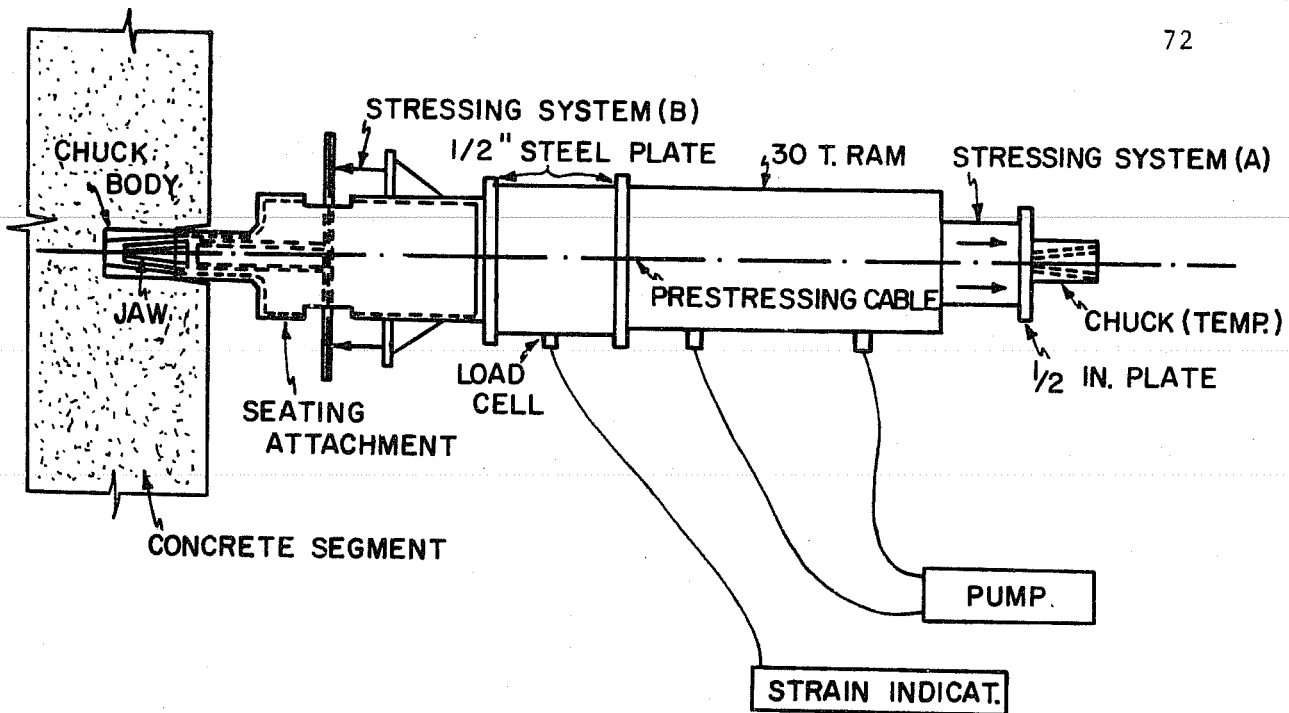


Fig. 6.11. General view of prestressing system for negative tendons

(13) Excess prestressing wire or strands protruding from anchors were cut with an electric grinder after seating of the jaws into the chuck



### PRESTRESSING PROCEDURES:

- (1) INSERT PRESTRESSING CABLE.
- (2) PUT JAW INTO CHUCK BODY.
- (3) SET SEATING ATTACHMENT, LOAD CELL AND 30 TON RAM.
- (4) INSERT TEMPORARY CHUCK AT THE END OF RAM AND HOLD IN POSITION.
- (5) EXTEND STRESSING SYSTEM (A) UNTIL  $0.8 f_s'$  IS REACHED IN PRESTRESSING CABLE.
- (6) DROP THE PRESTRESSING FORCE FROM  $0.8 f_s'$  TO  $0.65 f_s'$ .
- (7) SET SMALL RAMS AT STRESSING SYSTEM (B) AND APPLY 2 TO 3 KIPS OF LOAD TO PUSH THE JAWS INTO CHUCK BODY IN ORDER TO SEAT THE PRESTRESSING CABLE. RELEASE SYSTEM (B).
- (8) RELEASE SYSTEM (A), AND REMOVE SEATING ATTACHMENT, LOAD CELL AND 30 TON RAM.

Fig. 6.12. Details of prestressing system

bodies. Anchorage holes were filled with epoxy mortar ((Epoxy Resin): (Sand + Aggregate) = 1:1). These surfaces were ground smooth on the next day.

### 6.1.5 Correction of Horizontal and Vertical Alignment

Correction of horizontal and vertical alignment was performed after the 9th segment out from each pier was erected because the balanced cantilever sections were still symmetrical and easy to adjust.

The following are the correction procedure steps used:

(a) Horizontal Alignment. There are two possible errors in horizontal alignment which may occur in precast segmental cantilever construction (twin boxes construction) as shown in Fig. 6.13. Points a, b, c and d in Fig. 6.13 are the center points of the pier segments.

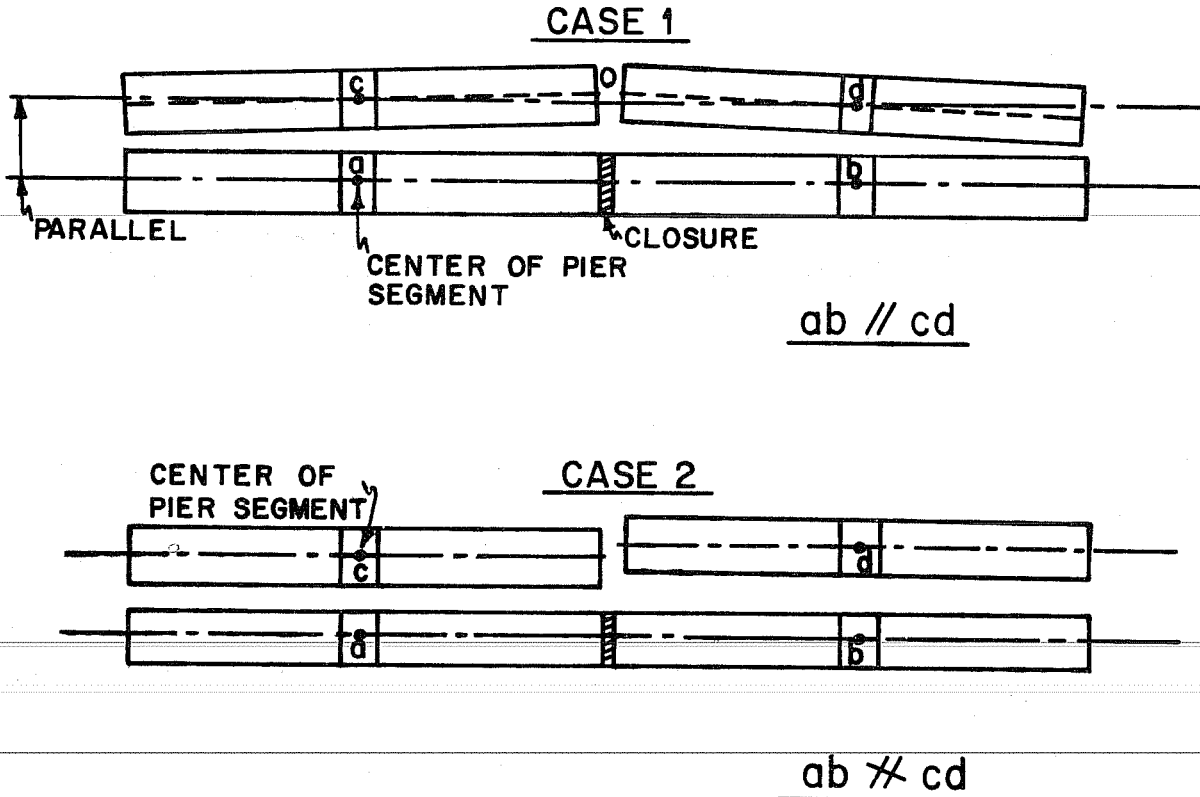


Fig. 6.13. Errors of horizontal alignment

In case (1), lines ab and cd are parallel, but the cantilever sections co and do extending from piers c and d are not in correct horizontal alignment.

In case (2), piers are not carefully cast and the distance between ac and bd are not equal so that ab and cd are not parallel.

Since the anchor bolts in the piers were carefully set in the correct position prior to casting, there was no error of the case (2) type in the model bridge construction.

During the construction of the second half, a piano wire was stretched between the points c and d (in Fig. 6.13) in order to provide a base line for the two sections. This provided much finer alignment. There was about  $3/4$  in. of correction required at the closure of the two cantilever sections during erection of the first half of the bridge, but less than  $1/4$  in. for the second half of the bridge.

Each cantilever section was adjusted after erection of nine segments so that the center line of each cantilever tip would meet on the base line. In order to adjust the cantilever sections with equipment which could be practically scaled up for the prototype construction, a small channel was connected at the web of the 8th and 9th segments and was pulled by a ratchet hoist whose base was connected to the end pier, as shown in Fig. 6.14. The maximum capacity of the ratchet hoist in the model was 4 kips.

(b) Vertical Alignment. There are three possible errors in vertical alignment at the closure of the two cantilever sections.

They are:

- (1) Error due to incorrect adjustment of the nuts underneath and supporting the pier segments.
- (2) Error due to variation in height of the soffit at the time of casting.
- (3) Error in joint widths at the time of cantilever erection.

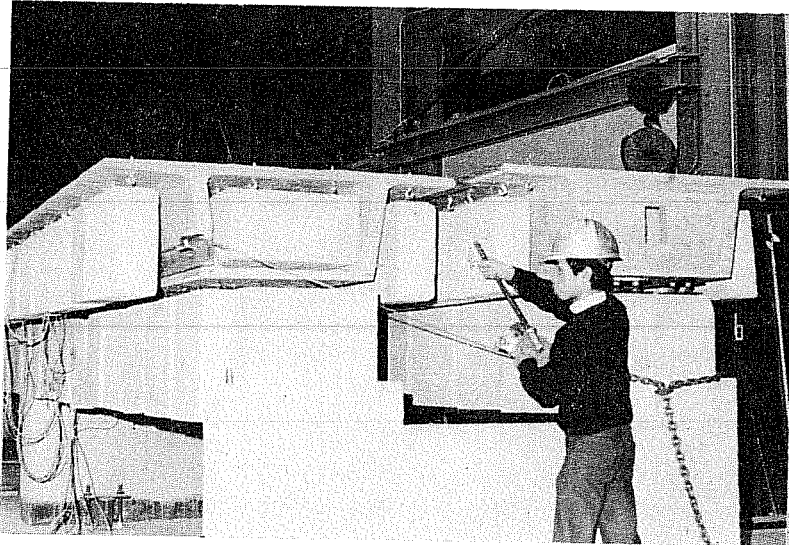
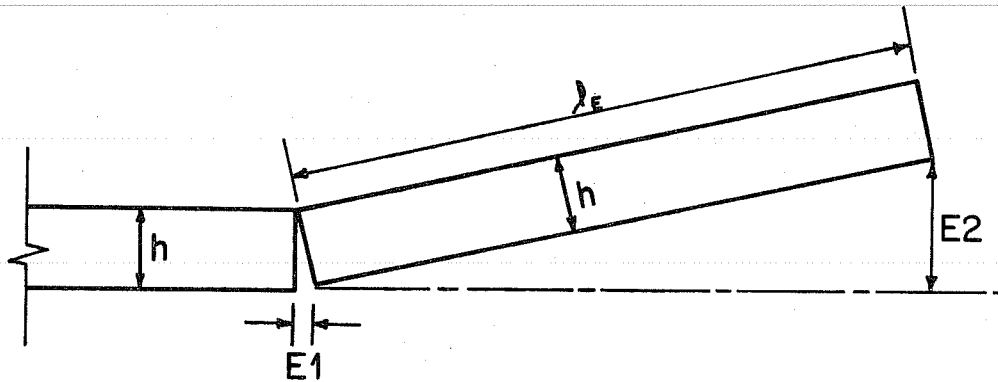


Fig. 6.14. Adjustment of horizontal alignment

It had been predicted in the design<sup>16</sup> that a small tensile stress would occur on the bottom fiber at a distance of 30 in. from the pier center (at the joint between 1st and 2nd cantilevered segments), when the cantilever arm length is 50 in. and 70 in. In the erection of the first half of the bridge there were definitely joining errors because the temporary prestressing system at the bottom of the segment was not used to carry these tensile forces during erection of the first several segments. Design procedures should ensure that there is no tension at the bottom of any joints during the cantilever erection. There were also other probable minor errors due to faulty joining work in the first half of the box girder bridge before crew experience was obtained. There were also some probable errors due to variation in the height of soffit in the first and second half of the model bridge. Therefore, substantial vertical adjustment had to be done at the end of the cantilever erection.

Jointing errors in the early stages of cantilever erection accumulate and are magnified at the end of the cantilever, as shown in Fig. 6.15.





$$E2 = \frac{\lambda_E}{h} \times E1$$

where,

$h$  = Depth of segment

$\lambda_E$  = Distance from the joint with the erection error

$E1$  = Thickness of error in joint at bottom

$E2$  = Accumulated error in height at the distance  $\lambda_E$

Fig. 6.15. Accumulation of joining error

Although the second half of the bridge was constructed with little error, adjustment of vertical alignment was necessary to minimize the deviation of the top slab at the midstrip closure with the previously constructed portion of the bridge.

For example, in order to correct the vertical alignment the nuts at D were released slightly and about 600 lbs. of unbalanced weight was put on the top of the M9 segment. The nuts at B in Fig. 6.16 were then backed down in small increments. If the nuts at B (13

threads per inch) were turned down one turn, then the end of the S9 segment was dropped 1-1/4 in. ( $(1/13) \times (196/12)$ ).

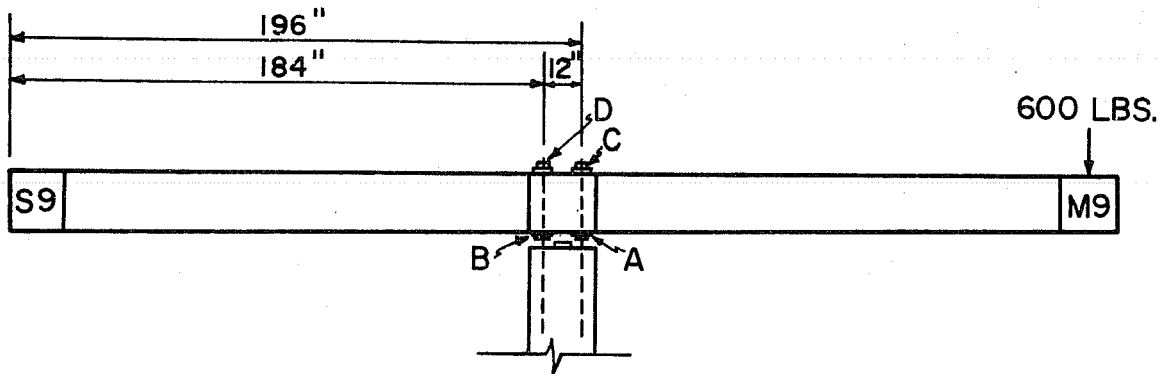


Fig. 6.16. Correction of the vertical alignment

In the erection of the first half of the bridge, the two cantilever sections were adjusted to the correct vertical alignment prior to the closure operation, but were not lowered to the neoprene pads until after the positive tendons had been stressed. However, for the second half of the bridge, the two cantilever sections were separately lowered to their final position on shims on the neoprene pads prior to the closure operation. It was easier to lower the balanced sections onto the neoprene pads prior to the closure operation and it simplified the positive tendon operation. All lowering was done by unbalancing the overhangs and backing the plate support nuts down in small increments.

#### 6.1.6 Casting of the Closure Segment

After adjusting the vertical and horizontal alignments, the half segments with diaphragms were erected over the end piers and the positive tendons in the side span were prestressed (details are in Sec. 6.1.7). Half segments (8.5 in. long) were erected for each cantilever in the main span, and the overlapping reinforcement extending from each half segment was joined by tie wires. In addition, the tendon ducts extending from each midspan half segment were connected by polyethelene

tubes at the closure and sealed by epoxy resin as shown in Fig. 6.17. The positive tendons for the main span were inserted immediately after the above operation was completed.

Figure 6.18 shows the simulation of the closure prior to the construction of the half segments. Since there was no space to work inside the segments, interior side and top slab forms were set in place prior to joining the reinforcement at the closure and the top slab forms were supported using the holes made for dead load blocks. Plexiglas windows were provided in the bottom of the exterior side forms, in order to observe any tendency for honeycombing around the tendon ducts. Also temporary bracing channels were rigidly attached to the top and bottom slabs of the half segments, as shown in Fig. 6.18. These channels were intended to provide temporary flexural stiffness across the closure equivalent to half of the flexural stiffness of the finished concrete box section at the closure until the concrete had cured.

In order to cast concrete in bottom slab at the closure, the concrete was placed through the gap between the top slabs and vibrated from outside the bottom form. The form for the top slab was then set in place prior to casting the web and top slab. Concrete in the closure was cured for a week until the positive tendon stressing operation was performed.

#### 6.1.7 Prestressing of the Positive Tendons

In order to minimize the effects of the secondary moments due to prestressing which occur in indeterminate structures, the prestressing operation for the positive moment tendons in the side spans was completed prior to the closure operation. The C3 and C4 tendons as shown in Fig. 2.3 were also intended to prevent tensile cracking in the top slab due to prestressing of the C1 and C2 tendons. The order of the prestressing operation was tendons C4, C3, C2 and C1 as designated in Fig. 2.3. All tendons were prestressed from the anchorages in the top slab as shown in Fig. 6.19. Details of the prestressing equipment were the same as reported in Sec. 6.1.4.2.

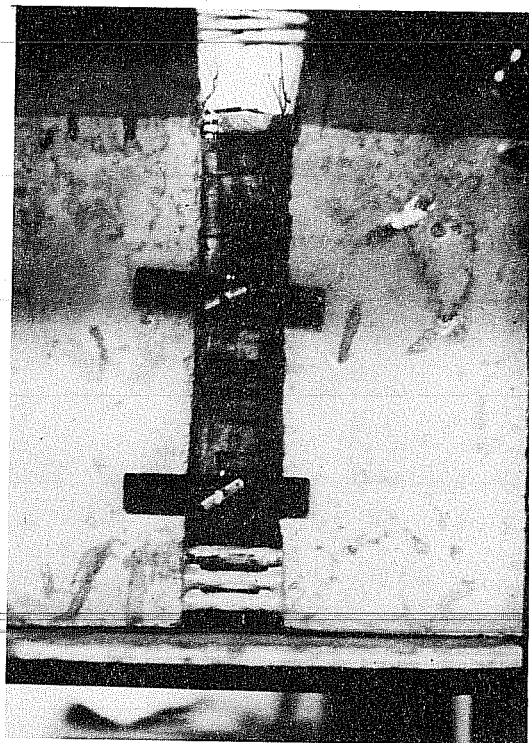


Fig. 6.17. Connection of tendon duct at the closure

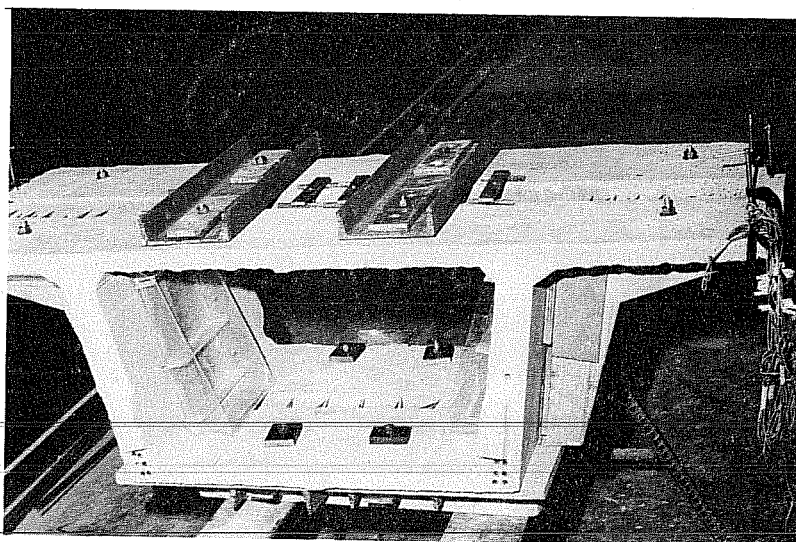


Fig. 6.18. Simulation of the closure

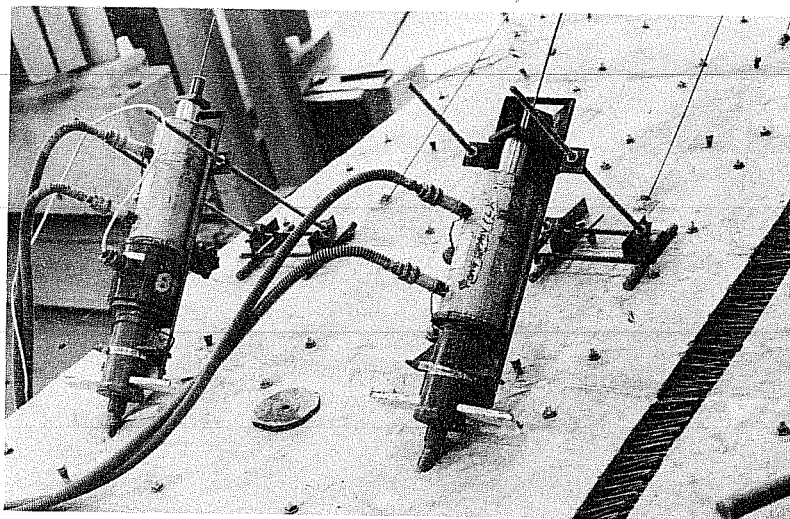


Fig. 6.19. Setup for prestressing of positive tendons

The procedure for the positive tendon operations in the main span was specified in the Texas Highway Department plans as follows:

- (1) Set jacks at end supports.
- (2) Stress tendons A1, A2, A3 and A4, in that order.
- (3) Lower restraining nuts at units PS and transfer load to bearing pads.
- (4) Adjust jacks at outer supports for a reaction of 15 kips (0.417 kips for the model) for each segment at each support.
- (5) Stress tendon A5, then A6.
- (6) Increase jacking reactions at outer supports to 92 kips (2.56 kips for the model) at each segment, at each support. Set bearing pads and shim to maintain this reaction.

This procedure was used as a guide for the model bridge construction. For the model box girder bridge construction, the procedure indicated in the Texas Highway Department plan except Step (3) and the amount of reaction in Step (4) was followed. Step (3) was done after stressing tendons A5 and A6. The reaction of 15 kips (0.417 kips for the model) was very small and was already produced by stressing A1, A2,

A3 and A4 tendons. Therefore, the reaction was increased by 0.28 kips (10.1 kips for the prototype) according to the preliminary design recommendation.<sup>16</sup>

The reaction at the ends was measured using load cells, while the deflections at the ends and at the center of the main span were measured with dial gages. Detailed results are given in Sec. 6.2.3 and 6.2.5. Details of the prestressing system were the same as in Sec. 6.1.4.2. Prestressing was performed from each end alternately.

In view of the experience gained in this erection sequence, recommended procedures for the prototype bridge construction were as follows:

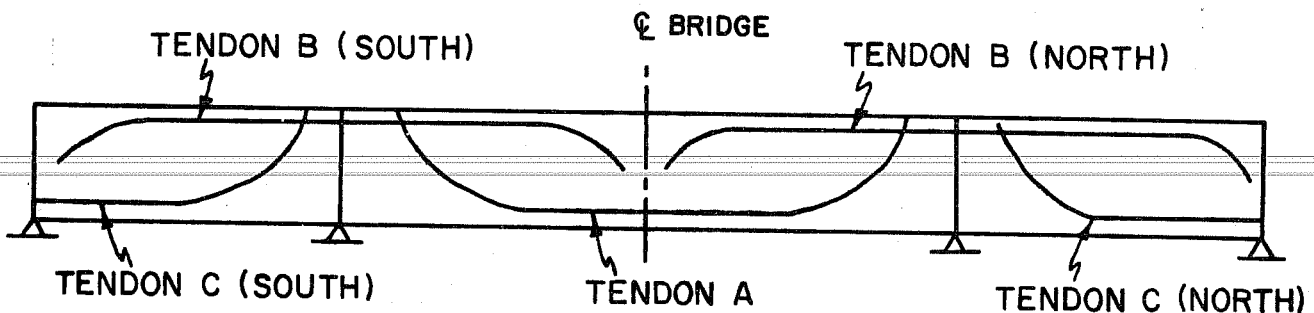
- (1) Lower the S9 - M9 completed sections to their final position over the main pier at the symmetrical cantilever stage.
- (2) Attach the end segments and prestress positive tendons in the side spans.
- (3) Erect the midspan half segments and insert the positive tendons in the main span, prior to casting the closure segment.
- (4) Cast the closure segment.
- (5) Set jacks at outer supports and stress tendon A1.
- (6) Release restraining nuts at the main piers and temporary stiffness at the closure.
- (7) - (9) Stress tendon, A2 - A4
- (10) Increase jacking reaction by 10 kips
- (11) - (12) Stress tendon, A5 - A6
- (13) Adjust elevation of the end segments to optimum amount of reaction (see Sec. 7.3.3.2)

#### 6.1.8 Grouting of Tendons

There were two options for grouting the tendons of the model bridge.

- (1) After prestressing each tendon.
- (2) After prestressing all tendons.

Procedure (1) was required in the prototype structure to minimize corrosion hazards. However, it was considered more time-consuming and more prone to the hazard of possible leakage of grout into the adjacent tendon ducts if there was any honeycombing in the concrete or if sufficient epoxy resin was not spread between the tendon ducts at the joints. Therefore, procedure (2) was used in the model bridge. Grouting was done separately for five groups of tendons as shown in Fig. 6.20. The grout pump and hoses were washed with clean water after grouting each group of tendons.



- ORDER OF GROUTING:
- 1) TENDON B (NORTH)
  - 2) TENDON B (SOUTH)
  - 3) TENDON C (NORTH)
  - 4) TENDON C (SOUTH)
  - 5) TENDON A

Fig. 6.20. Order of grouting for each tendon group

Tendons in each group were located close to each other, as shown in Fig. 6.21. When the B9 tendon was grouted, grout came out from the outlets of both the B9 and B7 tendons simultaneously. This happened because the distance between the B7 and B9 tendons was very small and epoxy resin was apparently not spread fully between the

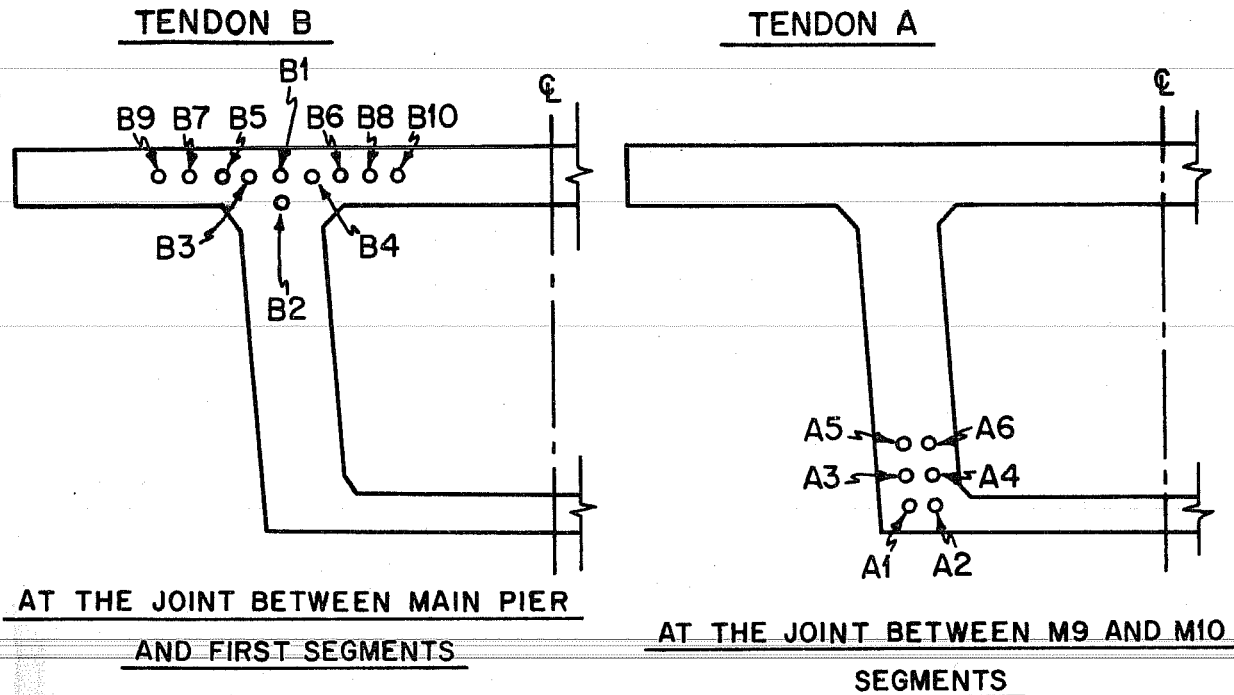


Fig. 6.21. Examples of tendon arrangement

tendons at some joint. However, it was not critical since grouting of the B7 tendon was completed immediately after grouting B9 tendon. It could have had very disadvantageous consequences in the prototype with sequenced grouting. Grout also came out from a joint which had damage on the concrete face near the tendon.

Grouting mix and grouting procedures were done according to Reference 27. The grouting mix used was:

Type III portland cement:	94 lbs.
Water:	42 lbs.
Admixture (INTRAPLAST C, SIKA):	1 lb.

In the first half of the bridge, all tendon ducts were flushed with clean water under pressure immediately before grouting. For the second half, all tendons were blown out with air pressure immediately prior to grouting and not flushed.



The following is the grouting procedure used:

- (1) Grouting injection pipes were screwed into the inlets of tendons as shown in Fig. 6.22.
- (2) Grout was pumped through the ducts and permitted to flow from the outlet until no visible slag of water or air was ejected.
- (3) The valves of the injection pipes were closed while maintaining pressure and the outlets were closed.
- (4) The injection pipes were removed from the inlets of the tendons and the inlets were closed.



Fig. 6.22. Connection of injection pipes and inlets of tendons

The B series tendons were grouted completely in both the first and second half of the bridge. It was initially felt that the A and C series tendons were only grouted with about 70% effectiveness because of some signs that grout might have leaked at some joints due to honeycombing of concrete around the joints. However, by cutting segments at

## 6.2 Behavior of the Bridge during Construction

### 6.2.1 Rotational Stiffness at the Main Pier

Unbalanced loading tests were performed at some stages of construction in order to find the rotational stiffness at the main pier and to check the performance of the temporary anchor bolts. These results are shown in Fig. 6.23.

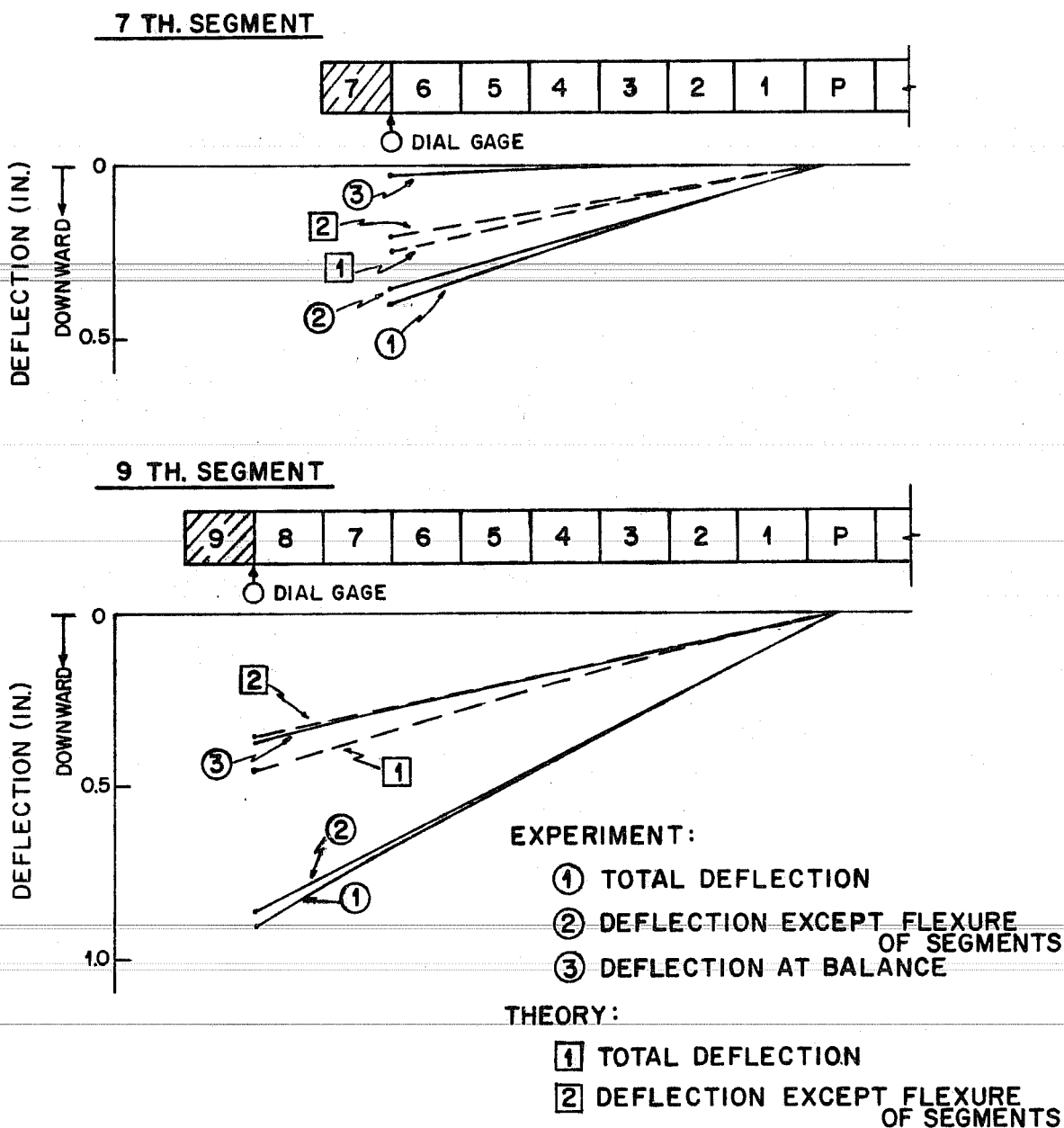


Fig. 6.23. Deflection at unbalanced loading

After each unbalanced loading test was completed, a balancing segment was joined at the other end. Although the bolts behaved elastically at the test of the 7th segment, there was residual deflection at the test of the 9th segment. When the structure was brought to a balanced configuration after the unbalanced loading experiment at the 9th segment, the bolts under the pier were carefully examined and it was found that the bolts on the compression side had deformed and showed evidence of yielding. Although the calculated direct compressive stress was under the actual yield strength, yielding was apparently caused by the large gap between the pier segments and the pier, with consequent local bending and accentuated by the stress concentration in the threads.

Experimental and theoretical values for unbalanced loading are compared in Fig. 6.23. In both cases, the experimental deflection was larger than the theoretical values. There are several factors affecting the deflection under unbalanced loading. These may be classified as follows:

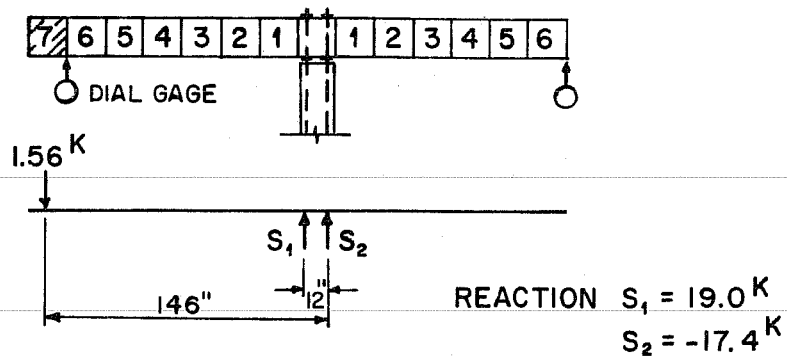
- (1) Flexure of segments.
- (2) Elongation of the pier bolts for temporary connection.
- (3) Bending of pier.
- (4) Moment connection of pier to the test floor.
- (5) Slippage of bolts with respect to pier concrete.

Although the moment connection of the pier was designed to connect to the floor rigidly, there is a slight possibility that bolts were not tight enough or welding of the I-beam to the pier was not strong enough. All cases except (4) and (5) were considered in the calculation of the theoretical deflection at the 7th segment, as follows:

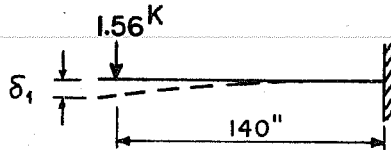
Deflection due to flexure of segments (Fig. 6.24 (1));

$$\delta_1 = Pl^3/3EI = 1.56 \times 140^3 / (3 \times 4.56 \times 10^3 \times 6060) = 0.052 \text{ in.}$$

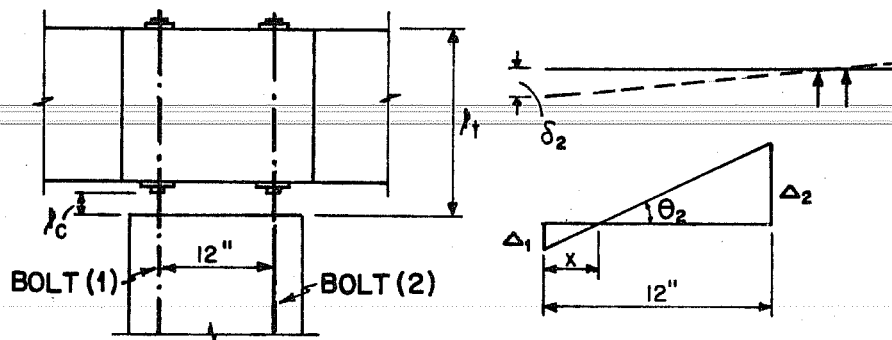
Deflection due to elongation of bolts (Fig. 6.24 (2));



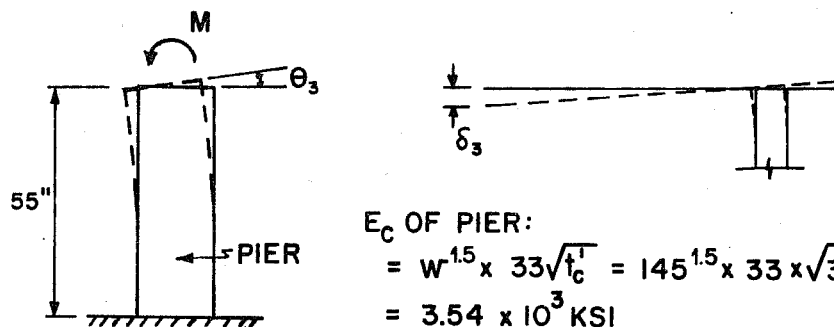
CASE (1) - FLEXURE OF SEGMENTS



CASE (2) - ELONGATION OF BOLTS



CASE (3) - BENDING OF PIER



$E_C$  OF PIER:  
 $= W^{1.5} \times 33 \sqrt{I_C} = 145^{1.5} \times 33 \times \sqrt{3770}$   
 $= 3.54 \times 10^3 \text{ KSI}$

$I_C$  OF PIER:  
 $= 8870 \text{ IN.}^4$

Fig. 6.24. Individual factors effecting the deflection

$$\Delta_1 = S_1 \ell_c / AE_s = (19.0 \times 1.5) / (6 \times 0.142 \times 29 \times 10^3)$$

$$= 1.15 \times 10^{-3} \text{ in.}$$

$$\Delta_2 = S_2 \ell_t / AE_s = (17.4 \times 19.0) / (6 \times 0.142 \times 29 \times 10^3)$$

$$= 13.4 \times 10^{-3} \text{ in.}$$

$$\theta_2 = (1.15 + 13.4) \times 10^{-3} / 12 = 1.21 \times 10^{-3} \text{ radian.}$$

$$\delta_2 = 1.21 \times 10^{-3} \times 125 = 0.151 \text{ in.}$$

Deflection due to bending of pier (Fig. 6.24 (3));

$$\theta_3 = Mh / E_c I = 218 \times 55 / (3.51 \times 10^3 \times 8870)$$

$$= 0.382 \times 10^{-3} \text{ radian.}$$

$$\delta_3 = 0.382 \times 10^{-3} \times 130 = 0.050 \text{ in.}$$

Therefore,

$$\delta_2 + \delta_3 = 0.151 + 0.050 = 0.201 \text{ in.}$$

$$\delta_1 + \delta_2 + \delta_3 = 0.253 \text{ in.}$$

While it is not possible to quantify the exact length of bolt required before full development of bond and prevention of any slip with reference to the concrete, it should be noted that if this length is as much as 20 percent of the development length specified for an equivalent deformed bar under the 1971 ACI Code,<sup>3</sup> the calculated deflection would increase by almost 20 percent and be in much better agreement with the observed values.

Deflection at the 9th segment was calculated in the same manner as follows:

$$\delta_1 = 0.110 \text{ in.} \quad \delta_2 = 0.259 \text{ in.} \quad \delta_3 = 0.084 \text{ in.}$$

$$\delta_2 + \delta_3 = 0.343 \text{ in.}$$

$$\delta_1 + \delta_2 + \delta_3 = 0.453 \text{ in.}$$

Although there are many ways to connect the pier segment to the pier temporarily or permanently, it is not recommended that the exact same system used in the model bridge be used in future bridges, because of the high compressive force applied to the bolts. If the same general type of moment connection is to be used, it should provide for temporary block supports to carry the compression and bolts to provide tensile force, as shown in Fig. 6.25.

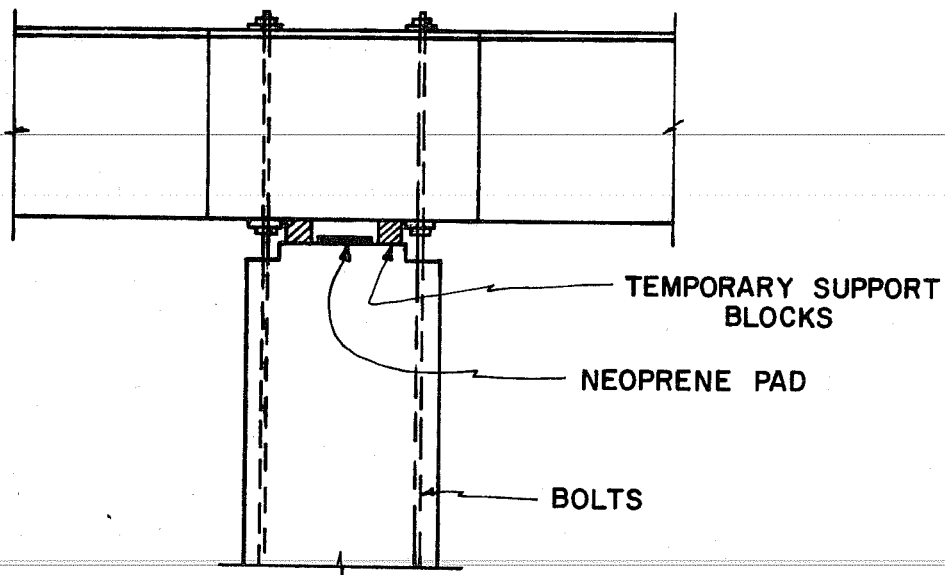


Fig. 6.25. Suggested improvement for temporary support

### 6.2.2 Prestressing Force

In Brown's incremental analysis,<sup>10</sup> he recommended that an initial  $0.8f'_s$  overstress be applied and then be reduced to a final level of  $0.6f'_s$  in order to get  $0.6f'_s$  in the straight portion of the prestressing cables. In the analysis of the bridge (using SIMPLA2 as explained in Sec. 6.2.3), friction coefficient ( $\mu$ ) and wobble coefficient ( $\lambda$ ) were assumed as 0.25/radian and 0.000017/in., respectively.

Friction loss tests were performed during stressing of three different cables (B6, A1, and A4 in the second half of construction). Prestressing force was applied at one end and the resulting force at the far end was measured using a load cell at that point. Prestressing force was applied up to the specified  $0.8f'_s$  and the elongation of the prestressing cables was also measured.

The generally accepted equation<sup>20</sup> to find prestressing force at any position after friction and wobble loss is given as follows:

$$P_{ij} = P_{io} e^{-(\mu\alpha + \lambda\ell_p)}$$

Where,

$P_{ij}$  = prestressing force at a certain point (kip).

$P_{io}$  = prestressing force applied at the end (kip).

$\mu$  = friction coefficient (per radian).

$\alpha$  = angle change of tendon (radian).

$\lambda$  = wobble coefficient (per in.).

$\ell_p$  = length of cables from the end to the point considered (in.).

Theoretical total elongation may be calculated by the following equation:

$$\Delta\ell_p = \int (P_{ij}/E_s A_p) d\ell_p$$

Where,

$P_{ij}$  = prestressing force at the certain point (kip).

$E_s$  = modulus of elasticity of prestressing cable (ksi).

$A_p$  = area of prestressing cable (in.<sup>2</sup>).

$l_p$  = length of prestressing cable (in.).

Experimental results were compared with the theoretical values as shown in Tables 6.1 and 6.2. Profiles of tendon input in the theoretical calculations were taken from the plans.

TABLE 6.1

FRICION LOSS TEST RESULTS

Tendon	Force (0.8f' <sub>s</sub> ) Applied (kip)	Force at the Other End (k)		(Experiment/Theory) at the Other End
		Experiment	Theory	
B6	11.9	8.94	9.26	0.966
A1	7.28	5.30	5.58	0.950
A4	7.28	5.26	5.59	0.942

The results in Table 6.1 indicate that the experimental force at the far end was less than the theoretical values by 5 to 6 percent. Five to 6 percent difference at the far end means that there will be about three percent difference in the prestressing force between the theoretical and experimental values in the straight portion. So a prestressing force of 0.6f'<sub>s</sub> was assumed in the straight portion in the theoretical calculations.

In Table 6.2 are listed some measured elongations during various stages of construction, including the friction loss tests. Experimental



TABLE 6.2

## ELONGATION OF PRESTRESSING CABLES IN SEVERAL STAGES

Tendon	Experimental Elongation (in.)	Theoretical Elongation (1)		Theoretical Elongation (2)			
		$E_s$ (ksi)	$\Delta\ell_p$ (in.)	Exp./Theo.	$E_s$ (ksi)	$\Delta\ell_p$ (in.)	Exp./Theo.
B6	1.67	$30.5 \times 10^3$	1.46	1.14	$27.0 \times 10^3$	1.65	1.01
B7	1.99		1.69	1.18		1.91	1.04
B9	2.28	$30.9 \times 10^3$	2.02	1.13	$27.0 \times 10^3$	2.31	0.986
B10	2.41		2.23	1.08		2.55	0.945
A1	2.46		2.64	0.931		---	---
A2	2.19	$27.0 \times 10^3$	2.37	0.924		---	---
A3	2.06		2.11	0.975		---	---
A4	1.78		1.85	0.961		---	---

(1) Wire  $E_s$  assumed as 30.5 or 30.9.(2) Wire  $E_s$  assumed as 27.0.

results are compared with the theoretical calculations. The ratio of (experiment/theory) for elongation of strands A1 and A4 showed the same trend as the results for forces shown in Table 6.1. However, the experimental elongation of the wires for the B tendons was much higher than the theoretical calculations. In spite of the fact that the force measurements agreed, the area of the prestressing cables or the value of  $E_s$  are the only factors which would affect elongations and not forces, and thus affect the results of Table 6.2. Therefore, it was judged that there might have been some error in the experimental method used to measure  $E_s$ , since the area of the wires was verified by measuring the diameter of several wires. If  $E_s$  is assumed as  $27 \times 10^3$  ksi for the wires, the results of wire elongation agree well with the theoretical calculations shown in Set (2) of Table 6.2.

---

When prestressing force was lowered to  $0.65f'_s$ , some change was observed in the experimental elongation of wire, and no change in the resulting force at the far end.

### 6.2.3 Deflections

It was difficult to measure vertical deflection during construction correctly because the deflection was so small in comparison to the span. Casting and construction of the model segments requires six times the accuracy of the prototype if it is necessary to maintain the same relative tolerance as the prototype. This was not completely feasible so that deflections were measured only to see the general trend of cantilever section behavior. Theoretical deflections were calculated by the computer program SIMPLA2<sup>10</sup> which provides an analysis at each stage of erection using the finite segment technique.

Since it is confusing to put the theoretical and experimental results in the same figures, separate results are shown in Figs. 6.26 and 6.27, respectively, for all stages of erection. Relative deflections for one typical case are compared in Fig. 6.28. There are many factors which affect the vertical deflections as mentioned in Sec. 6.1.5 (b). Therefore, it is very hard to indicate the cause of errors

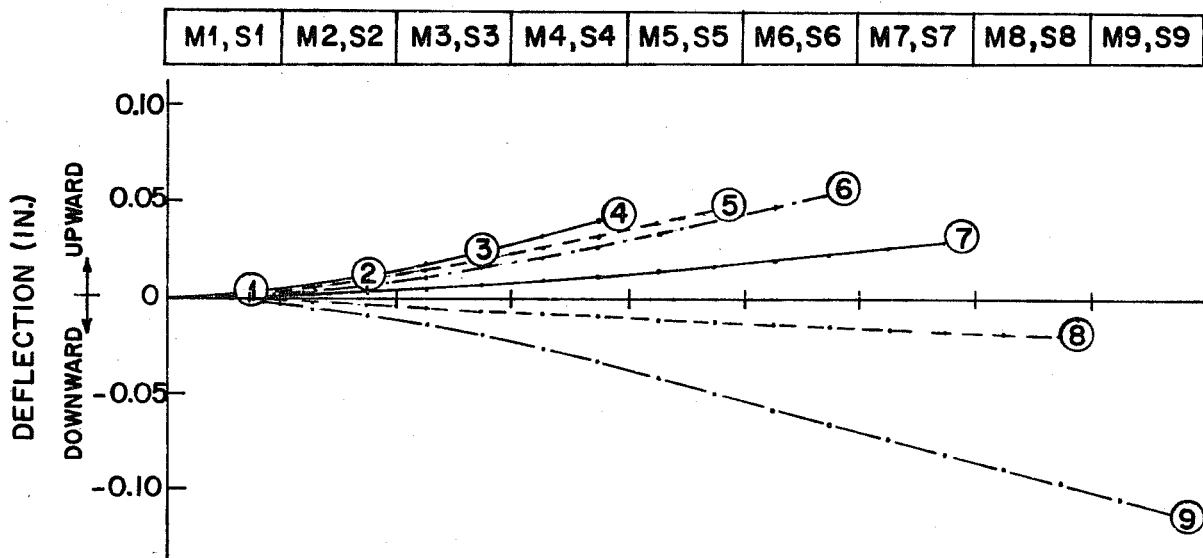


Fig. 6.26. Deflection predicted by SIMPLA2 for cantilever erection

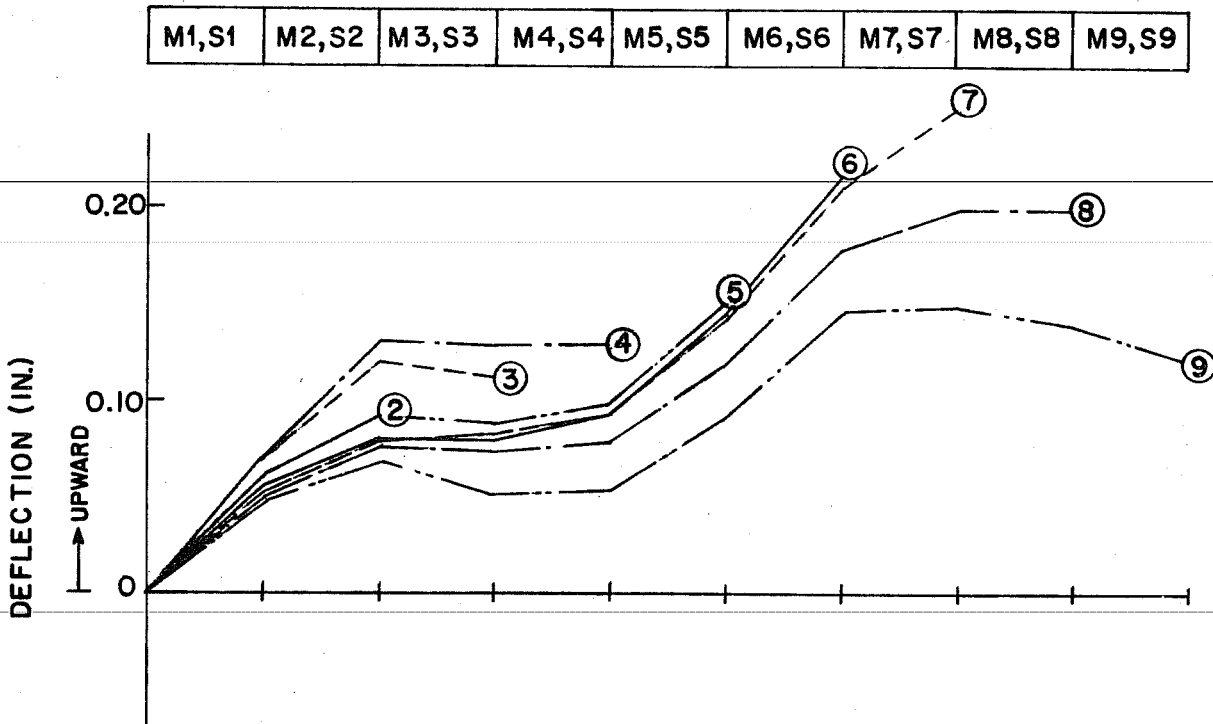


Fig. 6.27. Typical measured deflection during cantilever erection

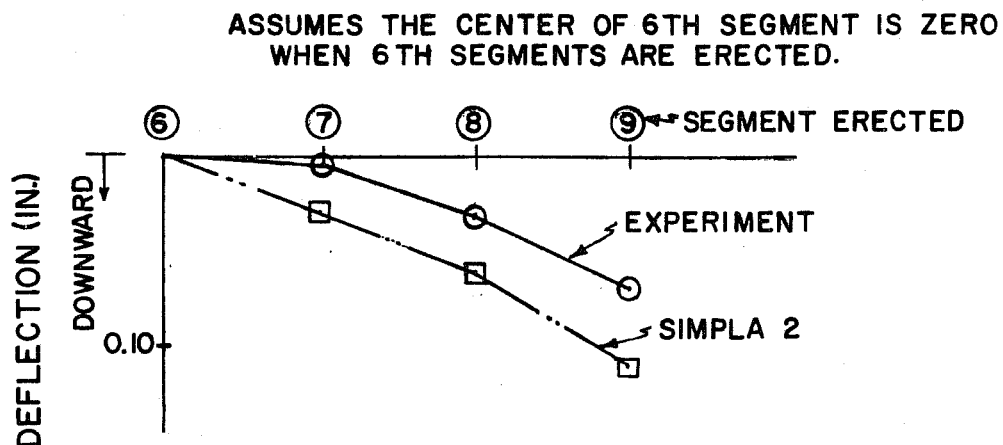


Fig. 6.28. Deflection relative to the center of 6th segment

in deflection and to find the component of deflection due to dead load and to the prestressing. Figures 6.26 and 6.27 indicate that the trend of the theoretical and experimental results agreed fairly well. Although the experimental deflection at construction of the 7th segment was still upward at the tip of the last unit, it dropped at the tip of the 8th and 9th segments, as did the theoretical results.

Experimental deflection measurements had to be taken for both cantilever ends and averaged at each symmetrical point because it was necessary to eliminate the effect of the unbalanced weight of the segments or the bending of bolts at the pier occurring under the extreme unbalanced loading. Readings of each symmetrical point were averaged and those values were plotted in Fig. 6.27. It can be observed from Fig. 6.27 that there were some soffit errors or jointing errors which showed up in the initial stages of cantilever erection.

During the positive tendon operations in the main span, the experimental and theoretical deflections agreed well, as shown in Fig. 6.29. The procedure used to calculate deflections using program BMCOL50<sup>22</sup> is explained in Sec. 6.2.5.

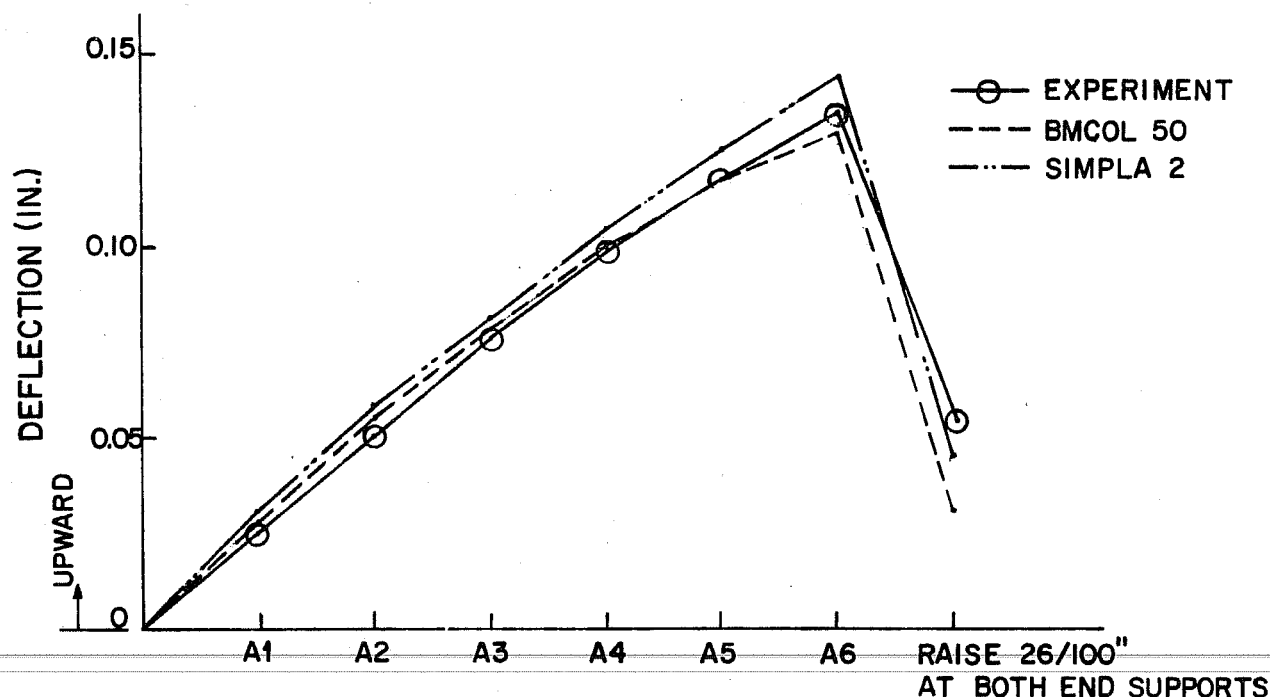


Fig. 6.29. Deflection at the center in main span during positive tendon operations

By superimposing results from Figs. 6.26 and 6.29, relative displacement at the center in the main span was almost zero when prestressing of all positive tendons were completed. However, the center of the main span was subsequently lowered 0.08 in. (0.48 in. in the prototype) from that point by the later upward jacking at the outer supports.

When a half segment (S10) in the side span was erected, the joint between the S9 and S10 segment lowered about 0.06 in., although SIMPLA2 predicted it as 0.2 in. This difference was caused by the reduced weight of the model segment (about 35 percent of the ideal weight). Some of the compensating dead load blocks were not able to be hung because this segment was located above the outer pier. During prestressing of positive tendons (C3, C2, and C1) in the side span, there was no change in elevation at the end segment (S10), although SIMPLA2 predicted 0.1 in. downward displacement.

#### 6.2.4 Strains

The sequence of construction referenced as stages in presentation of strain readings is listed in Table 6.3. Results of strain readings are shown in Figs. 6.30 to 6.38.

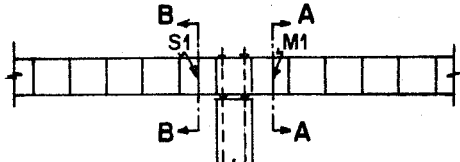
Longitudinal strains as plotted in these figures in most cases were the average for the duplicate readings at identical positions in the similar segments.

In the top slab of the M1 and S1 segments, the experimental strains varied across the cross section until the erection of the 5th segment and did not agree with either of the sets of theoretical calculations until the erection of the 6th segment, as shown in Fig. 6.30. Experimental strains were uniform across the cross section with the erection of the 6th and subsequent segments. Although the longitudinal strains at the top of the M1 and S1 segments varied across the cross sections in early erection stages, it is not a serious problem. All strains are in compression across the cross section and are well below the strains which would accompany the maximum allowable compressive stress. The increase of strain in the top slab over the web was probably influenced by the concentrated tendon forces and subsequent increases were less than the other portions of the top slab during the erection of the second through fifth segments, as shown in Fig. 6.30.

For strains in the M1 and S1 segments, SIMPLA2 gave reasonable predictions of the longitudinal strain distribution at the erection of the first segment, but then showed poor agreement with the experimental results until the erection of the 7th segments. Since beam theory cannot predict any variations in longitudinal strain distribution at a transverse section, the deviation with the experimental values for the first two stages were somewhat expected. There were some deviations between the two theoretical methods of calculation at the erection of the 3rd, 4th, 5th, and 6th segments. Calculation by beam theory was closer to the experimental values in these stages. Deviation of the experimental and beam theory results in the initial stages affects the accumulated values

TABLE 6.3  
 DETAILS AT EACH STAGE OF CONSTRUCTION

Stage	Segment Erected	Prestressing Cable	Amount of Force Per Cable at $0.8f'_s$ (kip)	Amount of Force Per Cable at $0.6f'_s$ (kip)
1	M1, S1	B1, B2	11.9	8.94
2	M2, S2	B3	18.3	13.8
3	M3, S3	B4	18.3	13.8
4	M4, S4	B5	11.9	8.94
5	M5, S5	B6	11.9	8.94
6	M6, S6	B7	11.9	8.94
7	M7, S7	B8	5.52	4.13
8	M8, S8	B9	5.52	4.13
9	M9, S9	B10	5.52	4.13
10	S10	C4	5.52	4.13
11	-----	C3	5.52	4.13
12	-----	C2	5.52	4.13
13	-----	C1	5.52	4.13
14	M10	B11	5.52	4.13
Closure segment was cast and supported at ends (3 span continuous beam).				
15	-----	A1	7.28	5.46
16	-----	A2	7.28	5.46
17	-----	A3	7.28	5.46
18	-----	A4	7.28	5.46
19	-----	A5	7.28	5.46
20	-----	A6	7.28	5.46
21	Raise 0.26 in. at outer supports.			



\* STRAIN READINGS AT A-A AND B-B WERE AVERAGED.  
 ○ - EXPERIMENT  
 △ - SIMPLA 2  
 --- BM THEORY

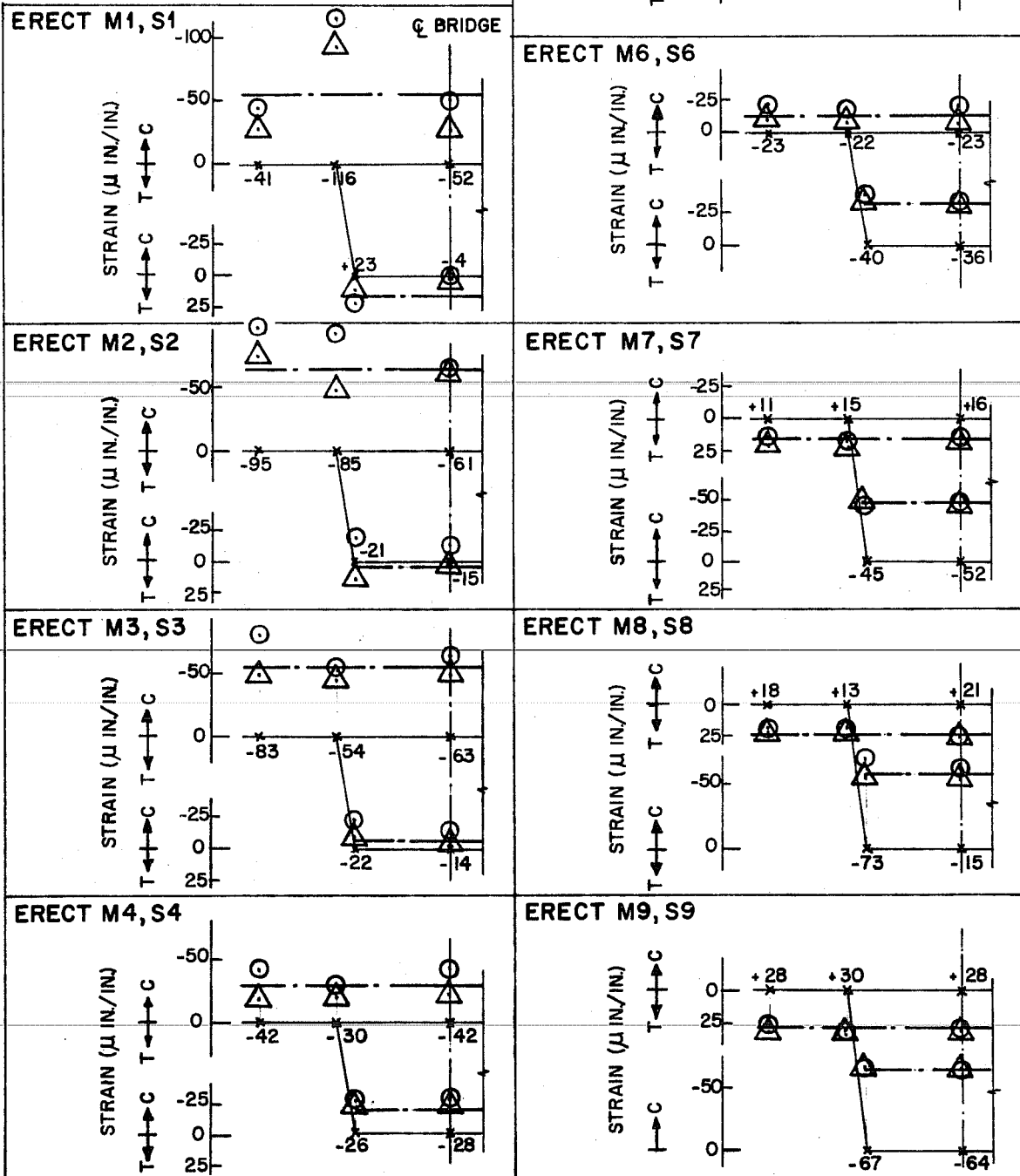
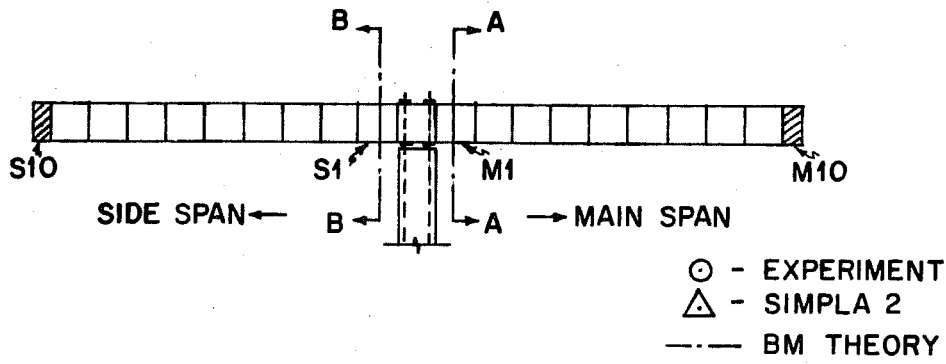


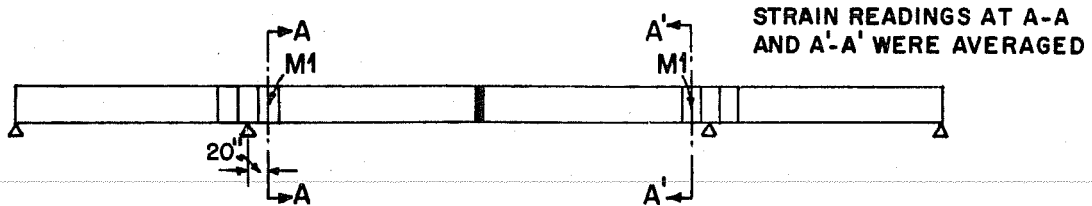
Fig. 6.30. Strain in M1 and S1 segments during balanced cantilever construction





STAGE	AT SECTION B-B	AT SECTION A-A
(10) → (13)	<p>PRESTRESS C4,C3,C2,C1</p> <p>STRAIN (<math>\mu</math> IN./IN.)</p> <p>☉ BRIDGE</p>	<p>PRESTRESS C4,C3,C2,C1</p> <p>STRAIN (<math>\mu</math> IN./IN.)</p> <p>☉ BRIDGE</p>
(14)	<p>ERECT M10</p> <p>STRAIN (<math>\mu</math> IN./IN.)</p> <p>☉ BRIDGE</p>	<p>ERECT M10</p> <p>STRAIN (<math>\mu</math> IN./IN.)</p> <p>☉ BRIDGE</p>

Fig. 6.31. Strains in M1 and S1 segments during erection of half segments



STRAIN READINGS AT A-A AND A'-A' WERE AVERAGED

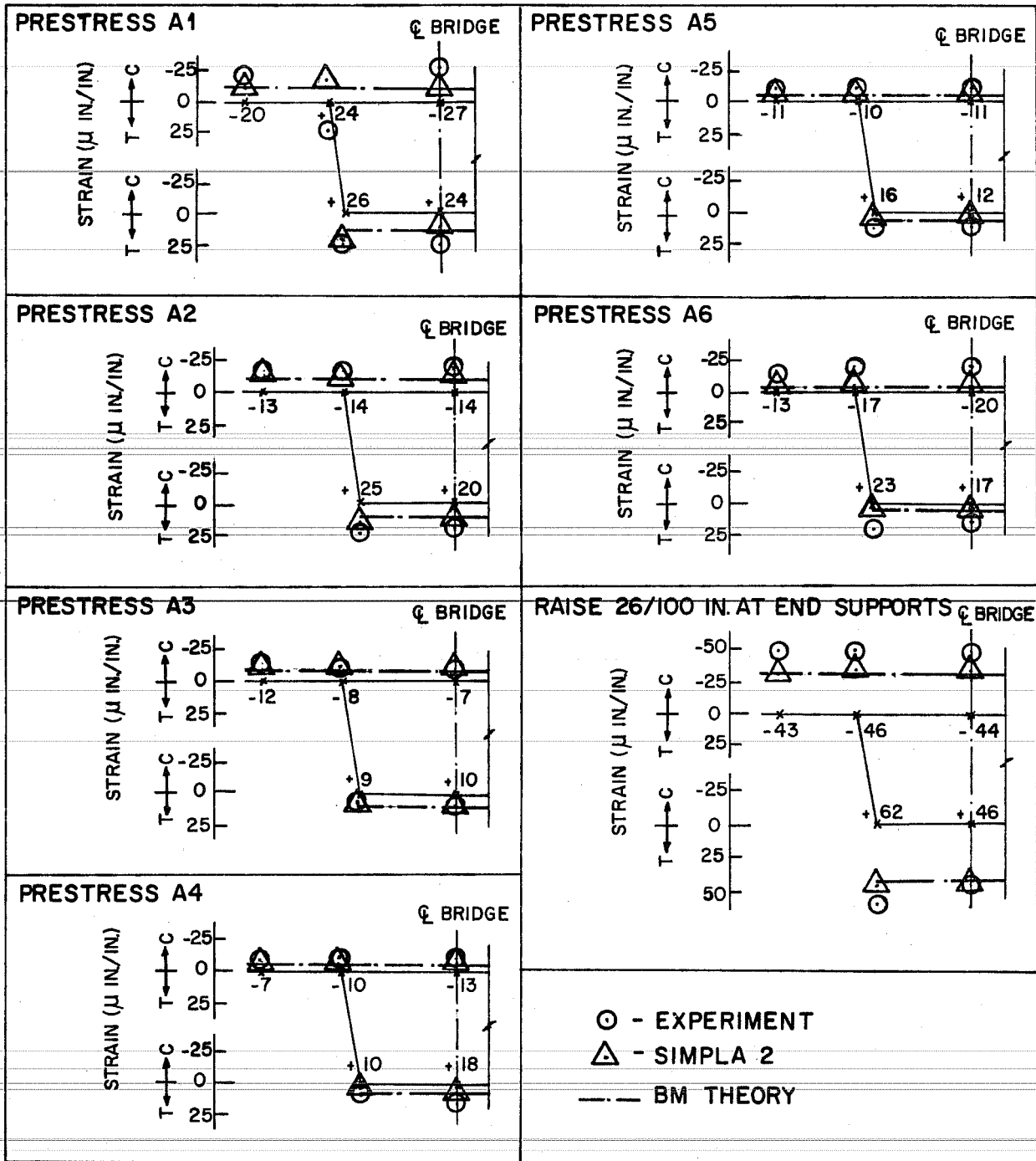


Fig. 6.32. Strains in M1 segments during closure operation

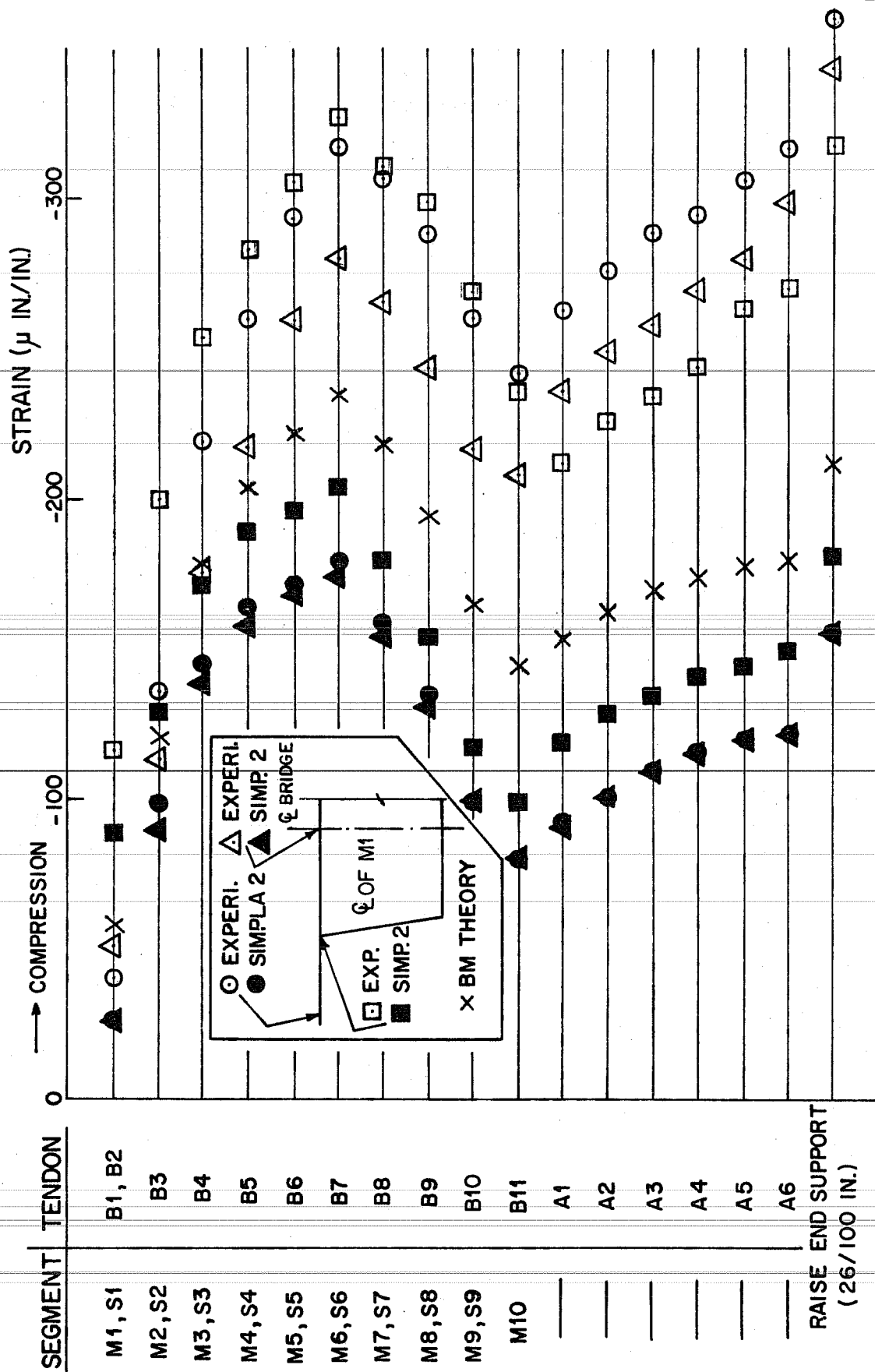


Fig. 6.33. Strains in the top slab of M1 segments during construction

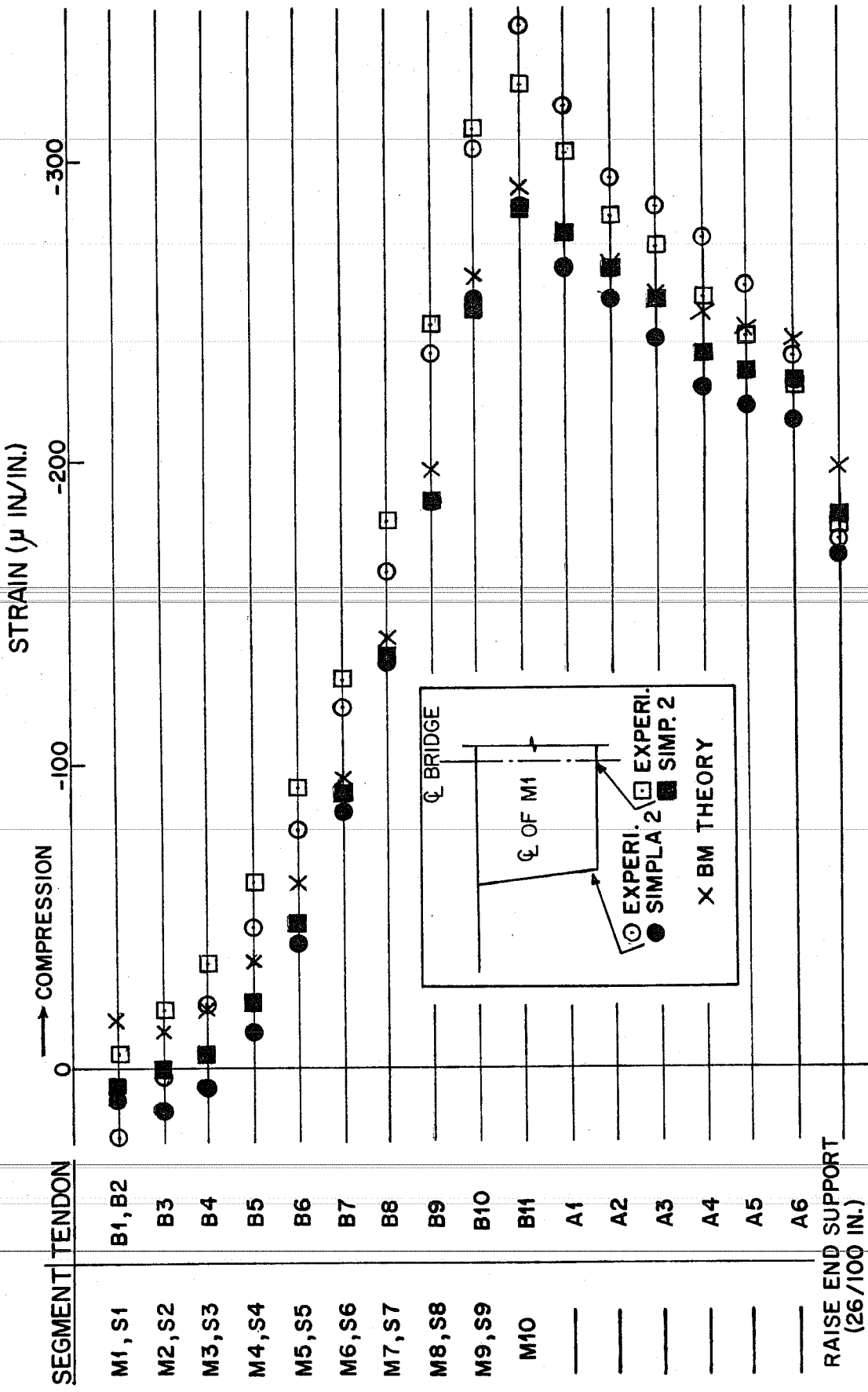


Fig. 6.34. Strains in the bottom slab of M1 segments during construction

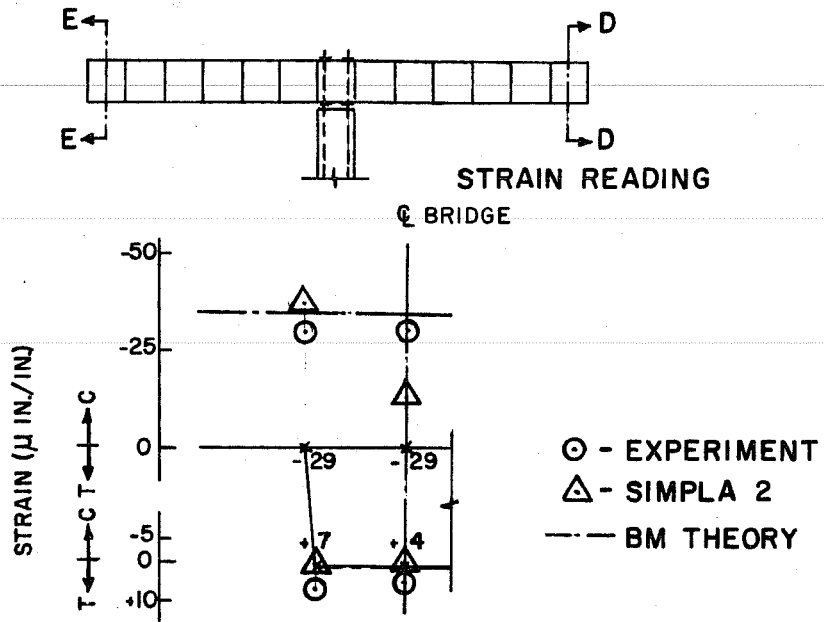


Fig. 6.35. Strains in the M6 and S6 segments at erection of the 6th segment

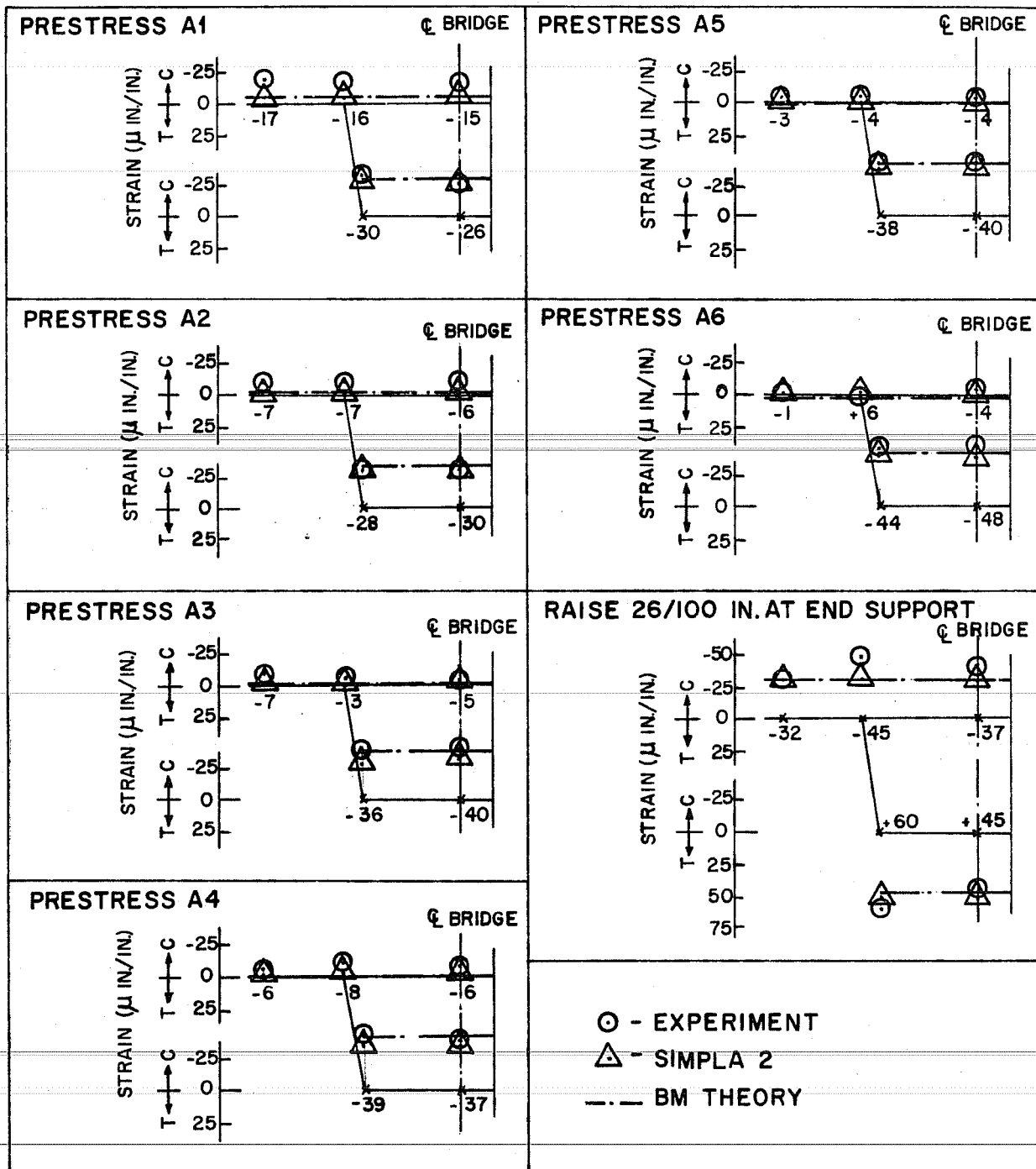
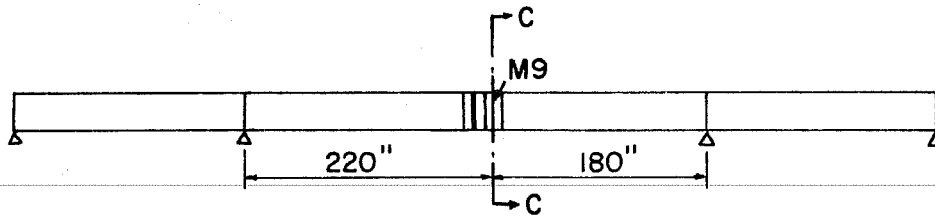


Fig. 6.36. Strains in the M9 segment during closure operations

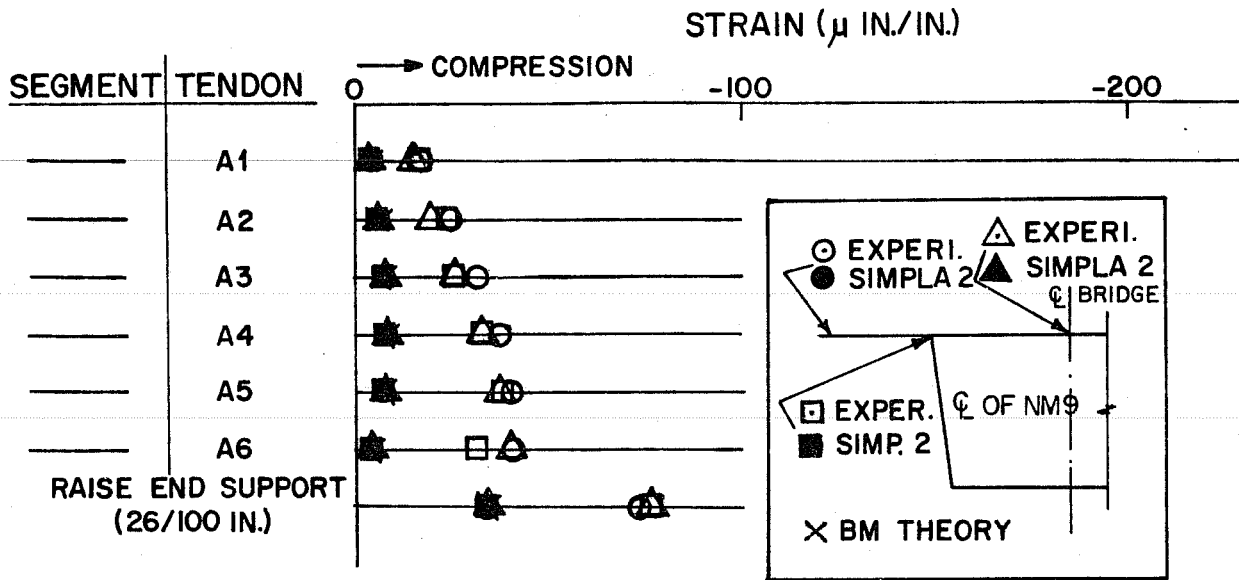


Fig. 6.37. Strains in the top slab around the center of the main span

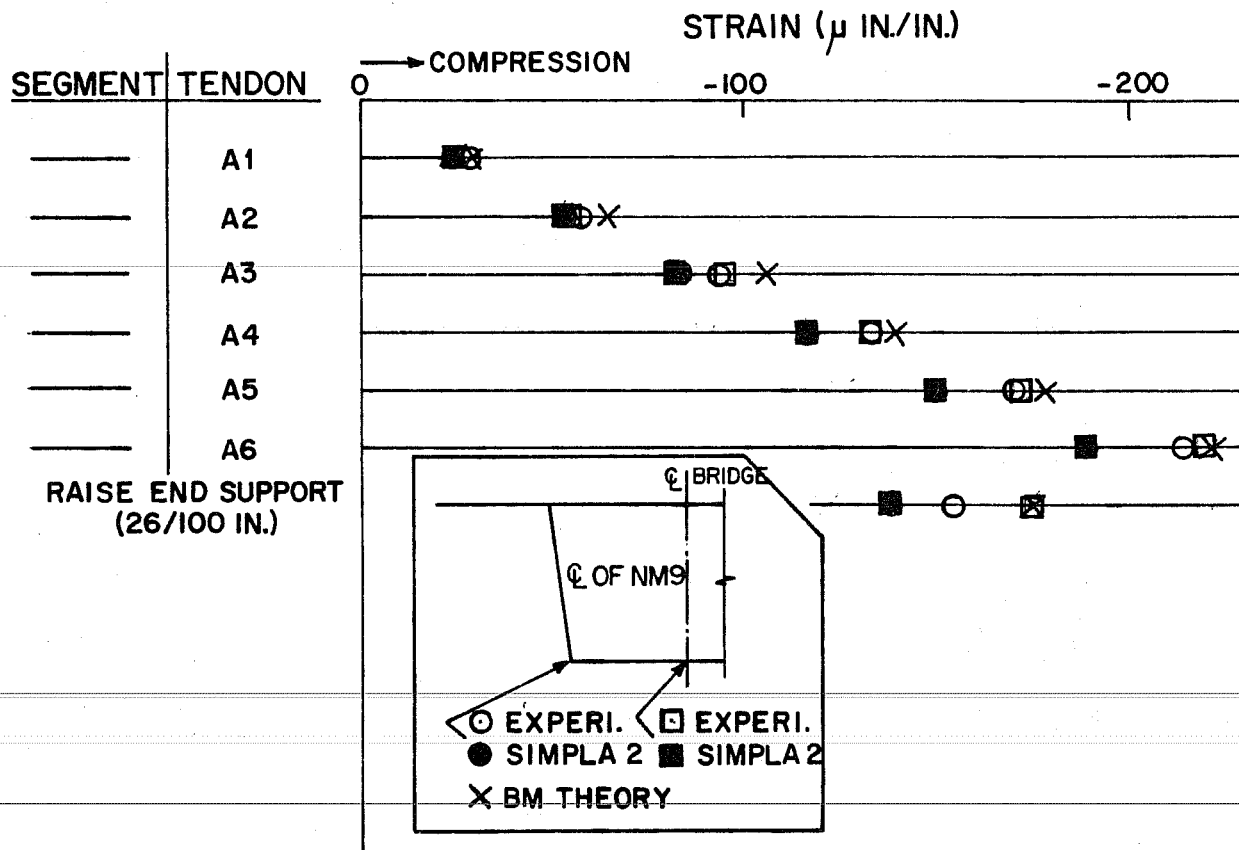


Fig. 6.38. Strains in the bottom slab around the center of the main span

of strain in the top slab of M1 and S1, as shown in Fig. 6.33, even though the subsequent longitudinal strain increments agreed during cantilever erection, as shown in Figs. 6.30 and 6.31.

Because Figs. 6.30 through 6.34 indicated so much deviation in the longitudinal strains across the cross section for the M1 and S1 segments during erection of the first groups of segments, the longitudinal strains in the 6th segments during its erection are shown in Fig. 6.35. At this stage the experimental strains measured in the top slab were uniform although SIMPLA2 predicted some deviation. The magnitude of this deviation was small in comparison to the first segment because of the lower prestressing force as the cantilever sections extended. Apparently little local compression effect existed. In the bottom slab the experimental and theoretical results agreed very well except for the erection of the first three segments, as shown in Figs. 6.30, 6.31, and 6.34. The strain produced was almost uniform in the bottom slab, except at the erection of the first three segments. Figure 6.34 shows tensile strains developed in the bottom of the M1-S1 segments at the erection of the first two segments as predicted.

During the positive tendon stressing operations after casting the closure segment, as shown by Figs. 6.33 through 6.38, the values predicted by both SIMPLA2 and beam theory deviated from the experimental results in the top slab of the M1 and M9 segments. Although the experimental results were consistently greater than the theoretical calculations, no ready explanation for the difference is known. The small absolute values of the strain might be one of the factors for the discrepancy due to inherent difficulties in accurately measuring these very small strains.

The maximum strain in the M1 and S1 segments occurred in the top slab at the erection of the 6th segments and at the completion of construction and in the bottom slab at the erection of the M10 segment, as shown in Figs. 6.33 and 6.34. The magnitude of the maximum compressive strain in the M1 and S1 segments was approximately 330  $\mu\text{in./in.}$  in both the top and bottom slab. Therefore, the maximum compressive stress was



about 1500 psi. This value was only 21 percent of the ultimate compressive strength of concrete (7090 psi) and about half of the maximum allowable stress. The maximum strain in the bottom slab at the center of the main span was about 200  $\mu$ in./in. during construction of the bridge.

All readings were taken before and after the application of load and not cumulative. Creep effects appear very small, although the experimental strain values were generally larger than the values given by beam theory. Since the beam theory agreed fairly well with the experimental results, the BMCOL50 program can be modified for use in theoretical calculations for construction stages for this type of bridge.

In general, both theoretical solutions and the experimental results were in reasonable agreement when the change of strain in each stage was reasonably large, except for the local strains in the top slab during initial stages when the large local compressive forces from the tendons seemed to effect the strain distributions.

#### 6.2.5 Reaction at Outer Supports during Positive Tendon Operations

Prior to positive tendon prestressing operations in the main span, the end supports were adjusted to just bear on the underside of each web at the edge of the end pier segments. Reactions at the end supports were measured by sensitive load cells during each stage. Comparison between theoretical and experimental results is shown in Table 6.4.

Figure 6.39 shows the simplified procedure used to calculate the reaction at the end. Prestressing forces were replaced by the vertical forces which produced the moment diagram due to prestressing. These reactions were calculated using the BMCOL50 program.<sup>22</sup>

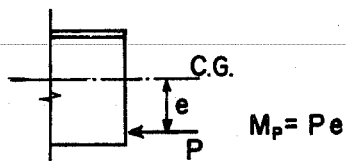
Experimental reactions agreed very well with the theoretical values for large values such as A1 and A2 tendons. But, as the amount

TABLE 6.4

REACTION AT OUTER SUPPORT DURING PRESTRESSING IN MAIN SPAN

Tendon	Experiment (kip)	BMCOL 50 (kip)
A1	0.245	0.251
A2	0.200	0.213
A3	0.115	0.169
A4	0.074	0.131
A5	0.012	0.091
A6	0.012	0.055
Raise 0.26 in. at outer supports	1.04	0.700
<b>Total</b>	<b>1.698</b>	<b>1.610</b>

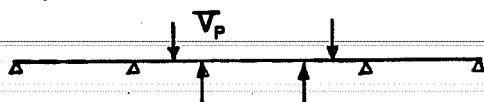
(A) PRESTRESSING FORCE AND ECCENTRICITY OF CABLE.



(B) MOMENT DUE TO PRESTRESSING.



(C) EQUIVALENT VERTICAL FORCE FOR  $M_p$ .



(D) POSITION OF LOAD FOR EACH CABLE.

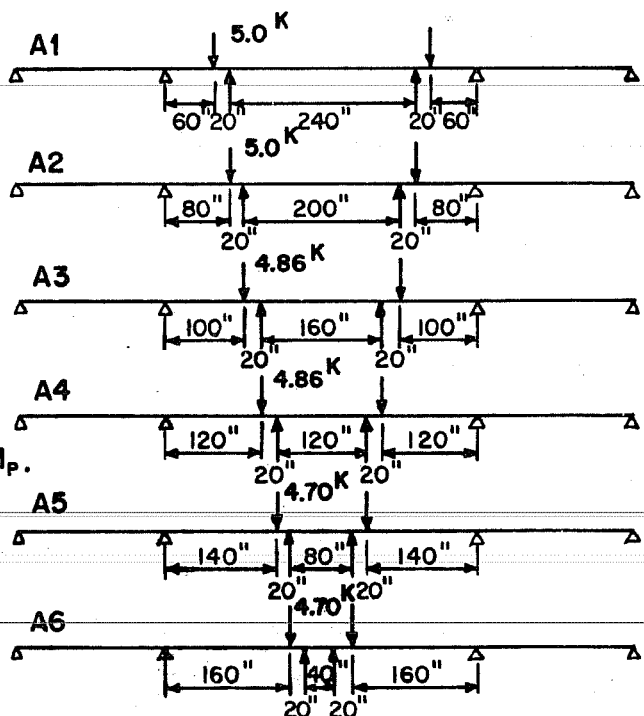


Fig. 6.39. Calculation of end reaction due to positive tendons

of reaction became smaller, the experimental readings became much smaller than the theoretical values. However, the total experimental reaction agreed well with the total theoretical values.

CHAPTER 7

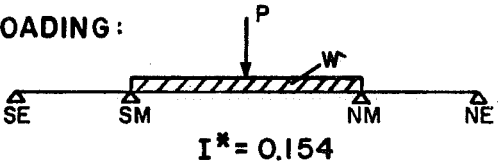
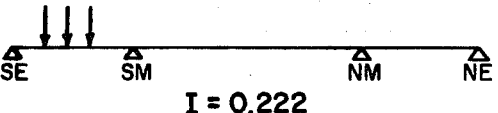
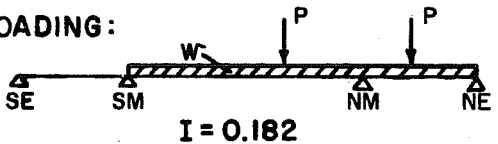
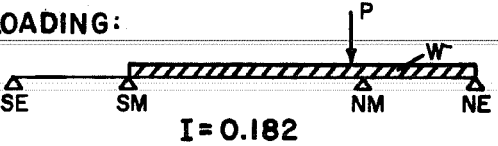
SERVICE AND DESIGN ULTIMATE LOAD TESTS

7.1 General

The loading plan was designed to test the completed bridge for all critical AASHO loading conditions used in the design.<sup>16</sup> Those are summarized in Table 7.1.

TABLE 7.1

CRITICAL LOADING CONDITIONS IN LONGITUDINAL DIRECTION

CASE	CRITICAL CONDITION	LOADING CONDITION
(1)	MAXIMUM POSITIVE MOMENT AT THE CENTER OF THE MAIN SPAN.	LANE LOADING:  $I^* = 0.154$
(2)	MAXIMUM POSITIVE MOMENT IN THE SIDE SPAN.	TRUCK LOADING:  $I = 0.222$
(3)	MAXIMUM NEGATIVE MOMENT AT THE MAIN PIER.	LANE LOADING:  $I = 0.182$
(4)	MAXIMUM SHEAR ADJACENT TO THE MAIN PIER.	LANE LOADING:  $I = 0.182$

\* I = IMPACT FACTOR

The order of testing was as follows:

(1) Service loading (1.0 DL + 1.0 (LL + IL)).

- (a) Case (2) in Table 7.1.
- (b) Case (1) in Table 7.1.
- (c) Case (3) in Table 7.1.
- (d) Case (4) in Table 7.1.

(2) Ultimate loading. The ultimate load used in the actual design of the bridge was specified by the Bureau of Public Roads 1969 Ultimate Design Criteria<sup>7</sup> as  $U = 1.35 \text{ DL} + 2.25 (\text{LL} + \text{IL})$ . Prior to applying any of the ultimate design live loads, supplementary concrete blocks corresponding to 0.35 dead load were added to the structure. Then, design ultimate live load was applied in the following sequence:

- (a) Case (1) in Table 7.1.
- (b) Case (3) in Table 7.1.
- (c) Case (4) in Table 7.1.
- (d) Case (2) in Table 7.1.

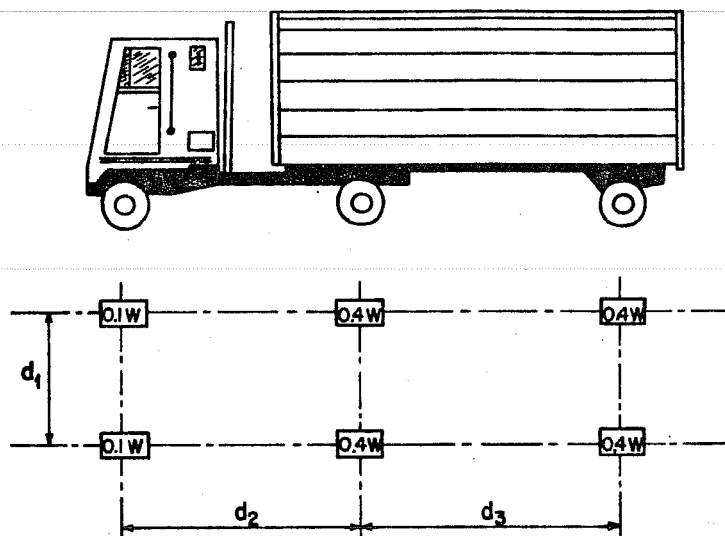
In all of the loading tests, the AASHO reduction factors for load intensity were not used. These factors (reflecting improbable coincident maximum loading in all lanes) would have allowed a 25 percent reduction in load when four-lane loading was considered. In addition to the main loading series special loads were applied to study transverse moment distribution for the different types of truck loadings and lane loading (two lanes). The weight of the asphalt topping, which is about 8 percent of the weight of the segment, was not included in the model bridge test.

## 7.2 Test Procedures

### 7.2.1 Simulation of Loading

#### 7.2.1.1 Truck Loading

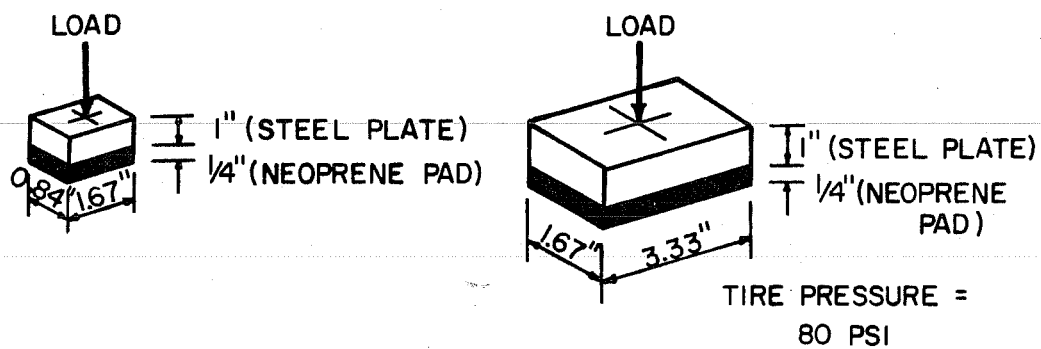
HS20-S16-44 truck loadings specified by AASHO<sup>6</sup> were scaled down, as shown in Fig. 7.1. Tire pressure was assumed as 80 psi for both



ITEM	FULL SIZE TRUCK	MODEL TRUCK
W (lbs)	40,000	1111
$d_1$ (ft.)	6.0	1.0
$d_2$ (ft.)	14.0	$2\frac{1}{3}$
$d_3$ (ft.)	14.0 ~ 30.0	$2\frac{1}{3}$ ~ 5.0

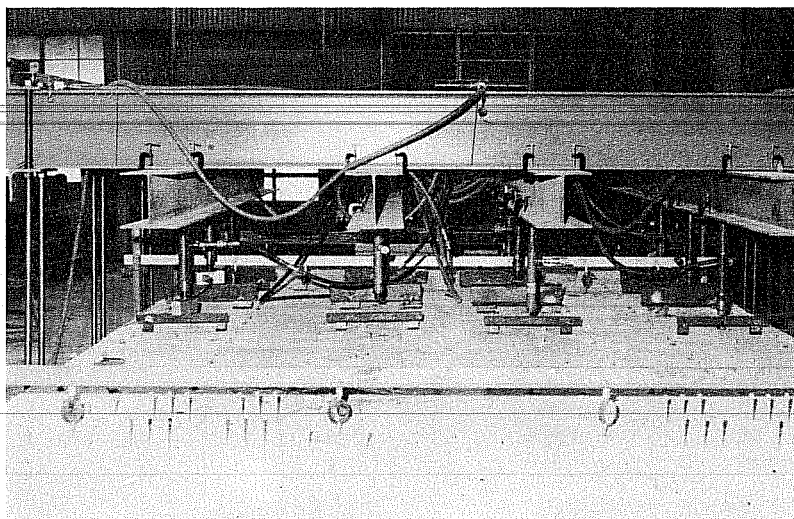
Fig. 7.1. Dimensions of full size and 1/6 scale model AASHO HS20-S16 truck

front and rear wheels in sizing the loading pads, as shown in Fig. 7.2. In single point load tests (punching shear test in Chapter 8), load was applied directly on the load pad by rams. To simulate axle loads, the loads were applied by using load spreaders.



(a) FRONT WHEEL

(b) REAR WHEEL



(c) 4 LANE AASHTO HS20-16 TRUCK

Fig. 7.2. Scaled wheels and AASHTO HS20-S16 truck

### 7.2.1.2 Lane Loading

It would have been very difficult to completely simulate uniform lane loadings on this bridge model. Uniform lane loads were closely simulated by applying a series of concentrated loads at 4 ft. intervals. Each lane is roughly centered over a web, as shown in Fig. 7.3, so this made it possible to apply load above each web in the main test series. Transverse distribution was checked in another series. These concentrated loads were applied on the top slab at the webs by using  $4 \times 4 \times 1$  in. steel bearing plates and  $4 \times 4 \times 1/2$  in. neoprene pads. Details are shown in Figs. 7.3 and 7.4.

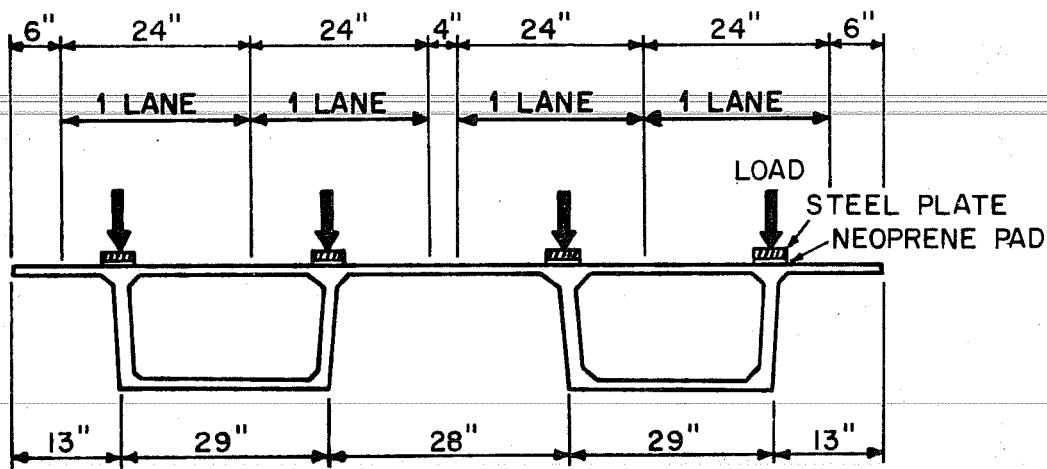


Fig. 7.3. Application of concentrated loads above the webs (in each lane)

Prior to loading tests, moment and shear diagrams for the uniform loading and the equivalent concentrated loads were compared as shown in Table 7.2. Although extremely close agreement is shown for bending moment, there are some differences with shear loadings because of the change of loading (uniform load  $\rightarrow$  concentrated loads). Loads shown in Fig. 7.4 are for 4 lanes fully loaded. Reduction in load intensity was not used although the AASHTO specification would call for this structure to resist only 75% of 4 lane traffic. Hence all results represent very conservative design loads.



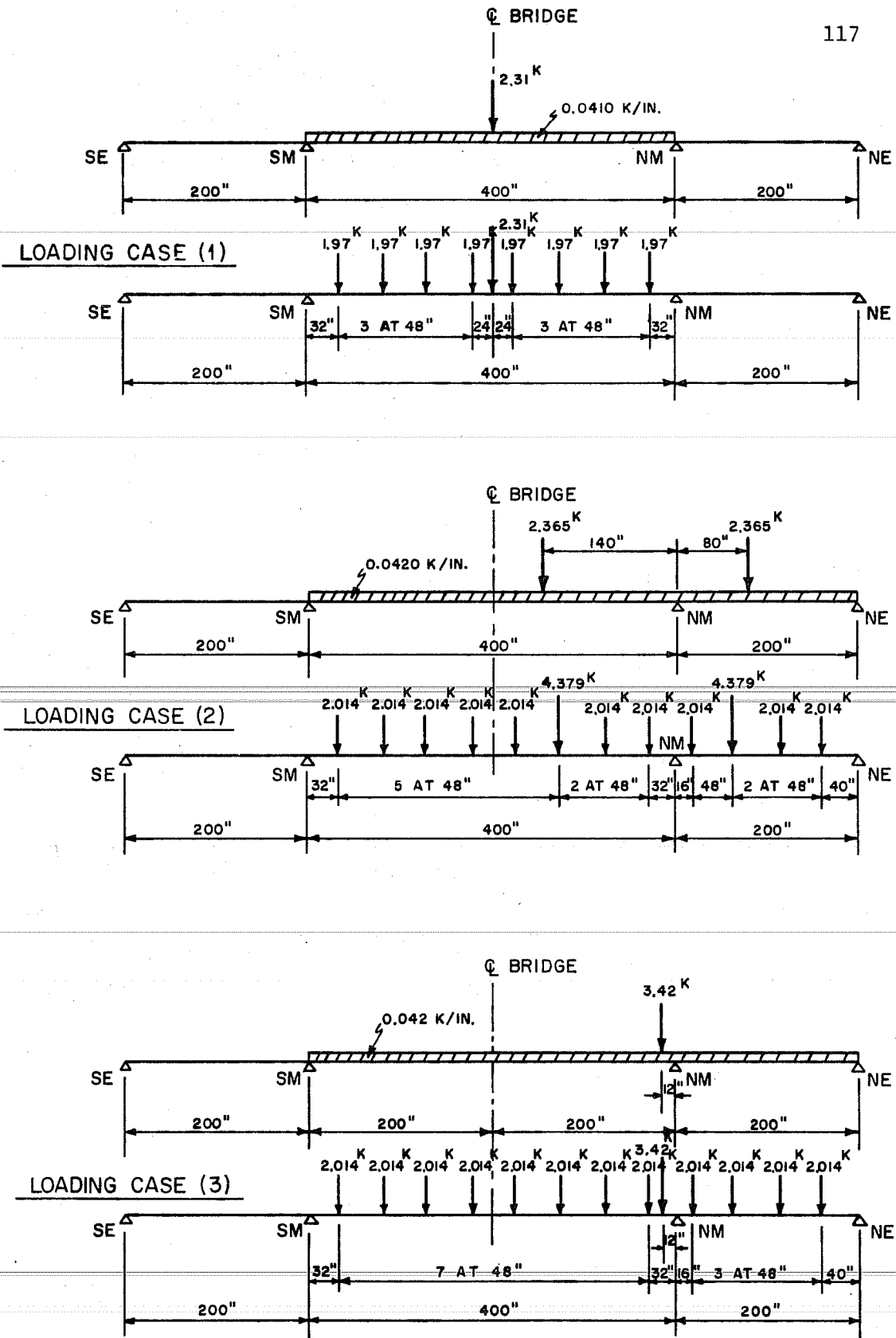


Fig. 7.4. Lane loads and equivalent concentrated loads for four lanes with impact allowances



## 7.2.2 Loading System and Instrumentation

### 7.2.2.1 Loading System

Wide flange beams were mounted sufficiently above the bridge to leave enough space for loading equipment. These members spanned across the bridge and were supported by 1-in. diameter high strength bolts as shown in Fig. 7.5. The bolts were attached to the structural test floor. Rams were mounted on these wide flange beams to apply load to the top of the webs as shown in Fig. 7.5 (a) or (b).

The wide flange beams were set at 4 ft. intervals longitudinally. Rams were connected to pumps with hoses and the number of pumps was minimized by using many manifolds.

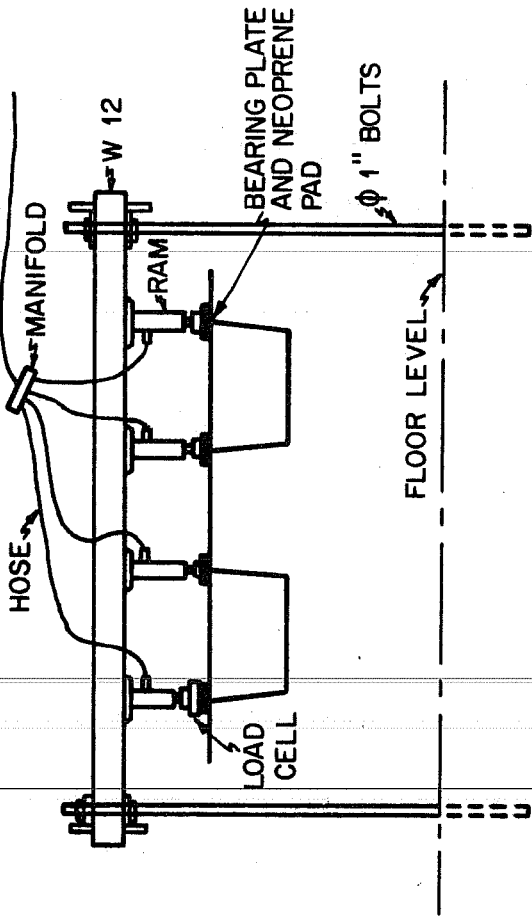
An example of the loading setup for critical shear next to the NM pier in main span is shown in Fig. 7.6.

Load was applied by electric or manual pumps. Two load cells were generally used in the loading system. One load cell indicated the amount of load and was used to regulate pump pressure while the other load cell was used to check the load applied. In addition hydraulic system pressure gage readings were also recorded for check purposes. Load control procedures worked well.

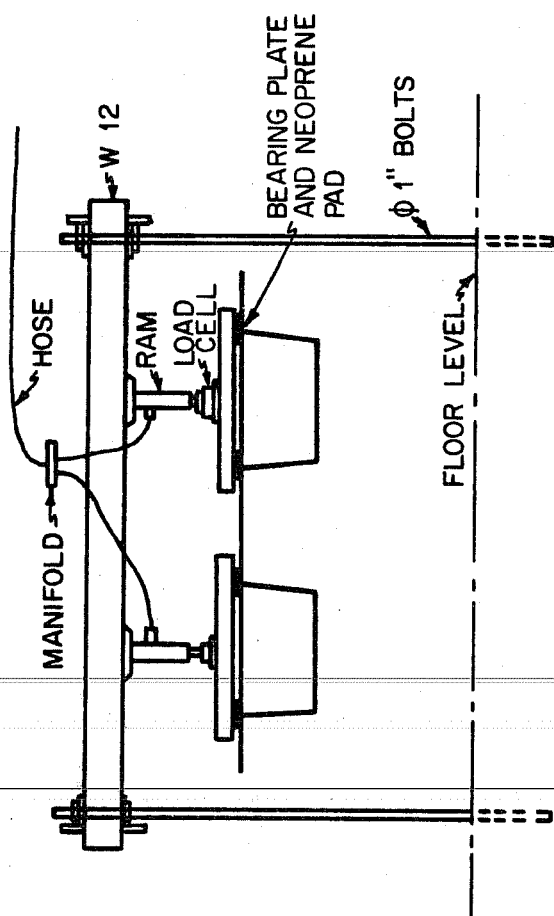
### 7.2.2.2 Instrumentation and Observation

Strain gage measurements were taken at the four positions shown in Fig. 4.14. Dial gages referenced to the test floor measured deflections of the top slab. Four or nine dial gages were set at each position, as shown in Fig. 7.7. Although nine gages were set at some points, only the dial gage readings above the four webs were averaged to get longitudinal deflections. Also, slip gages were provided to check relative movement across the critical joint for the maximum shear loading case.

Reactions were measured by load cells at the outer supports (SE and NE in Fig. 7.7). Load cells could not be set at the main piers (SM and NM in Fig. 7.7) because of the temporary bolt support devices. Load



(a) LOADING SETUP 1



(b) LOADING SETUP 2

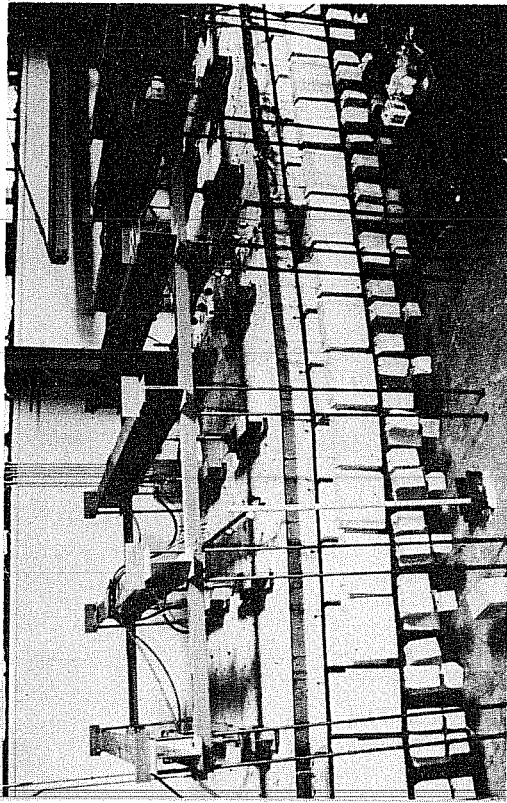


Fig. 7.5. Application of lane load

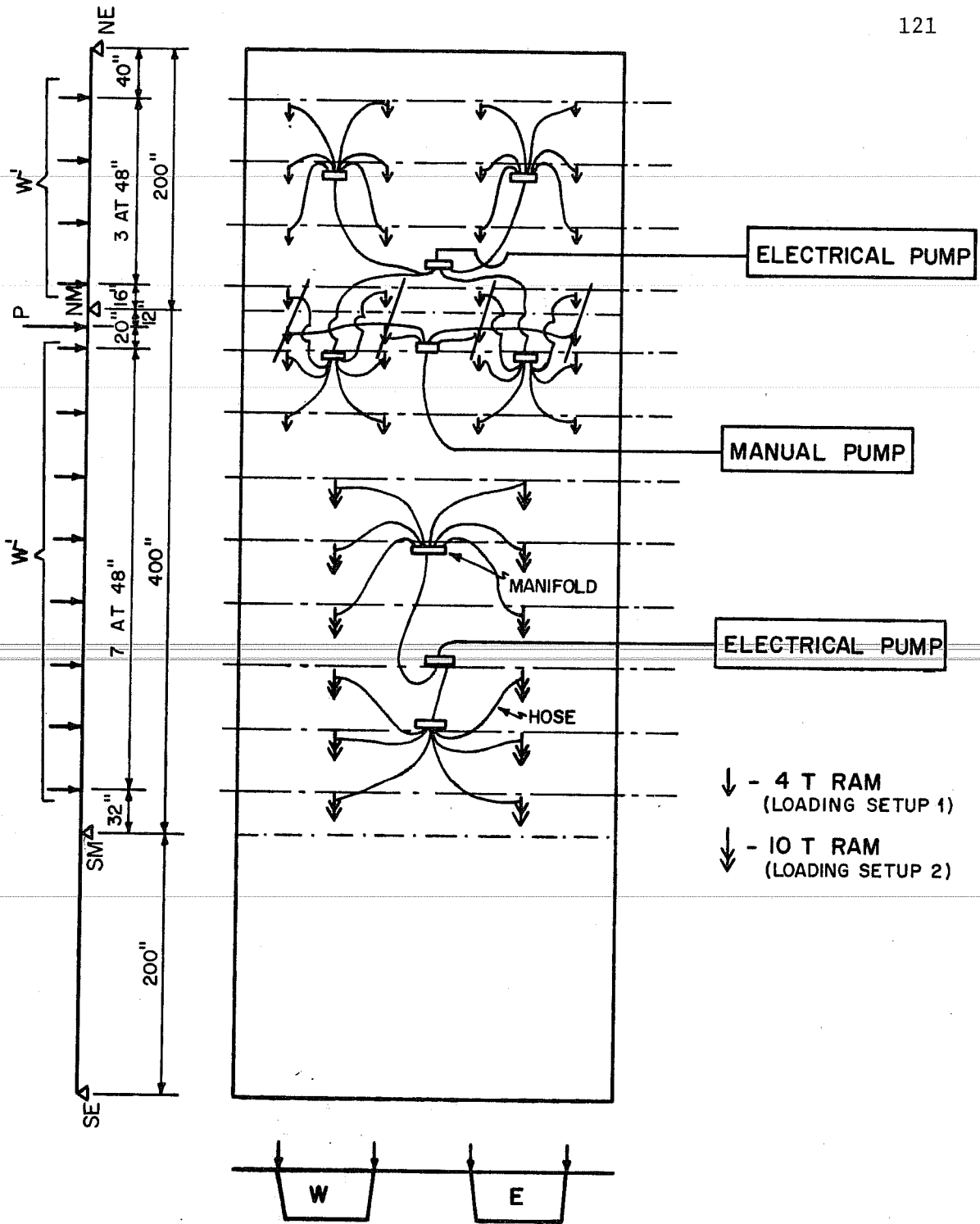
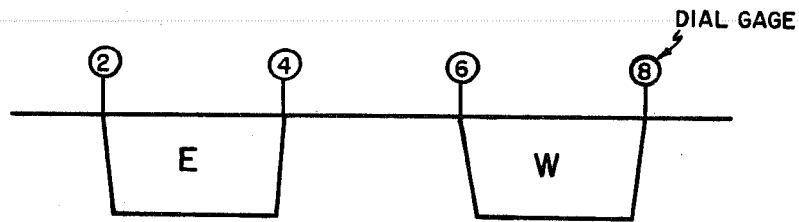
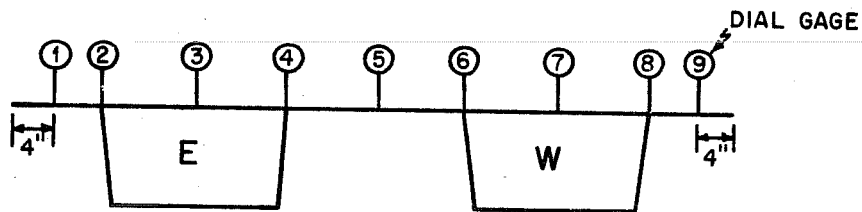


Fig. 7.6. Arrangement of rams, hoses, manifolds and pumps



CASE (1) - 4 DIAL GAGES



CASE (2) - 9 DIAL GAGES

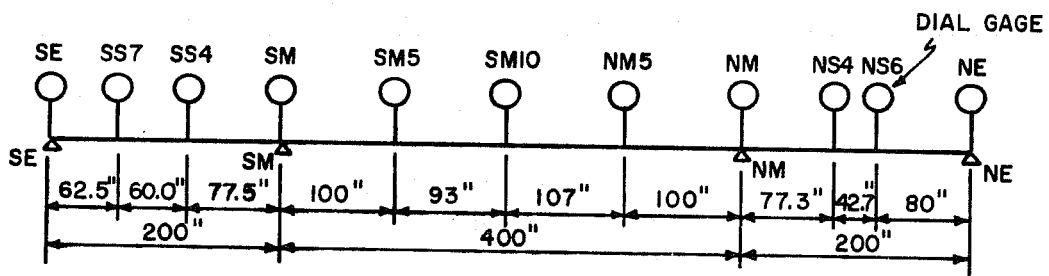


Fig. 7.7. Locations of dial gage readings

cells were only placed under two webs (a box) at each outer support, since only a limited number of load cells were available. These reaction readings are generally sufficient because most of the loadings were applied uniformly (four lane loads). In the case of two lane loadings, the same type of loadings were repeated on the opposite side to allow reactions for four webs to be determined, taking advantage of symmetry. Pancake load cells were used to measure the reactions in service load tests. The area of neoprene pad support was only  $2 \times 2\text{-}1/2$  in. ( $1/4$  in. thick), since the pancake load cell is small. For the ultimate loadings, the area of the pier neoprene pad used was exactly as scaled down from the prototype. Pads were  $2 \times 4\text{-}5/32$  in. ( $1/4$  in. thick) and the diameter of the load cell which supported the bearing plate was  $2\text{-}1/2$  in., as shown in Fig. 7.8. Load cells used for the ultimate load test were not as sensitive as the pancake load cells.

Prior to any loading test,  $1/4$  of service load was preloaded in order to get stable initial readings.

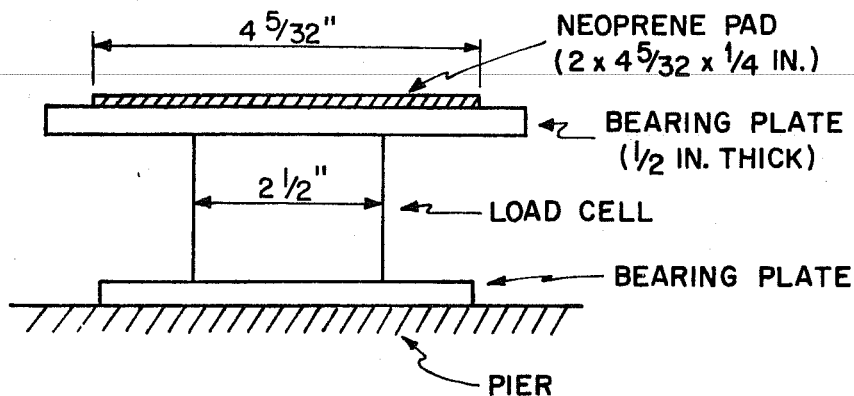


Fig. 7.8. Load cell to measure the reaction at ultimate loading

### 7.3 Test Results and Interpretations

#### 7.3.1 General

The results of deflection, strain, and reaction measurements are compared with solutions of BMCOL50<sup>22</sup> and MUPDI<sup>28</sup> programs.

BMCOL50 is a beam type analysis program which solves the linearly elastic beam or column by a discrete element analysis procedure. This program takes into account variable loads and non-linear supports. Load-deflection relations for each neoprene pad were measured and these values were input to BMCOL50 as the spring constant at the supports.

MUPDI is a versatile generalized elastic analysis program which can analyze folded plate or box structures with interior rigid diaphragms or supports using folded plate theories which consider cross section warping.

Although BMCOL50 can treat variable sections, the section for MUPDI has to be uniform. For MUPDI all sections were assumed uniform in the analysis because the effect of variations in the sections should be small (thickened bottom slabs only at main pier and 1st segments from main pier). BMCOL50 was used for uniform loadings (four lane loadings) and MUPDI was used primarily for two lane loadings or in the transverse moment study. To check the performance of MUPDI and compare it with BMCOL50, it was also run for one uniform loading case.

All external and thickness dimensions for each member of typical box sections were measured for several segments and averaged section properties were calculated by the BOX2 program.<sup>16</sup> These "as built" section properties and the measured properties of the materials used in the theoretical calculations were listed in Table 4.2.



### 7.3.2 Service Loading

#### 7.3.2.1 Four Lane Loadings

(a) **Truck Loading.** Truck loadings (four lanes) were applied in the south side in order to get critical moment at the designer's calculated position, 60 in. from the outer support. The positions of load longitudinally and transversely are shown in Fig. 7.9. Theoretically, additional truck loads should be applied simultaneously in the north side span in order to get the maximum moment at the critical section. But the calculated effect of loadings in the other side span was so small that they could be safely disregarded and truck loads were applied only on one side span.

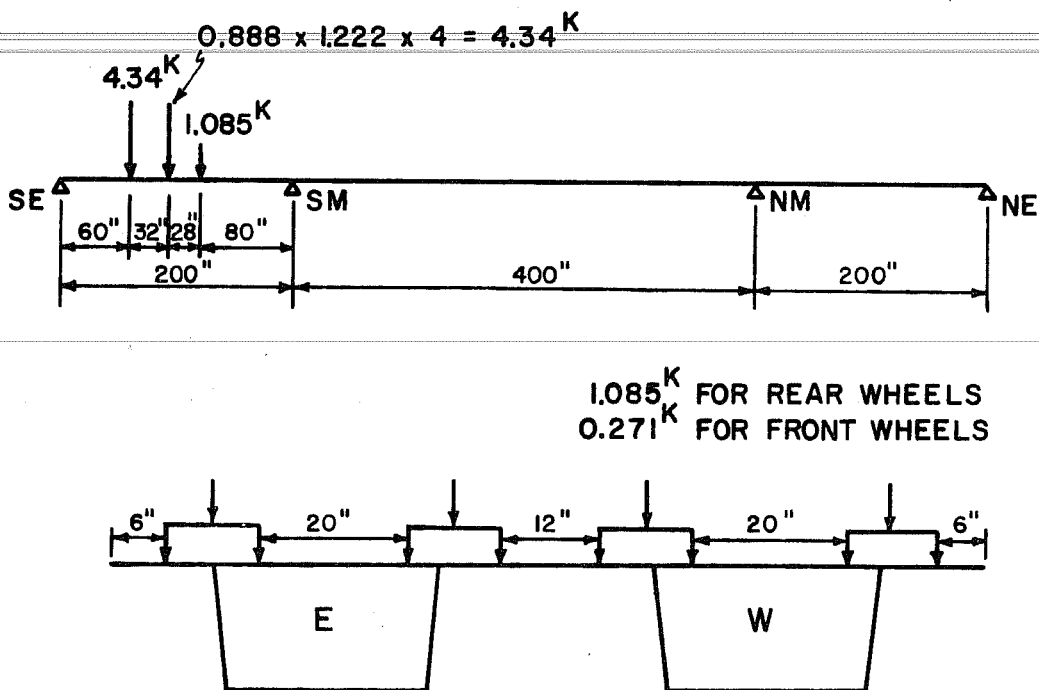


Fig. 7.9. Position of truck loading

As shown in Fig. 7.10, experimental and computed vertical deflections (in longitudinally) agreed very well. However, the deflections of the cantilever slabs and the center of the midstrip closure along the SS7

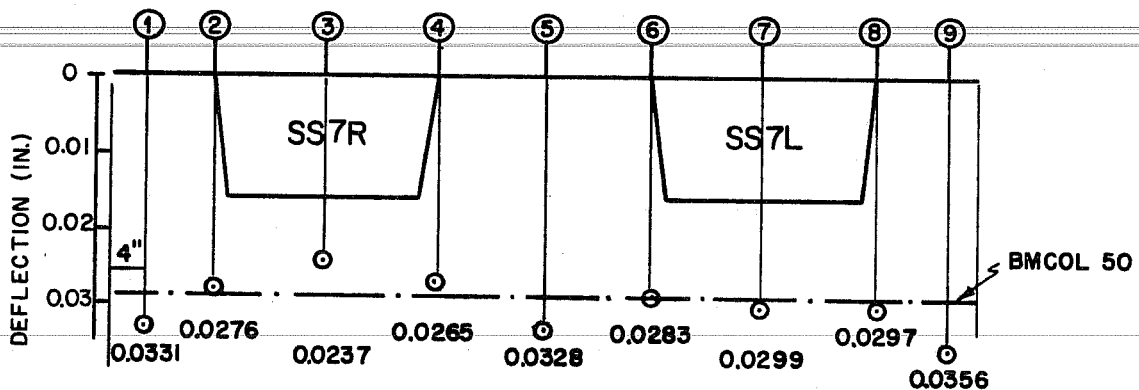
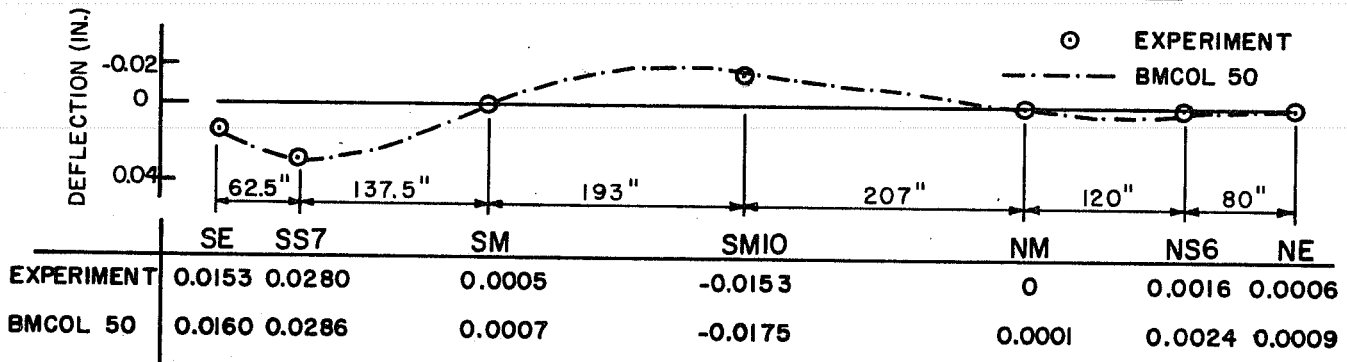
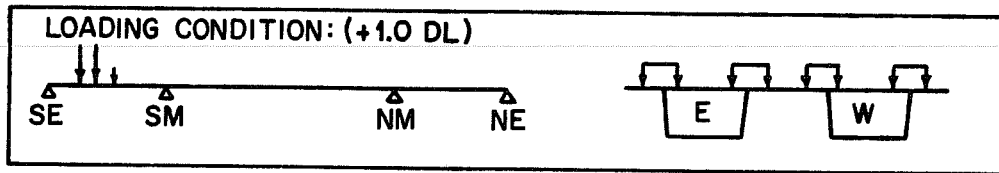


Fig. 7.10. Deflections for truck loadings (four lanes) in side span

segment were larger than predicted by BMCOL50, which does not consider transverse behavior. Although the deflection at (7) in SS7L was equal to that at the top of webs (6) and (8), the deflection at (3) in SS7R was less than that at the webs. This apparently was due to instrumentation errors, because some of the dial gages were tight and acted very slowly. These were replaced in the initial stage of load tests. The deflection/span ratio under full design load was approximately 1/7200 in the side span, which is much smaller than 1/300, which is generally considered as acceptable.



For reactions, experimental and BMCOL50 results, shown in Fig. 7.11, agreed fairly well at the outer support (in loaded span), but did not agree as well on a percentage basis at the far end support because of the very small amount of reaction.

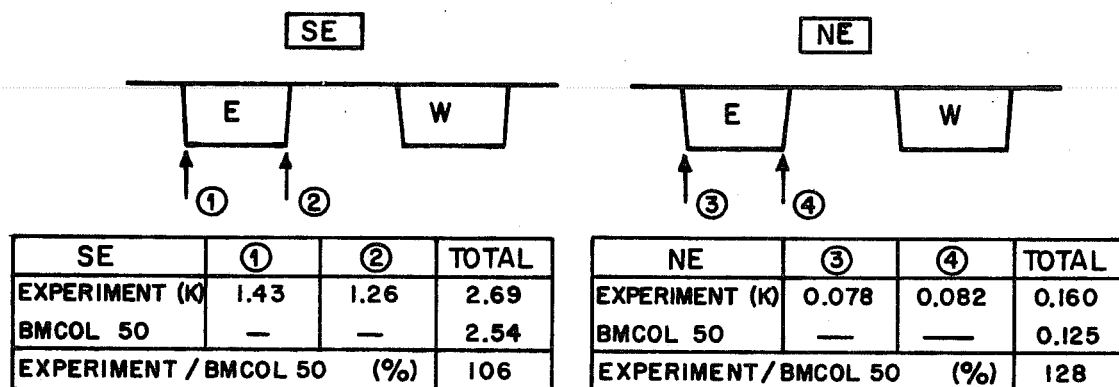


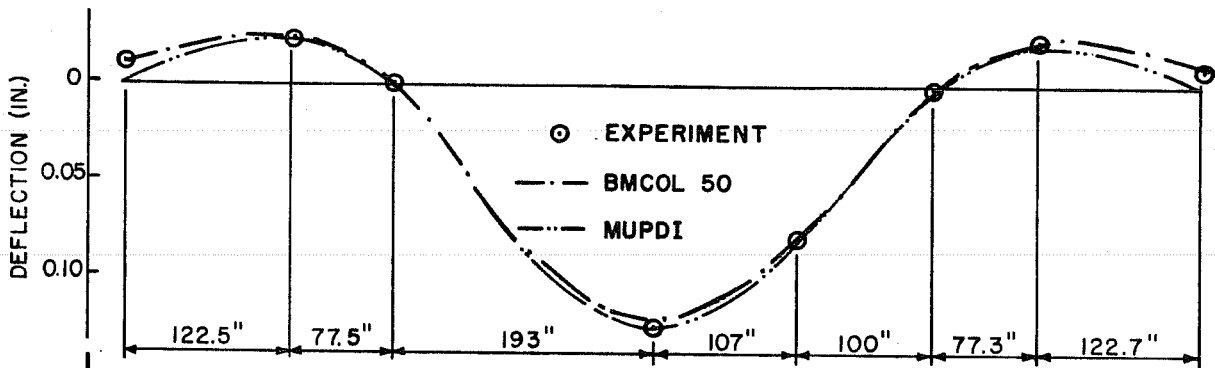
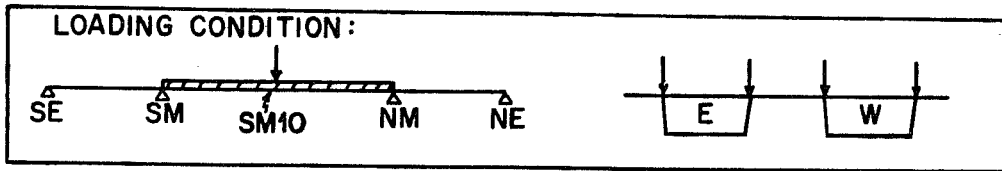
Fig. 7.11. Reactions at outer supports for truck loadings (four lanes) in side span

Strains in the top slab above the webs showed larger values than at midspan of the top slab (see Fig. 7.12). The bottom slab strains were almost uniform. The experimental and BMCOL50 results agreed well generally, except for the inability of BMCOL50 to treat warping.

(b) Lane Loadings. Lane loadings were applied for maximum positive moment in the main span and maximum negative moment at an interior pier. These results are shown in Figs. 7.13 to 7.18.

In comparisons of the experimental and theoretical data for four lane loadings, all instrument readings agreed very well with the theoretical values, especially for the larger values. BMCOL50 showed excellent agreement with the experimental results, especially for longitudinal deflection.

Tensile strains produced by the service level loadings were smaller than the compressive strains produced by prestressing during construction so that the sections remained completely in compression.



	SE	SS4	SM	SM10	NM5	NM	NS4	NE
EXPERIMENT	-0.0127	-0.0241	0.0015	0.127	0.0781	0.0016	-0.0236	-0.0112
BMCOL 50	-0.0114	-0.0256	0.0016	0.124	0.0813	0.0016	-0.0256	-0.0114
MUPDI	0	-0.0226	0	0.129	0.0839	0	-0.0226	0

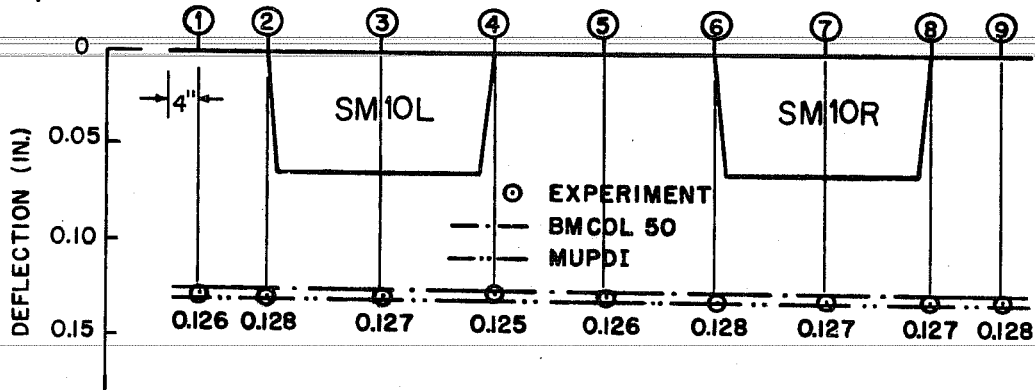
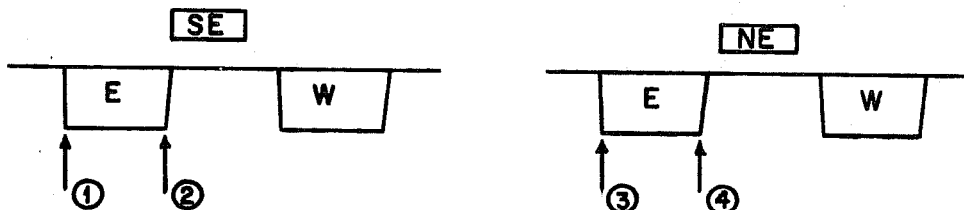


Fig. 7.13. Deflections for lane loadings (four lanes) in main span



SE	①	②	TOTAL
EXPERIMENT (K)	-0.583	-0.670	-1.253
BMCOL 50	—	—	-1.24
EXPERIMENT/BMCOL 50 (%)			101

NE	③	④	TOTAL
EXPERIMENT (K)	-0.658	-0.672	-1.33
BMCOL 50	—	—	-1.24
EXPERIMENT/BMCOL 50 (%)			107

Fig. 7.14. Reactions at outer supports for lane loadings (four lanes) in main span

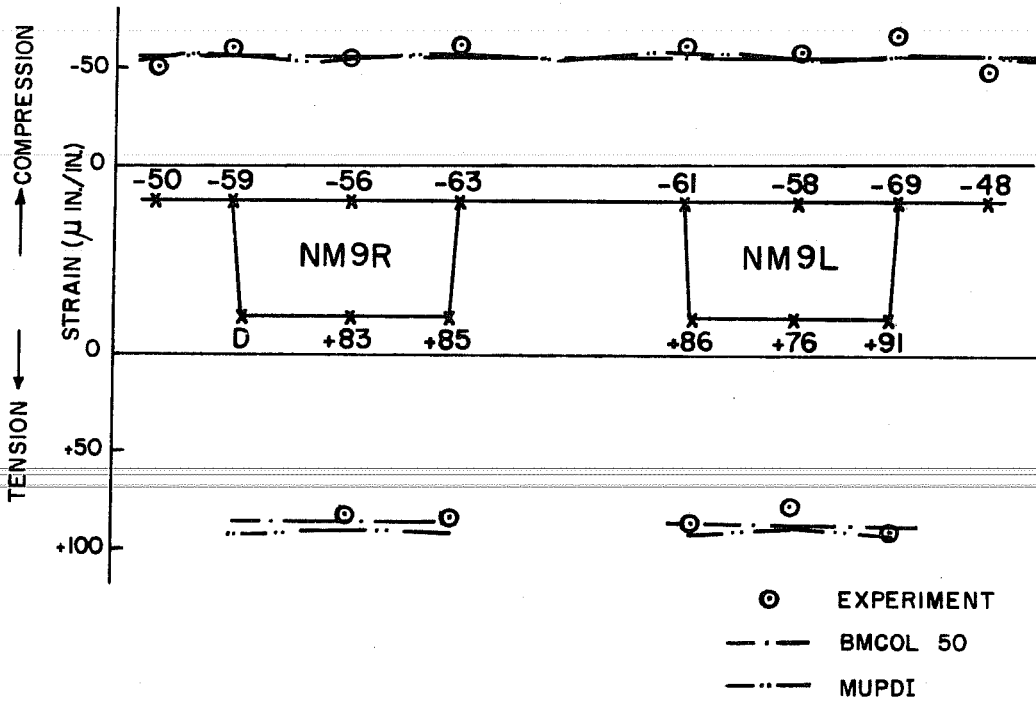
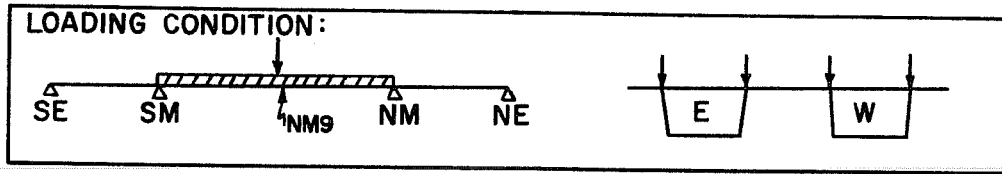
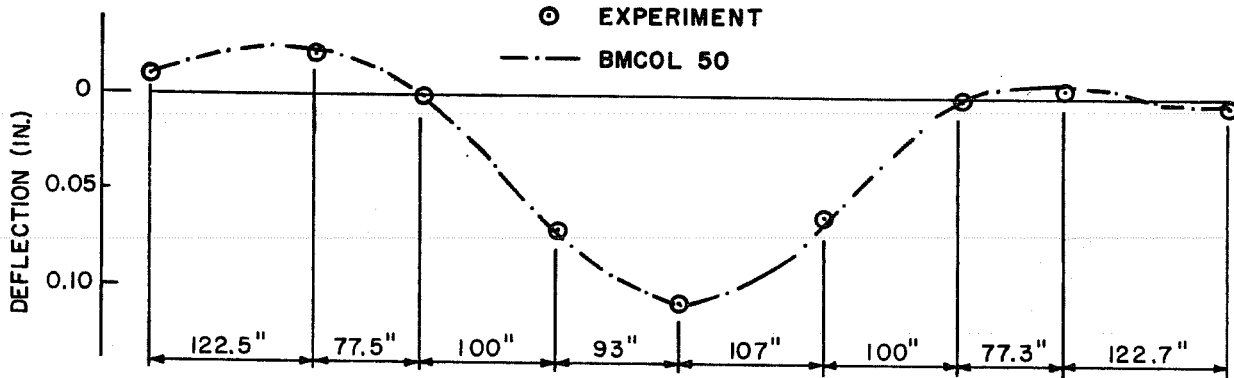
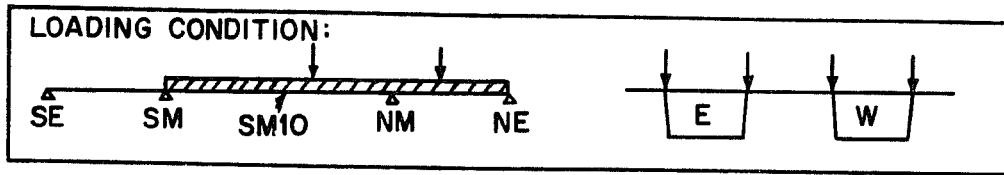


Fig. 7.15. Longitudinal strains along NM9 for lane loadings (four lanes) in main span



	SE	SS4	SM	SM5	SM10	NM5	NM	NS4	NE
EXPERIMENT	-0.0099	-0.0207	+0.0016	+0.0699	+0.107	+0.0641	+0.0023	-0.0035	+0.0035
BMCOL 50	-0.0106	-0.0268	+0.0014	+0.0703	+0.106	+0.0620	+0.0027	-0.0056	+0.0042

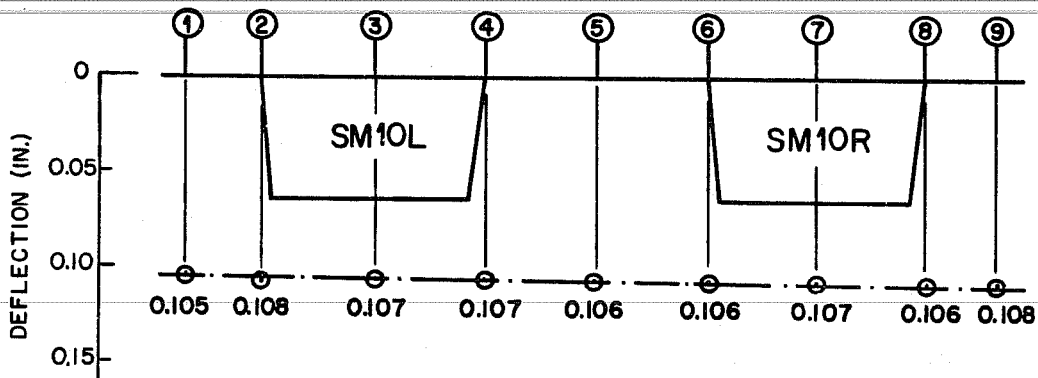
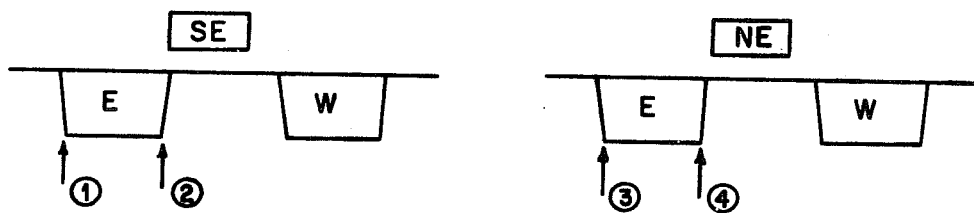


Fig. 7.16. Deflections for lane loadings (four lanes) in main and one side span



SE	①	②	TOTAL
EXPERIMENT (K)	-0.550	-0.570	-1.120
BMCOL 50	—	—	-1.08
EXPERIMENT / BMCOL 50 (%)			104

NE	③	④	TOTAL
EXPERIMENT (K)	0.312	0.272	0.584
BMCOL 50	—	—	0.516
EXPERIMENT / BMCOL 50 (%)			113

Fig. 7.17. Reactions at outer supports for lane loadings in main and one side span

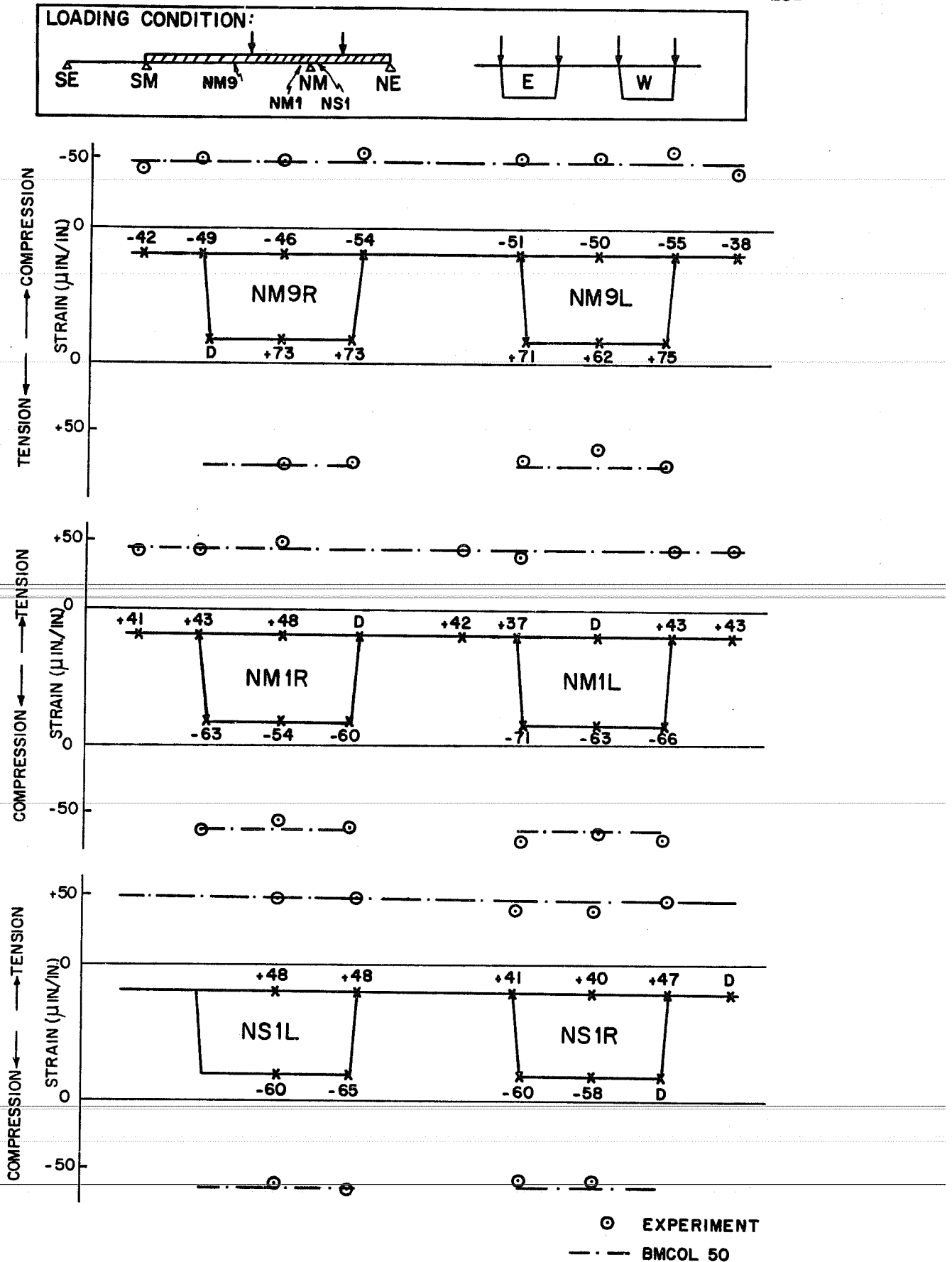


Fig. 7.18. Longitudinal strains for lane loadings (four lanes) in main and one side span



The deflection/span ratio under full design service loads was approximately 1/3200 in the main span. This value is much smaller than 1/300 which is generally considered as acceptable.

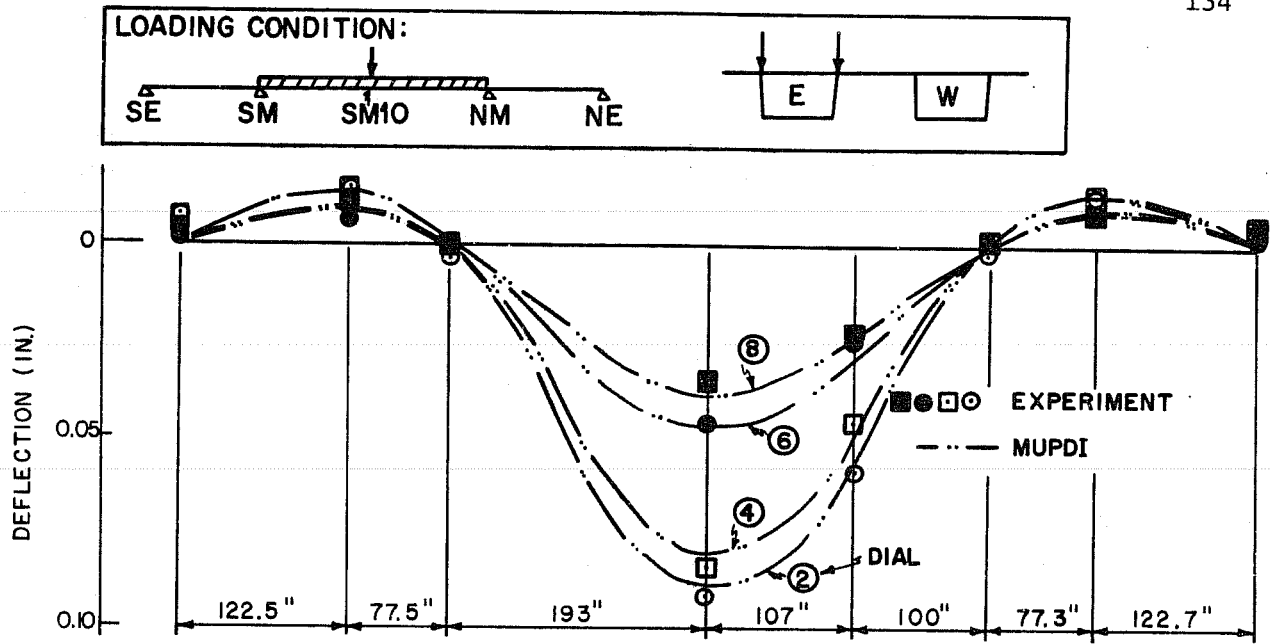
It is very difficult to determine possible warping or shear lag from the experimental data, because the low magnitude strain readings are very sensitive to the exact position of strain gages and dimensional placement tolerances. By observing the results of the strain readings, it appeared that there was some effect of shear lag on the top slab, but it was negligible for design purposes. The twin box sections were generally acting as a beam and little warping occurred. Comparison of the predicted strains using BMCOL50 and MUPDI in Fig. 7.15 show this effect would be expected to be negligible.

Although no special instrumentation was included for the critical shear stress locations, the maximum shear loading case was also applied. There was no visible diagonal tension cracking around the NM pier and no slip at the joints.

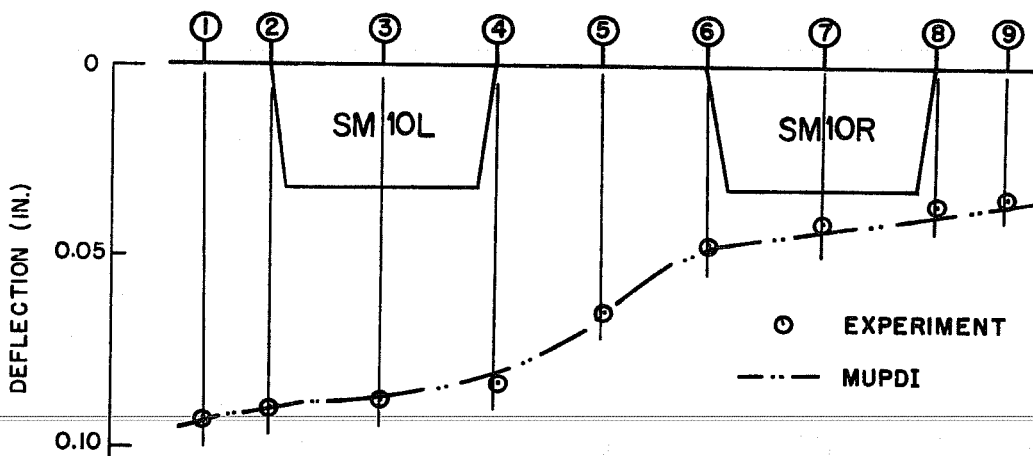
#### 7.3.2.2 Two Lane Loadings (Loads on One Box)

Two lanes on one side of the bridge were loaded with lane loadings to produce the critical moment at the midspan of the main span and then at the main pier. Test results for deflections and strains were compared with the results of MUPDI, since BMCOL50 cannot treat unsymmetrical loading across the section.

Comparison of the theoretical and experimental deflection and strain diagrams (Figs. 7.19, 7.20, 7.22, and 7.23) show that experimental results and the MUPDI analysis agreed very well in general. Approximately one-third of the load was distributed to the unloaded box section around midspan of the main span. Loading only in the main span was more critical transversely than was loading of both main and side spans. The far side webs away from the loaded box raised up at the main supports in both loading cases.



		SE	SS4	SM	SM10	NM5	NM	NS4	NE
EXPERIMENT	②	-0.0068	-0.0140	+0.0029	+0.0913	+0.0586	+0.0019	-0.0125	-0.0057
	④	-0.0072	-0.0150	+0.0007	+0.0834	+0.0465	+0.0004	-0.0118	-0.0064
	⑥	-0.0013	-0.0067	+0.0002	+0.0463	+0.0239	+0.0013	-0.0089	-0.0033
	⑧	-0.0039	-0.0089	-0.0006	+0.0363	+0.0227	-0.0005	-0.0091	-0.0036
MUPDI	②	0	-0.0137	0	+0.0895	+0.0588	0	-0.0137	0
	④	0	-0.0143	0	+0.0811	+0.0524	0	-0.0143	0
	⑥	0	-0.0083	0	+0.0479	+0.0316	0	-0.0083	0
	⑧	0	-0.0090	0	+0.0394	+0.0251	0	-0.0090	0



	①	②	③	④	⑤	⑥	⑦	⑧	⑨
EXPERIMENT	0.0931	0.0913	0.0875	0.0834	0.0653	0.0463	0.0408	0.0363	0.0339
MUPDI	0.0925	0.0895	0.0858	0.0811	0.0646	0.0473	0.0430	0.0389	0.0368

Fig. 7.19. Deflections for lane loadings (two lanes) in main span

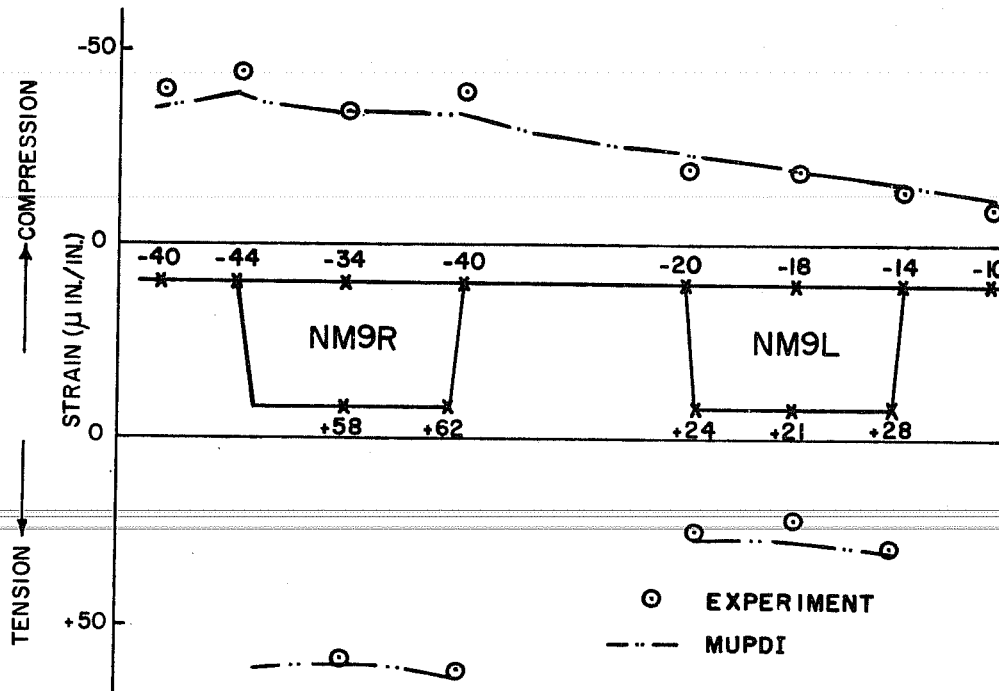
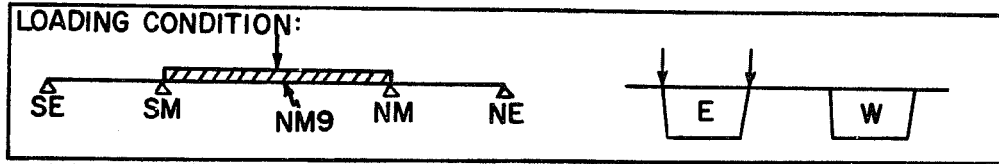


Fig. 7.20. Longitudinal strains along NM9 for lane loadings (two lanes) in main span

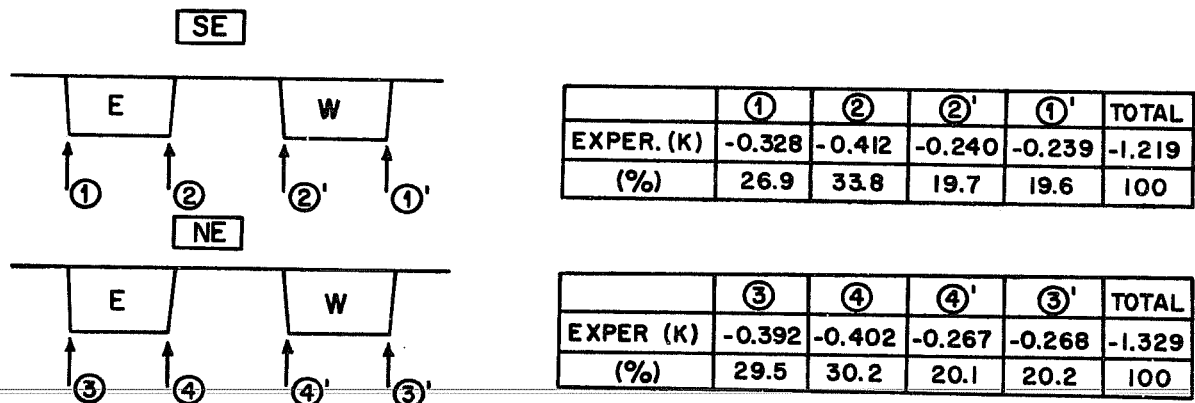
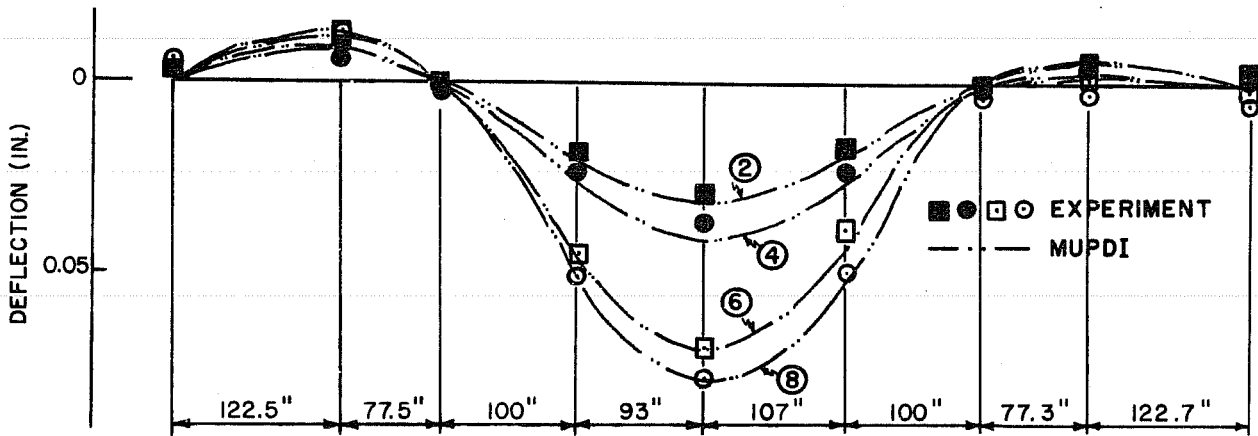
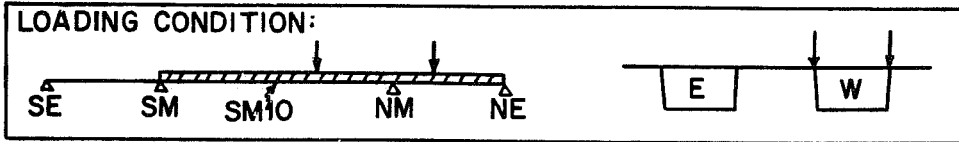
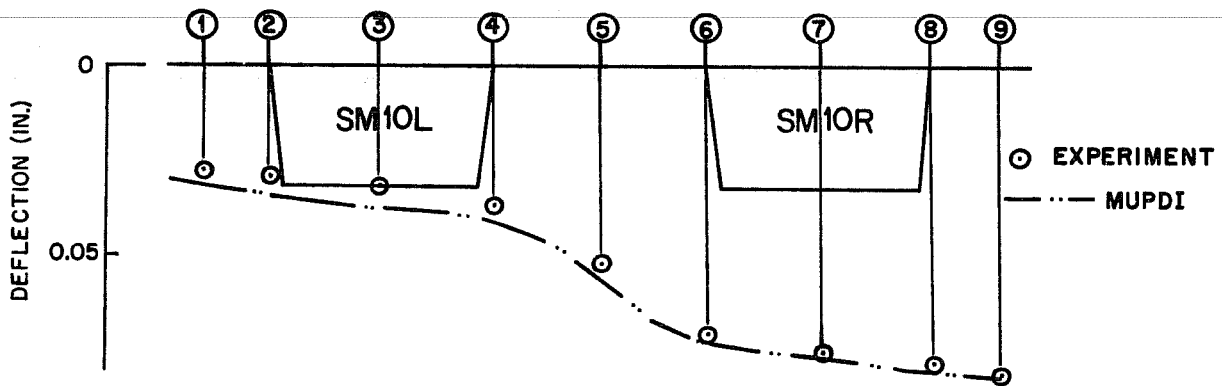


Fig. 7.21. Reactions at outer supports for lane loadings (two lanes) in main span



		SE	SS4	SM	SM5	SM10	NM5	NM	NS4	NE
EXPERIMENT	②	-0.0033	-0.0080	-0.0005	+0.0193	+0.0296	+0.0175	-0.0010	-0.0046	-0.0029
	④	-0.0025	-0.0060	+0.0016	+0.0234	+0.0368	+0.0232	+0.0010	-0.0032	-0.0007
	⑥	-0.0022	-0.0138	+0.0020	+0.0455	+0.0698	+0.0386	+0.0010	-0.0005	+0.0029
	⑧	-0.0050	-0.0129	+0.0018	+0.0513	+0.0775	+0.0501	+0.0038	+0.0031	+0.0061
MUPDI	②	0	-0.0080	0	+0.0218	+0.0339	+0.0209	0	-0.0063	0
	④	0	-0.0073	0	+0.0277	+0.0417	+0.0270	0	-0.0048	0
	⑥	0	-0.0129	0	+0.0467	+0.0713	+0.0461	0	-0.0014	0
	⑧	0	-0.0123	0	+0.0526	+0.0791	+0.0521	0	0	0



	①	②	③	④	⑤	⑥	⑦	⑧	⑨
EXPERIMENT	0.0276	0.0296	0.0321	0.0368	0.0522	0.0698	0.0739	0.0775	0.0804
MUPDI	0.0315	0.0339	0.0372	0.0417	0.0566	0.0713	0.0756	0.0791	0.0819

Fig. 7.22. Deflections for lane loadings (two lanes) in main and one side span

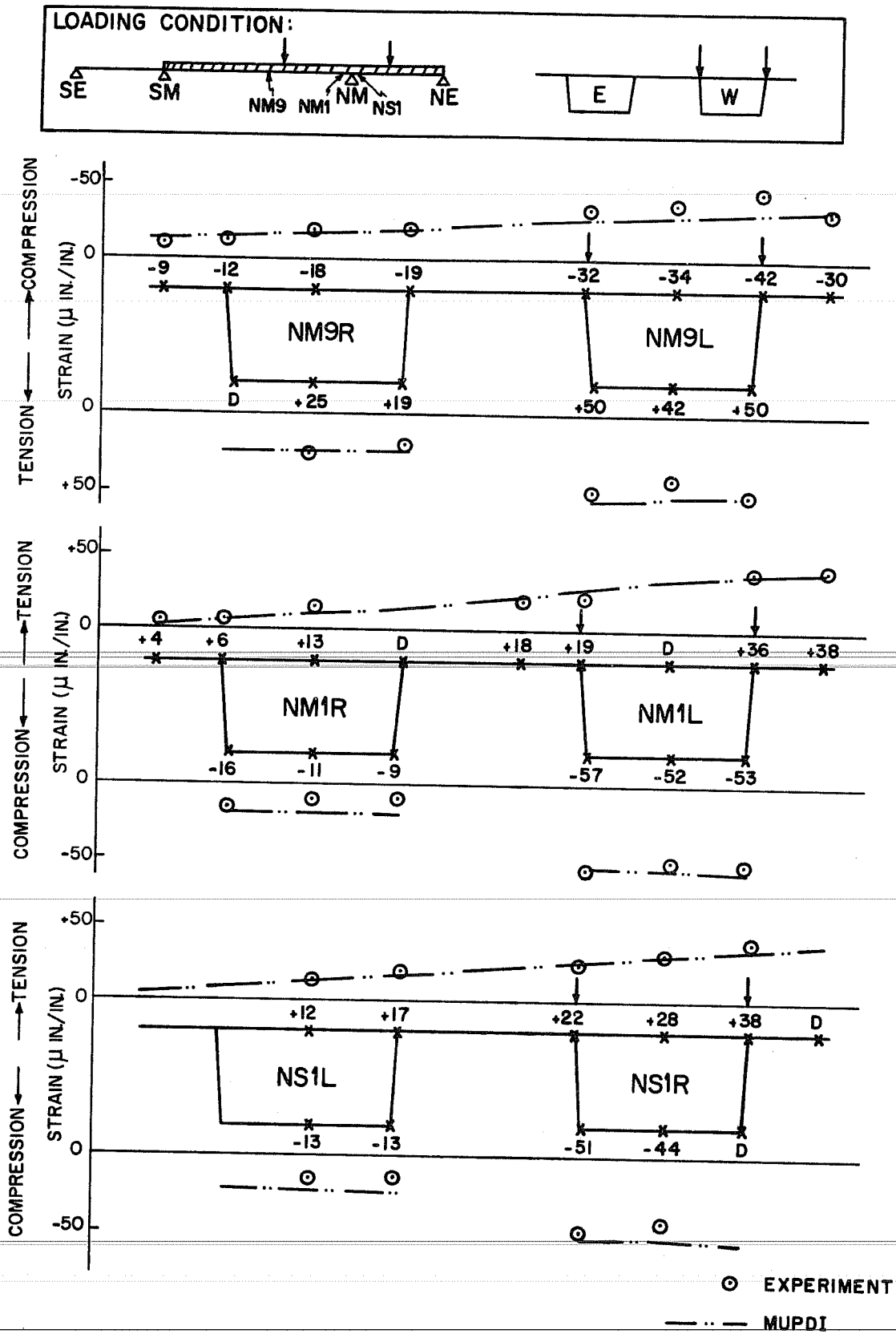


Fig. 7.23. Longitudinal strains for lane loadings (two lanes) in main and one side span

Strains across the bottom slab of each box were fairly uniform because of high torsional rigidity of the box section. But strain across the top slab gradually decreased from one end to the other end. Also, reactions at the outer supports indicated that the loaded box is acting almost as a beam because reactions under the two webs of the box section were almost equal with loading only in the main span (Fig. 7.21). When the loads were applied in both the main and side spans, the end reactions were not uniform under each box of the loaded side span and showed substantial twist effects. However, the reaction under each box was reasonably uniform at the end support of the unloaded side span (Fig. 7.24).

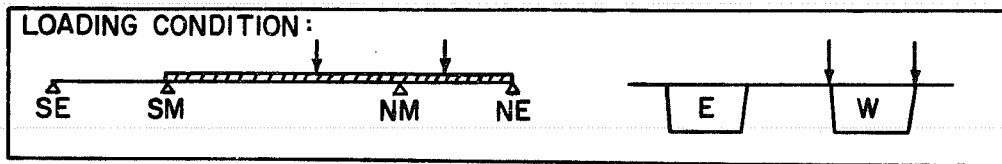
Although the support conditions and section properties input into MUPDI differed slightly from the actual model, MUPDI results agreed very well with the experimental results. Therefore, MUPDI can be used in design to predict the longitudinal load distribution. Transverse moments from these loadings are discussed in Sec. 7.3.4 and are compared with MUPDI.

### 7.3.3 Ultimate Design Loading Specified by BPR Criteria

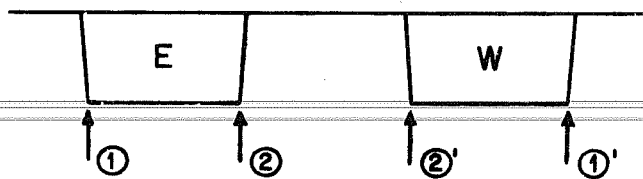
#### 7.3.3.1 Additional 0.35 DL

Ultimate design dead load is specified as 1.35 DL by BPR.<sup>7</sup> The additional 0.35 DL was applied to the structure by using additional concrete blocks to supplement the previously adjusted 1.0 DL segment weight. Typical arrangement of concrete blocks per box is shown in Fig. 7.25. These blocks were permanently added to the bridge, so 1.35 DL has to be considered as the effective dead load in all later tests.

The experimental results are generally larger than the theoretical values for both deflection and reactions, as shown in Figs. 7.26 and 7.27. Strain readings show considerable scatter and do not agree with the theoretical values, as shown in Fig. 7.28. The maximum moment due to loading is less than that due to the service live load producing maximum

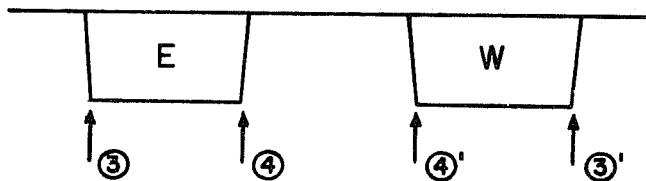


SE



SE	①	②	②'	①'	TOTAL
EXPERIMENT (K)	-0.239	-0.197	-0.347	-0.314	-1.097
(%)	21.8	18.0	31.6	28.6	100

NE



NE	③	④	④'	③'	TOTAL
EXPERIMENT (K)	-0.170	-0.067	0.334	0.486	+0.583
(%)	-29.1	-11.5	57.3	83.3	100

Fig. 7.24. Reactions at outer supports for lane loadings (two lanes) in main and one side span

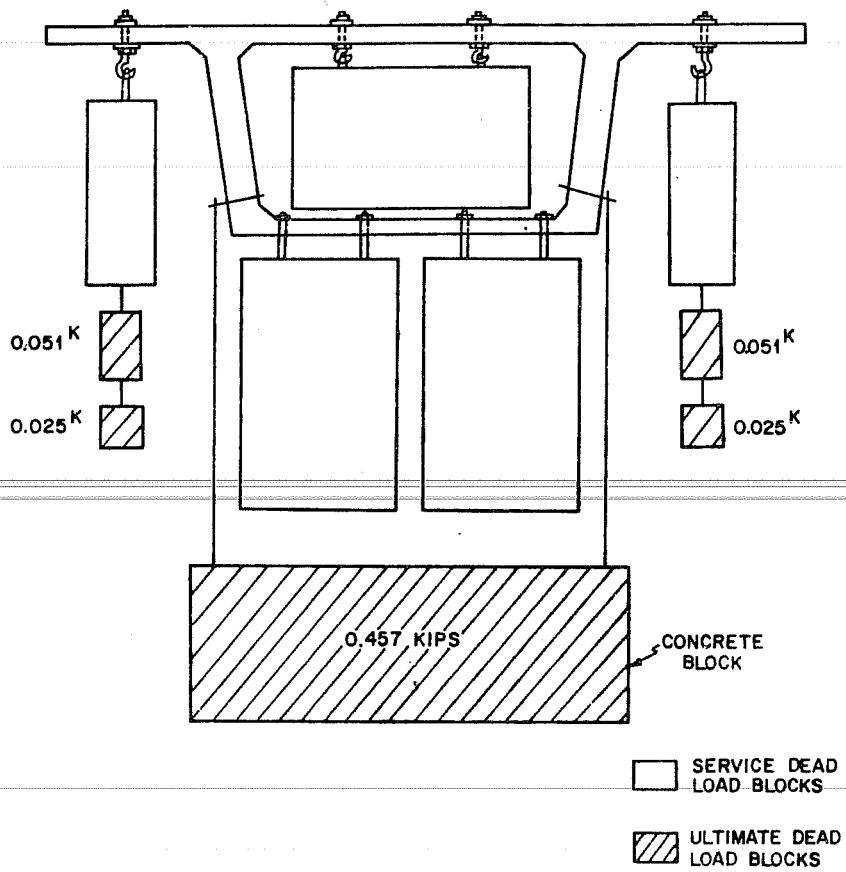


Fig. 7.25. Concrete blocks for 0.35 DL



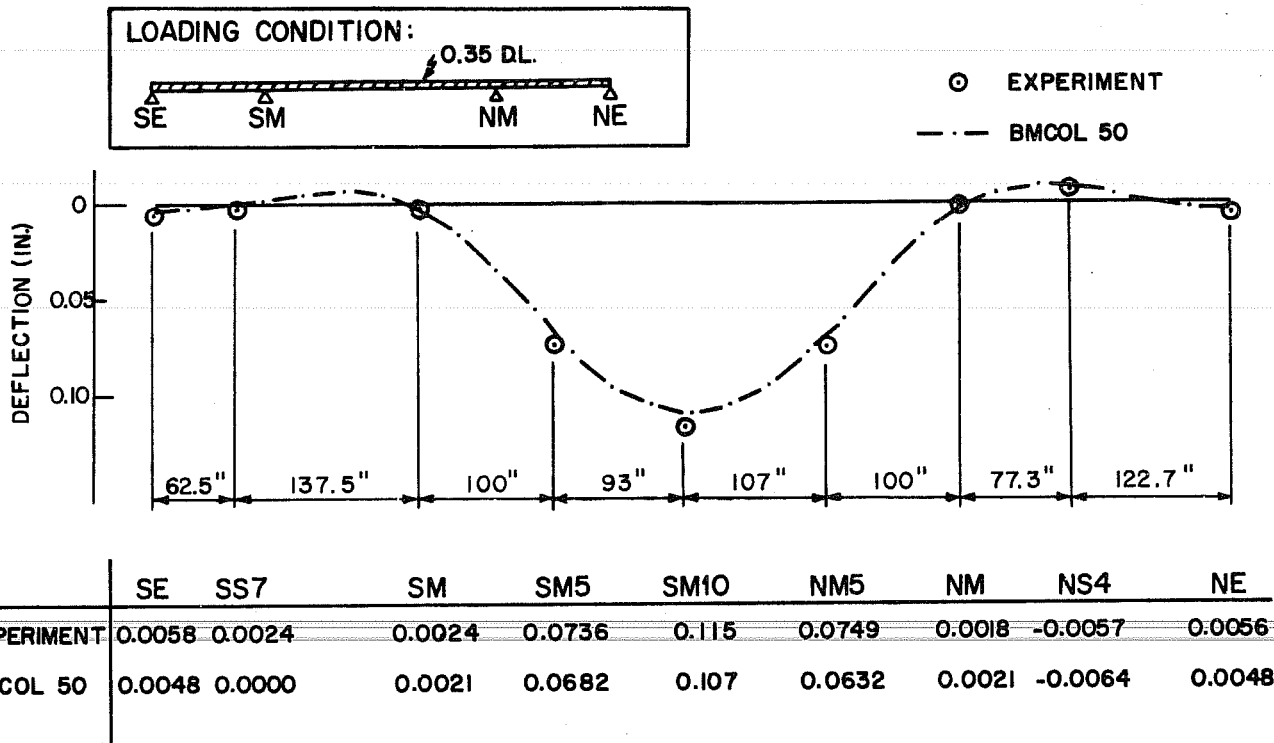


Fig. 7.26. Deflections for 0.35 DL

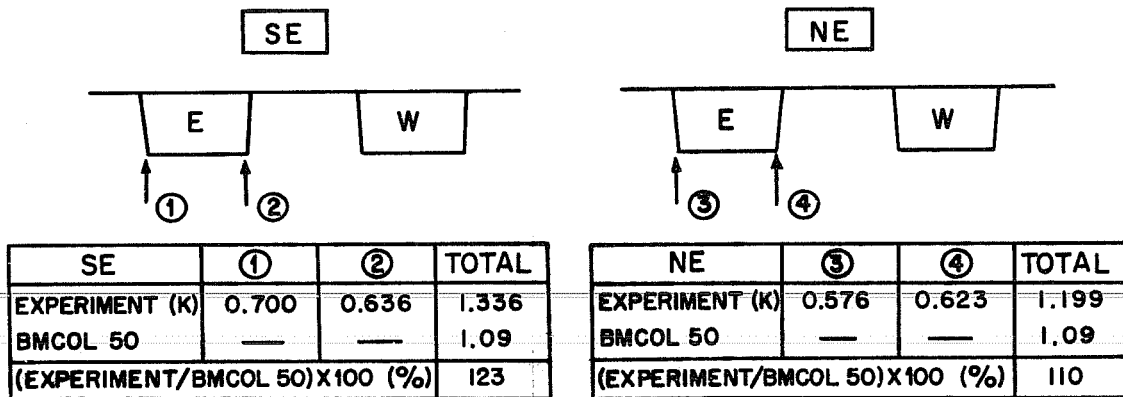


Fig. 7.27. Reactions at outer supports for 0.35 DL



positive moment at midspan of the main span. Thus, the bridge should still be in the elastic range. Deviation of the experimental results from the theoretical values is probably due to temperature and time variations in the electrical data recording instruments (it took about 10 hours to hang all concrete blocks).

### 7.3.3.2 Maximum Positive Moment, Main Span

As shown by the deflection diagram of Fig. 7.29, the measured deflections at midspan in the main span were slightly larger than the theoretical values calculated by BMCOL50. Increase of deflection at midspan of the main span was linear up to the  $(1.35 \text{ DL} + 0.75 \text{ (LL} + \text{IL)})$  increment and started to change slope as the load increased. An appreciable change in slope was noted with formation of the first crack at  $(1.35 \text{ DL} + 1.75 \text{ (LL} + \text{IL)})$ . The increase of deflection at the increment of  $(1.35 \text{ DL} + 2.25 \text{ (LL} + \text{IL)})$  was very large and the outer supports raised up suddenly, as shown in Fig. 7.30. The deflection at the midspan of the main span did not immediately come back to its original value after releasing load. However, it recovered almost completely after several hours.

Figure 7.31 shows the increase of end reactions was linear up to the  $(1.35 \text{ DL} + 1.25 \text{ (LL} + \text{IL)})$  increment and agreed with the theoretical values very well up to that point. The actual reactions become zero at about  $2.13 \text{ (LL} + \text{IL)}$ , which is less than the actual design ultimate if advantage is taken of the 25 percent design load reduction for a four lane bridge.

From the strain diagrams shown in Fig. 7.32, it can be seen that the rate of strain increase did not change very much up to the  $(1.35 \text{ DL} + 1.5 \text{ (LL} + \text{IL)})$  level. Strain at the outer edges of the top slab was consistently less than the other positions. Strains along the bottom slab in the service loading test (Fig. 7.15) were almost uniform, but there was some deviation in this test even if the amount of live load was small. Strains in the bottom slab (tension side) started to deviate substantially

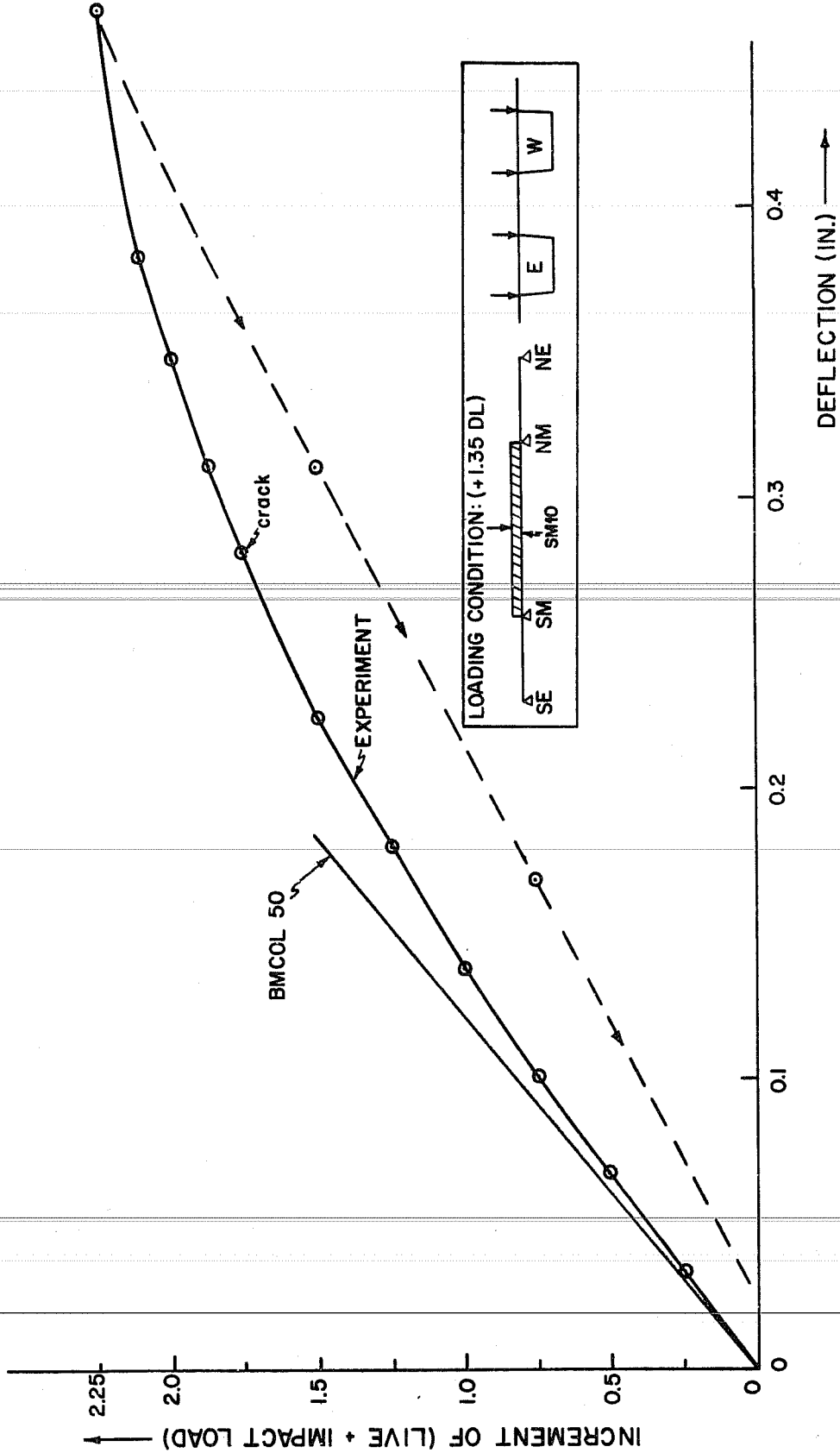
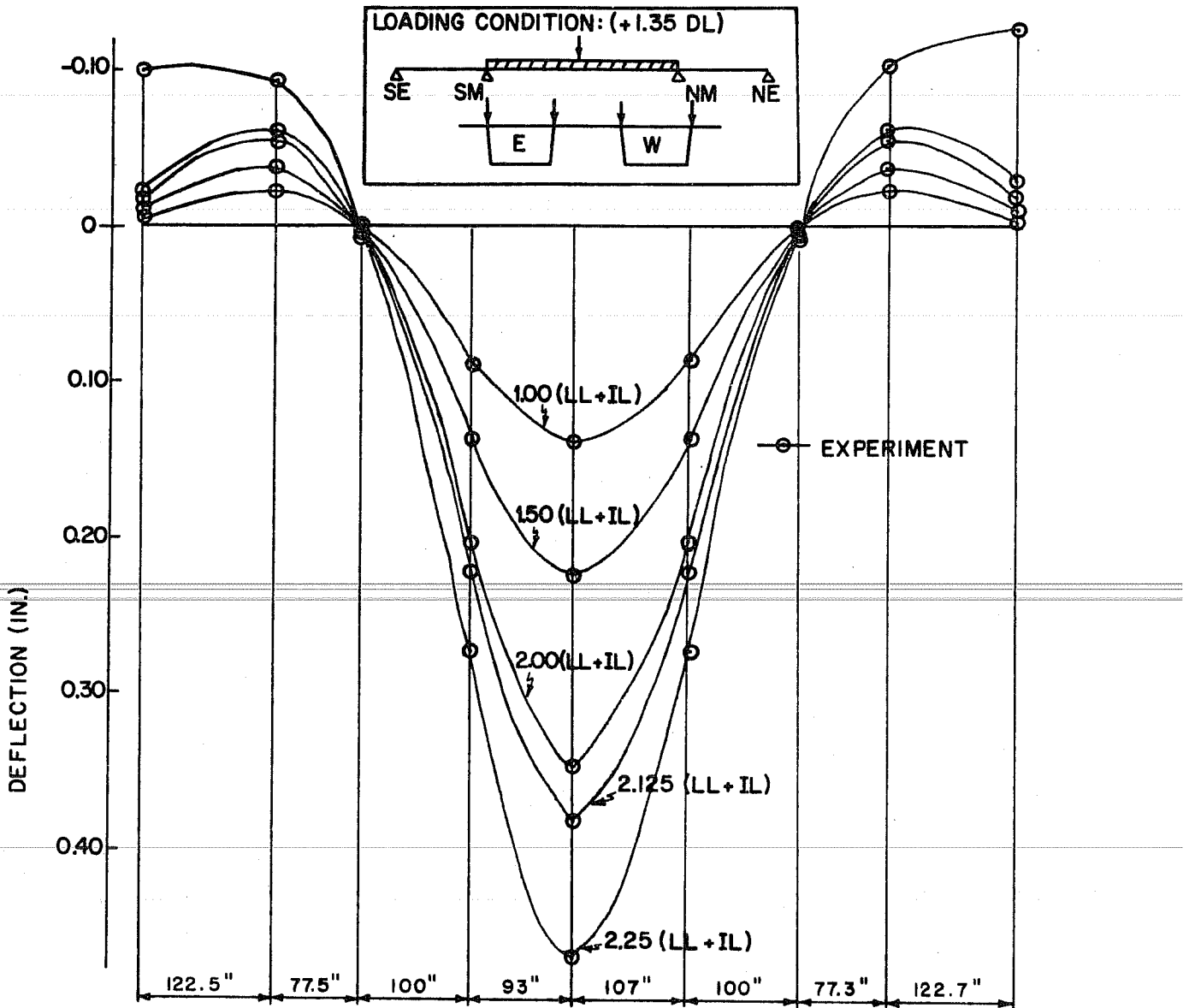


Fig. 7.29. Deflections at SM10 for lane loadings (four lanes) in main span (design ultimate)



(LL+IL)	SE	SS4	SM	SM5	SM10	NM5	NM	NS4	NE
1.00	-0.0041	-0.0229	+0.0013	+0.086	+0.137	+0.083	+0.0014	-0.0239	-0.0049
1.50	-0.0079	-0.0367	+0.0025	+0.136	+0.224	+0.134	+0.0020	-0.0381	-0.0090
2.00	-0.0155	-0.0553	+0.0048	+0.203	+0.348	+0.202	+0.0032	-0.0563	-0.0175
2.125	-0.0229	-0.0617	+0.0052	+0.221	+0.382	+0.221	+0.0038	-0.0637	-0.0321
2.25	-0.101	-0.0948	+0.0059	+0.271	+0.469	+0.272	+0.0040	-0.1038	-0.128

Fig. 7.30. Deflections for lane loadings (four lanes) in main span (design ultimate)

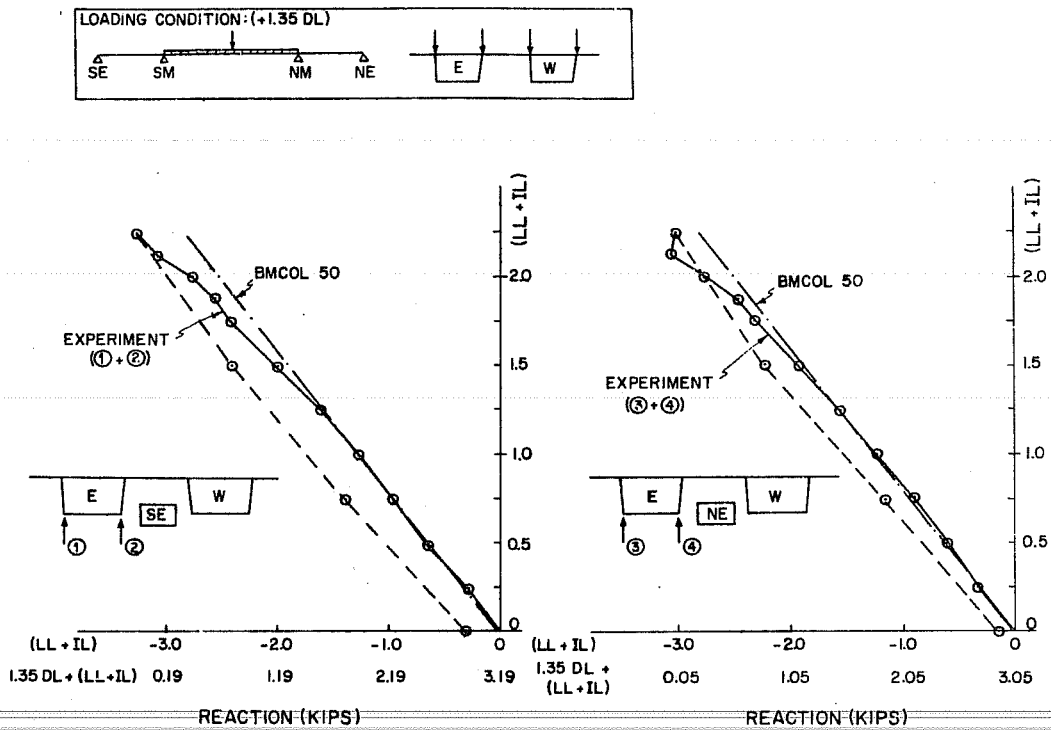


Fig. 7.31. Reactions at outer supports for lane loadings (four lanes) in main span (design ultimate)

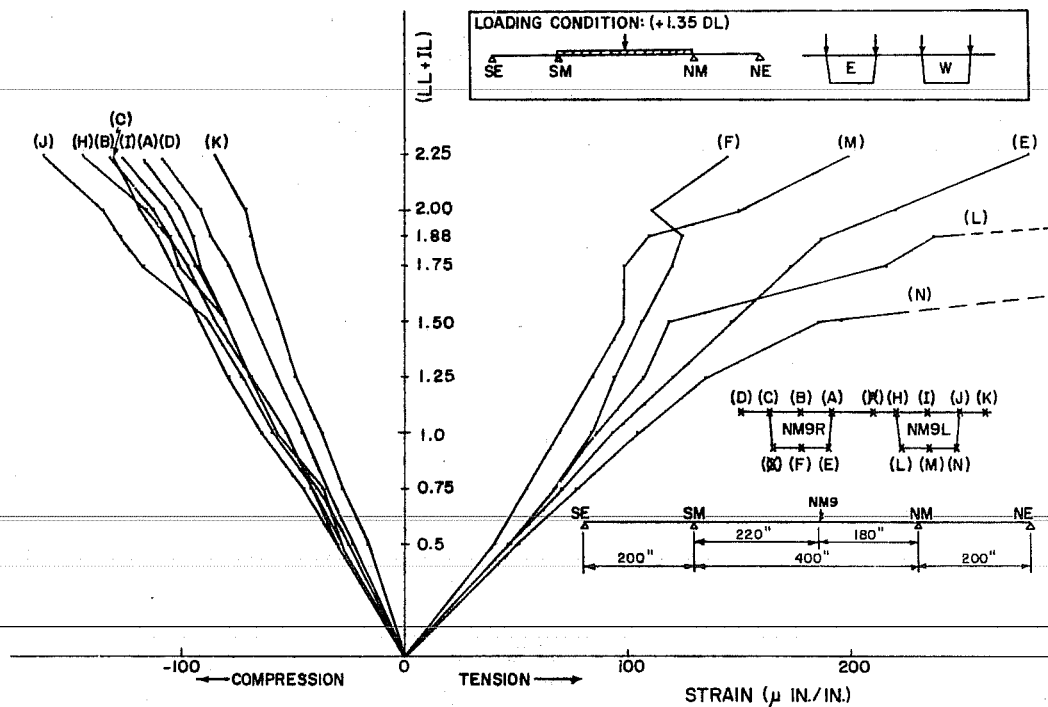


Fig. 7.32. Longitudinal strains along NM9 for lane loadings (four lanes) in main span (design ultimate)

at the (1.35 DL + 1.50 (LL + IL)) increment and varied widely at the (1.35 DL + 1.75 (LL + IL)) level.

As shown in Fig. 7.33, a crack appeared at the center of the closure segment (OE side) at the (1.35 DL + 1.75 (LL + IL)) increment and developed along the joint of the closure segment. On the OW side, the first crack appeared at the (1.35 DL + 1.88 (LL + IL)) increment. At the (1.35 DL + 2.25 (LL + IL)) increment, cracks extended to the midheight of the webs.

The theoretical cracking moment at the closure segment, as predicted by the 1963 ACI Building Code, is calculated as follows:<sup>2</sup>

$$\begin{aligned} M_{cr} &= W_b (f_{pe} + 6\sqrt{f'_c}) - M_s \\ &= 1230 (1.34 + 0.505) - 740 \\ &= 1529 \text{ k-in.} \end{aligned}$$

where,

$W_b$  = section modulus at bottom.

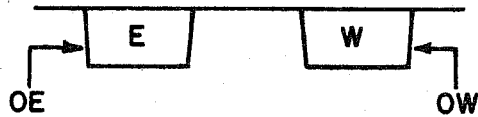
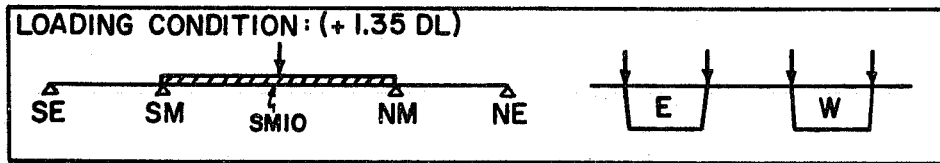
$f_{pe}$  = compressive stress of concrete due to prestressing only at bottom fiber.

$f'_c$  = compressive strength of concrete.

$M_s$  = moment due to end reaction caused by prestressing of the positive tendons in the main span and seating force at the outer supports.

Therefore the LF (load factor) of (LL + IL) for the load at which cracks might appear can be calculated as:

$$M_{cr} = 1.35 M_{DL} + LF \times M_{(LL + IL)}$$



\* NUMBERS ALONG THE CRACK ARE MULTIPLES OF (LL + IL)

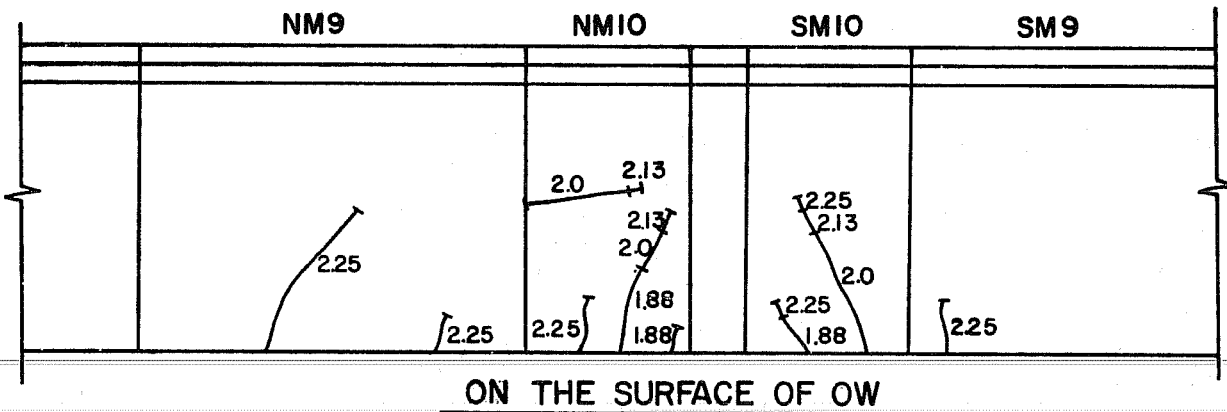
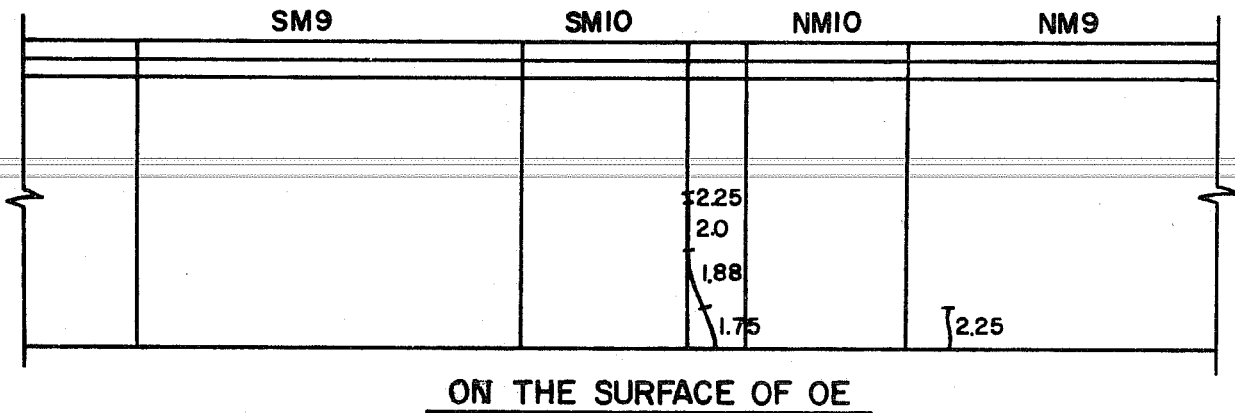


Fig. 7.33. Development of cracks for lane loadings (four lanes) in main span (design ultimate)



$$1529 = 481 + LF \times 552$$

$$LF = 1048/552 = 1.90.$$

Since initial cracks appeared on one web at the  $LF = 1.75$  level and on the other web at the 1.88 increment, the theoretical value (1.35 DL + 1.90 (LL + IL)) was very accurate.

This method of calculation shows that the cracking moment is greatly affected by the adjusting force at the end supports. If the reaction force provided at the end supports is large, midspan cracks will appear at lower increments of (LL + IL). If the adjusting force provided at the end is small, the end segments will raise up from the neoprene pads under very small increments of (LL + IL). Therefore, the end reactions for the prototype bridge should be selected at an optimum point which balances these two factors. Figure 7.34 shows the relation between the initial and reaction applied, the LF of (LL + IL) at which the end segments will raise up from the neoprene pads and the LF of (LL + IL) at which first cracks will appear. Therefore, 4.9 kips (176 kips in the prototype bridge) total for two boxes is the optimum initial reaction at each outer support. Although the weight of the asphalt topping, which is about 8 percent of the weight of the segment, was not included in the model bridge test, the effect of the asphalt is also included in the dead load calculations on which Fig. 7.34 is based.

### 7.3.3.3 Maximum Negative Moment at the Main Pier

Under this loading condition the experimental deflection at midspan in the main span was slightly larger than the theoretical values (BMCOL50), as shown in Fig. 7.35. Increase of deflection was linear up to the (1.35 DL + 0.75 (LL + IL)) increment. Increases of deflection at the unloaded span outer support (SE) became rapid at the (1.35 DL + 2.12 (LL + IL)) increment, as shown in Fig. 7.36.

The trend of strains at the NM9 segment, as shown in Fig. 7.37, was the same as noted in Sec. 7.3.3.2. Strains in the top slab increased almost linearly up to the (1.35 DL + 2.25 (LL + IL)) increment,

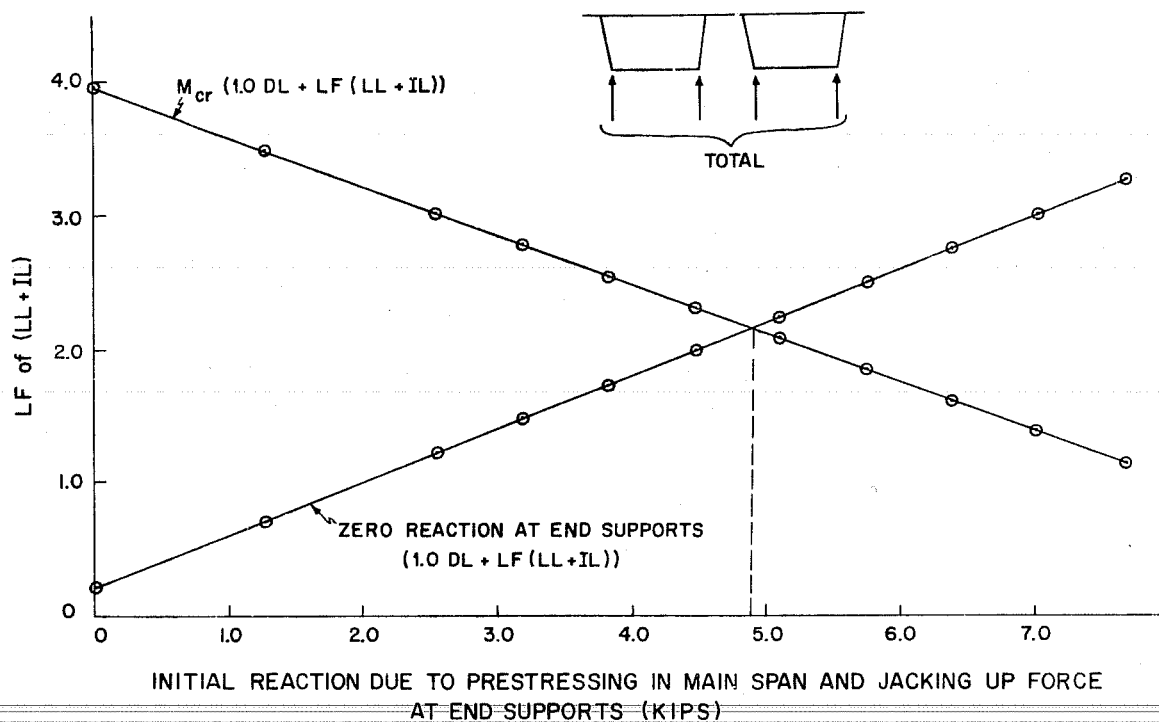


Fig. 7.34. Relation between the end reaction and cracking moment

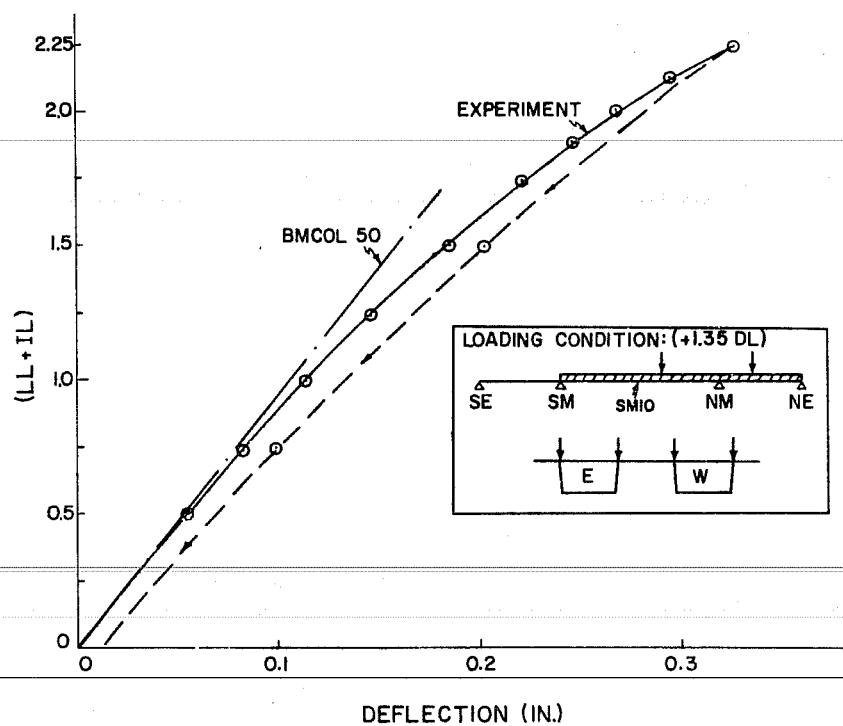
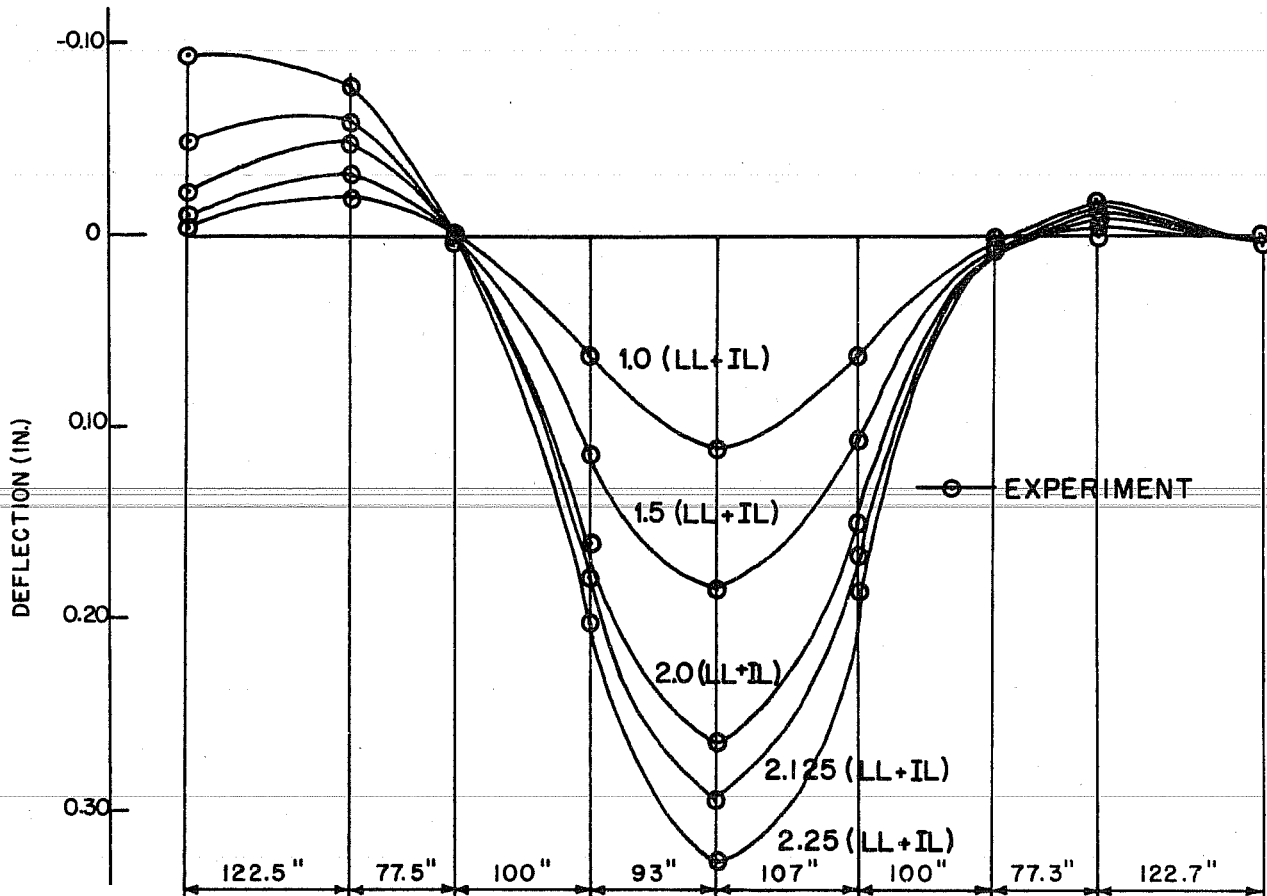
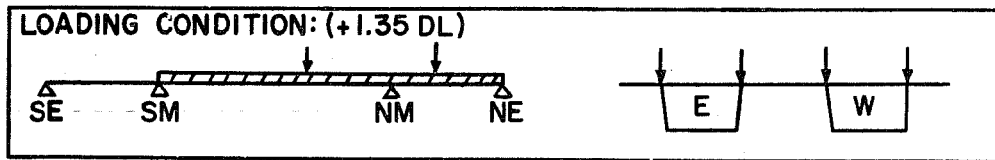


Fig. 7.35. Deflections at SM10 for lane loadings (four lanes) in the main and one side span (design ultimate)



(LL+IL)	SE	SS4	SM	SM5	SM10	NM5	NM	NS4	NE
1.00	-0.0035	-0.0203	+0.0007	+0.0727	+0.113	+0.0641	+0.0023	-0.0032	+0.0014
1.50	-0.0073	-0.0311	+0.0011	+0.1150	+0.184	+0.1060	+0.0038	-0.0063	+0.0022
2.00	-0.0212	-0.0471	+0.0019	+0.1620	+0.266	+0.1510	+0.0050	-0.0098	+0.0031
2.125	-0.0464	-0.0579	+0.0027	+0.1790	+0.293	+0.1660	+0.0053	-0.0117	+0.0034
2.25	-0.0921	-0.0756	+0.0028	+0.2020	+0.327	+0.1840	+0.0058	-0.0136	+0.0035

Fig. 7.36. Deflections for lane loadings (four lanes) in the main and one side span (design ultimate)

but the strain in the bottom slab was linear only up to the (1.35 DL + 0.5 (LL + IL)) increment and started to deviate after that increment. The strains in the bottom slab showed considerable difference between the webs and the middle of the bottom slab. In the N1 segment, strains in the top and bottom slabs increased linearly until (1.35 DL + 1.50 (LL + IL)) and (1.35 DL + 1.75 (LL + IL)) increments, respectively, as shown in Fig. 7.38.

Reaction at the NE support increased linearly until the (1.35 DL + 1.00 (LL + IL)) increment and that at the SE support decreased linearly up to the (1.35 DL + 1.50 (LL + IL)) increment, as shown in Fig. 7.39.

Besides reopening positive moment zone cracks developed in the earlier test (Sec. 7.3.3.2), cracks appeared along the trajectories of the negative moment prestressing cables in the 2nd and 3rd segment from the NM pier, as shown in Fig. 7.40. Appearance of these cracks along the tendons was probably due to a combination of high bending moments and shears around the NM pier and relatively thin covers in relation to the large diameter of the tendons (3/8 in. diameter) which were used to construct the 2nd and 3rd segments. It is believed that N1 and NS1, which were subjected to higher moments and shears, did not have such cracks because of double tendons and the smaller size of tendon ducts. Because of high compressive stress due to negative tendons in the top slab around the main pier, no flexural cracks appeared around the main pier. Therefore, this loading condition was not critical.

#### 7.3.3.4 Maximum Shear Loading Adjacent to the Main Pier

As mentioned in Sec. 7.3.2.1, no special strain instrumentation was provided for shear loadings. Design loadings for maximum shear were applied until the (1.35 DL + 2.25 (LL + IL)) ultimate design increment.

The moment diagram for this loading is very similar to the maximum negative moment loading case in Sec. 7.3.3.3 and the magnitudes

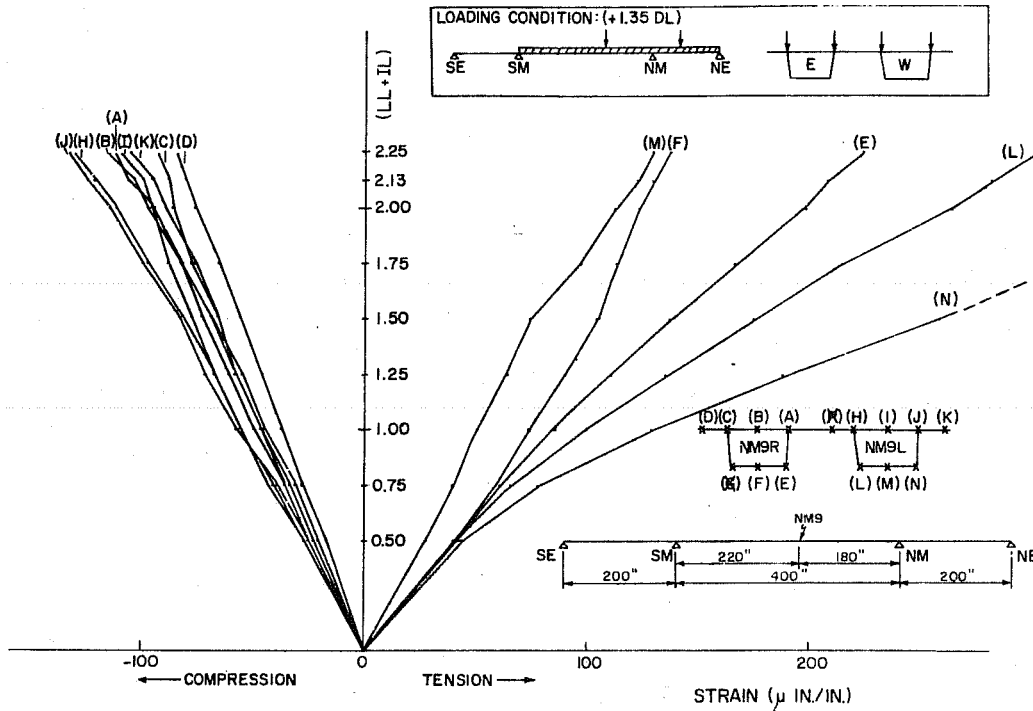


Fig. 7.37. Longitudinal strains at NM9 for lane loadings (four lanes) in the main and one side span (design ultimate)

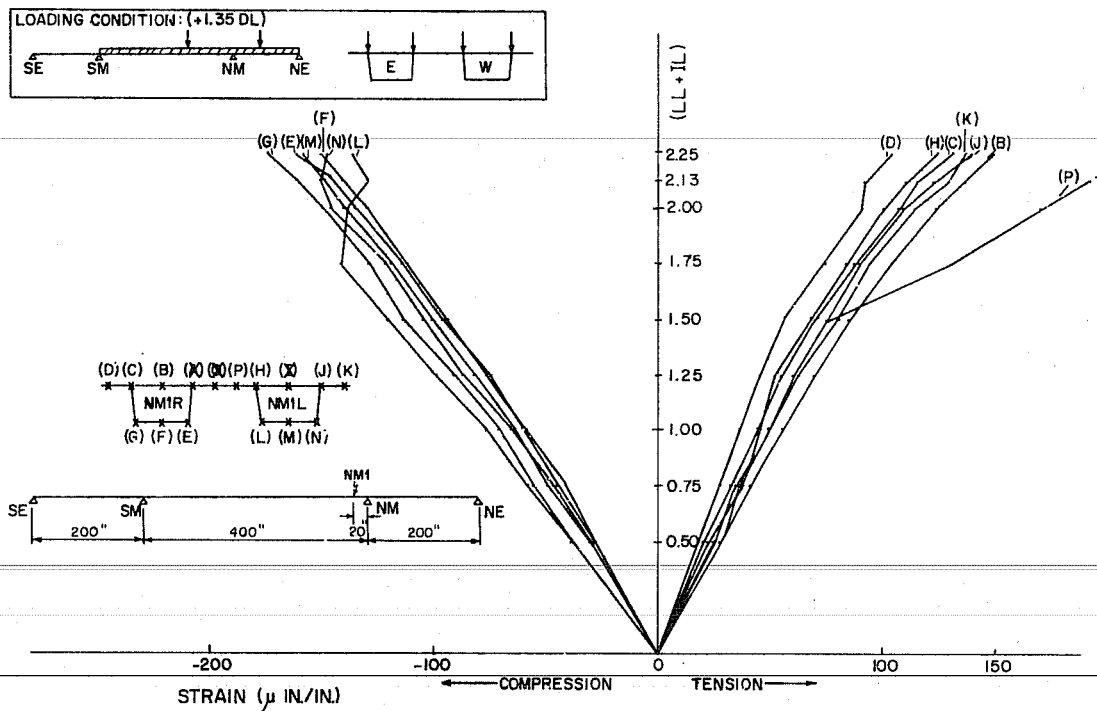


Fig. 7.38. Longitudinal strains at NM1 for lane loadings (four lanes) in the main and one side span (design ultimate)

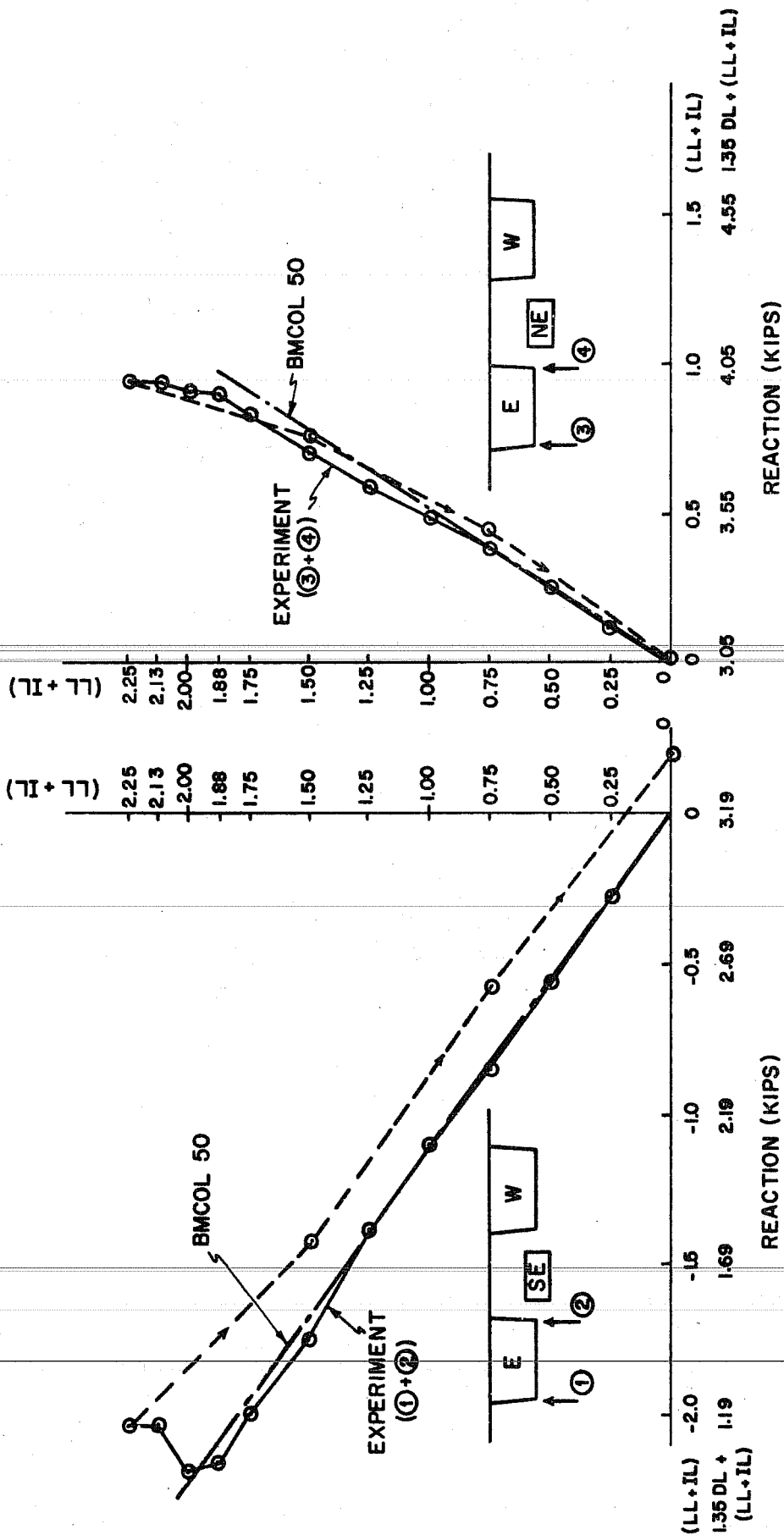
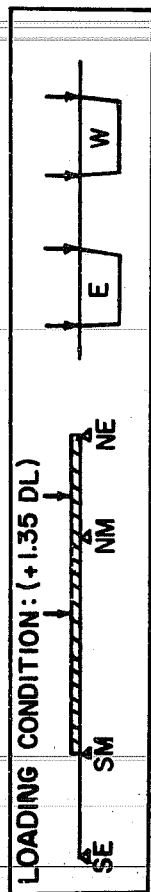


Fig. 7.39. Reactions at outer supports for lane loadings (four lanes) in the main and one side span (design ultimate)



of the maximum positive and negative moments for this loading are only about 17 percent less than this previous loading case. Therefore, the experimental results were very similar to those of Sec. 7.3.3.3, except slightly reduced at each level of load. Because one of the major questions was the dependability of the joints under high shear, this type of loading was applied to the bridge in a later test to failure.

No additional flexural or diagonal tension cracks were observed in this test. Slip gages set across the critical first joint in the main span (as shown in Fig. 7.41) showed zero movement during the loading test.

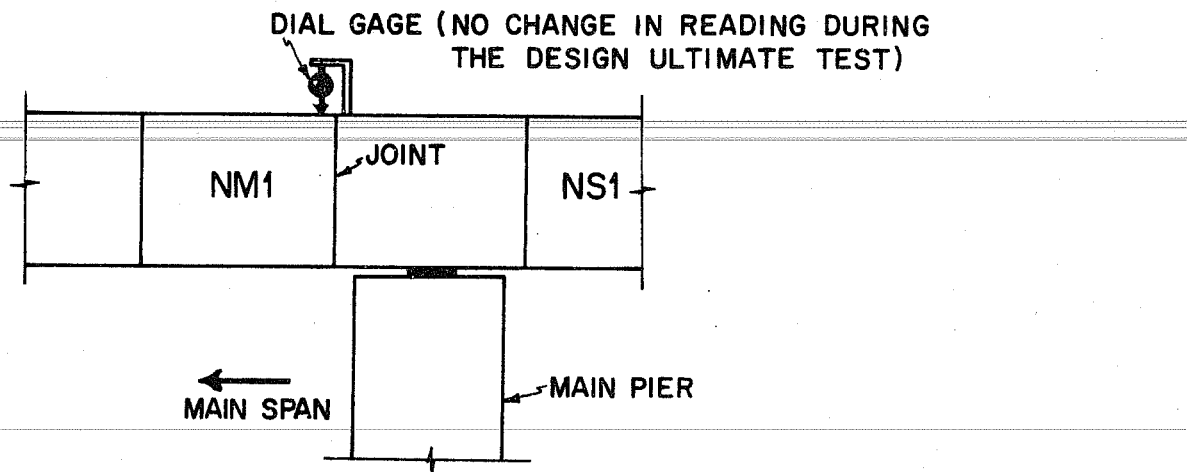


Fig. 7.41. Arrangement of slip gage at the first joint

#### 7.3.3.5 Maximum Positive Moment in Side Span

Truck loads (four lanes) were applied at the same longitudinal position as shown in Fig. 7.9, but the transverse positions were changed to those shown in Fig. 7.42.



Deflection at the center of the SS7 segment, as shown by Fig. 7.43, was exactly the same as the theoretical values at the  $(1.35 \text{ DL} + 0.5 (\text{LL} + \text{IL}))$  increment. The experimental deflections became larger than the theoretical values after this point. The experimental deflection was about 14 percent larger than the theoretical deflection at the  $(1.35 \text{ DL} + 2.25 (\text{LL} + \text{IL}))$  increment. Also, the deflection transversely at the center of the box section (3), in Fig. 7.44, was increasing as the load increased. Details of transverse moment distributions are discussed in Sec. 7.3.4. Observed strains and reactions, as shown in Figs. 7.45 to 7.47, were generally linear. No cracking was observed during this loading test.

Transverse strain was measured at the center of the top slab of SS7R and compared very favorably with MUPDI results, as shown in Fig. 7.48. Transverse strain increased almost linearly up to the 2.25 (LL + IL) increment and agreed with MUPDI.

#### 7.3.4 Study of Transverse Moment

It is very hard to simulate the behavior of the prototype bridge transversely because of the increased difficulty in reducing the scale correctly for the very shallow slab sections used.

Transverse strain gages were put on the surface of the segments at some points and these strain readings were compared with MUPDI analysis results.

The loading cases considered in this section are shown in Fig. 7.49. Since the transverse effect of dead load is small,<sup>16</sup> (LL + IL) only was considered at the service load level. Experimental transverse deflections agreed very well with MUPDI for case (3), as shown in Fig. 7.19. Transverse gages on the SS7 segment are shown for cases (1) and (2) in Fig. 7.49 and experimental strain readings agreed very well with MUPDI results, as shown in Table 7.3.

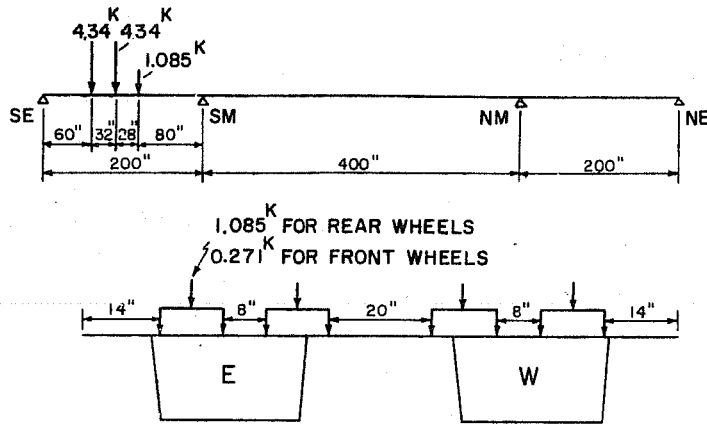


Fig. 7.42. Position of truck loadings (design ultimate)

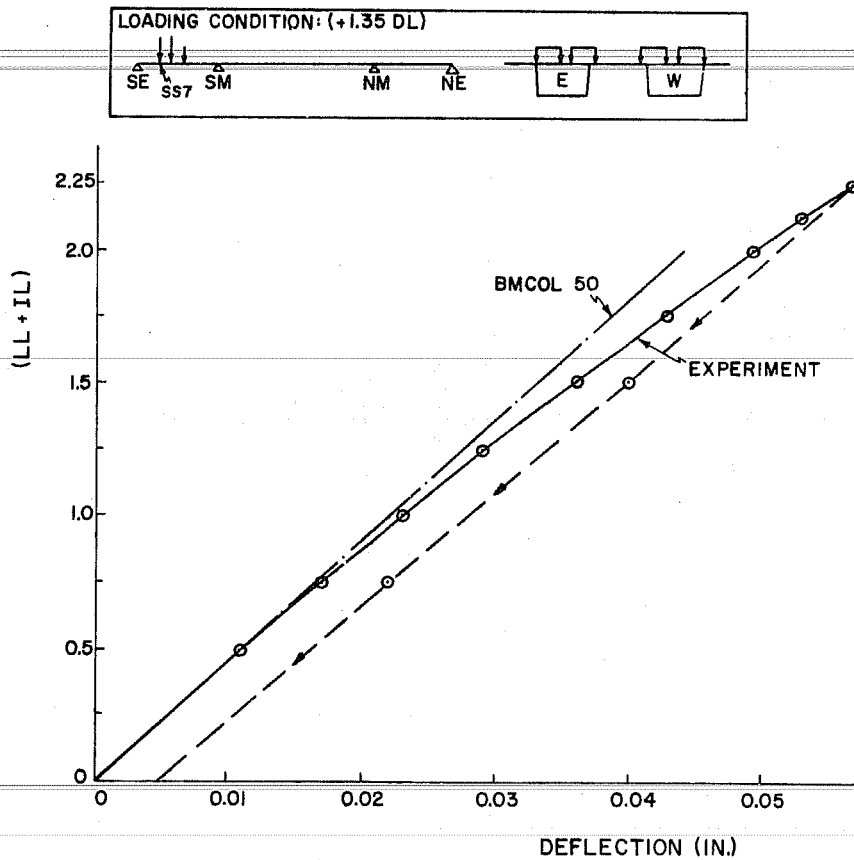
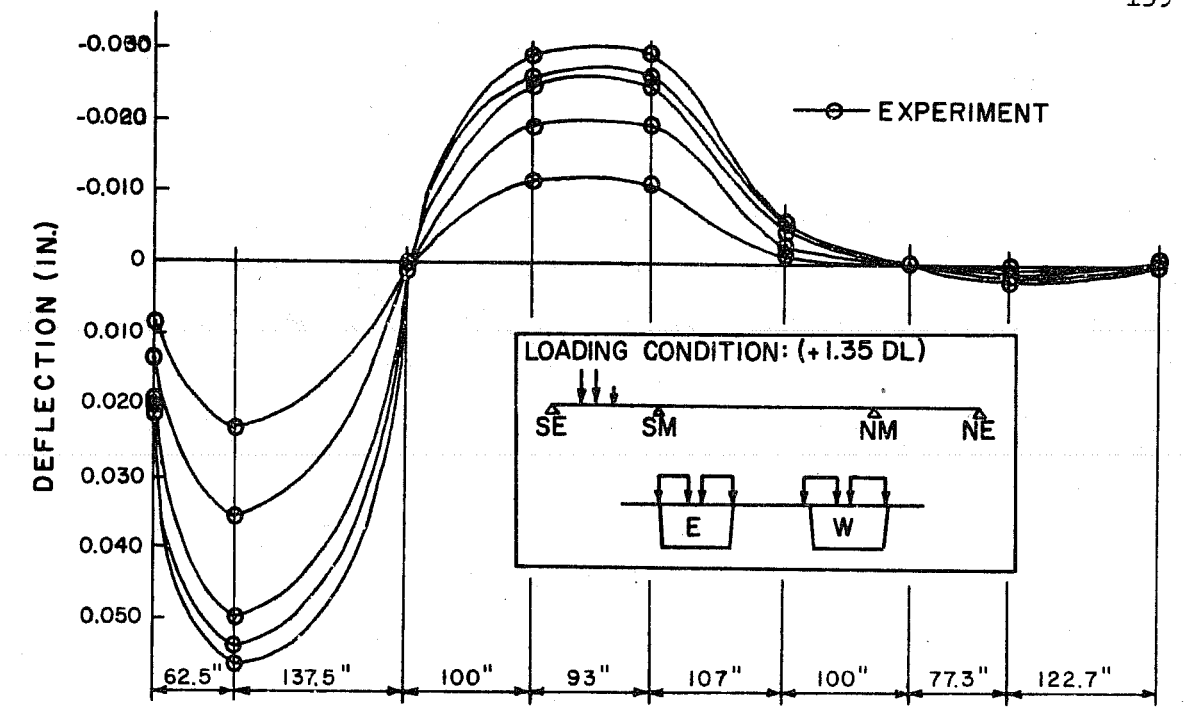


Fig. 7.43. Deflections at SS7 for truck loadings (four lanes) in side span (design ultimate)



(LL+IL)	SE	SS7	SM	SM5	SM10	NM5	NM	NS4	NE
1.00	+0.0082	+0.0228	+0.0003	-0.0121	-0.0119	-0.0020	+0.0002	+0.0010	+0.0002
1.50	+0.0130	+0.0362	+0.0006	-0.0185	-0.0181	-0.0031	+0.0001	+0.0017	+0.0005
2.00	+0.0184	+0.0495	+0.0012	-0.0247	-0.0245	-0.0041	0.0000	+0.0025	+0.0010
2.125	+0.0198	+0.0530	+0.0016	-0.0262	-0.0257	-0.0043	-0.0001	+0.0026	+0.0010
2.25	+0.0209	+0.0568	+0.0017	-0.0278	-0.0274	-0.0047	+0.0001	+0.0028	+0.0010

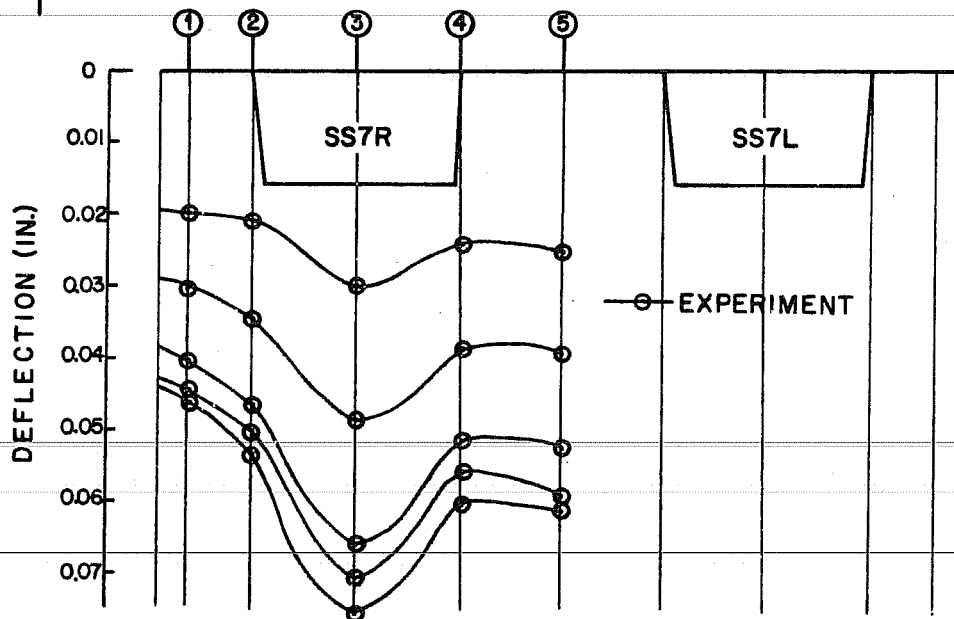


Fig. 7.44. Deflections for truck loadings (four lanes) in side span (design ultimate)

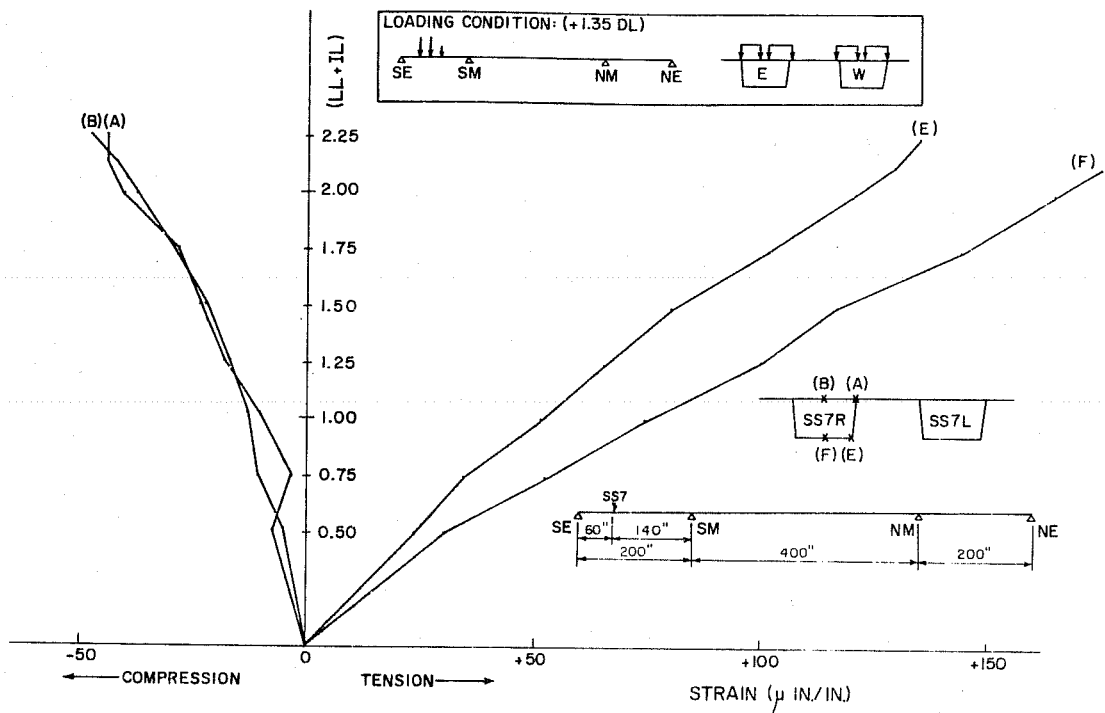


Fig. 7.45. Longitudinal strains at SS7 for truck loadings (four lanes) in side span (design ultimate)

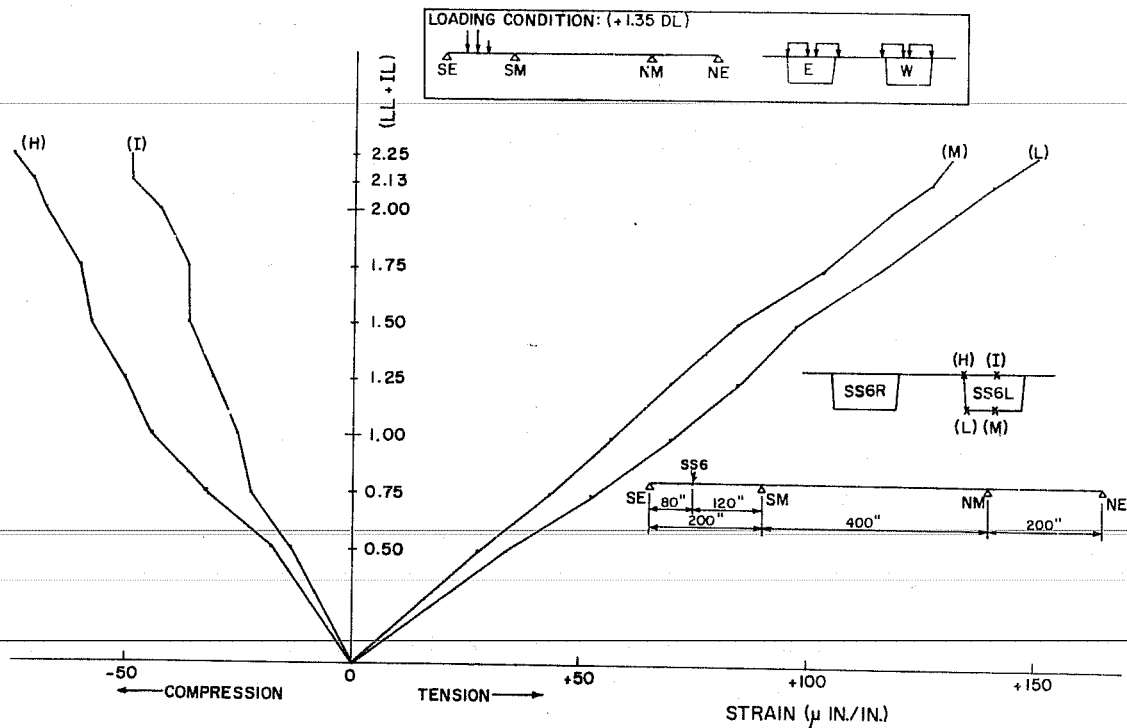


Fig. 7.46. Longitudinal strains at SS6 for truck loadings (four lanes) in side span (design ultimate)

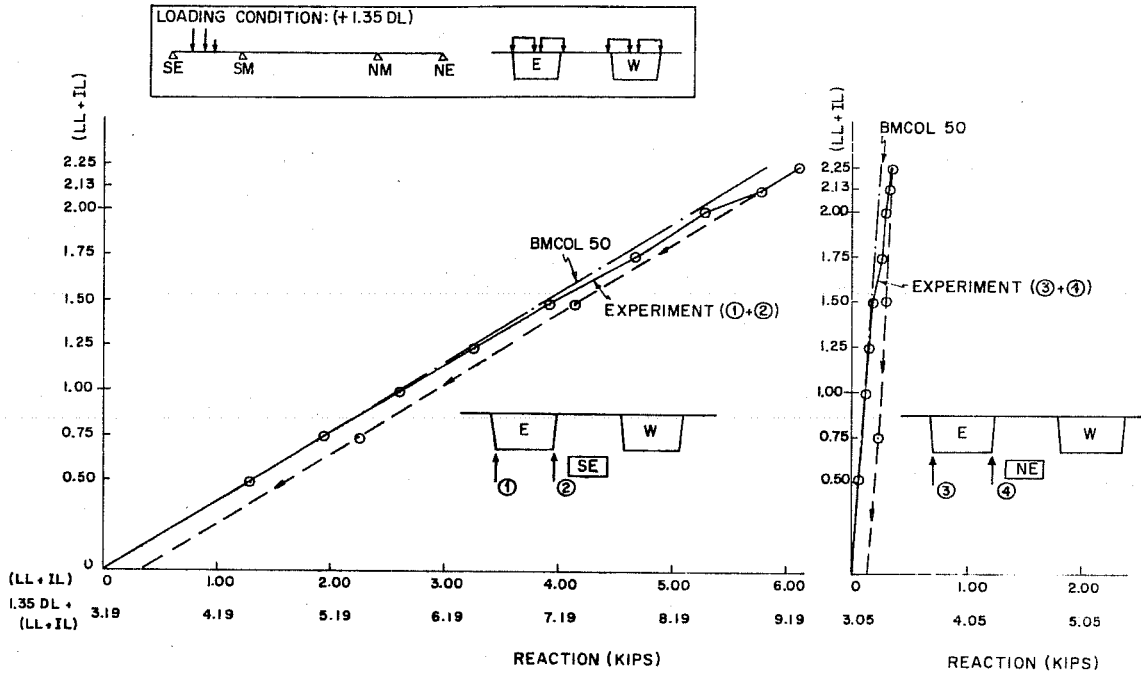


Fig. 7.47. Reactions at outer supports for truck loadings (four lanes) in side span (design ultimate)

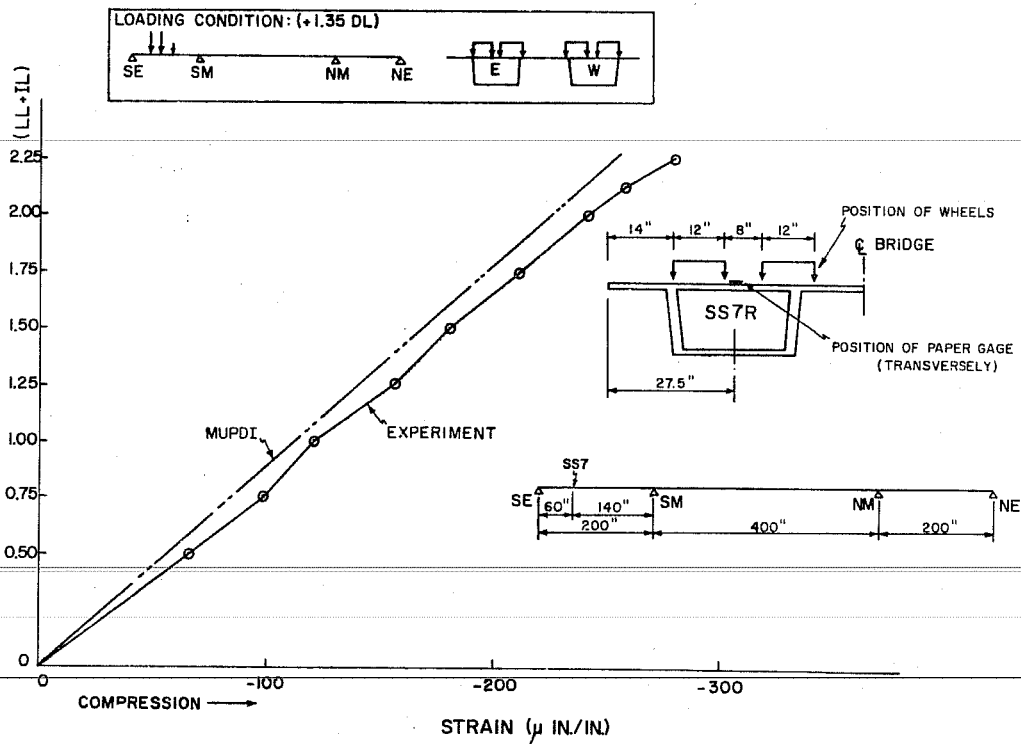
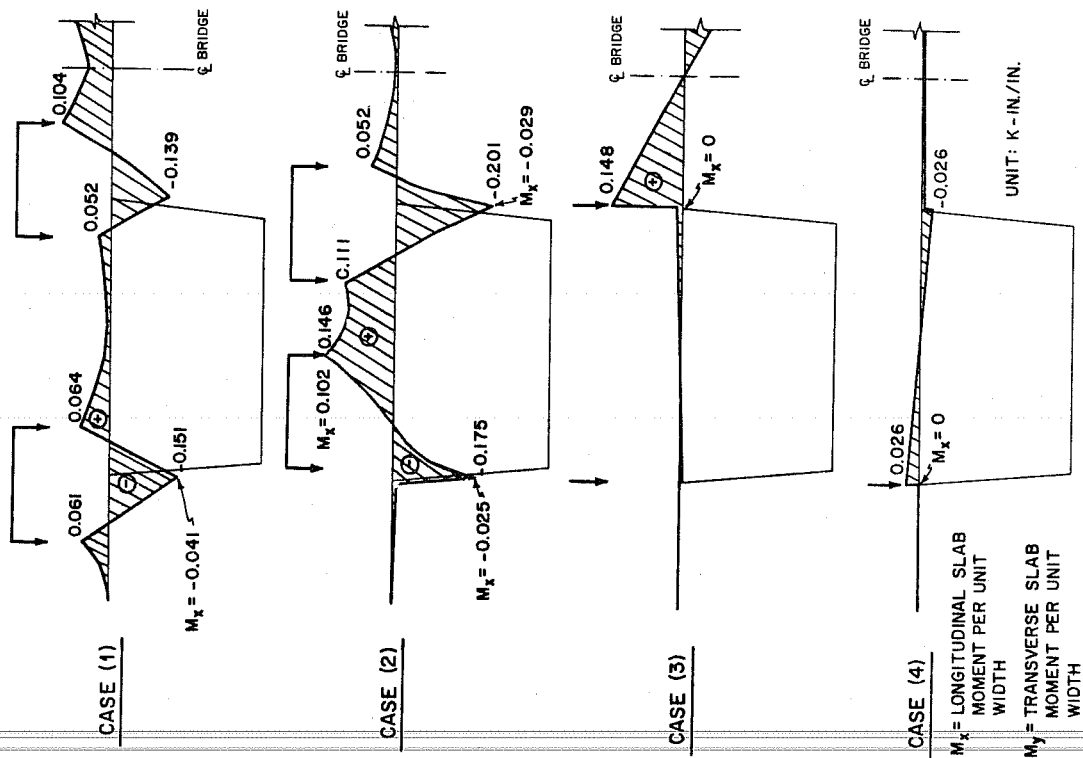


Fig. 7.48. Transverse strain at SS7 R for truck loadings (four lanes) in side span (design ultimate)



CASE (1) - DETAILS OF LOADING ARE IN SEC. 7.3.2.1.

CASE (2) - DETAILS OF LOADING ARE IN SEC. 7.3.2.2.

CASE (3) - DETAILS OF LOADING ARE IN SEC. 7.3.2.3.

CASE (4) - NOT TESTED.

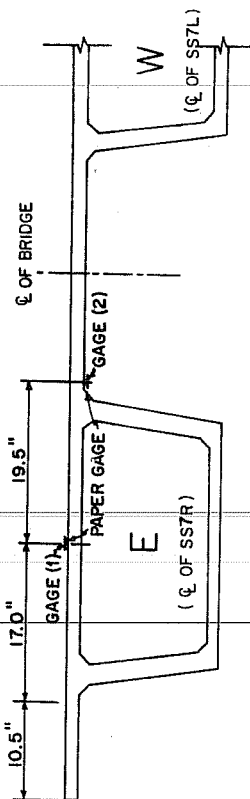


Fig. 7.49. Transverse slab moment ( $M_y$ ) diagram for different loading cases by MUPDI

TABLE 7.3

COMPARISON OF EXPERIMENTAL AND THEORETICAL  
TRANSVERSE STRAINS

Loading Case	Cage No.	Strain ( $\mu$ in./in.)		Experiment/MUPDI
		Experiment	MUPDI	
(1)	(2)	64	63	1.02
(2)	(1)	122	107	1.14

Because MUPDI showed good agreement with the experimental results, transverse moment diagrams for each case were drawn (Fig. 7.49) using the MUPDI results and the computed longitudinal slab moment ( $M_x$ ) at the location of the maximum transverse moment is also shown in Fig. 7.49. Among these four cases, case (2) gave the largest values in transverse positive and negative moments. In order to judge the transverse strength of the section, several strain gages were put at these critical positions in later punching shear tests (punching shear test results are given in Sec. 8.4) and strain readings were taken almost to failure. Transverse and longitudinal slab moments at the service load level were calculated from the experimental results for the loading cases shown in Fig. 7.50. These moments are much larger than the values calculated for the above four cases and strains increased linearly almost to the punching shear failure loads which were about 18 and 7 times (LL + IL) at the middle of the twin boxes and the edge cantilever, respectively. Also, loading case (1) in Fig. 7.49 was applied at the 5.25 (LL + IL) increment in the failure test of Sec. 8.2 and no visible crack was observed in the top slab. Although it is not possible to relate these results directly to the prototype because of casting tolerances being exceeded in the model

(the thickness of the top slab was about 15 percent thicker than thickness specified), the above results indicate that there is ample safety in transverse bending for the top slab.



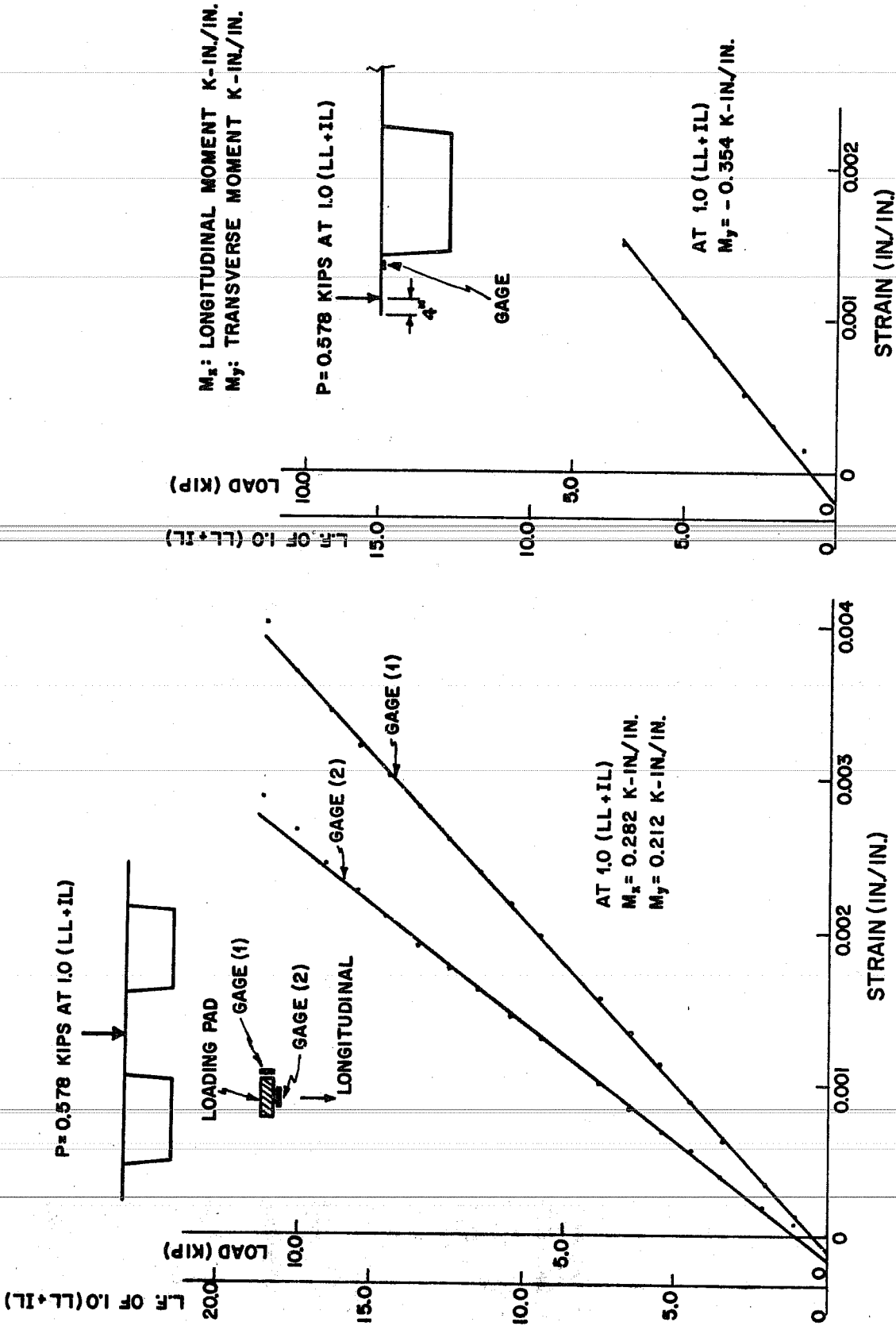


Fig. 7.50. Typical strain readings in punching shear tests

## CHAPTER 8

### LOADING TO FAILURE TESTS

#### 8.1 General

The model bridge carried the BPR design ultimate load safely for all critical loading conditions, as shown in the previous chapter. To obtain maximum return from the model, several failure tests were planned to determine capacity. It was decided that truck loads would be first applied to the side span, as shown in Fig. 8.1 (b), to cause a bending failure. This was decided even though the calculated ultimate live load factor for this case was larger than that which was calculated for maximum moment in the main span. Since both failures would be flexural, it was felt that a failure test in the side span could verify flexural ultimate calculations. Such a test would leave the structure with two relatively undamaged spans so that a shear test to failure could also be run by applying lane loadings to the main and side spans to produce maximum shear at the main pier, as shown in Fig. 8.1 (c). Truck loading on the side span (Fig. 8.1 (b)) was stopped after distinct yielding had occurred, but before complete collapse of the side span. The loading increment at which testing was stopped was judged by the deflection and strain readings. Although loads continued to be applied after formation of another hinge at the SM pier segment, the effect of this loading on the ultimate bending and shear strength of spans (B) and (C) was judged negligible because no live load would be applied on span (A) and the end segment at SE would raise up during the second failure loading test shown in Fig. 8.1 (c).

## 8.2 Failure Test of the Side Span

### 8.2.1 General

Scaled HS20-S16 (AASHO) truck loads were applied to all four lanes of the side span to produce critical bending.

Longitudinal and transverse truck loadings are shown in Fig.

8.2. These are the same as shown in Fig. 7.9.

Strain gage measurements were taken at the positions shown in Fig. 4.14. Positions of dial gages were the same as in the previous test (see Fig. 7.7). Reaction readings were taken at outer supports.

In addition to the 1.35 dead loads, live and impact loads were applied using rams up to the 5.25 (LL + IL) level. Load increments of 0.25 (LL + IL) or 0.125 (LL + IL) were used after the 0.75 (LL + IL) level.

### 8.2.2 Test Results

At the 2.88 (LL + IL) increment, there were some deviations from the previous linear load vs. deflection diagram (Fig. 8.3). Strains in the bottom slab at the SS6L segment changed rapidly at the 2.75 (LL + IL) increment as shown in Fig. 8.4. It appears as though cracking may have started to develop in the inner webs although no cracking was visible in the outer webs.

At the 3.25 (LL + IL) increment, a flexural crack on the outer web around the center of the SS7R segment was visible almost up to mid-height and the strain gages in the bottom slab showed a large increase in strain, as shown in Fig. 8.5.

At the 4.25 (LL + IL) increment, a wide crack (more than 1/8 in. visually) developed suddenly at the SS6-7 joint in the outer web of the west side (OW) as shown in Fig. 8.6. At the 4.38 (LL + IL) increment a major crack formed near the SS6-7 joint in the outer web of the east side (OE) as shown in Fig. 8.6. After these cracks developed, Figs. 8.3 to 8.5

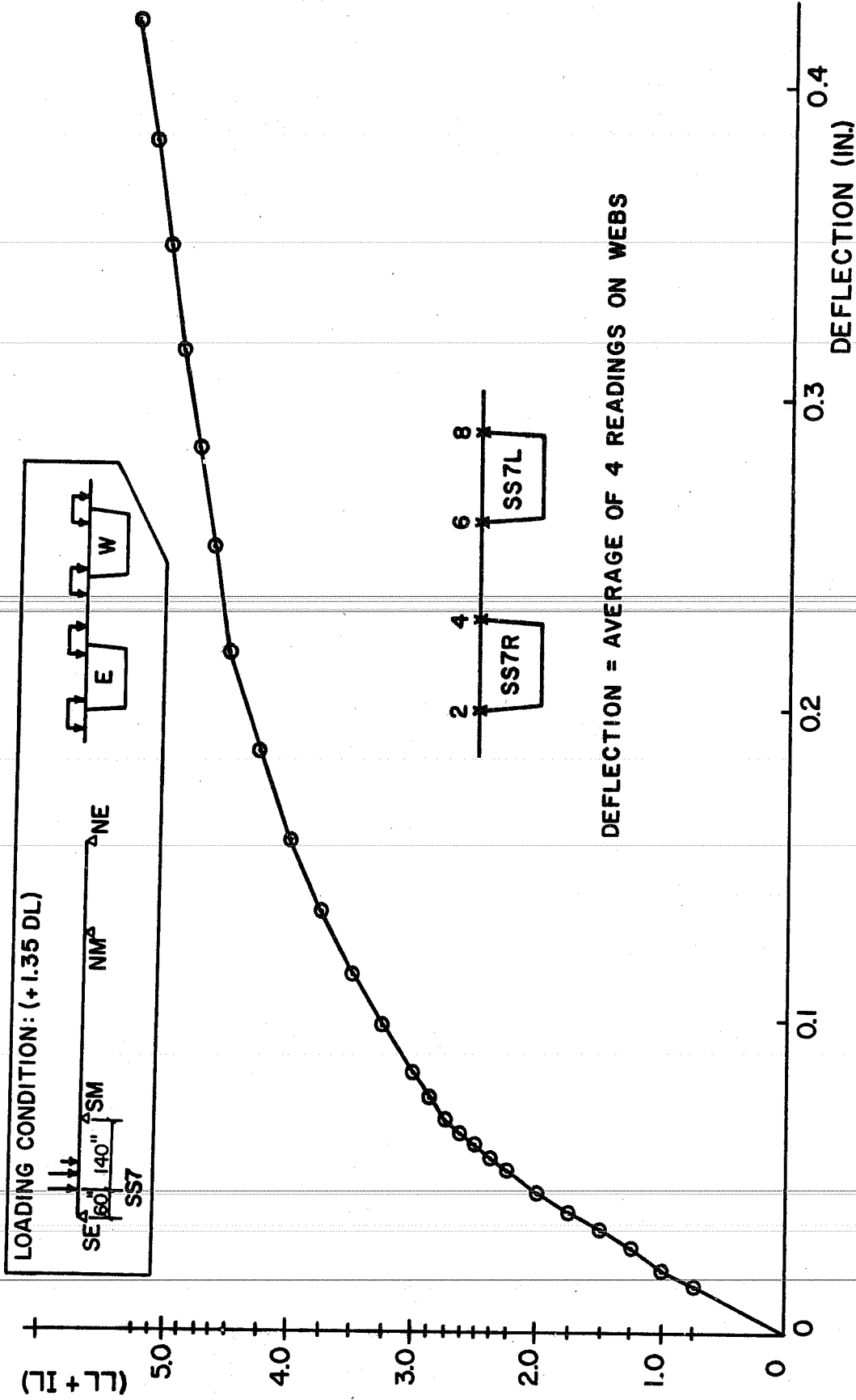


Fig. 8.3. Deflections at the center of the SS7 segment in side span

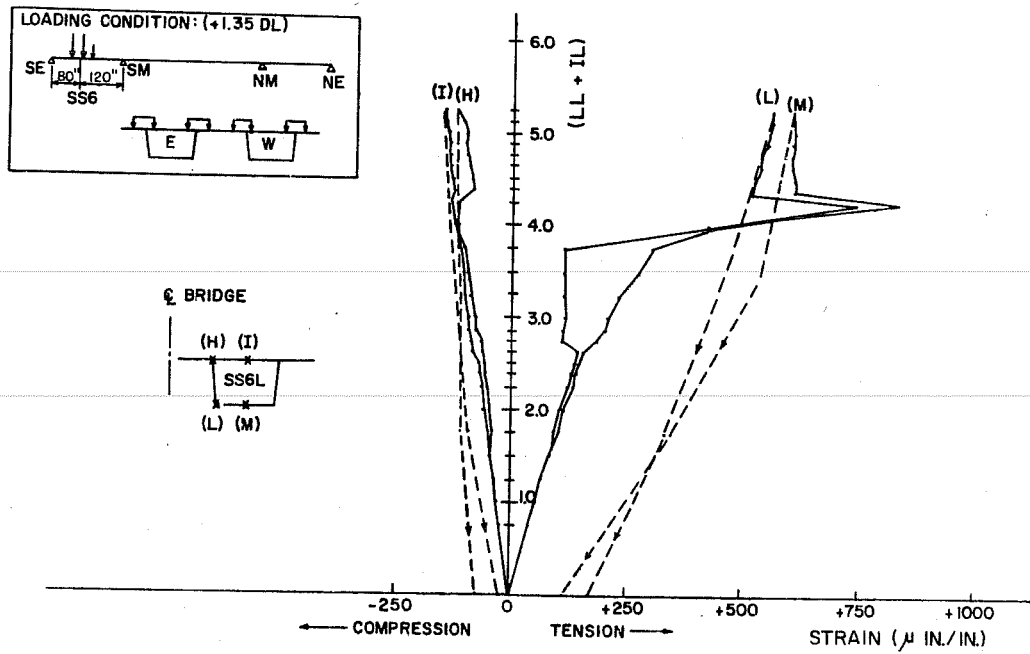


Fig. 8.4. Longitudinal strains at the center of the SS6L segment

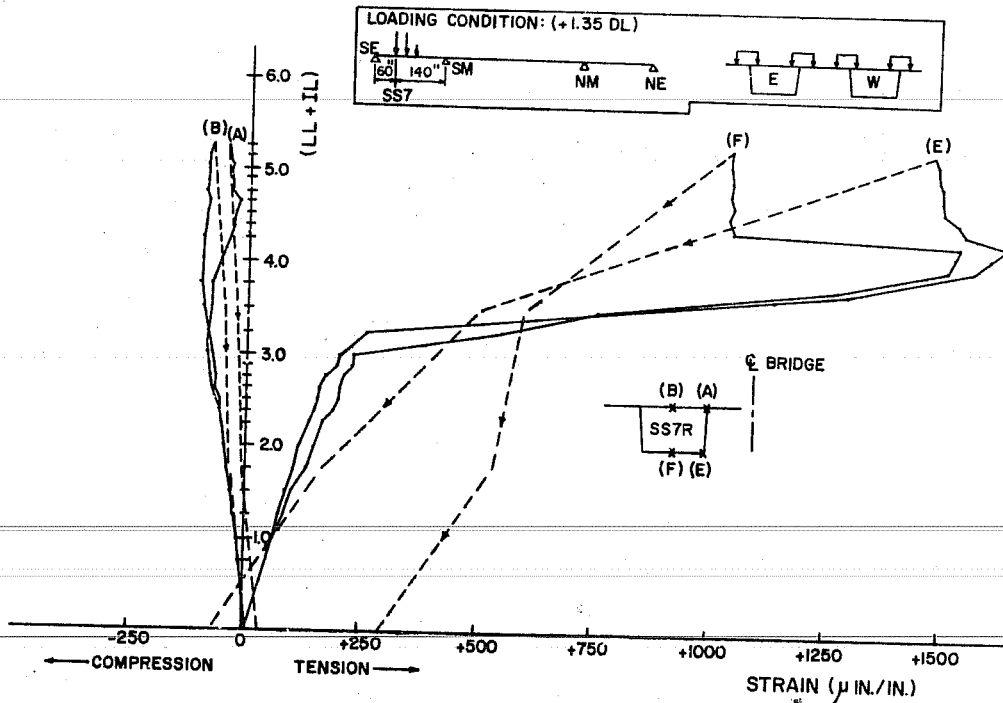
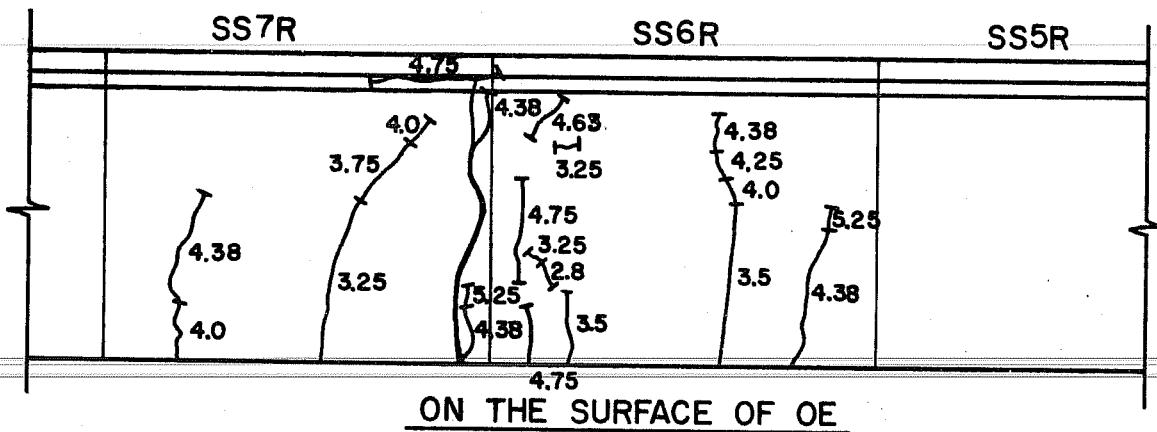
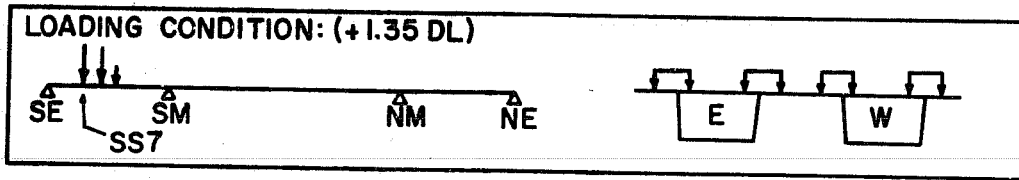
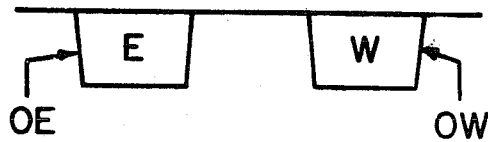


Fig. 8.5. Longitudinal strains at the center of the SS7R segment



\* NUMBERS ALONG THE CRACKS ARE MULTIPLES OF (LL+IL)

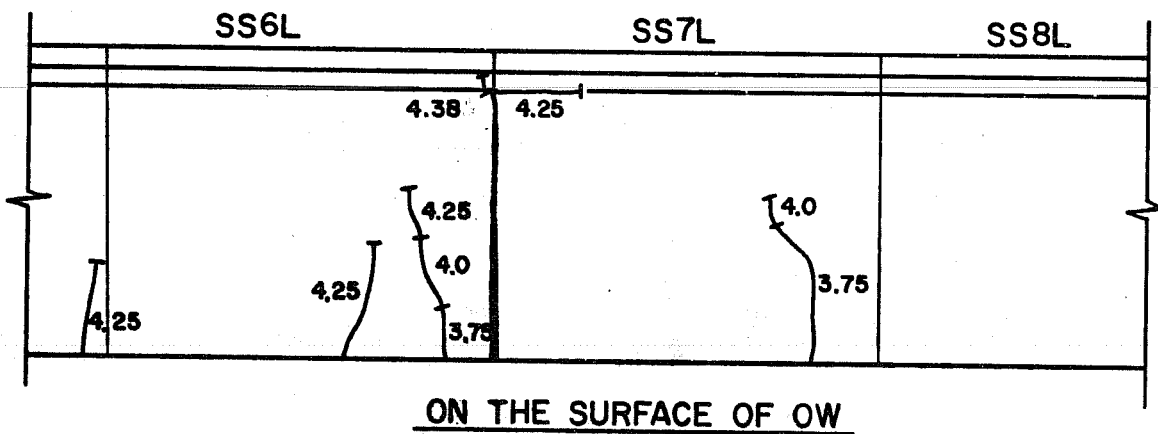


Fig. 8.6. Development of cracks during loading

indicate changes in strain at the center of the SS7R and SS6L segments stopped, and deformations were concentrated in the vicinity of these large cracks. By observing the strain diagram of the SS1 segment (as shown in Fig. 8.7), the strains are seen to increase rapidly at the 4.38 (LL + IL) increment and to increase less rapidly after that increment. The rapid increase of the strain at the SS1 segment, and in the reaction at the NE support (as shown in Fig. 8.8) around the 4.25 or 4.38 (LL + IL) increment means that a plastic hinge was formed at the SS6-7 joint. After forming the plastic hinge the loads were redistributed and more load was carried at the SM pier region. Since the bridge is a three-span continuous beam, plastic hinges have to be formed at (A) and (B) in Fig. 8.9 to have complete failure for loading in the side span. The average reaction at the SE support increased fairly linearly, as shown in Fig. 8.8. Changes in each reaction at the SE support can be seen at the 2.88 and 4.38 (LL + IL) increments.

Due to the extreme widening of the crack at the SS6-7 joint, an unexpected horizontal force occurred on the top of the SE pier. It could be visually observed at high load levels that the SE pier was tilting and inclining after the large cracks opened around the SS6-7 joint. Apparently a horizontal force acted on the top of the SE pier, due to the deformation of the bridge, as shown in Fig. 8.10. The moment connection between the end pier and the testing floor was not strong enough to keep the pier from tilting under this force.

Because it was obvious that a plastic hinge had formed near the 4.38 (LL + IL) increment and because of the inclination of the end pier, it was decided to stop loading and release all live load at the 5.25 (LL + IL) increment. This represented practical failure of the side span although collapse did not occur. In this way further loading testing could be completed in the other two spans.

The maximum width of the crack at the SS6-7 joint was  $1/4$  in. on the outer west web (OW) and about  $1/8$  in. on the outer east web (OE) under the maximum load increment. Cracks were distributed more in the outer east web than in the outer west web. This might be due to a

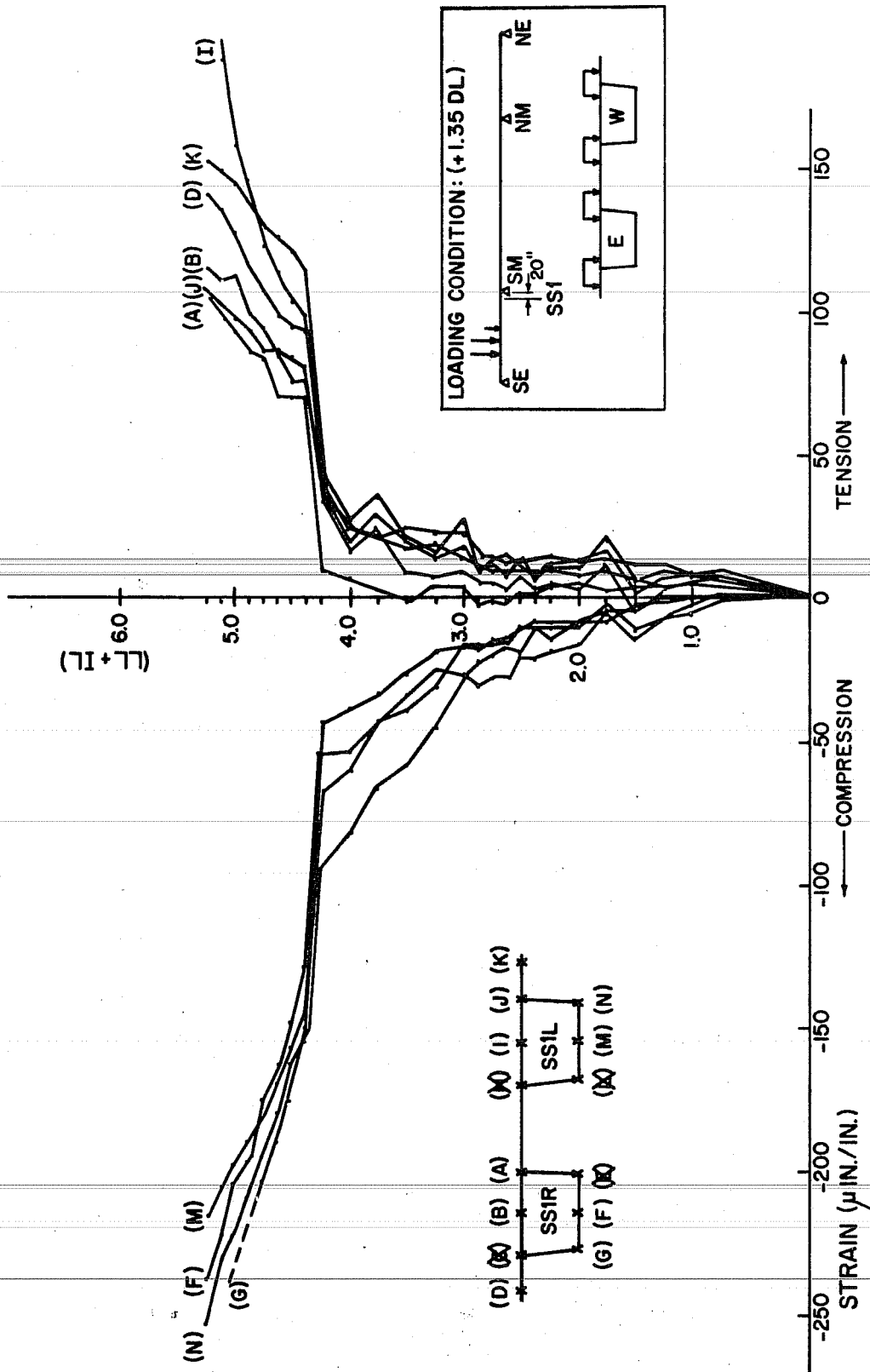


Fig. 8.7. Longitudinal strains at the center of the SS1 segment



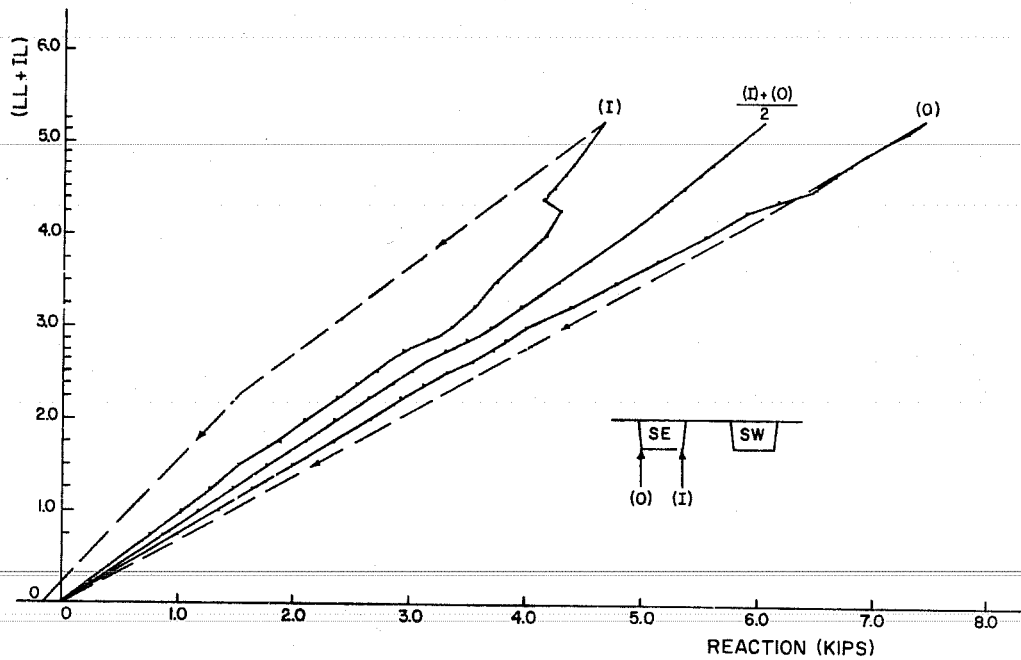
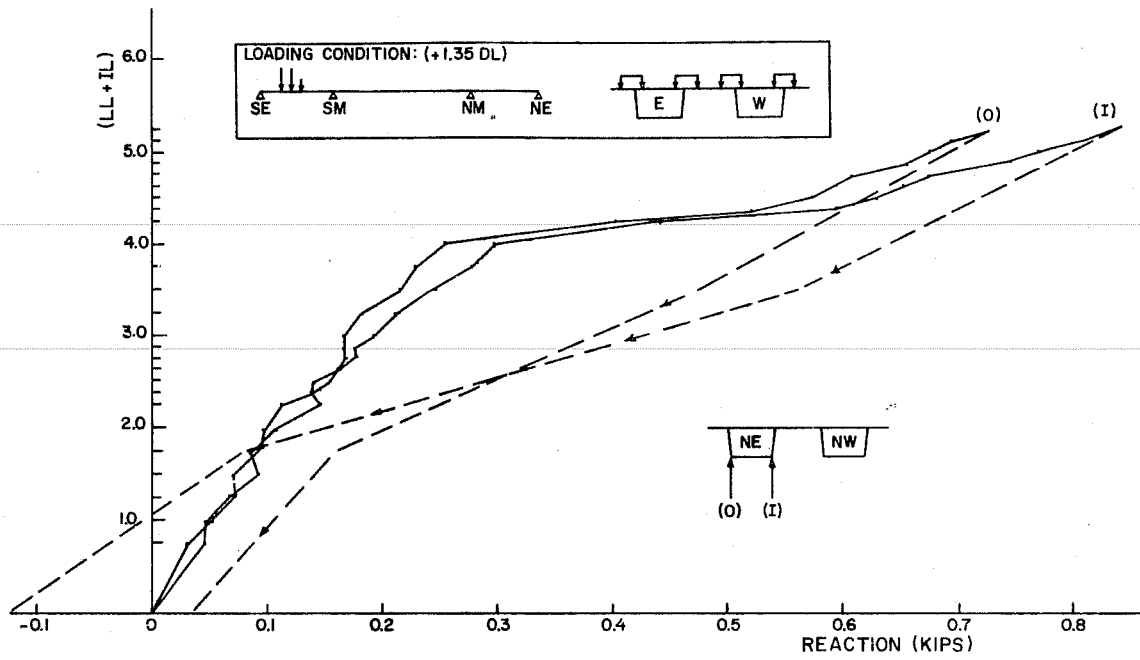
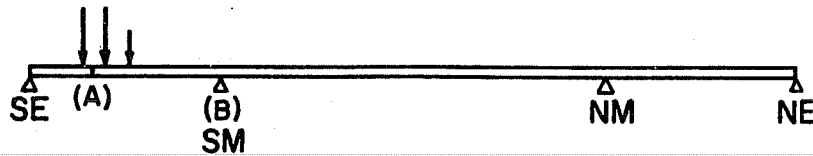
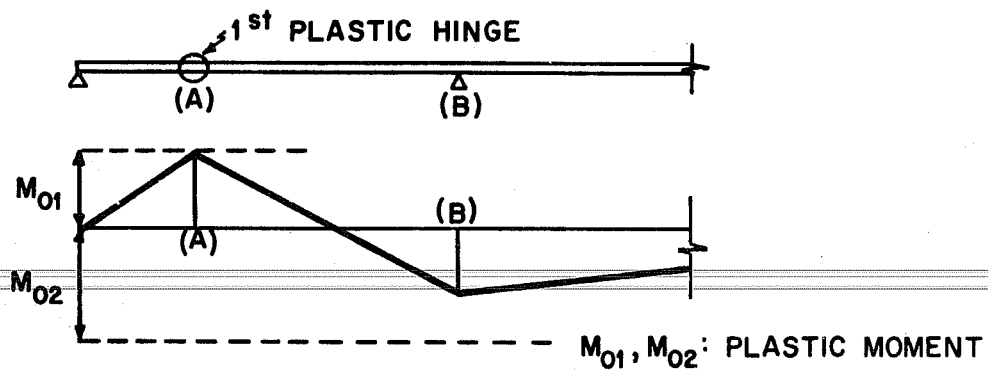


Fig. 8.8. Reactions at the outer supports

(A) LOADING CONDITION: (+1.35 DL)



(B) FIRST PLASTIC HINGE AND MOMENT DIAGRAM.



(C) SECOND PLASTIC HINGE AND MOMENT DIAGRAM AT COLLAPSE.

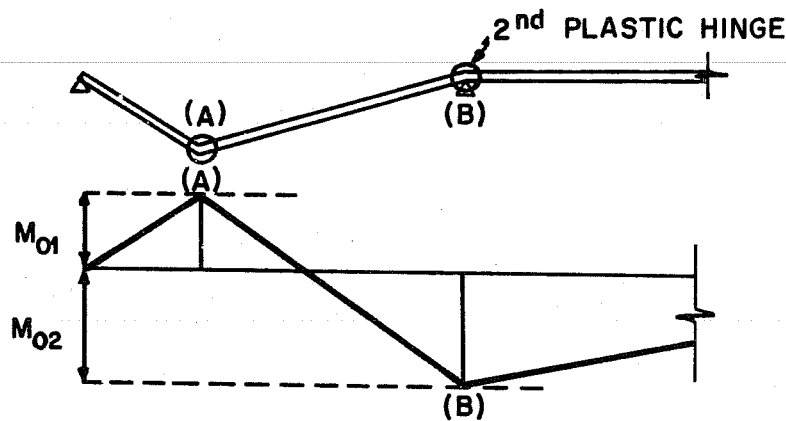


Fig. 8.9. Failure mechanism for truck loadings in the side span

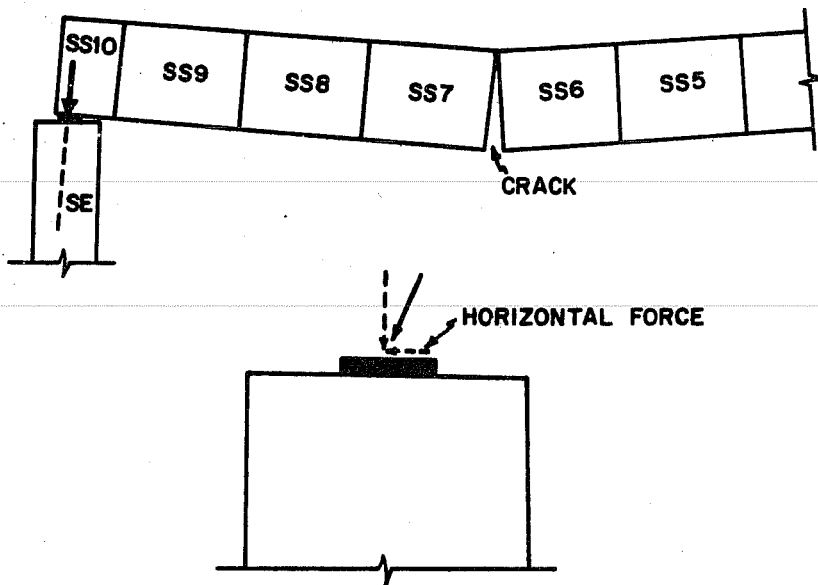


Fig. 8.10. Horizontal force on the top of the outer pier

weaker joint in the west side of the box because there was not much apparent difference in grouting.

In the transverse direction, deflections were reasonably uniform across the SS1 segment at small loading increments. Relative deflections increased in the cantilever slabs and at the middle of the midstrip closure (in Fig. 8.11) as loading increased. Transverse strains on the bottom face near the end of the cross slabs were measured by paper gages, as shown in Fig. 8.12. Transverse strains also increased rapidly at the 4.38 (LL + IL) increment.

### 8.2.3 Determination of Side Span Live Load Capacity

In order to find the actual live load capacity factor (LF) for the truck loading on the side span, it is necessary to consider all forces and moments acting on the bridge.

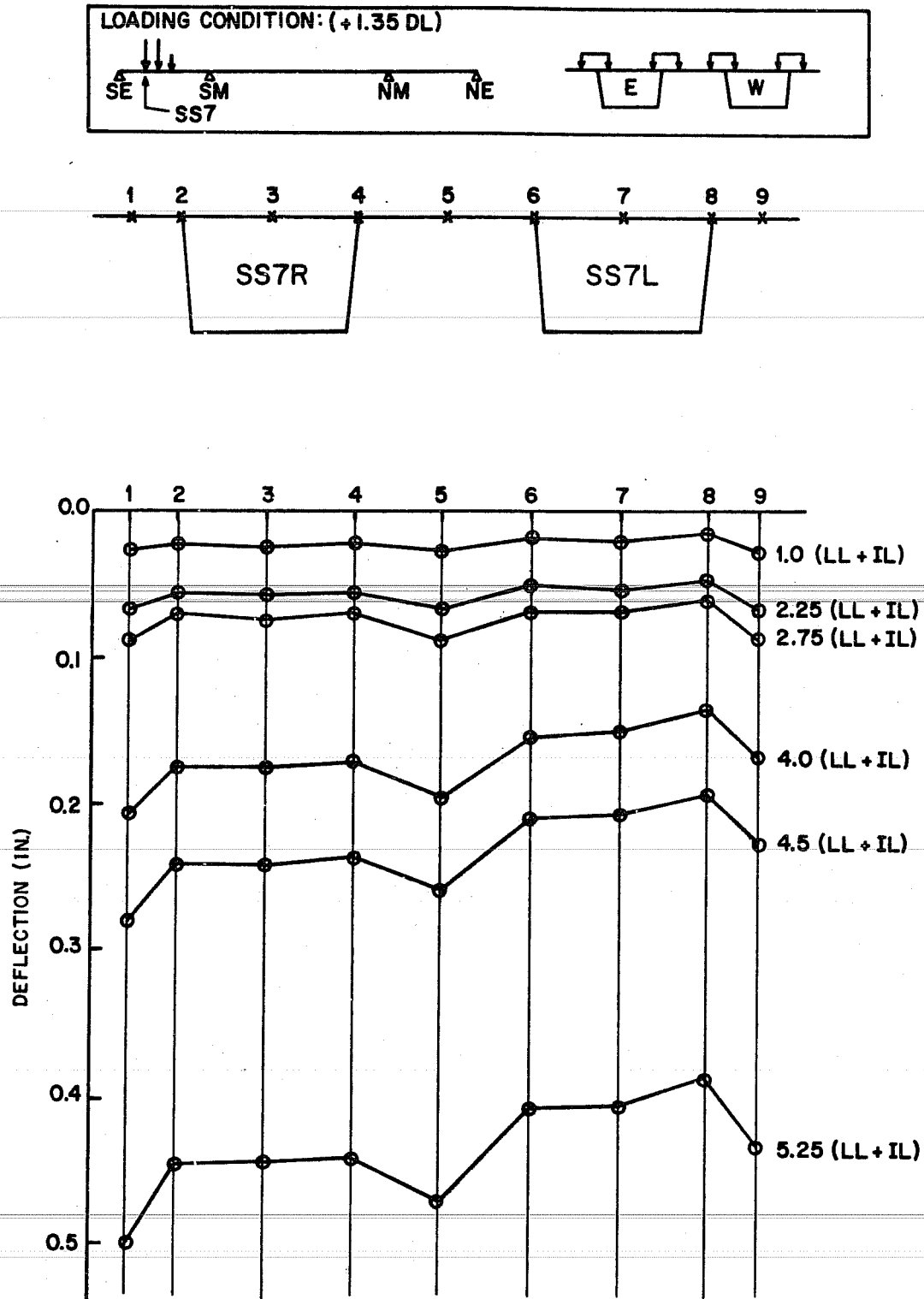


Fig. 8.11. Deflections along the center of the SS7 segment in side span

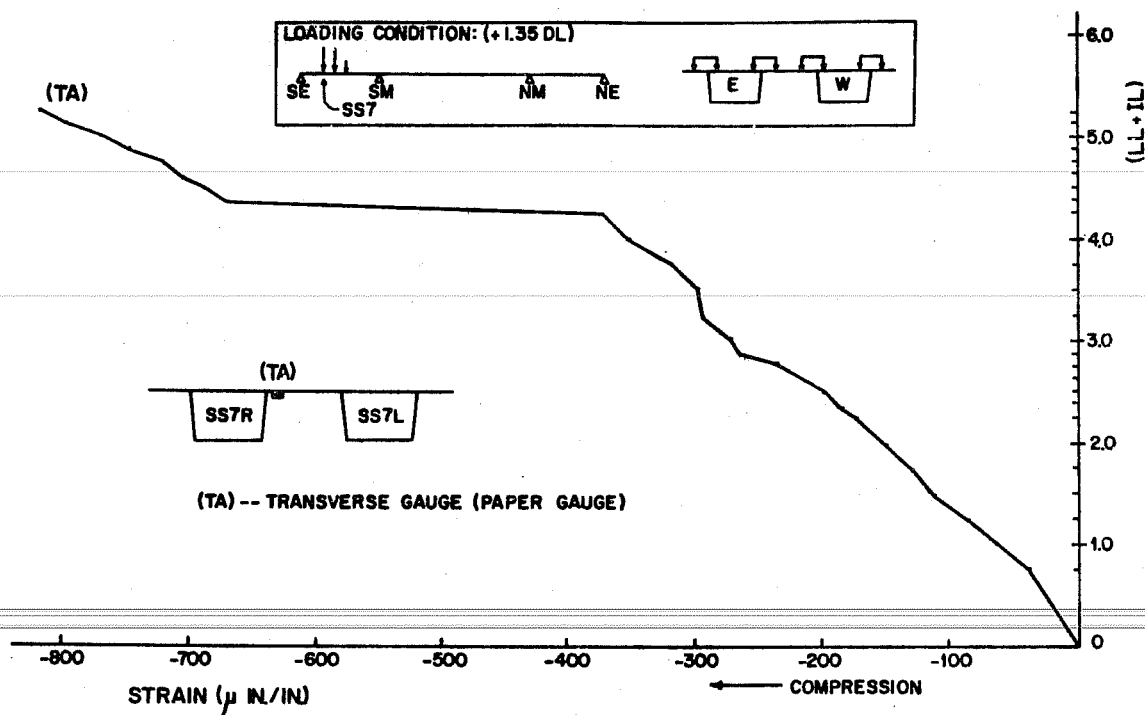
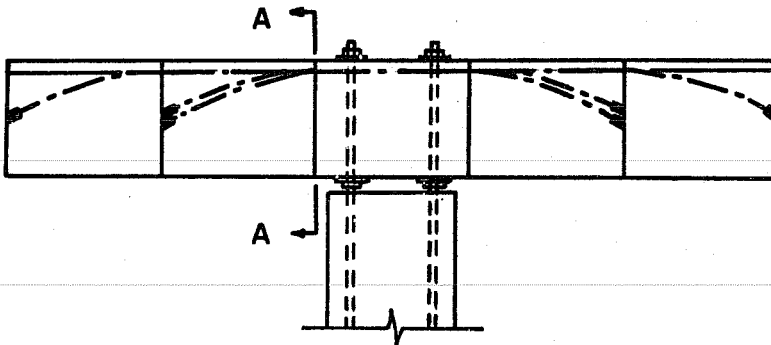


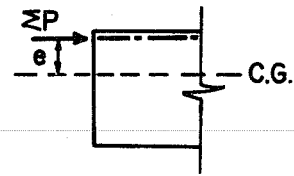
Fig. 8.12. Transverse strains at the center of the SS7 segment

Each time the precast segments were erected and joined in symmetrical cantilever construction, negative tendons were prestressed in order to hold the precast segments in the proper balanced position, as shown in Fig. 8.13 (a). For a typical construction stage, if a section is cut at A-A, the prestressing force  $\Sigma P$  is acting as shown in Fig. 8.13 (b) and it also produces a moment  $M_p$  ( $[\Sigma P] \times e$ ). These forces and moments can be calculated at each section and a force diagram for  $\Sigma P$  and a moment diagram for  $M_p$  can be drawn as in Fig. 8.13 (c) and (d), respectively. The opposing dead load moment due to the weight of the segments is shown in Fig. 8.13 (e). Although vertical forces are acting along the curved portions of the tendon ducts, no vertical forces are included in subsequent figures, since all negative tendons are horizontal at the joint. At the completion

## (A) CANTILEVER CONSTRUCTION

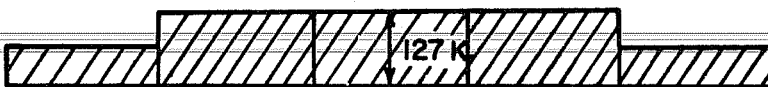


## (B) PRESTRESSING FORCES AND MOMENTS AT A-A

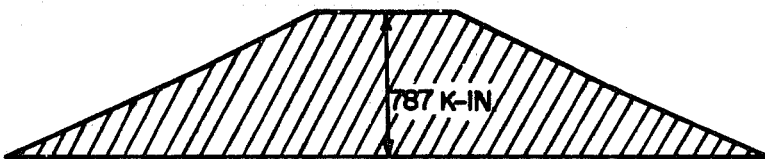


$$M_p = (\Sigma P) \times e$$

## (C) PRESTRESSING FORCES ALONG SEGMENTS



## (D) MOMENTS DUE TO PRESTRESSING FORCES



## (E) MOMENTS DUE TO WEIGHT OF SEGMENTS



Fig. 8.13. Forces and moments acting on the bridge for a typical cantilever stage

of the balanced cantilever construction scheme, the diagrams of the total force and the total moment due to prestressing cables (negative tendons) and the total moment due to dead load (weight of segments) are shown in Fig. 8.14. The moment due to the external load (weight) and prestressing cables were designated as the external moment ( $M_E$ ) and the internal moment ( $M_I$ ), respectively. The force due to the prestressing cables was designated as the internal force ( $F_I$ ).

Positive tendons in the side spans were inserted and prestressed after completing the cantilever construction. Prestressing of positive tendons in the side spans cause an internal force ( $F_{I2}$ ) and moment ( $M_{I2}$ ), as shown in Fig. 8.15.

The closure segment at the center of the main span was then cast. At this stage there were external moments due to 1.0 DL, ( $M_{E1}$ ), and internal force ( $F_{I1}$ ) and moment due to negative tendons ( $M_{I1}$ ) in the main span. However, the moment at the closure segment was zero. The positive moment cables at midspan essentially need to resist only live loads. Thus, the amount of center span positive prestressing cables should be less in a bridge constructed by cantilever construction than in a bridge constructed on falsework. Details of those differences are referred to in Muller's paper.<sup>24</sup>

After the required strength of concrete in the closure was developed, positive tendons in the main span were prestressed. Outer supports were set in position touching the girder ends prior to prestressing the positive tendons in the main span. Thus, resultant forces were produced at the outer supports when the positive tendons were prestressed since the side span outer ends tried to deflect downward. In addition, to ensure that no uplift at the outer supports occurs at service level loading, specified additive vertical reactions were jacked into the outer supports at completion of the stressing (see Sec. 7.3.3.2). Internal forces ( $F_{I3}$ ) and moments ( $M_{I3}$ ) due to positive tendons in the main span are shown in Fig. 8.16. The moment ( $M_{E2}$ ) caused by the resultant forces due to prestressing and the applied

## (A) COMPLETION OF CANTILEVER CONSTRUCTION

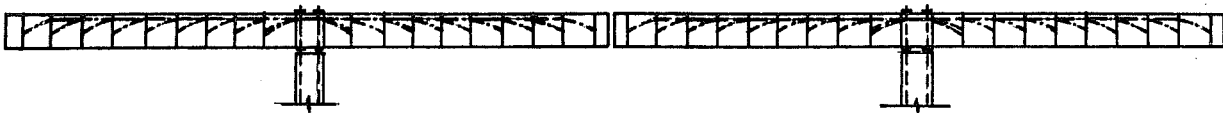
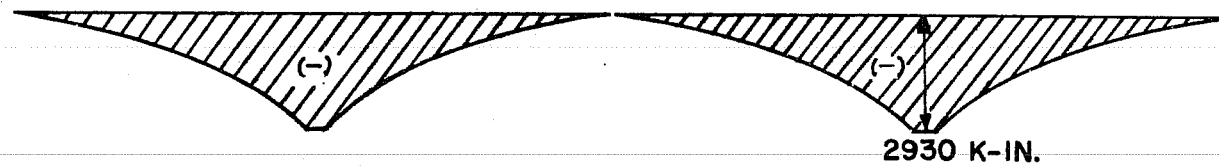
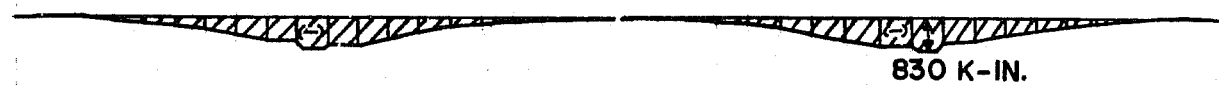
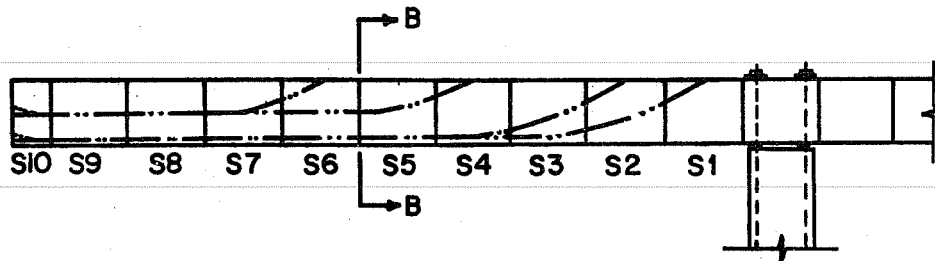
(B) HORIZONTAL FORCES DUE TO PRESTRESSING ( $F_{I1}$ )(C) MOMENTS DUE TO PRESTRESSING ( $M_{I1}$ )(D) MOMENTS DUE TO WEIGHT OF SEGMENTS ( $M_{E1}$ )(E)  $M_{I1} + M_{E1}$ 

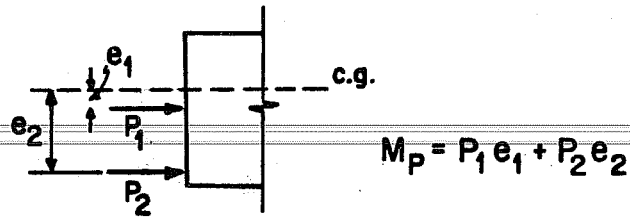
Fig. 8.14. Horizontal forces and moments at completion of cantilever erection



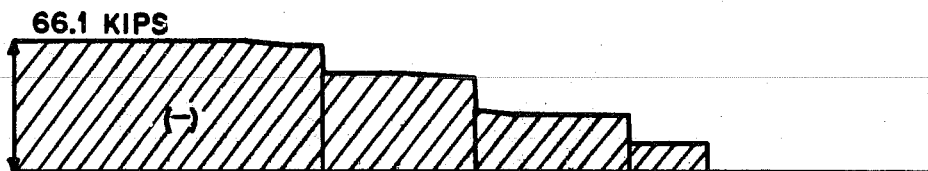
(A) PRESTRESSING OF POSITIVE TENDONS IN SIDE SPAN



(B) PRESTRESSING FORCE AND MOMENT AT B-B



(C) HORIZONTAL FORCES DUE TO PRESTRESSING IN SIDE SPAN ( $F_{I2}$ )



(D) MOMENTS DUE TO PRESTRESSING IN SIDE SPAN ( $M_{I2}$ )

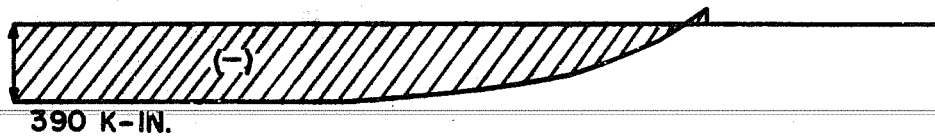


Fig. 8.15. Horizontal forces and moments due to prestressing in side span

## (A) PRESTRESSING OF POSITIVE TENDONS IN MAIN SPAN

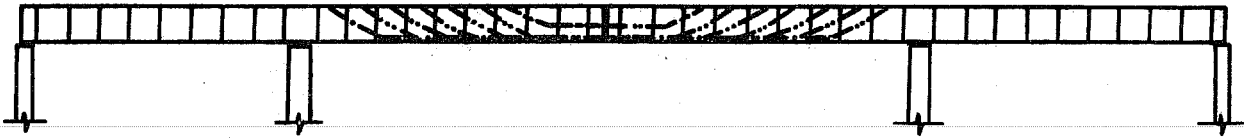
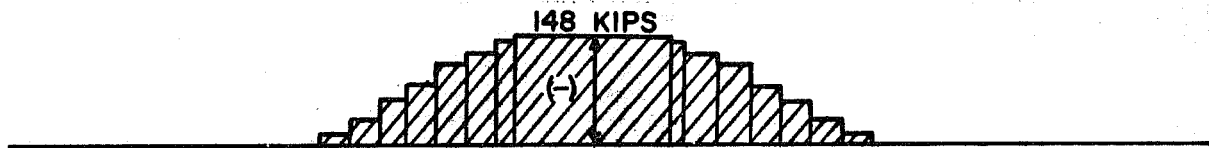
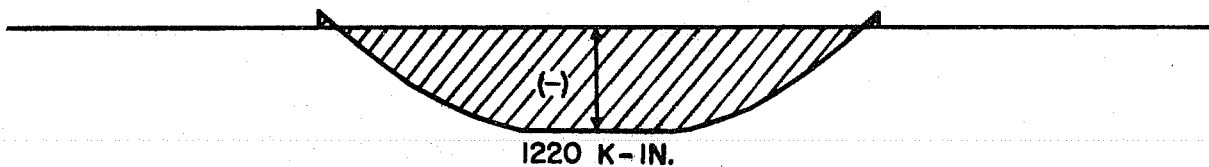
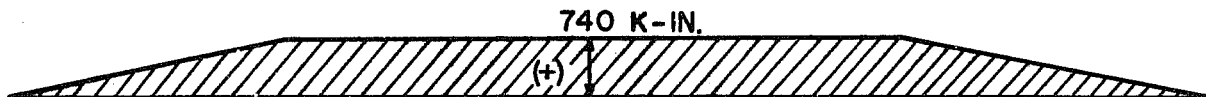
(B) HORIZONTAL FORCES DUE TO PRESTRESSING IN MAIN SPAN ( $F_{I3}$ )(C) MOMENTS DUE TO PRESTRESSING IN MAIN SPAN ( $M_{I3}$ )(D) MOMENTS DUE TO RESULTANT FORCE OF PRESTRESSING IN MAIN SPAN AND JACKING FORCES AT OUTER SUPPORTS ( $M_{E2}$ )

Fig. 8.16. Horizontal forces and moments due to prestressing in main span

forces used to adjust the reactions and elevations at the outer supports are shown in Fig. 8.16 (d).

$F_{I1}$ ,  $F_{I2}$ ,  $F_{I3}$ , and  $M_{I1}$ ,  $M_{I2}$ ,  $M_{I3}$ ,  $M_{E1}$ , and  $M_{E2}$  are the forces and moments acting on the bridge at the time of completion of construction. Figure 8.17 shows the total or net horizontal forces and moments at each joint at the completion of all prestressing operations.

In order to compute the ultimate capacity of the bridge for the additional dead and live load, the following procedure was used. The basic ultimate design guide used, the 1969 BPR "Strength and Serviceability Criteria, Reinforced Concrete Bridge Members, Ultimate Design,"<sup>7</sup> specifies  $1.35 M_{DL}$  as the ultimate dead load moment. This value ( $1.35 M_{DL}$ ) was used for designing the bridge<sup>16</sup> by assuming the basic structural configuration as the same for both the 1.0 DL and 0.35 DL. In designing the positive tendons of the prototype, the external design ultimate moment was calculated as an ideal three span continuous beam as follows:

$$M_u = 1.35 M_{DL} + 2.25 M_{(LL + IL)} + M_{s1} + M_{s2} + M_{s3}$$

to be computed as an ideal three span continuous beam

where

$M_{DL}$  = moment due to dead load

$M_{(LL + IL)}$  = moment due to (live + impact) load

$M_{s1}$  = secondary moment due to prestressing of negative tendons

$M_{s2}$  = secondary moment due to prestressing of positive tendons in the main span

$M_{s3}$  = secondary moment due to prestressing of positive tendons in the side span

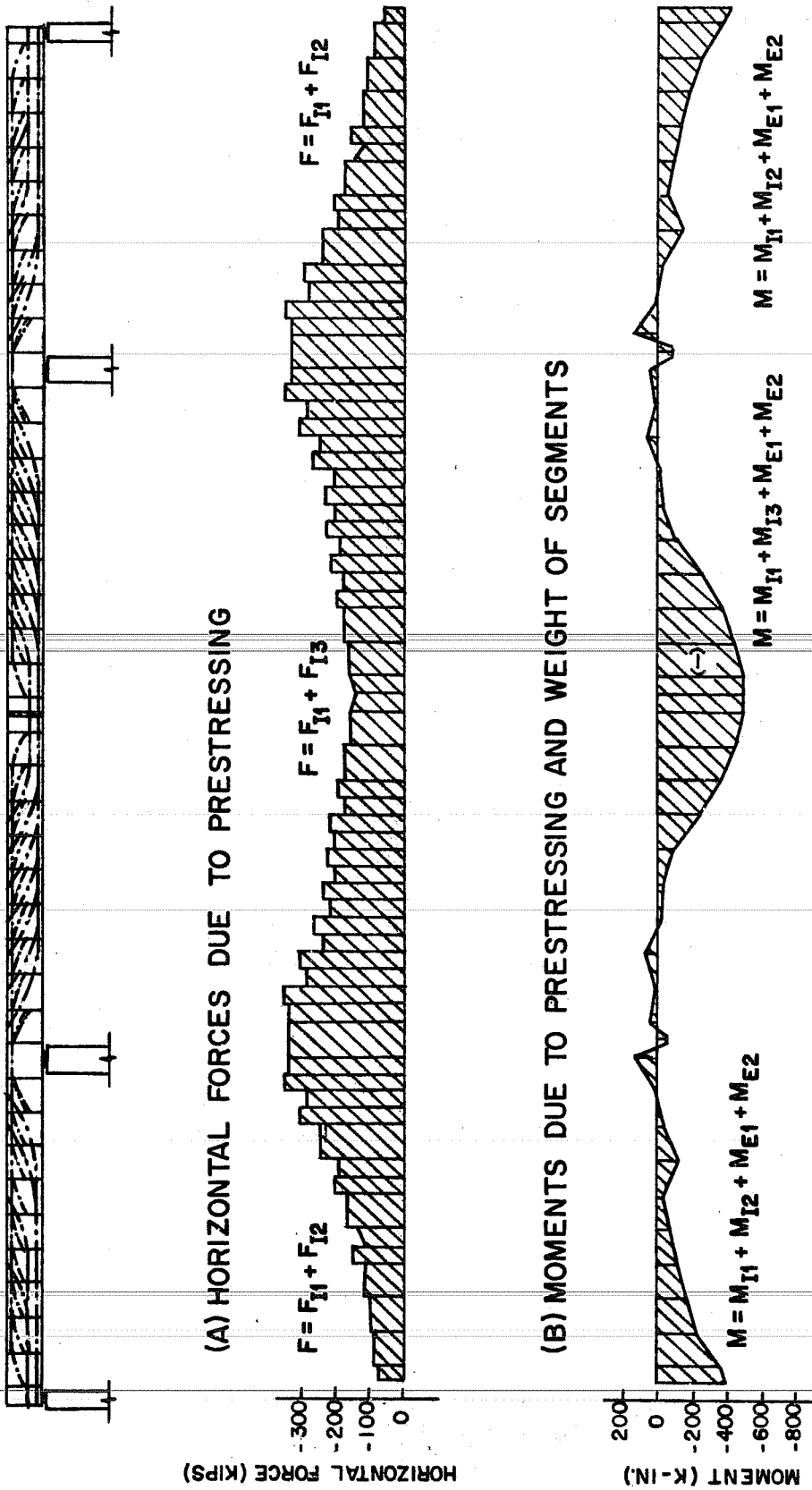


Fig. 8.17. Horizontal forces and moments at completion of all prestressing operations

Secondary moments due to prestressing of all negative and positive tendons were calculated in the design ultimate moment as shown in the above equation.<sup>16</sup> An additional 0.35 DL may represent additional weight due to heavier sections which would be caused by casting errors or allow for later changes in the bridge. Since these types of segments are cast in a factory under close control of an engineer, there seems to be less possibility of occurrence. It may be logical to apply some of the 0.35 DL on a balanced cantilever and the rest of 0.35 DL on the completed continuous structure. However, that condition could not be simulated on the completed model structure and the additional 0.35 DL was applied as a type of live load on the structure after completion of construction. It is necessary to calculate the moment due to 1.0 DL and 0.35 DL separately. The moment for 1.0 DL should be calculated for the determinate structure (balanced cantilever) and that for the 0.35 DL (which was applied to the completed structure after service load testing) should be calculated for the indeterminate three span continuous beam structure. The moment due to 0.35 DL ( $M_{E3}$ ) is shown in Fig. 8.18. Figure 8.19 shows the critical design truck loading in the side span and the corresponding moment diagram at service load of 1.0 (LL + IL). If the increment of the service (live + impact) load is increased, a flexural failure of the bridge will occur in either rupture of the concrete or of the prestressing cables. The positive tendons in the positive moment region and the negative tendons in the negative moment region as well as the concrete compression zones present primary resistance to live load.

The following equations for the ultimate external moment were used to calculate the LF of (LL + IL) in the model tests as if the structure was an ideal three span continuous beam after completion.

$$M_u = M_{u1} + M_{u2}$$

$$M_{u1} = 1.0 M_{DL} \text{ to be computed as a balanced cantilever } (= M_{E1})$$

$$M_{u2} = 0.35 M_{DL} + LF \times M_{(LL+IL)} + M_s \text{ to be computed as an ideal}$$

three span continuous beam

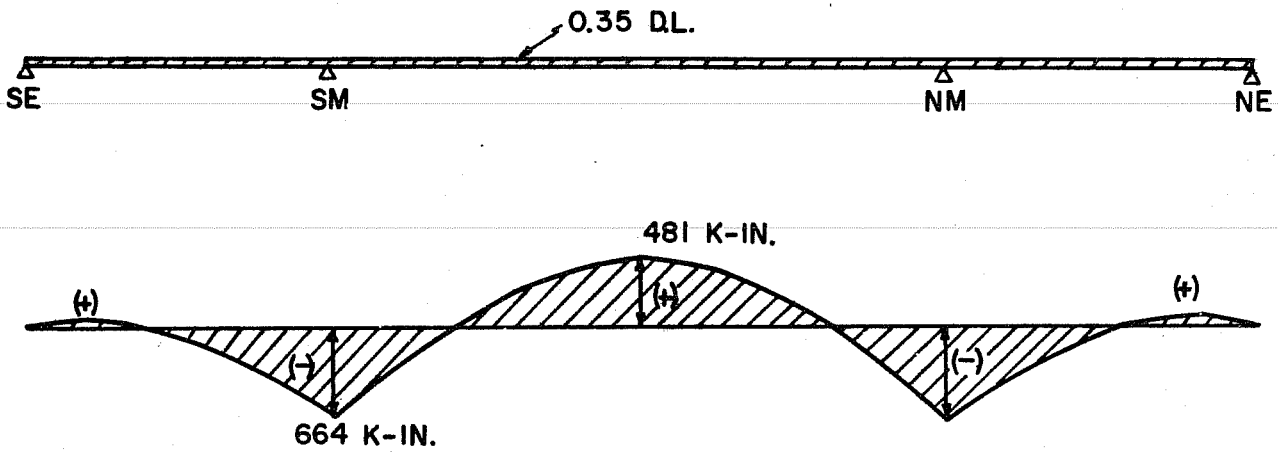


Fig. 8.18. Moment diagram for 0.35 DL ( $M_{E3}$ )

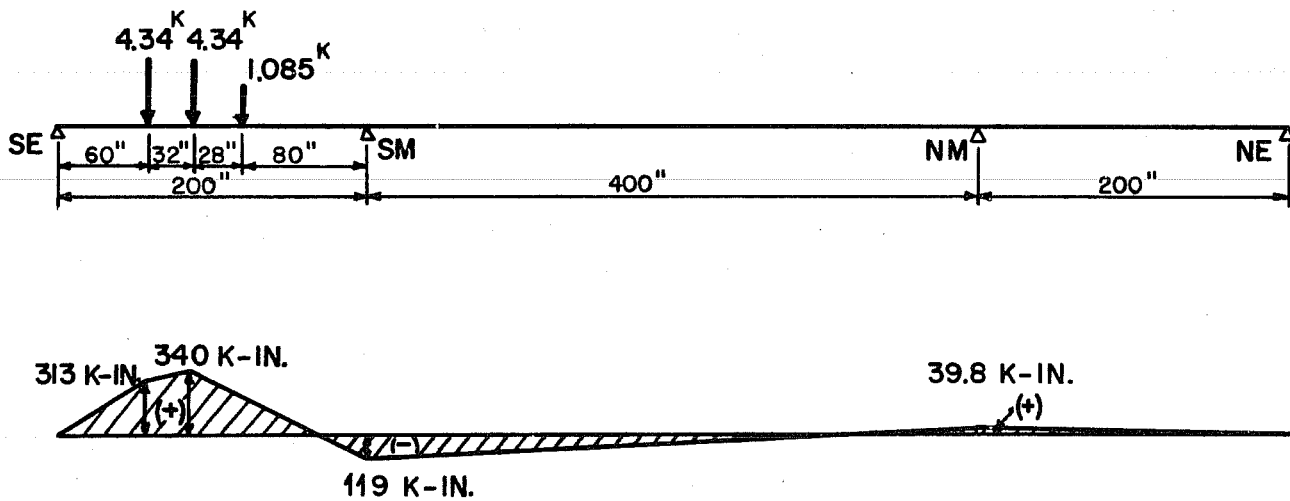


Fig. 8.19. Moment diagram for truck loads in side span ( $M_{E4}$ )

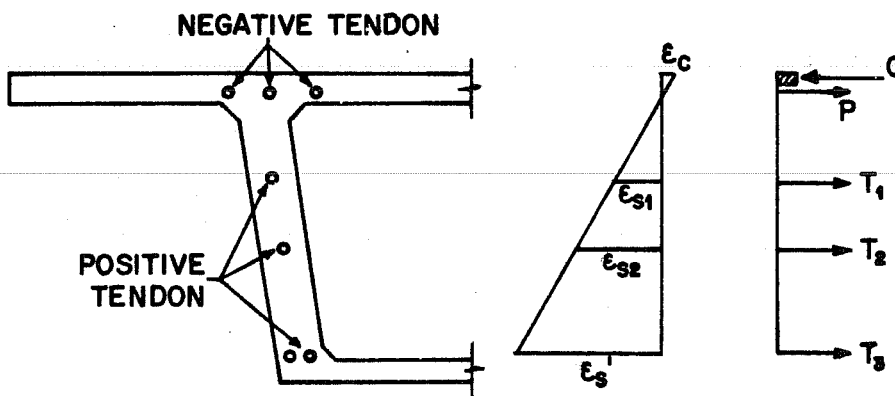
where

$$0.35 M_{DL} = M_{E3}$$

$$M_{(LL+IL)} = M_{E4}$$

$$M_s = M_{E2}$$

In very underreinforced sections, as in the positive moment region, the ultimate compressive force ( $C$ ) and the tensile force ( $\Sigma T_i$ ) may be calculated by assuming the bottom layer of prestressing cables as its ultimate strain ( $\epsilon'_s$ ). If joint 6-7 in the side span is taken, prestressing forces ( $P$ ) due to negative tendons add to  $C$  and  $T$ , as shown in Fig. 8.20. These  $P$  forces have to be taken into account for the ultimate moment capacity, except at the closure segment.



$C$  : ULTIMATE COMPRESSIVE FORCE  
 $P$  : FORCE DUE TO NEGATIVE TENDON  
 $T$  : ULTIMATE TENSILE FORCE

Fig. 8.20. Ultimate force at a certain section

Since the positive tendons were placed in multiple layers in some sections, it is necessary to use the stress-strain curve of each

cable in order to find  $T_1$ . Although several specimens were tested in an attempt to obtain stress-strain curves for wires and strands up to failure, a complete stress-strain curve up to failure was not obtained. This type of steel usually failed at the grips in the testing machine. A stress-strain curve for a 270K grade 7-wire strand tested by a manufacturer was modified as shown in Fig. 8.21, since the ultimate strength of all prestressing cables and  $E_s$  of some prestressing cables were known from the material tests. The ultimate strain of prestressing cables was assumed as 0.06 in./in.<sup>20</sup>

In order to find the ultimate forces at joint 6-7 in the side span,  $T_1$  was found first by using the stress-strain curves of Fig. 8.21. Compressive strains for the concrete in the top fiber were assumed for three different cases ( $\epsilon_c = 0.003, 0.002, \text{ and } 0.0015 \text{ in./in.}$ ) and then  $\Sigma T_1$  was found, as shown in Fig. 8.22. There was no difference in  $\Sigma T_1$  whether  $\epsilon_c$  at the compression fiber was 0.003, 0.002 or 0.0015 in./in., and it was not necessary to make further iterations for  $T_1$  in order to find the internal ultimate moment capacity. By assuming  $\epsilon_c = 0.003 \text{ in./in.}$  at the extreme compression fiber and a rectangular stress block, as shown in Fig. 8.23 (a), C and P were calculated as follows:

$$\epsilon'_s = 0.06 \text{ in./in.}$$

$$\epsilon_c = 0.003 \text{ in./in.}$$

$$c = 0.72 \text{ in.}$$

$$a = 0.70 \times 0.72 = 0.504 \text{ in.}$$

$$C = 0.85 f'_c \times a \times b = 0.85 \times 7.09 \times 0.504 \times 112 = 340 \text{ kips.}$$

$$P = 49.6 - A_p \times E_s \times \epsilon_p = 49.6 - 0.348 \times 30.9 \times 10^3 \times 0.00025 \\ = 49.6 - 2.7 = 46.9 \text{ kips.}$$

$$C = 340 \gg P + T_1 = 46.9 + 127 = 174 \text{ kips.}$$



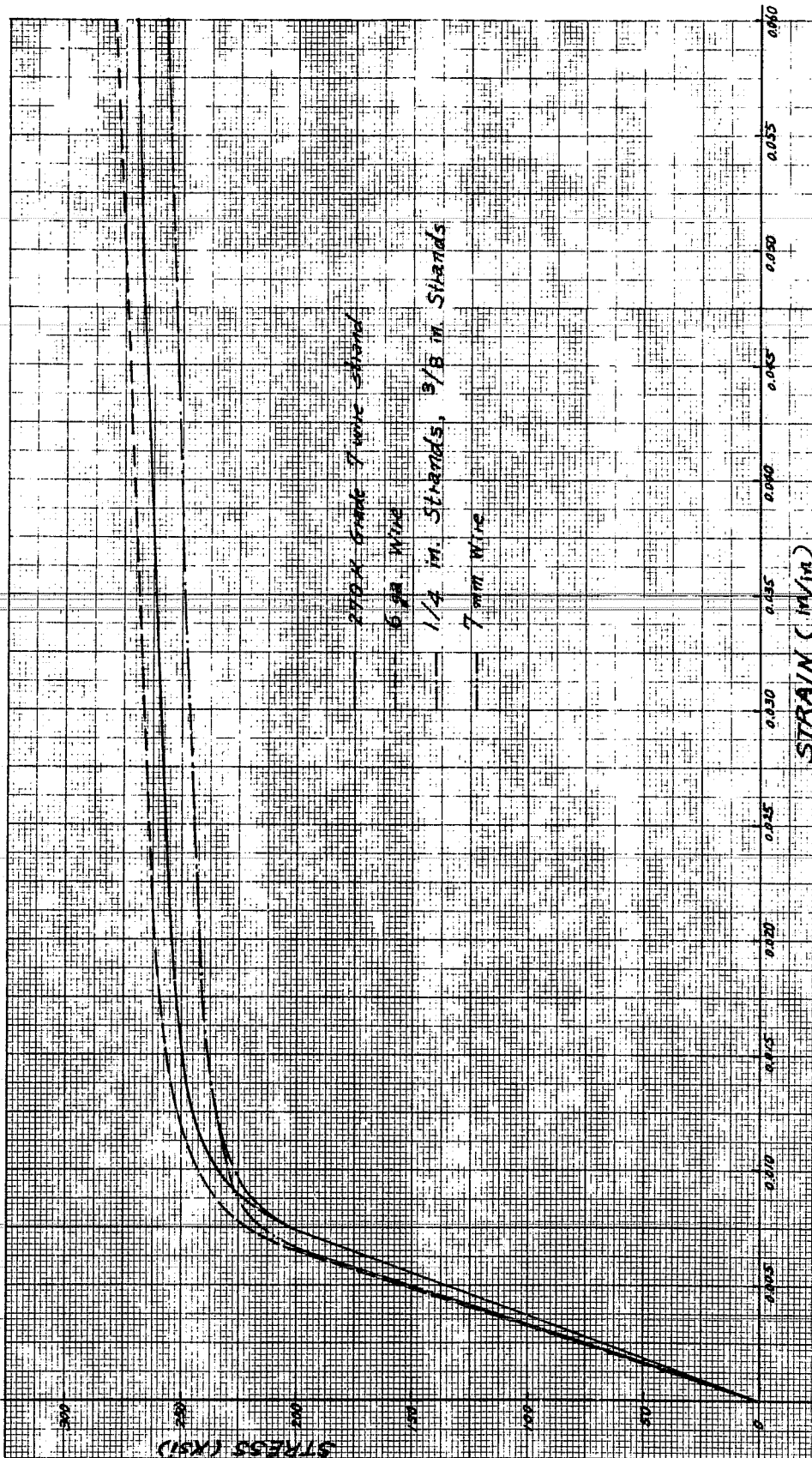
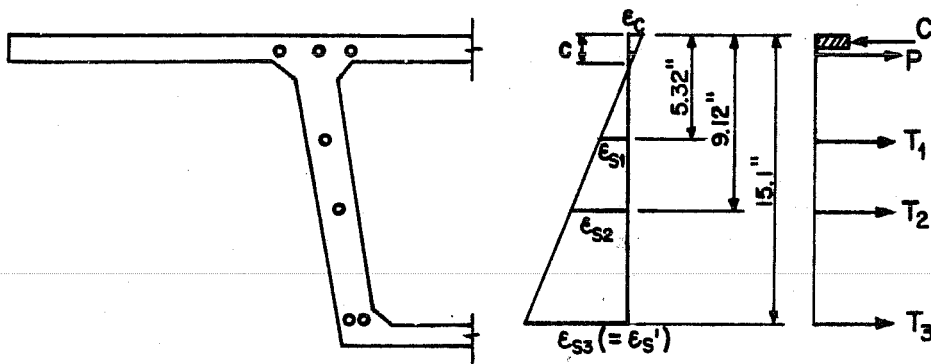


Fig. 8.21. Stress-strain curves of prestressing cables



CASE (1) -  $\epsilon_{s3} = 0.06$  IN./IN.,  $\epsilon_c = 0.003$  IN./IN.,  $c = 0.72$  IN.

$\epsilon_s$ (IN./IN.)	$\sigma_s$ (KSI)	$T_i$ (KIPS)	$T_i$ for 2 boxes (KIPS)	$\Sigma T_i$ (KIPS)
$\epsilon_{s1} = 0.019$	261	7.57	30.3 ( $T_1$ )	127
$\epsilon_{s2} = 0.035$	269	7.80	31.2 ( $T_2$ )	
$\epsilon_{s3} = 0.06$	280	8.11	65.0 ( $T_3$ )	

CASE (2) -  $\epsilon_{s3} = 0.06$  IN./IN.,  $\epsilon_c = 0.002$  IN./IN.,  $c = 0.49$  IN.

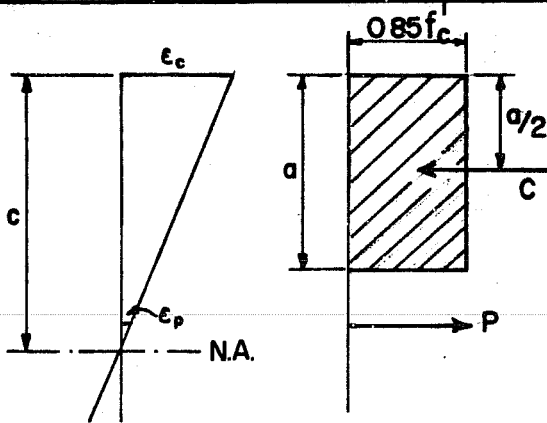
$\epsilon_s$ (IN./IN.)	$\sigma_s$ (KSI)	$T_i$ (KIPS)	$T_i$ for 2 boxes (KIPS)	$\Sigma T_i$ (KIPS)
$\epsilon_{s1} = 0.020$	262	7.60	30.4 ( $T_1$ )	127
$\epsilon_{s2} = 0.035$	269	7.80	31.2 ( $T_2$ )	
$\epsilon_{s3} = 0.06$	280	8.11	65.0 ( $T_3$ )	

CASE (3) -  $\epsilon_{s3} = 0.06$  IN./IN.,  $\epsilon_c = 0.0015$  IN./IN.,  $c = 0.37$  IN.

$\epsilon_s$ (IN./IN.)	$\sigma_s$ (KSI)	$T_i$ (KIPS)	$T_i$ for 2 boxes (KIPS)	$\Sigma T_i$ (KIPS)
$\epsilon_{s1} = 0.020$	262	7.60	30.4 ( $T_1$ )	127
$\epsilon_{s2} = 0.036$	269	7.80	31.2 ( $T_2$ )	
$\epsilon_{s3} = 0.06$	280	8.11	65.0 ( $T_3$ )	

Fig. 8.22. Calculation of  $T_i$  for different strain profiles

**(A) RECTANGULAR STRESS BLOCK**



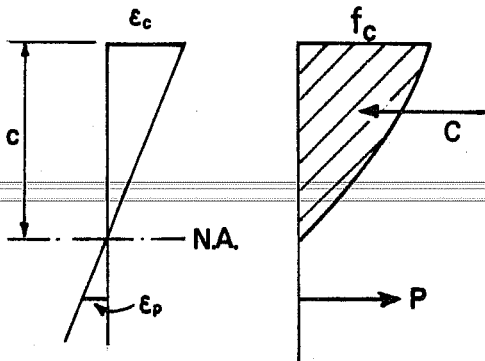
$\epsilon_c$  = CONCRETE STRAIN

$c$  = DISTANCE FROM EXTREME COMPRESSION FIBER TO NEUTRAL AXIS AT ULTIMATE STRENGTH

$a$  = DEPTH OF EQUIVALENT RECTANGULAR STRESS BLOCK =  $k_1 c$

$f_c'$  = COMPRESSIVE STRENGTH OF CONCRETE

**(B) PARABOLIC STRESS BLOCK**



$b$  = WIDTH OF COMPRESSION FACE OF FLEXURAL MEMBER

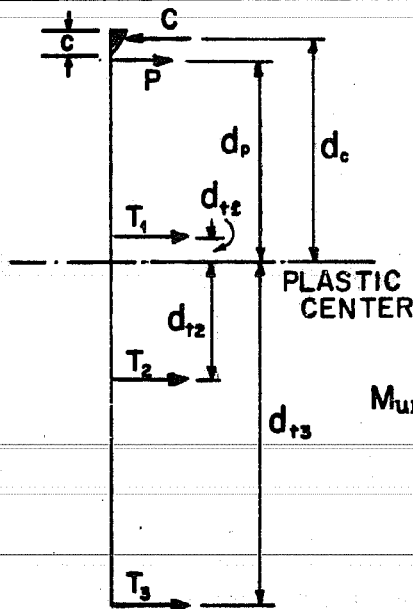
$\epsilon_p$  = STRAIN AT LEVEL OF PRESTRESSING CABLES (NEGATIVE TENDONS)

$A_p$  = AREA OF PRESTRESSING CABLES

$C$  = ULTIMATE COMPRESSIVE FORCE

$P$  = FORCE DUE TO NEGATIVE TENDON

**(C) CALCULATION OF ULTIMATE INTERNAL MOMENT**



$T$  = ULTIMATE TENSILE FORCE

$d_c, d_p, d_{ti}$  = DISTANCE FROM PLASTIC CENTER TO EACH FORCE

$$M_{ULT} = C \times d_c - P \times d_p - T_1 \times d_{t1} + T_2 \times d_{t2} + T_3 \times d_{t3}$$

Fig. 8.23. Calculation of ultimate internal moment

This indicated that the compressive strain at the top fiber had not reached 0.003 in./in. Then, by assuming the strain at the bottom of steel as 0.06 in./in. and the parabolic stress block shown in Fig. 8.23 (b), C and P were found after several trials using  $C = \Sigma T_i + P$ . The internal ultimate moment was then calculated as follows (see Fig. 8.23 (c)):

$$\epsilon'_c = 0.0015 \text{ in./in.}$$

$$c = 0.37 \text{ in.}$$

$$f_c = 0.95 \times f'_c = 0.95 \times 7.09 = 6.74 \text{ ksi.}$$

$$\epsilon_p = 0.0012 \text{ in./in.}$$

$$P = 49.6 + 0.348 \times 30.9 \times 10^3 \times 0.0012 = 62.5 \text{ kips.}$$

$$C = 187 \text{ kips.}$$

$$C = 187 \neq \Sigma T_i + P = 62.5 + 127 = 189.5 \text{ kips.}$$

$$\begin{aligned} M_{UI} &= C \times d_c - P \times d_p - T_1 \times d_{t1} + T_2 \times d_{t2} + T_3 \times d_{t3} \\ &= 187 \times 5.90 - 62.5 \times 5.46 - 30.4 \times 0.8 + 31.2 \times 3.0 + \\ &\qquad\qquad\qquad + 65 \times 8.98 \\ &= 1103 - 341 - 24.3 + 93.6 + 584 = 1415 \text{ k-in.} \end{aligned}$$

At the peak compressive strength of concrete, strains reach about 0.002 in./in. for various strengths of concrete, as found in experiments.<sup>19</sup>

If the strain at the peak stress is assumed as 0.002 in./in., about 95 percent of  $f'_c$  will develop at the extreme fiber for 0.0015 in./in. strain.<sup>21</sup> Therefore,  $f_c$  was calculated by  $0.95 \times f'_c$  in the above calculation.

In all calculations of the ultimate moment and shear capacity,  $\phi = 1.0$  was used in the model, since all dimensions and internal strengths were known.

In overreinforced sections (around the main pier), the concrete strain at failure at the bottom fiber was assumed as 0.003 in./in. according to the ACI Code<sup>2</sup> and strains were calculated at the position of the prestressing cables. The compressive stress block was assumed as rectangular. Several trials were made until C was equal to T by changing c in Fig. 8.24 (c). T was calculated by using stress-strain curves of Fig. 8.21 for  $\epsilon_s = \epsilon_{sp} + \epsilon_{sl}$ . Although some compressive strain existed at the bottom fiber before applying any live load, the magnitude (about 0.00015 in./in.) was very small compared to  $\epsilon_c = 0.003$ . Therefore, this effect was neglected and the strain was simply assumed as 0.003 in./in. at the bottom fiber in order to calculate the ultimate moment at the pier. After several trials, the internal ultimate moment at the pier. After several trials, the internal ultimate moment was calculated as follows:

$$c = 2.46 \text{ in.}$$

$$\epsilon_c = 0.003 \text{ in./in.}$$

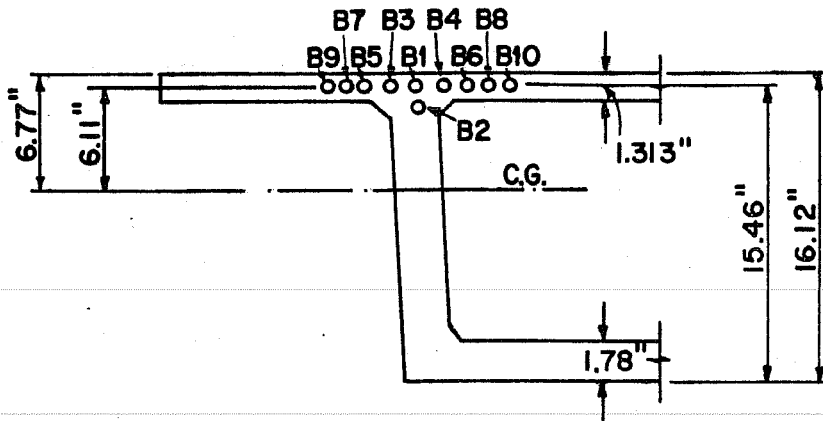
$$a = 0.7 c = 1.72 \text{ in.}$$

$$b = 52 \text{ in.}$$

$$C = 0.85 f'_c \times a \times b = 0.85 \times 7.09 \times 1.72 \times 52 = 539 \text{ kips.}$$

	Area (in. <sup>2</sup> )	$\epsilon_{sp}$ (in./in.)	$\epsilon_{sl}$ (in./in.)	$\epsilon_s = \epsilon_{sp} + \epsilon_{sl}$	$\sigma_s$ (ksi)	T (kip)	T for 2 boxes (k)
3/8 in. strands	0.085	0.00600	0.0159	0.0219	243	20.7	166
7mm wire	0.0593	0.00495	0.0159	0.0199	242	14.4	288
6 ga. wire	0.029	0.00462	0.0159	0.0205	242	7.0	84
Total T =						538	

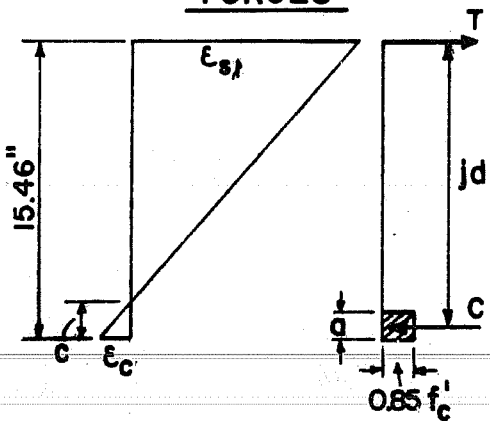
**(A) POSITION OF TENDONS AT MAIN PIER**



**(B) PROPERTIES OF EACH TENDON**

TENDONS		AREA (IN. <sup>2</sup> )	EXPERIMENTAL VALUE			APPLIED VALUE		
			F <sub>s</sub> ' (KIPS)	f <sub>s</sub> ' (KSI)	E <sub>s</sub> (KSI)	0.6 F <sub>s</sub> ' (KIPS)	0.6 f <sub>s</sub> ' (KSI)	ε <sub>SP</sub> AT 0.6f <sub>s</sub> ' (IN./IN.)
7 MM. WIRE	B1, B2, B5, B6, B7	0.0594	15.31	258	30.5 × 10 <sup>3</sup>	8.94	151	0.00495
8/16" STRANDS	B3, B4	0.085	22.05	259	27.0 × 10 <sup>3</sup>	13.75	162	0.00600
6 GA. WIRE	B8, B9, B10	0.029	8.13	280	30.9 × 10 <sup>3</sup>	4.14	143	0.00462

**(C) ULTIMATE INTERNAL FORCES**



- ε<sub>SP</sub> = STRAIN DUE TO PRESTRESSING (IN./IN.)
- ε<sub>S<sub>l</sub></sub> = STRAIN DUE TO EXTERNAL LOAD (IN./IN.)
- ε<sub>S</sub> = ULTIMATE STRAIN OF PRESTRESSING CABLE = ε<sub>SP</sub> + ε<sub>S<sub>l</sub></sub> (IN./IN.)
- ε<sub>c</sub> = 0.003 IN./IN.
- f'<sub>c</sub> = COMPRESSIVE STRENGTH OF CONCRETE
- T = TENSILE FORCE AT ULTIMATE (KIPS)
- C = ULTIMATE COMPRESSIVE FORCE
- c = DISTANCE FROM EXTREME COMPRES. FIBER TO NEUTRAL AXIS AT ULT. STRENGTH (IN.)
- jd = DISTANCE BETWEEN T & C (IN.)
- a = DEPTH OF EQUIV. RECT. STRESS BLOCK (IN.)
- b = WIDTH OF COMPRESSION FACE OF FLEXURAL MEMBER (IN.)

Fig. 8.24. Calculation of ultimate internal moment at pier section

$$jd = 15.46 - a/2 = 15.46 - 0.86 = 14.6 \text{ in.}$$

Ultimate Internal Moment:

$$M_{UI} = 538 \times 14.6 = 7855 \text{ k-in.}$$

Since the completed bridge is a three span continuous beam, it has to form two additional hinges for complete failure in the side span as shown in Fig. 8.25 (b). The LF for (LL + IL) to produce the first plastic hinge was calculated as follows:

Internal moment and external moment at the ultimate capacity are equated.

$$M_{UI} = M_{E1} + M_{E2} + M_{E3} + LF \times M_{E4}$$

$$LF \text{ for (LL + IL)} = \frac{M_{UI} - M_{E1} - M_{E2} - M_{E3}}{M_{E4}}$$

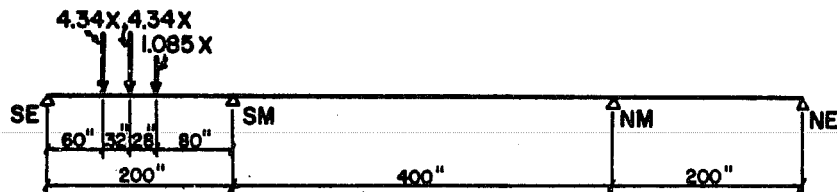
$$= \frac{1415 + 319 - 259 - 34}{322}$$

$$= 1441/322 = 4.48$$

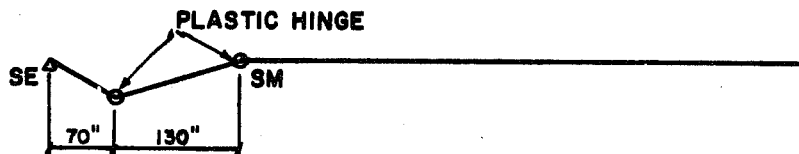
Therefore, a first plastic hinge should form at the 4.48 (LL + IL) increment (1.35 DL + 4.48 (LL + IL)), at the SS6-7 joint. Since the plastic hinge at the SS6-7 joint was observed to form between 4.25 to 4.38 (LL + IL) in the experiment, the calculated value (4.48) is very accurate.

Tensile strength of the only available 6 gage wire, which was used for the positive tendons in the side span was about 18 percent higher than the specified minimum, although all other prestress wires or strands had tensile strengths very close to the minimum values specified. It would therefore be expected that the first plastic hinge

## (A) LOADING CONDITION



## (B) FORMATION OF PLASTIC HINGE



## (C) PLASTIC MOMENT

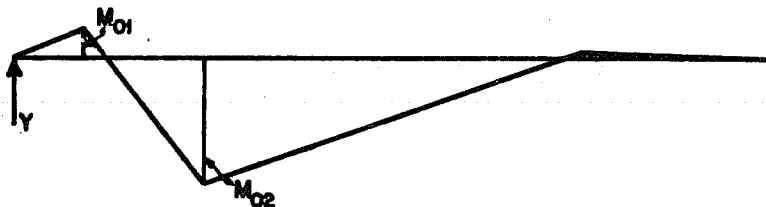


Fig. 8.25. Plastic hinges and moment diagram

in a prototype with strands having exactly the specified minimum tensile strength would form at a loading somewhat less than the test 4.48 (LL + IL) increment (at about 3.8 (LL + IL)).

If a second plastic hinge is assumed to form at the SM pier segment as shown in Fig. 8.25 (b) and the LF of (LL + IL) for complete failure is calculated as follows:

Assume

Y = reaction at the SE support.



$M_{01}$  = plastic moment at the SS6-7 joint ( $M_{UI}$  at the SS6-7 joint).

$M_{02}$  = plastic moment at the SM pier segment ( $M_{UI}$  at the SM pier segment).

$X$  = LF of (LL + IL).

From equilibrium, at the SS6-7 joint

$$M_{01} = - 4.34 \times 10X + 70Y \quad (1)$$

and at the center of the SM pier segment

$$\begin{aligned} - M_{02} &= - (4.34 \times 140 + 4.34 \times 108 + 1.085 \times 80)X \\ &+ 200 Y \quad (2) \end{aligned}$$

From Eq. (1)

$$1415 = - 43.4 X + 70 Y \quad (1)'$$

From Eq. (2)

$$- 7855 = - 1164 X + 200 Y \quad (2)'$$

$$[(2)' \times 0.35] - 2750 = - 408 X + 70 Y \quad (3)$$

$$[(1)' - (3)] \quad 4165 = 364 X \quad \therefore X = 11.4$$

Therefore the second plastic hinge would form around the 11.4 (LL + IL) increment (1.35 DL + 11.4 (LL + IL)) and the SM pier segment would fail in compression, if the initial plastic hinge had sufficient ductility. It is conservative to assume that the side span is fully capable of carrying (1.35 DL + 4.48 (LL + IL)) considering four lanes fully loaded. Using AASHTO load reduction factors for a four lane bridge, this would become (1.35 DL + 6.0 (LL + IL)).

### 8.3 Failure in the Main Span

#### 8.3.1 General

Four lane loads were applied to the main span and one adjacent side span to produce the critical shear condition at the first joint in the main span. It was anticipated from computations that with full development of shear strength the bridge would fail in flexure even though under a maximum shear loading. However, it was decided to check the shear capacity since basic information about flexural capacity was obtained by applying the truck loads to the side span. Lack of published information made it very desirable to check the performance of the epoxy joints under realistic high shear loadings.

In addition to the 1.35 dead load, live and impact loadings, shown in Fig. 8.26, were applied by rams and increased until failure.

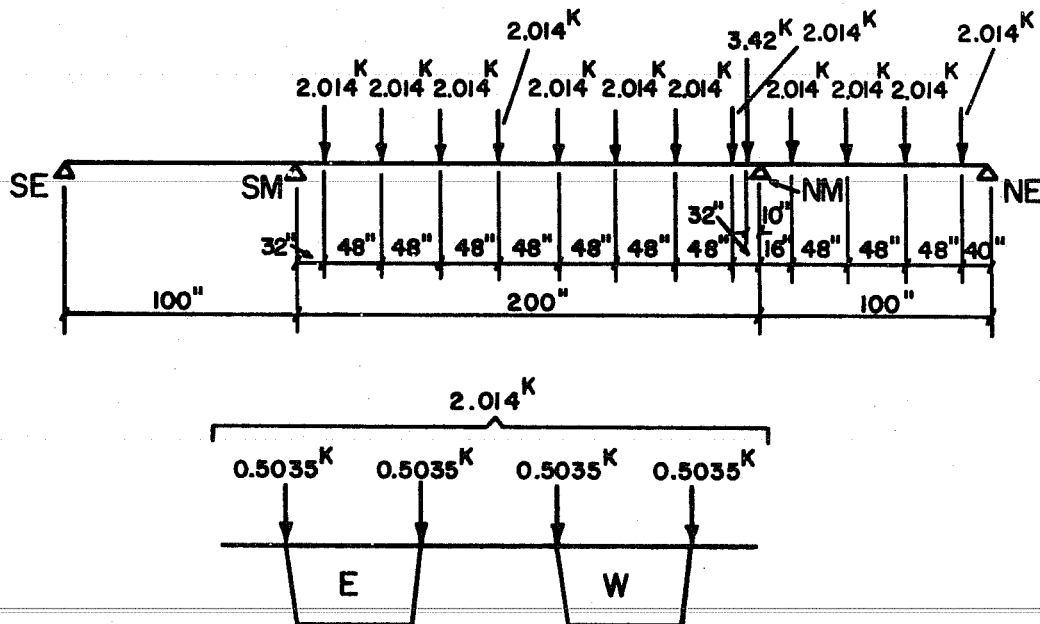


Fig. 8.26. 1.0 (LL + IL) loading for maximum shear at the NM pier

The position of the heavy concentrated load could greatly affect the shear strength of the bridge. It was considered that the direct shear failure might occur as the effective depth decreased due to flexural cracks, so concentrated loads were applied next to the first joint in the main span.

Strain gage measurements were taken at the positions shown in Fig. 4.14. The positions of dial gages were shown in Fig. 7.7.

Reaction readings were taken at outer supports. Crack formation was observed on the outer webs of the two boxes in both the main and side spans. Loading increments of 0.5 (LL + IL) were used up to loading of 2.0 (LL + IL), after which the increments were reduced to 0.25 (LL + IL) up to failure.

---

### 8.3.2 Test Results

---

After the loading of 2.25 (LL + IL), the reaction at the north end (NE) started to decrease, as shown in Fig. 8.27. At the 2.63 (LL + IL) increment, the south end segment (SE) raised completely from the neoprene pad support. At this load level the crack which had previously developed at the joint of the main span closure segment during the ultimate positive moment design test (see Sec. 7.3.3.2) started to reopen. In the strain diagrams of Figs. 8.28 to 8.30, strains in segments SS7, SS6, SS1, and SM1 increased almost linearly up to 2.63 (LL + IL), but remained constant after that increment because all end reaction was erased and no load was applied to the unloaded side span. Strain at NS6 was almost zero until the 2.5 (LL + IL) increment, then increased steadily until failure as shown in Fig. 8.31. This change was caused by the alteration in structural configuration when the south side span became a free cantilever.

---

At the 3.25 (LL + IL) increment, the strain increase at the NM6 segment stopped, as shown in Fig. 8.32. This was due to the concentration of deformation in the crack around the center of the main span. By observing the deflection diagram for the SM10 segment in Fig. 8.33, it is seen that the rate of deflection increase changed substantially at

---

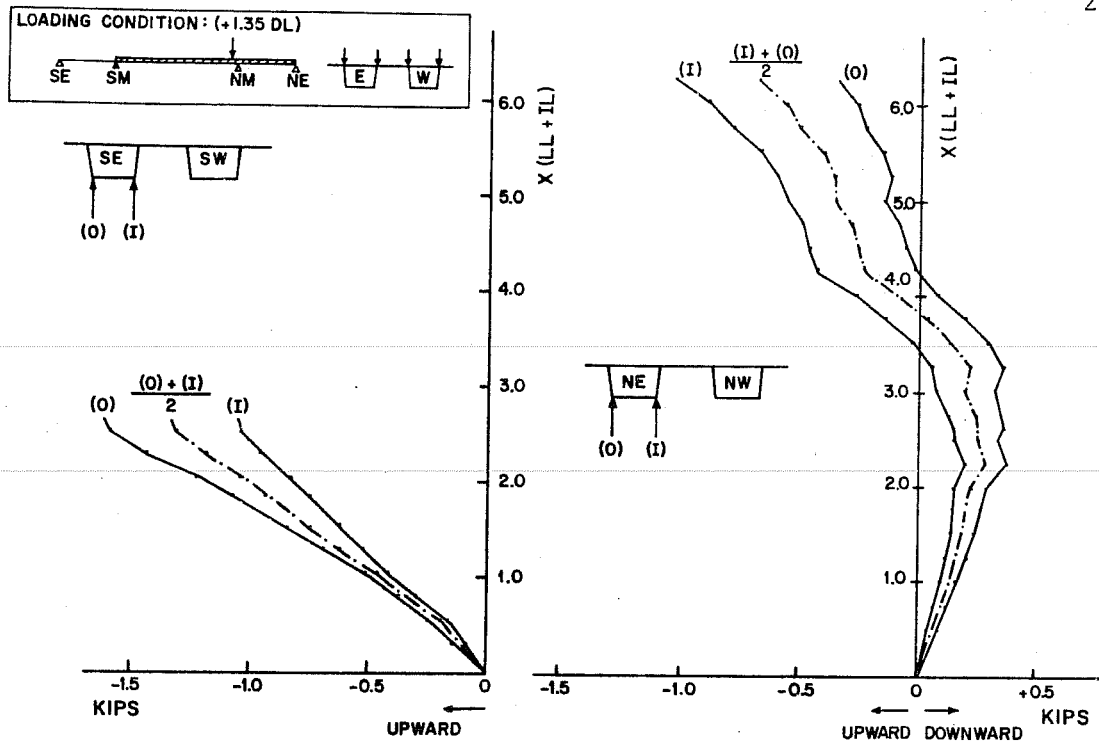


Fig. 8.27. Reaction at outer supports during loading to failure

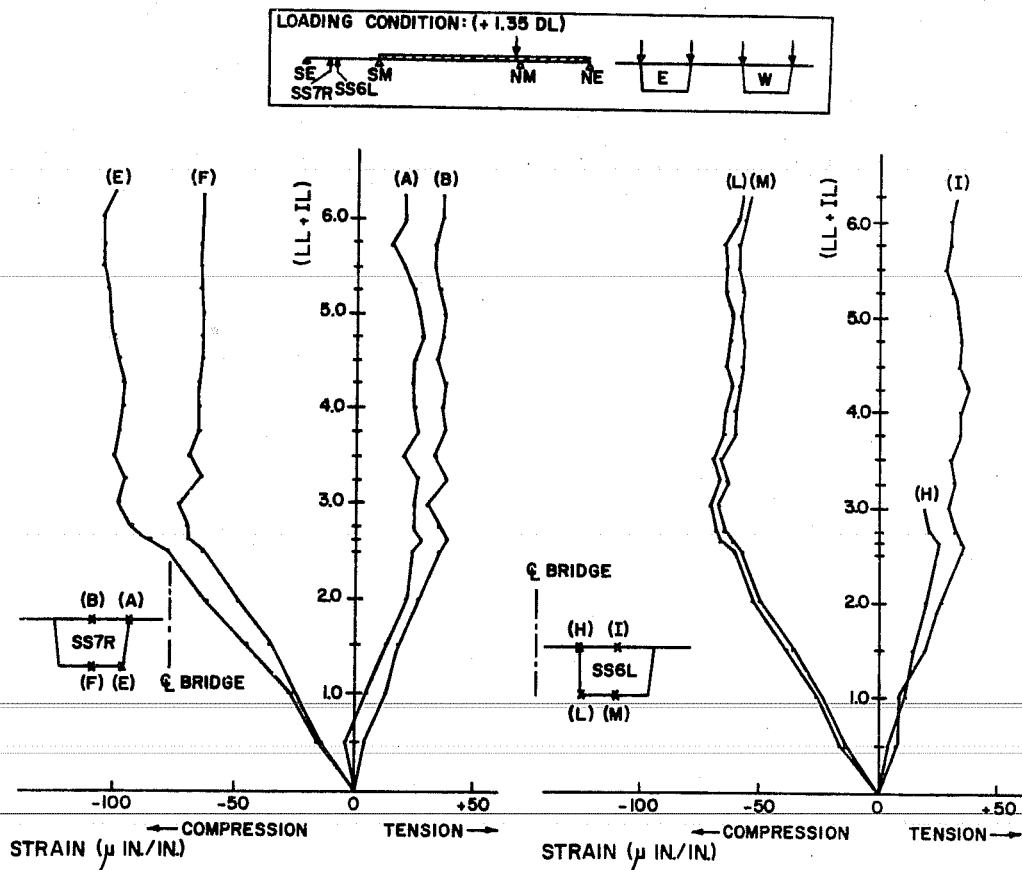


Fig. 8.28. Longitudinal strains at SS7R and SS6L during loading to failure

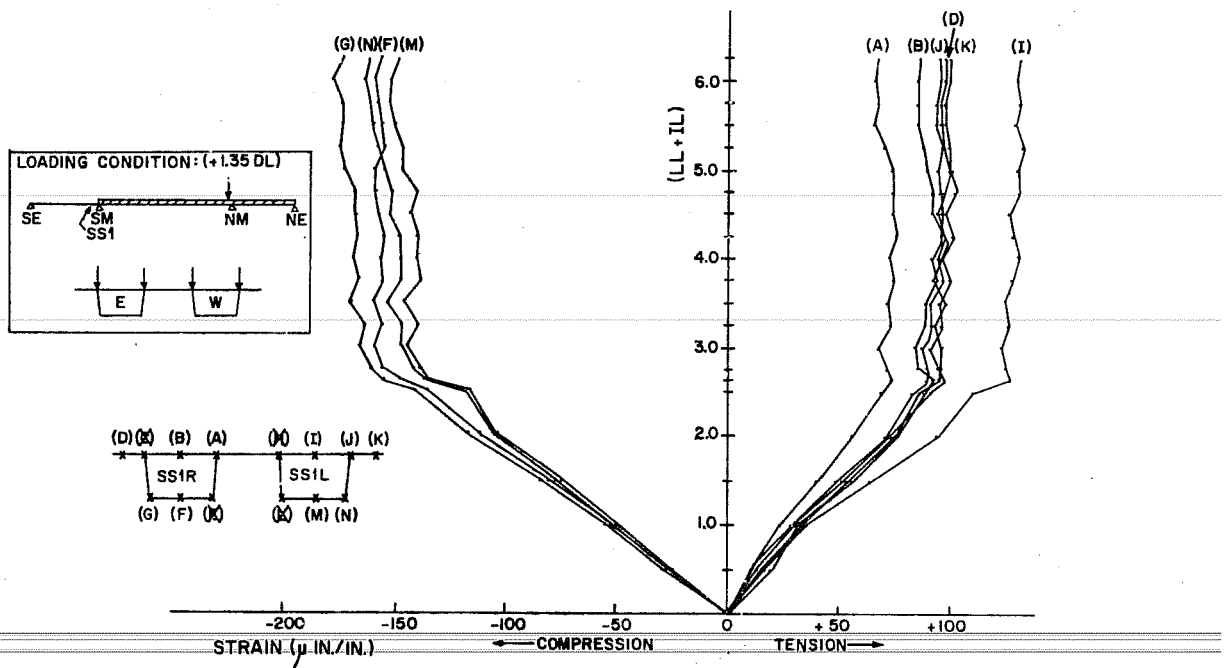


Fig. 8.29. Longitudinal strains at SS1 during loading to failure

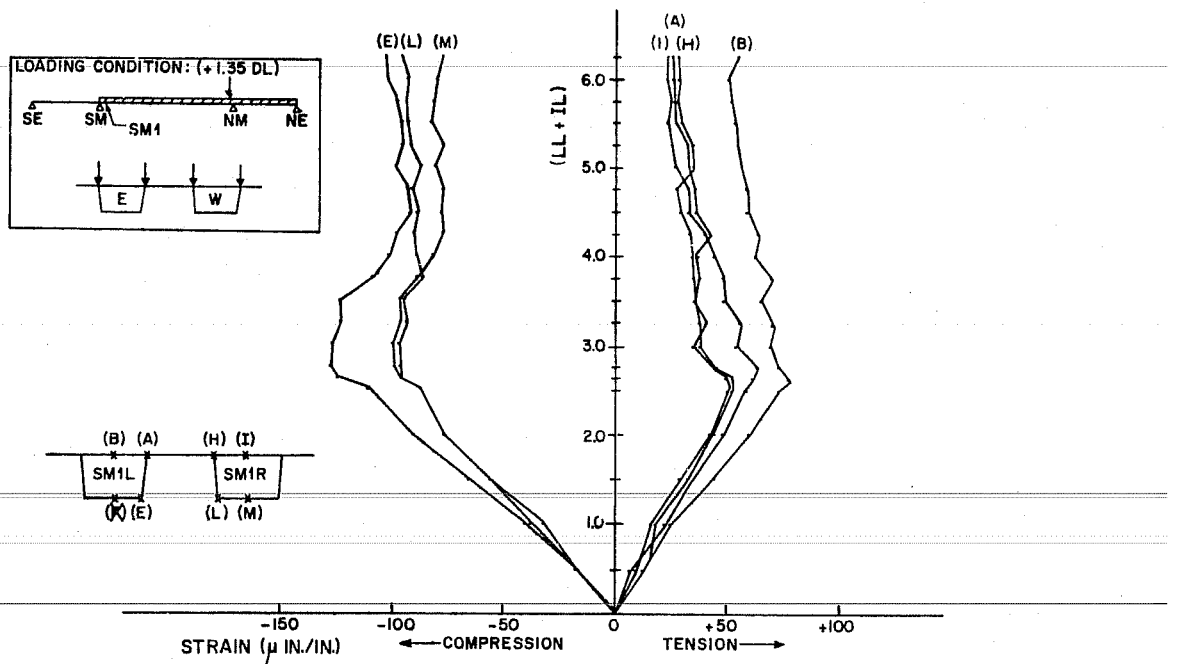


Fig. 8.30. Longitudinal strains at SM1 during loading to failure

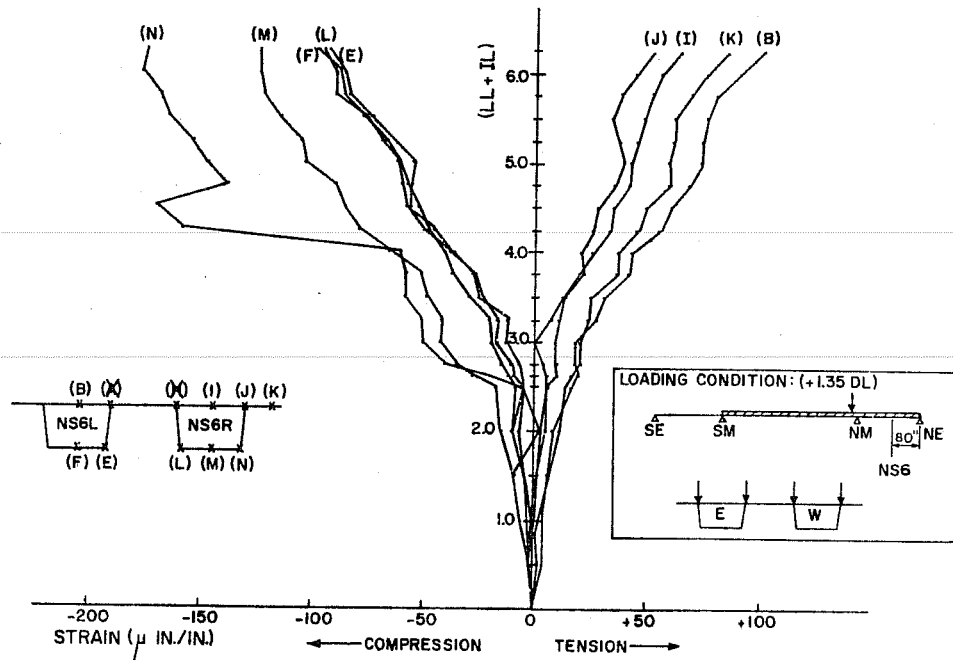


Fig. 8.31. Longitudinal strains at NS6 during loading to failure

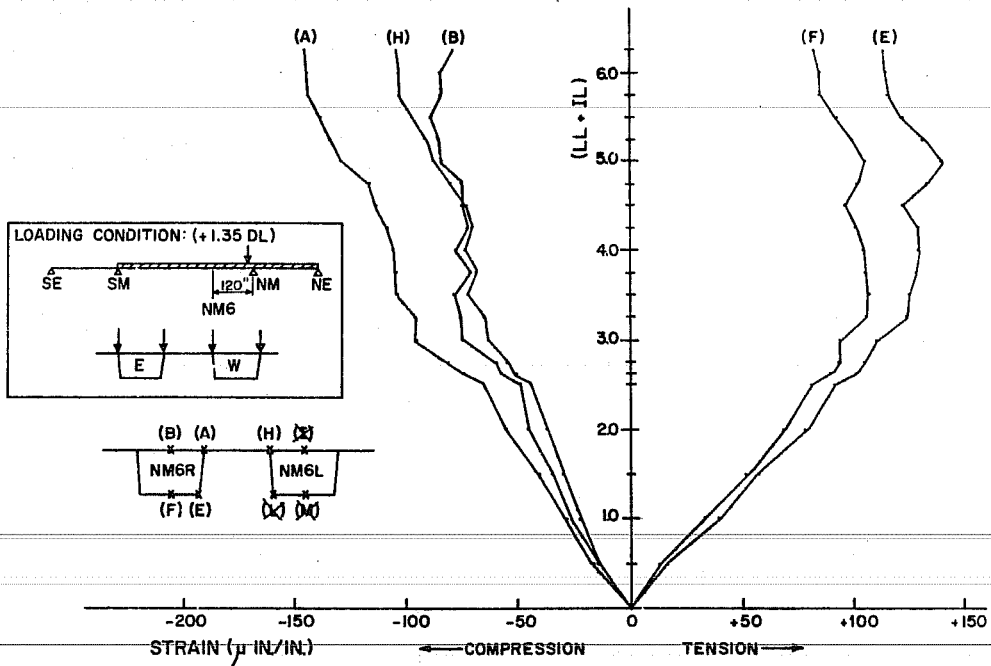


Fig. 8.32. Longitudinal strains at NM6 during loading to failure

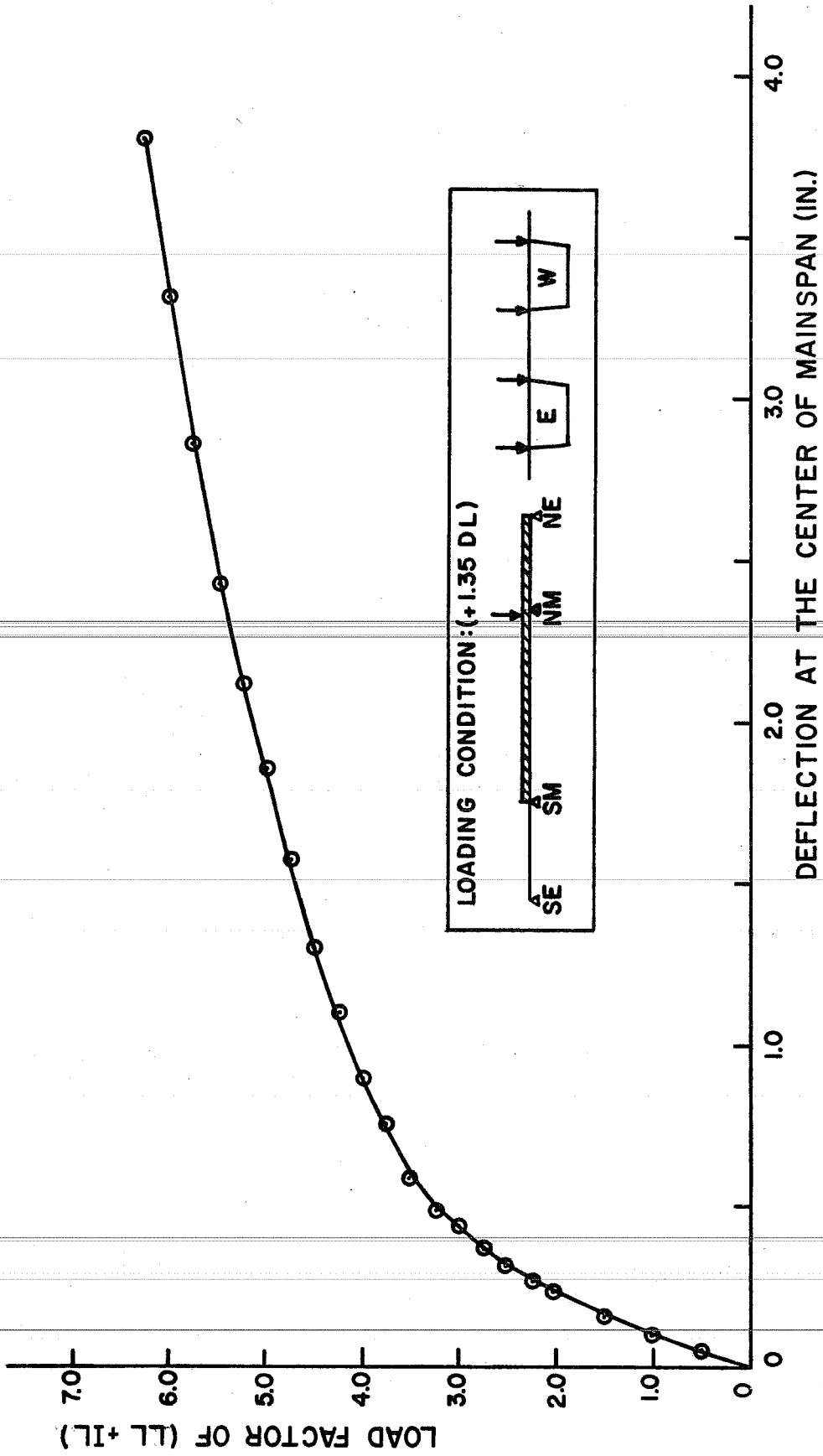


Fig. 8.33. Deflections at SM10 during loading to failure

3.25 (LL + IL). Also, a diagonal tension crack started to develop at the first segment in the main span (outer web on the west side) as shown in Fig. 8.34.

At the 3.75 (LL + IL) increment, a flexural crack at the joint of the closure segment extended to near the top of the web and many cracks started to develop in the region of segments SM6 to SM9, as shown in Fig. 8.35.

At the 4.25 (LL + IL) increment, the diagonal tension crack and the flexural crack around the NM pier joined and a wide flexural crack developed about 1 in. away from the first joint in the main span. At this stage, the flexural crack on the top slab was only in the outer cantilever portion. At this loading the south end segment raised up about 1 in. from the surface of the neoprene pad support.

At the 4.25 (LL + IL) increment in the east side and the 4.75 (LL + IL) increment in the west side, very wide flexural cracks developed at the SM6-7, SM7-8, and SM8-9 joints, as shown in Fig. 8.35. These cracks developed near the epoxy joints in the web portion (in the flexural tension zone) and about 1 in. away from the joint in the bottom slab (in the pure tension zone), as shown in Fig. 8.36. The cracks at these joints went nearly to the top of the web with an increase of one increment of loading. The increase of strain around the 4.00 to 4.75 (LL + IL) increment range at NM9, NM1, and NS1 stopped because of concentration of deformations at these joints and at the first joints from the main pier. Figure 8.37 to 8.39 show the effect of the concentration of deformation on strain at higher load.

At the 5.0 (LL + IL) increment, the crack on the top slab of segment NS1 and the NM pier segment extended the full width of the slab (on the east side of the box).

At the 5.75 (LL + IL) increment, the flexural cracks at the top slab near the NM pier extended the full width of the slab (two boxes). The flexural cracks at the SM6-7 and SM7-8 joints were getting



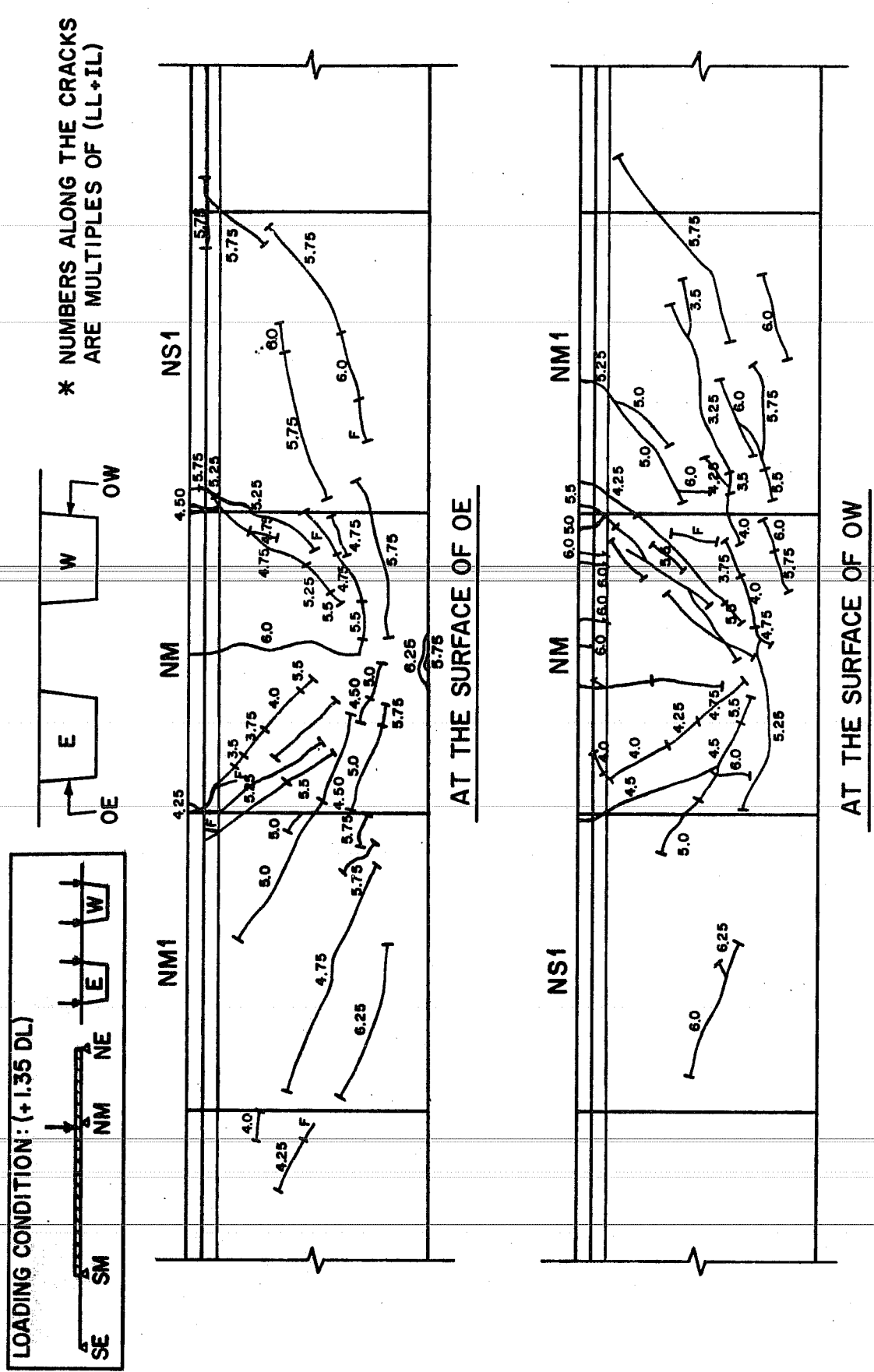


Fig. 8.34. Development of cracks around NM pier during loading to failure

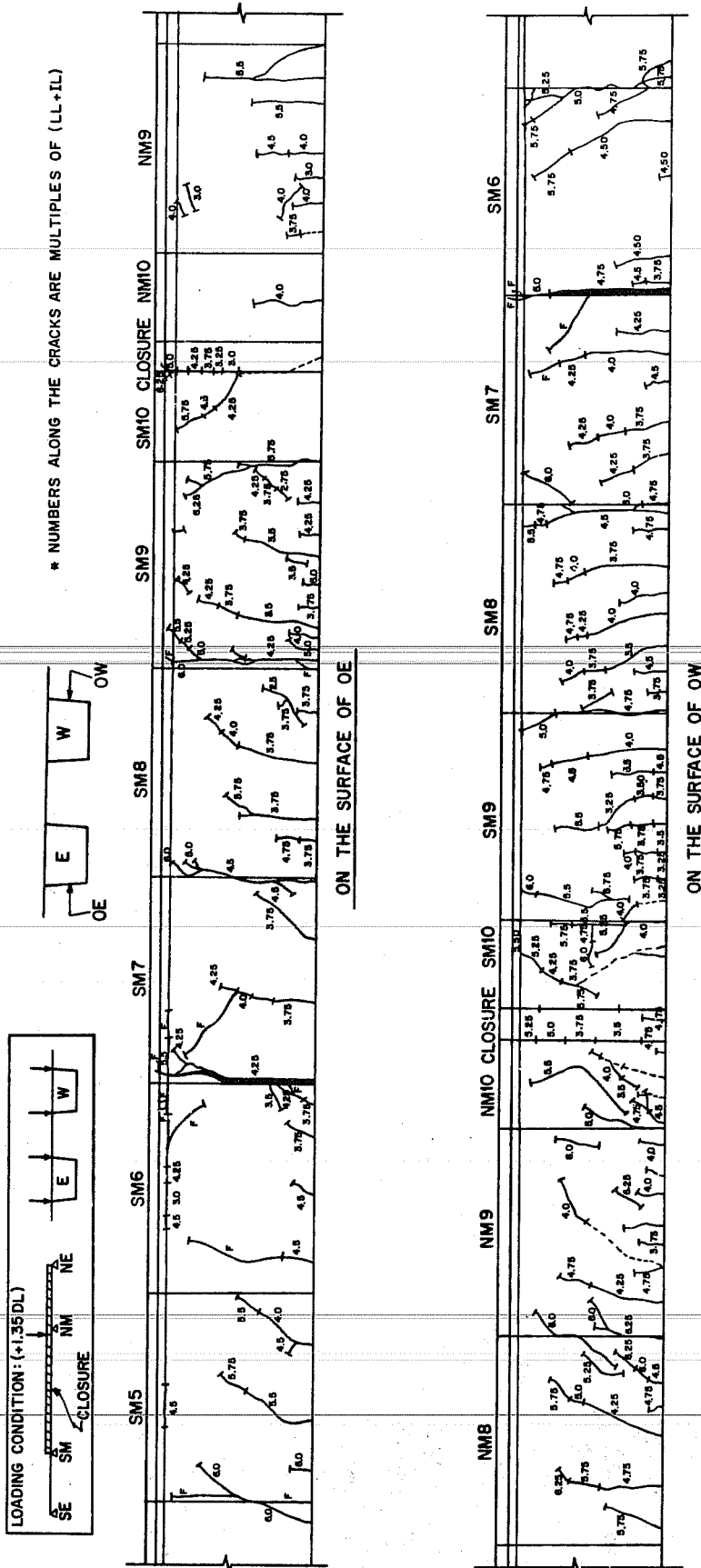


Fig. 8.35. Development of cracks around the center of main span during loading to failure

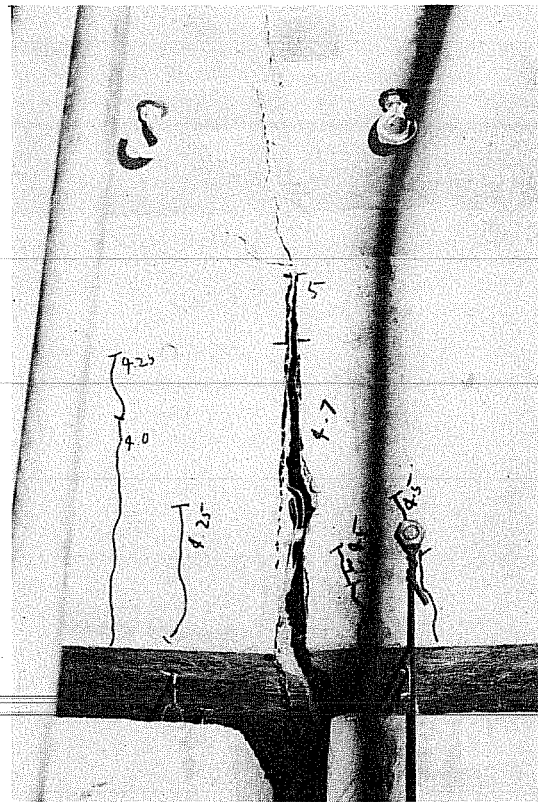


Fig. 8.36. Typical crack around the joint (after failure)

wider, but the width of cracks in some other portions were small. At this stage, the bridge looked straight from the SE pier to the SM6-7 joint and all major deformation was concentrated at the SM6-7 joint. The NM pier segment on the neoprene pad support started to crush on the east side, due to the high compression force.

At the 6.0 (LL + IL) increment, the width of the flexural crack at the SM6-7 joint was about 1/8 in. and the SE segment raised up about 4.5 in.

After taking the instrument readings at the 6.25 (LL + IL) increment, the loads were being increased to the 6.50 (LL + IL) increment when a sudden rupture of the positive moment prestressing cables occurred on the west side. This failure occurred before

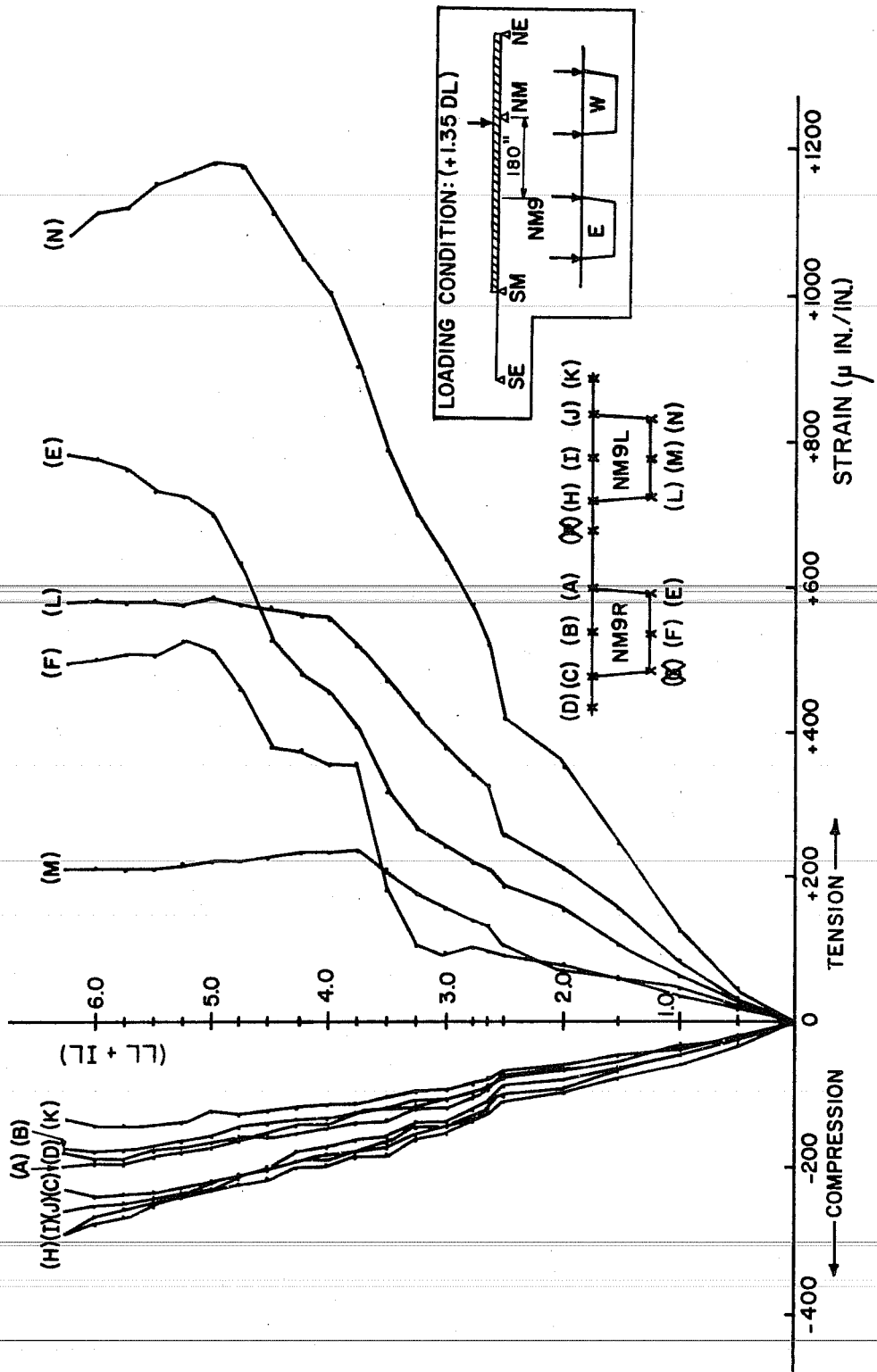


Fig. 8.37. Longitudinal strains at NM9 during loading to failure

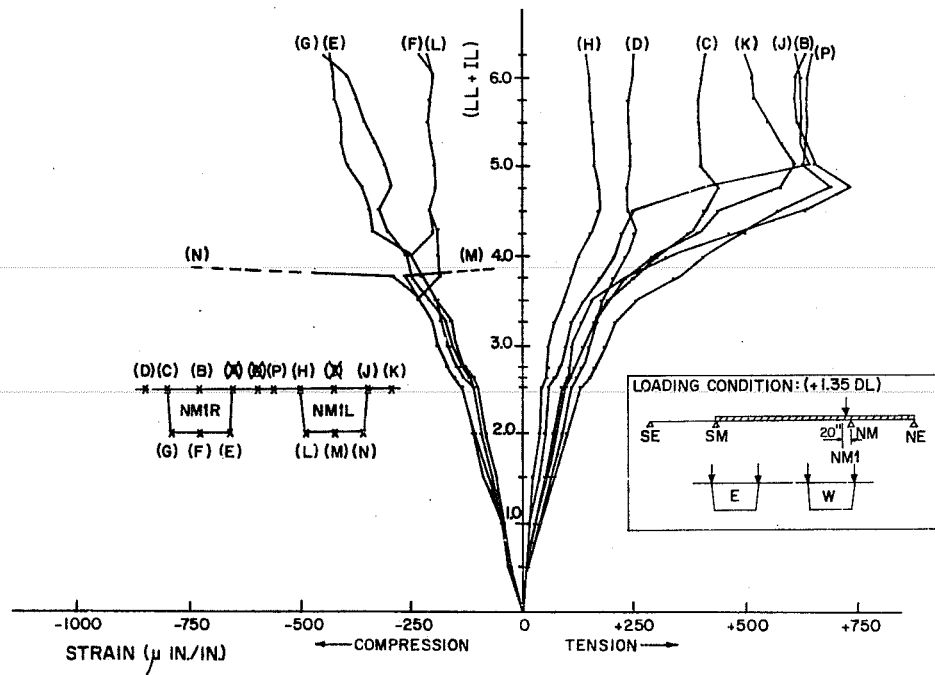


Fig. 8.38. Longitudinal strains at NMI during loading to failure

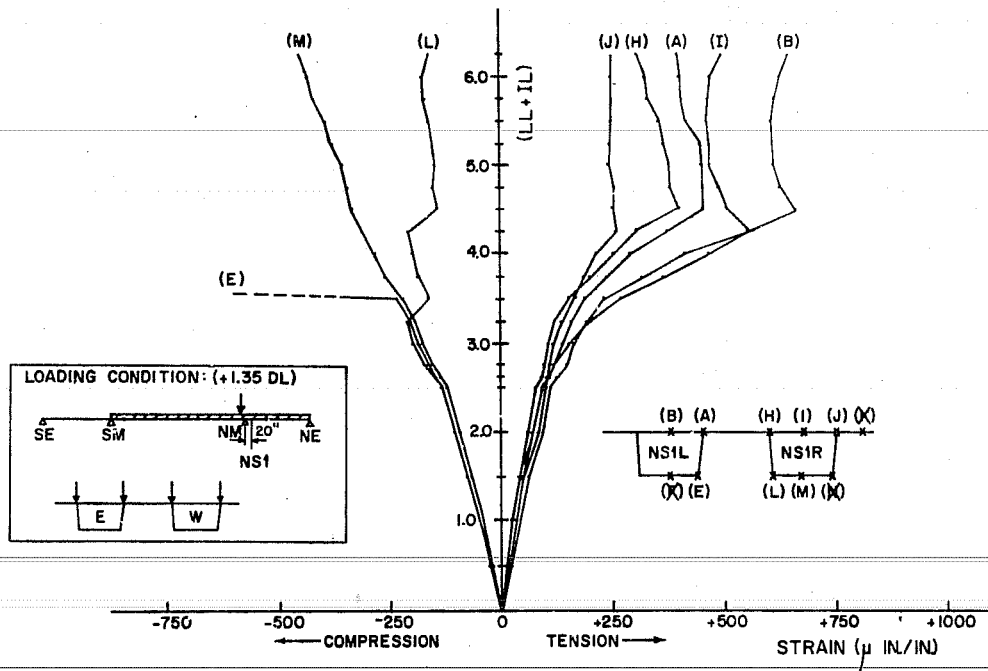


Fig. 8.39. Longitudinal strains at NS1 during loading to failure

applying less than half of the planned increment and the load dropped immediately after the failure. The load was then brought back to the 6.25 (LL + IL) increment and rupture of the positive moment prestressing cables in the east side box occurred after a small increase in load. Figure 8.40 shows the general view of the failed bridge.

The strain at the various positions in the same cross section varied as the load increased, although the tendency of strain change was similar at each position. However, the increase of deflection at the same station in each cross section was uniform as the load increased. Figure 8.41 shows the deflection along the bridge during the failure loading test.

### 8.3.3 Determination of the Main Span Live Load Capacity

#### 8.3.3.1 Flexure

One major difference between this bridge and the generally considered three-span continuous bridge is that there is no upward vertical restraint as usually assumed for pin supports, because the bridge rests on neoprene pads at all four piers with no hold-down devices. The bridge behavior could be kept as that of a three-span continuous beam by restricting the tendency for uplift at the outer supports, as the increment of (LL + IL) increases. However, to match the prototype support conditions, it was decided not to add any upward motion restriction at the outer supports. Therefore, under high levels of loading in the center span, the bridge started to act as a two-span continuous beam with an overhang or a simple beam with two overhangs.

It is, therefore, necessary to calculate  $M_{UI}$ ,  $M_{E1}$ ,  $M_{E2}$ ,  $M_{E3}$ , and  $M_{E4}$  for three different support conditions ( $M_{UI}$  and  $M_{E1}$  are the same for the three cases). The latter are calculated using the same procedure as explained in Sec. 8.2.3. Moment diagrams for  $M_{E2}$ ,  $M_{E3}$ , and  $M_{E4}$  for the three different support conditions are shown in Figs. 8.42, 8.43, and 8.44.

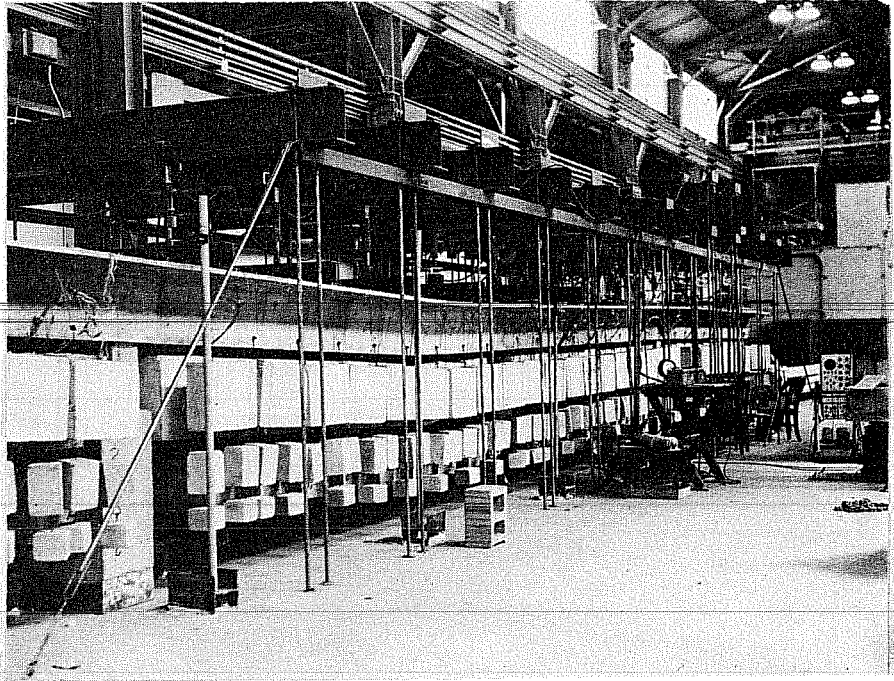


**Fig. 8.40. General view of the bridge after failure**

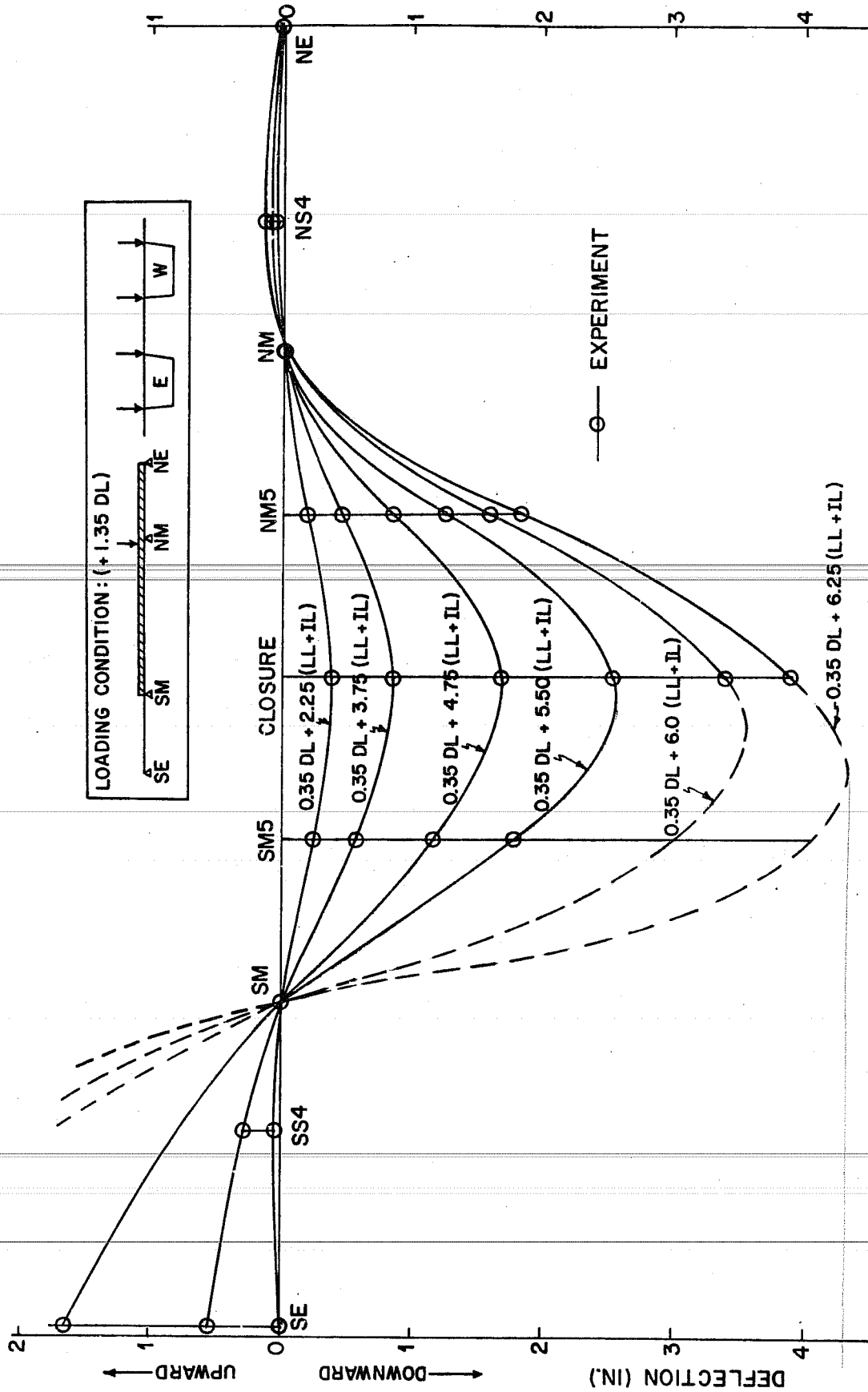
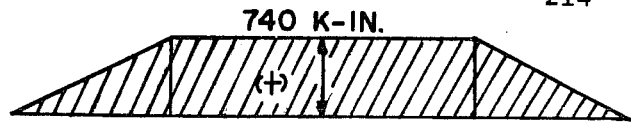


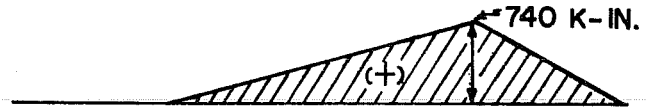
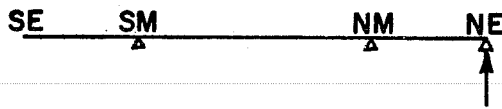
Fig. 8.41. Deflections along the bridge during loading to failure



(A) THREE SPAN CONTINUOUS BEAM



(B) TWO SPAN CONTINUOUS BEAM WITH AN ADDITIONAL OVERHANG SPAN



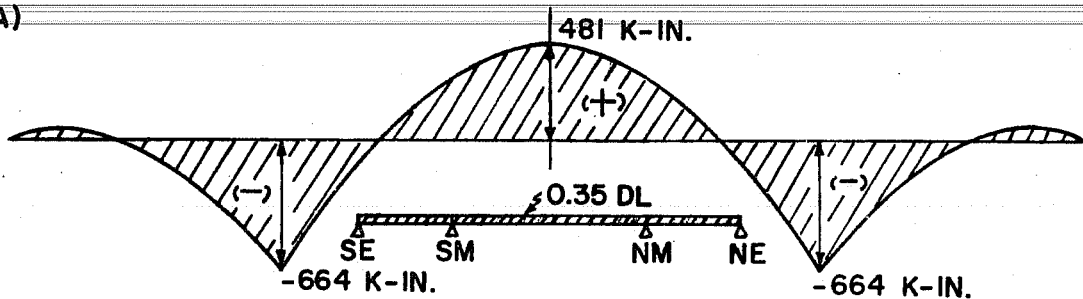
(C) SIMPLE BEAM WITH TWO OVERHANG SPANS



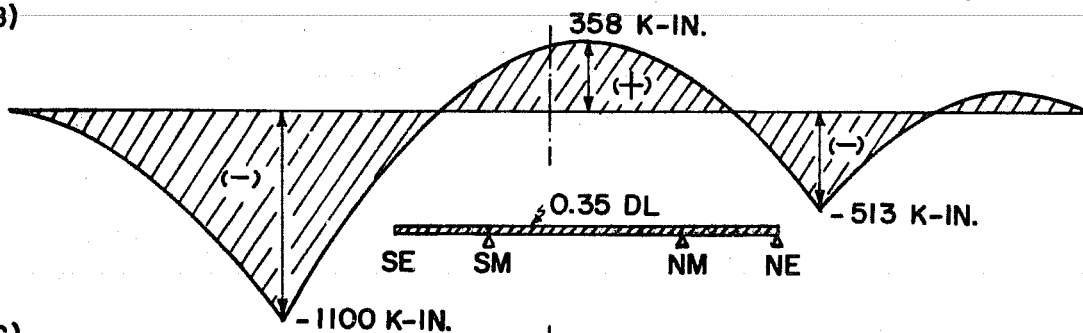
MOMENT DUE TO END REACTION IS ZERO BECAUSE OF NO RESTRAINT AT SE AND NE

Fig. 8.42. Moment diagram due to resultant force of prestressing and jacking force at end supports ( $M_{E2}$ )

(A)



(B)



(C)

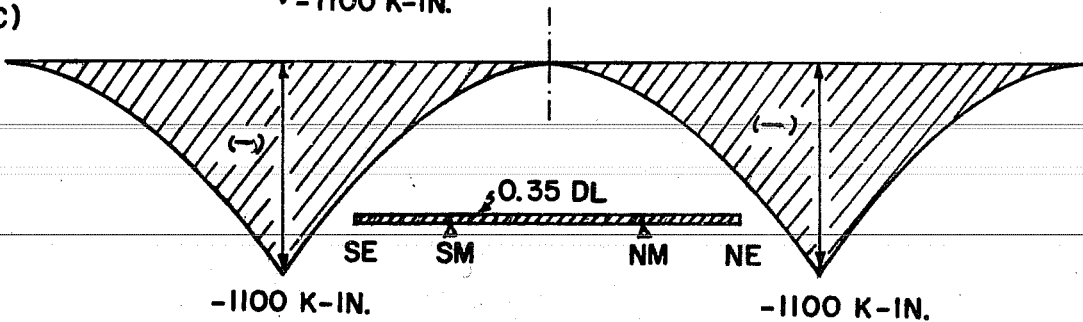


Fig. 8.43. Moment diagram for 0.35 DL for three different conditions ( $M_{E3}$ )

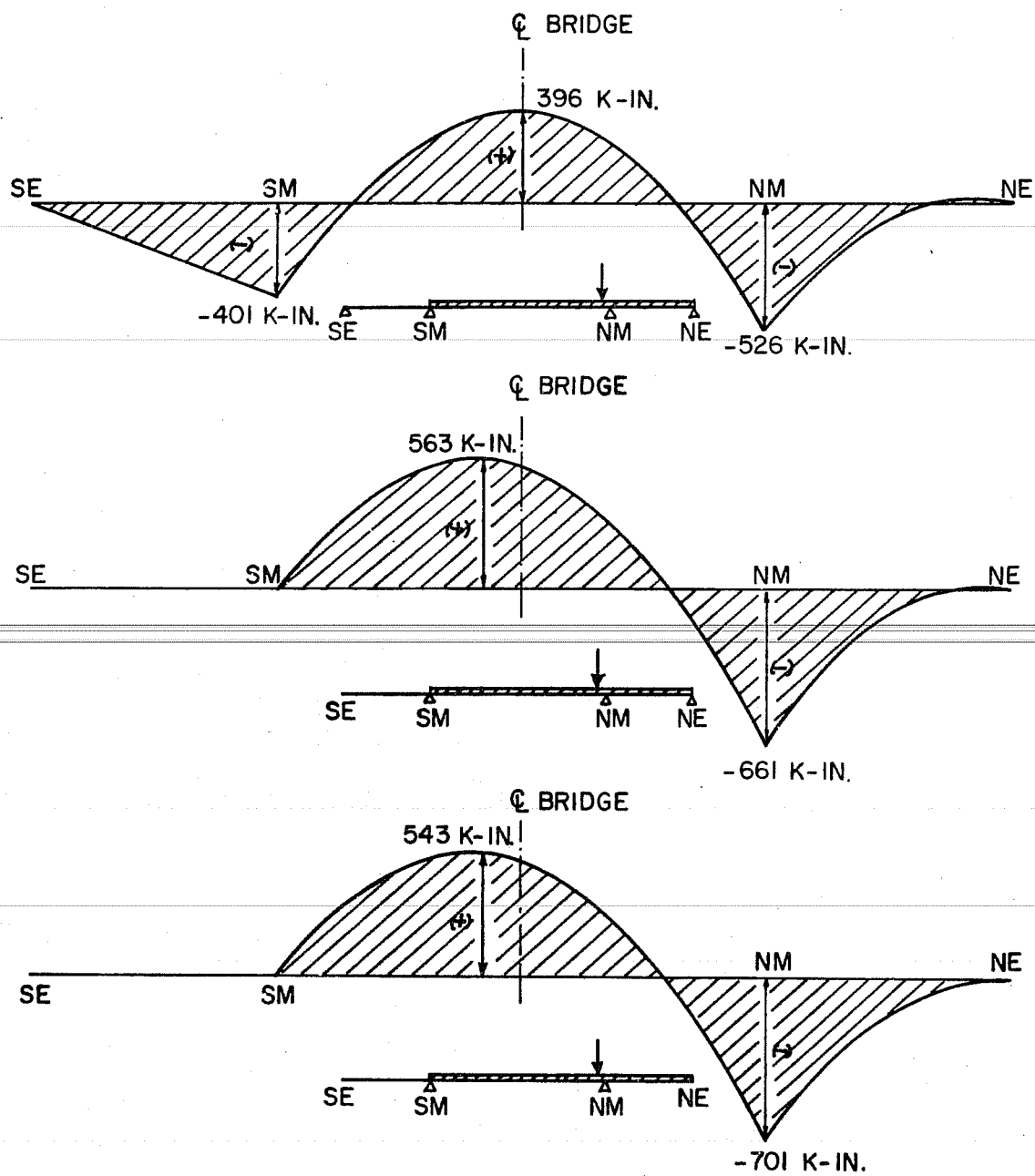


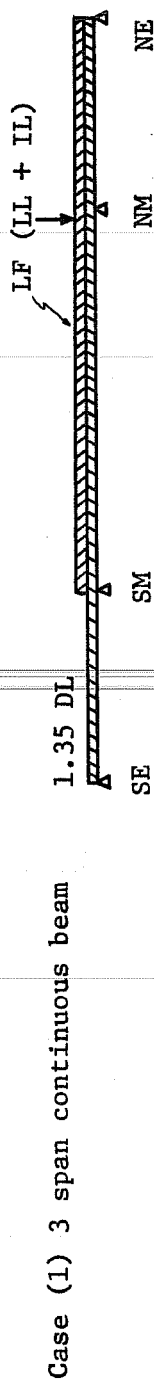
Fig. 8.44. Moment diagram for 1.0 (LL + IL) for three different conditions ( $M_E$ )

By examining Fig. 8.44, it can be seen that the moment of positive moment for 1.0 (LL + IL) in the main span increased 20 to 100 percent in the critical region due to the change of structural configuration. Also, the shift in position of the maximum moment point is clearly shown in Fig. 8.44. There is not much difference in moment between the two-span continuous beam with an overhang and the simple span beam with two overhangs for this loading case (Fig. 8.44).

In contrast, Fig. 8.43 indicates that the moment caused by the additional 0.35 DL around the positive moment region is erased by the change of structural configuration from three continuous spans or two continuous spans with an overhang to a simple beam with overhangs. However, the moment around the NM pier increased.

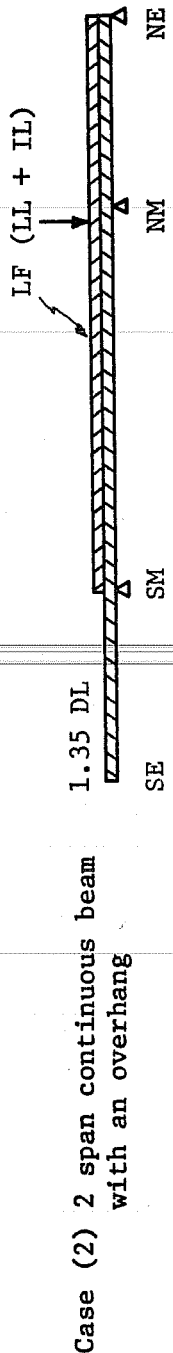
The LF or level of (LL + IL) which would form the first plastic hinge for this loading was calculated for each structure type (Table 8.1). The first plastic hinge would form at the joint of the closure segment at an increment of (1.35 DL + 5.21 (LL + IL)) if the structure was ideally supported by pins and there was no uplift possible at the end supports. However, it is not proper to calculate the LF for a three-span continuous beam since the SE support raised off its support pad at the (1.35 DL + 2.63 (LL + IL)) increment. Since the south end support raised completely from the neoprene pad supports, all forces applied at the time of construction (such as end reaction due to positive tendon prestressing in the main span or the jacking force at the end supports to adjust the reaction) were erased and the structure became a two-span continuous beam with an overhang. If the structure were an ideal two-span continuous beam with an overhang, the reaction at the NE support would have to increase as the load increased. But the reaction at the NE support decreased after the (1.35 DL + 2.25 (LL + IL)) increment due to the appearance of cracks and concentration of deformation around the center of the main span. Observations indicated that a plastic hinge was not formed at the closure segment as would be indicated by Table 8.1 (2) for a two-span continuous beam with an overhang. Since the calculation for case (3) in Table 8.1 indicated that the minimum LF of

TABLE 8.1  
LF OF (LL + IL) FOR THE FIRST PLASTIC HINGE AT EACH JOINT



Joint	Ultimate Internal Moment $M_{UI}$ (k-in.)	Moment due to 1.0 DL $M_{E1}$ (k-in.)	Moment due to end support forces $M_{E2}$ (k-in.)	Moment due to 0.35 DL $M_{E3}$	$\Sigma M = M_{UI} - M_{E1} - M_{E2} - M_{E3}$ (k-in.)	Moment due to 1.0 (LL + IL) $M_{E4}$ (k-in.)	LF of (LL + IL) $\frac{\Sigma M}{M_{E4}}$
SM 5 - 6	2342	-603	740	255	1950	245	7.96
6 - 7	2873	-361	740	346	2148	318	6.75
7 - 8	3395	-181	740	415	2421	354	6.84
8 - 9	3558	-62	740	458	2422	390	6.21
9 - 10	3558	-6	740	479	2345	398	5.89
closure	3285	0	740	481	2064	396	5.21
NM 10 - 9	3558	-6	740	479	2345	394	5.95
9 - 8	3558	-62	740	458	2422	378	6.41
8 - 7	3395	-181	740	415	2421	333	7.27
7 - 6	2873	-361	740	346	2148	289	7.43
6 - 5	2342	-603	740	255	1950	208	9.38

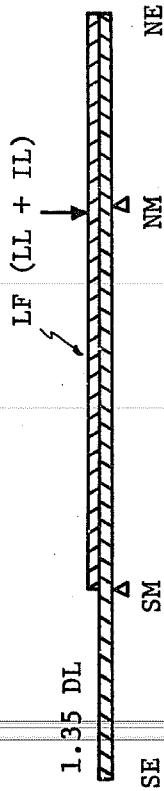
TABLE 8.1 (Continued)



Case (2) 2 span continuous beam with an overhang

Joint	Ultimate Internal Moment $M_{UI}$ (k-in.)	Moment due to 1.0 DL $M_{E1}$ (k-in.)	Moment due to end support forces $M_{E2}$ (k-in.)	Moment due to 0.35 DL $M_{E3}$	$\Sigma M = M_{UI} - M_{E1} - M_{E2} - M_{E3}$ (k-in.)	Moment due to 1.0 (LL + IL) $M_{E4}$ (k-in.)	LF of (LL+IL) $\frac{\Sigma M}{M_{E4}}$
SM 5 - 6	2342	-603	204	- 22	2763	498	5.55
6 - 7	2873	-361	241	99	2894	544	5.32
7 - 8	3395	-181	278	196	3102	554	5.60
8 - 9	3558	- 62	315	270	3035	563	5.39
9 - 10	3558	- 6	352	320	2892	544	5.32
closure	3285	0	370	337	2578	529	4.87
NM 10 - 9	3558	- 6	389	350	2825	513	5.51
9 - 8	3558	- 62	426	358	2836	470	6.03
8 - 7	3395	-181	463	344	2769	399	6.94
7 - 6	2873	-361	500	307	2427	328	7.40
6 - 5	2342	-603	537	245	2163	220	9.83

TABLE 8.1 (Continued)



Case (3) Simple beam with overhangs

1.35 DL

LF (LL + IL)

Joint	Ultimate Internal Moment $M_{UI}$ (k-in.)	Moment due to 1.0 DL $M_{E1}$ (k-in.)	Moment due to end support forces $M_{E2}$ (k-in.)	Moment due to 0.35 DL $M_{E3}$	$\Sigma M = M_{UI} - M_{E1} - M_{E2} - M_{E3}$ (k-in.)	Moment due to 1.0 (LL + IL) $M_{E4}$ (k-in.)	LF of (LL + IL) $\frac{\Sigma M}{M_{E4}}$
SM 5 - 6	2342	-603	0	-207	3152	485	6.50
6 - 7	2873	-361	0	-120	3354	530	6.33
7 - 8	3395	-181	0	-57	3633	536	6.78
8 - 9	3558	-62	0	-16	3636	543	6.70
9 - 10	3558	-6	0	0	3564	523	6.81
closure	3285	0	0	0	3285	507	6.48
NM 10 - 9	3558	-6	0	0	3564	487	7.32
9 - 8	3558	-62	0	-16	3636	445	8.17
8 - 7	3395	-181	0	-57	3633	372	9.77
7 - 6	2873	-361	0	-120	3354	295	11.4
6 - 5	2342	-603	0	-207	3152	188	16.8

(LL + IL) for the first plastic hinge was at the SM6-7 joint for a simple beam with overhangs, it will be proper to calculate the LF of (LL + IL) for that case and then take into account the reaction left at the NE support. If the structure is an ideal simple beam with overhangs, the first plastic hinge would form at the 6.33 (LL + IL) increment. The effect of the reaction left at the NE support was small and 5.88 (LL + IL) is the calculated increment to form the first plastic hinge when taking into account the end reaction at the NE support. This value agreed well with the 6.25 (LL + IL) experimental value.

All section properties used to calculate LF of (LL + IL) in Table 8.1 were based on the measured values.

After demolishing the bridge, the joints where failure occurred were carefully examined and it was found that the five positive tendons in each web were completely broken through.

Although the positive tendons were generously designed for the ideal three-span continuous beam as shown in Sec. 8.2, this reserve was reduced in the main span because the designer did not consider the unrestrained support condition. Therefore, it is also necessary to check the LF for the loading condition which produces maximum moment at the center of the main span, as shown in Fig. 8.45. In the loading case of Fig. 8.45 it is certain that the end supports (SE and NE) would raise up at failure (because the supports raised up in the previous test in Sec. 7.3.3.2). The structure at failure will be a simply supported beam with overhangs and the calculated LF is (1.35 DL + 3.13 (LL + IL)), as shown in the following calculation:

$$M_{E4} \text{ at } 1.0 \text{ (LL + IL)} = 1051 \text{ k-in.}$$

$$\Sigma M = M_{UI} - (M_{E1} + M_{E2} + M_{E3}) = 3285 \text{ (case (3) in Table 8.1)}$$

$$\text{LF of (LL + IL)} = 3285/1051 = 3.13$$

Therefore the support condition does not unduly affect the safety of the bridge, although the flexural capacity is reduced to (1.35 DL + 3.13

(LL + IL)) if the AASHO load reduction for multiple lanes is ignored. This would be (1.35 DL + 4.17 (LL + IL)) if the normal design specifications are used for a four lane bridge.

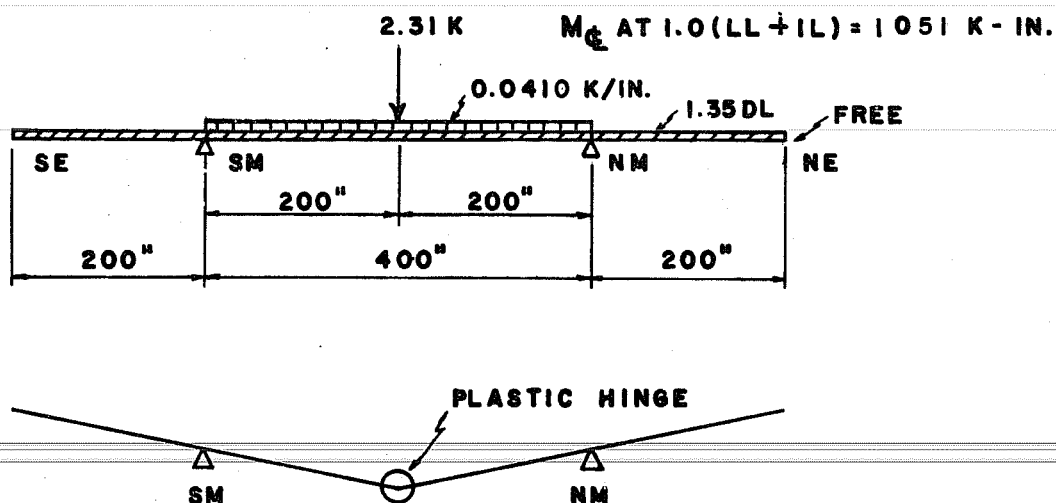


Fig. 8.45. Failure loading at the center of the main span

In order to match the test loading conditions, the model's external dead load moment was computed with 1.0 DL acting on a balanced cantilever and 0.35 DL acting on the completed continuous structure. It has been shown that it is not logical to base the analysis of the completed structure on continuous beam dead load moments for 1.35 DL. A more sensible load factor procedure for computation of the ultimate design moments in the completed structure should consider possible uncertainty in the dead load at various stages of construction. Based on experience in this program the following factors are suggested for analysis of the completed structure to determine proper positive moment tendons and to check the negative moment and shear capacity:

$$U = 1.35 \text{ DL} + 2.25 (\text{LL} + \text{IL}) \text{ (as specified by BPR)}$$

but



$$U = U_1 + U_2$$

$U_1 = 1.15$  DL to be computed for a balanced cantilever

$U_2 = 0.20$  DL +  $2.25$  (LL + IL) + SL to be computed for the completed continuous structure

where

DL = dead load

LL = live load

IL = impact load

SL = resultant reactions due to prestressing of positive

tendons and seating forces at outer supports

Negative tendons can be designed by WSD or USD to balance the dead load of segments and the weight of construction equipment on the segments during the balanced cantilever stages. However, the negative moment capacity of the cantilever structure should be checked for  $U = 1.35$  DL +  $2.25$  (LL + IL), where, in this case, LL + IL should be based on construction live loads.

#### 8.3.3.2 Shear

Initial formation of shear cracking is practically independent of the amount of web reinforcement,<sup>20</sup> so this design appears to have an adequate safety factor for shear without reliance on shear reinforcement, since the initial diagonal tension crack began to appear at the (1.35 DL + 3.25 (LL + IL)) increment. This exceeds the specified design ultimate loads.

Observation of cracks around the main pier showed there was no shear weakness of the epoxy joint. The flexural cracks which formed on the top slab of the first joint in the main span did not extend straight along the joint and these flexural cracks connected to the diagonal tension cracks in the web.

The truss analogy is widely accepted as a simple and safe design procedure for shear. Shear reinforcement at ultimate strength can be checked by ignoring the effect of the concrete, but a portion of the shear is carried by concrete at the ultimate.<sup>20</sup> The ACI Code<sup>2</sup> specifies that shear reinforcement should be not less than  $A_v = (V_u - \phi V_c) / (\phi d f_y)$ . The ACI Code also specifies another equation for shear reinforcement (not less than  $A_v = (A_p / 80) \times (f'_s / f_y) \times (s/d) \times \sqrt{d/b'}$ ).

It is suggested by Lin<sup>20</sup> that the critical section for shear computation be taken at a distance  $d (= 15.4 \text{ in.})$  away from the theoretical point of maximum shear. However, the critical section for shear was considered to be at the first joint from the pier in this bridge because the flexural cracks occurred at the top slab of the first joint and extended into the diagonal tension cracks. Many of the diagonal tension cracks appeared around the first joint in the main span. The LF of (LL + IL) for shear capacity was calculated by using the prestressed concrete equations in the 1963 ACI Code.<sup>2</sup> Since the bridge at failure was a simply supported beam with overhangs, shear and moment due to dead and live load were calculated for a simple beam with overhangs, as follows:

(a) Shear capacity carried by concrete and web shear reinforcement.

Shear carried by concrete:

$$\begin{aligned}
 V_{ci} &= 0.6 b' d \sqrt{f'_c} + \frac{M_{cr}}{M/V - d/2} + V_d \\
 &= 0.6 \times 8.81 \times 15.4 \times 0.0842 + 1490/36.0 + (10.9 + 28.6) \\
 &= 6.85 + 41.4 + 39.5 = 87.75 \text{ kips}
 \end{aligned}$$

where,

$$b' = 8.81$$

$$d = 15.4$$

$$\sqrt{f'_c} = \sqrt{7090}/1000 = 84.2/1000 = 0.0842 \text{ ksi}$$

$$f_{pe} = -P/A - M/W_T = -338/(2 \times 179) - \frac{338 \times 6.20}{2 \times 1020}$$

$$= -0.944 - 1.027 = -1.971 \text{ ksi}$$

$$f_d \text{ (= due to 1.35 DL)} = M/W_T$$

$$= 2630/2040 + 990/2090$$

$$= 1.29 + 0.474 = 1.764 \text{ ksi}$$

$$M_{cr} = \frac{I}{y} (6\sqrt{f'_c} + f_{pe} - f_d)$$

$$= 2090 (6 \times 0.0842 + 1.97 - 1.76)$$

$$= 1494 \text{ k-in.}$$

$$M/V - \frac{d}{2} = 572/13.1 - 15.4/2$$

$$= 43.7 - 7.7 = 36.0$$

$$V_d \text{ (due to 1.35 DL)} = 10.9 + 28.6$$

$$= 39.5 \text{ kips}$$

$$V_{cw} = b'd (3.5 \sqrt{f'_c} + 0.3 f_{pc}) + V_p$$

$$= 8.81 \times 15.4 (3.5 \times 0.0842 + 0.3 \times 0.944) + 0$$

$$= 78.5 \text{ kips}$$

where,

$$b' = 8.81 \text{ in.}$$

$$d = 15.4 \text{ in.}$$

$$\sqrt{f'_c} = 0.0842 \text{ ksi}$$

$$f_{pc} = 0.944 \text{ ksi}$$

$$V_p = 0 \text{ kip}$$

Therefore,

$$V_c = 78.5 \text{ kips } (= V_{cw})$$

Shear carried by the shear reinforcement:

$$\begin{aligned} V_s &= A_v d f_y / s \\ &= 0.165 \times 15.4 \times 70 / 2.5 = 71.1 \text{ kips} \end{aligned}$$

where,

$$A_v = 0.0206 \times 8 = 0.1648 \text{ in.}^2$$

$$f_y = 70 \text{ ksi}$$

$$d = 15.4 \text{ in.}$$

$$s = 2.5 \text{ in.}$$

Total shear carried by concrete and shear reinforcement:

$$V_u = \phi (V_c + V_s) = 1.0 (78.5 + 71.1) = 149.6 \text{ kips}$$

(b) Shear due to dead and live load.

$$\begin{aligned} V_u &= 1.35 \text{ (DL shear)} + LF \text{ (LL + IL shear)} \\ &= 39.5 + LF \times 13.1 \end{aligned}$$

(c) LF of (LL + IL) for shear capacity at the first joint in the main span.

$$\text{LF of (LL + IL)} = (150 - 39.5)/13.1 = 8.44$$

Therefore, the shear capacity was not critical at the time of flexural failure. The test developed 75 percent of the calculated shear capacity prior to the flexural failure, and indicates successful jointing.

As explained in Sec. 7.2.1.2, simulation for shear was not as accurate as that for bending moment. The LF of (LL + IL) for the ideal loading condition would be higher than the value obtained in the model test.

#### 8.4 Punching Shear Tests

After failure of the bridge in the longitudinal tests, a series of punching shear tests were performed by using a rear wheel (HS20) loading pad in the side span which did not get any appreciable damage. Since the positive tendons in the main span were broken and wide flexural cracks appeared around the main pier segments in the previous failure test, no estimate of the amount of compressive stress in the top slab is possible. Compressive stress of 150 to 250 psi would exist in the longitudinal direction in the top slab where punching shear tests were performed, if the grouting were still effective. Ultimate two-way shear stress  $V_{u2}$  was assumed as  $4\sqrt{f'_c}$  for the calculations, as used in reinforced concrete. If longitudinal compressive stress in the top slab is taken into account, the principal stresses will increase 25 to 45 percent.

Most of the experimental values of punching shear were approximately twice the ACI value in the normal punching shear test (case (A) in Table 8.2). Even if the increase in shear stress due to the longitudinal

TABLE 8.2 - PUNCHING SHEAR TEST RESULTS

CASE	TRANSVERSE POSITION OF LOADING	LONGITUDINAL POSITION OF LOADING	ULTIMATE LOAD (KIPS)	AVERAGE ULT. LOAD AND $\bar{S}$ (KIPS)	L.F. OF (LL+IL) = L.F. OF 1.3 LL	CALCULA. BY EQUA. IN ACI (KIPS)
A			9.81	10.3 ( $\bar{S} = 0.9$ )	17.8	5.09
			11.8			
			9.30			
A			10.3	10.9	18.9	
B			5.63	5.12 ( $\bar{S} = 0.37$ )	8.85	4.11*
			4.76			
			4.97			
B						* ASSUME ONE FACE IS OPEN

compressive stress is considered it appears that the value of the ultimate shear stress as specified by the 1963 ACI Code is underestimated. Punching shear tests on the cantilever overhangs of case (B) in Table 8.2 were an abnormal condition. Several flexural cracks appeared at 60 to 70 percent of the punching shear load and ringed the loading pad. Shear failure still occurred in a small area around the loading pad. Even under this abnormal condition, failure loads were more than eight times that of a service load level rear wheel (HS20). Thus, the bridge should have no problem with punching shear failure. Punching tests across the joints show there was no weakness of the joints under punching shear in the top slab.

## C H A P T E R 9

### CONCLUSIONS AND RECOMMENDATIONS

#### 9.1 Conclusions

##### 9.1.1 Primary Conclusions

(1) The model bridge carried safely the ultimate design loads for various critical moment and shear loading configurations as specified by the 1969 Bureau of Public Roads Ultimate Strength Design Criteria as shown in Sec. 7.3.3.

(2) The deflection under full four lane design live load was approximately  $L/3200$  in the main span. This is much smaller than  $L/300$  which is generally considered as acceptable.

(3) Positive tendons in the main span were conservatively designed as an ideal three-span continuous beam. Even though the bridge was supported on neoprene pads which have no vertical restraint against uplift at the outer supports and, hence, the structure need not act continuously at ultimate, there was sufficient reserve strength in the main span, as shown in Sec. 8.3.

(4) Under the high combined moment and shear loading (see Sec. 8.3), flexural cracks appeared around the joints of the top slab near the main pier but they connected with the diagonal tension cracks and did not extend along the joint. Therefore, there was no sign of any direct shear failure at the joints. Approximately 75 percent of the theoretical ultimate shear load was applied in the maximum shear loading test prior to failure of the bridge during that test by flexure with no sign of shear distress evident.



(5) During erection of the first few segments, tensile stress occurred in the bottom slab as predicted in the design (Sec. 6.1.5 (b) and 6.2.3). Temporary prestress devices were successfully developed to control the effects of these stresses.

(6) Theoretical calculation of the failure load, defined as the load factor for live and impact loads required to form the first plastic hinge agreed very well with the experimental results, as shown in Sec. 8.2 and 8.3, and these tests proved that the calculation procedure explained in Sec. 8.2.3 was correct.

#### 9.1.2 Secondary Conclusions

(1) Near failure, cracks concentrated around the joints which had no continuous conventional reinforcement (Secs. 8.2 and 8.3). However, cracks were generally well-distributed because of the effective grouting (Secs. 7.3.3, 8.2, and 8.3).

(2) Good agreement between the theoretical and experimental strains evident in most load cases indicated that  $E_c$  taken directly from the cylinder tests was reasonable as shown in Chapters 6 and 7.

(3) Although most of the epoxy resins tests should perform adequately for joining dry specimens, strengths of most epoxy joints were very weak if joined when in a saturated condition, as shown in Sec. 3.3.2.

(4) Transverse moment capacity of the model bridge girder section was very adequate, as shown by the punching shear load test results of Secs. 7.3.4 and 8.4.

(5) There was no adverse effect of the epoxy joints on the slab punching shear strengths, as shown in Sec. 8.4.

(6) Bolts used for the temporary connection of the pier segments to the main piers yielded locally under the most critical unbalanced loading, although the calculated direct compressive stress was under the actual yield strength. The bolts used in the model were

also below the yield strength specified for the bolts in the prototype. Yielding was apparently caused by the large gap between the pier segments and the pier, with consequent local bending and was accentuated by the stress concentrations in the threads (Chapter 6).

(7) Most of the theoretical calculations were in good agreement with the experimental results although there were some appreciable deviations between the experimental and theoretical values of strain in the top slab in some stages of cantilever construction (Chapters 6 and 7).

The BMCOL50 program was very useful in predicting the behavior of the bridge during construction and for uniform loading tests. The BMCOL50 results agreed very well with the experimental results for longitudinal strains and deflections. The relatively simple data input for BMCOL50 is another advantage when compared to the folded plate theory programs.

The SIMPLA2 program reasonably predicted the variation of the longitudinal strain under very high stress levels across the top slabs of the newly erected segments.

The MUPDI program, which can be used only for a constant cross section, agreed very well with the experimental results at the service load level. The variation of sections along the bridge was very small. MUPDI can determine the transverse moments and can be used effectively in designing the transverse reinforcement.

(8) The initial overstressing to  $0.8f'_s$  with release to  $0.65f'_s$  before seating, suggested by Brown,<sup>10</sup> worked well. The friction factor and wobble coefficient used with SIMPLA2 were reasonable as confirmed by the tests (Sec. 6.2.2).

(9) Separation of the match cast segments was smoothly carried out without any damage to the segments, by careful application of uniform force using hydraulic rams (Sec. 4.4).

## 9.2 Recommendations

### 9.2.1 Design Recommendations

(1) Since the structural configuration changes during construction for this type of bridge, the ultimate design load after completion of the bridge should be specified as follows:

$$U = U_1 + U_2$$

$U_1 = 1.15$  DL to be computed for a balanced cantilever

$U_2 = 0.20$  DL +  $2.25$  (LL + IL) + SL to be computed for the completed continuous structure

where

DL = dead load

LL = live load

IL = Impact load

SL = resultant reaction due to prestressing of the positive tendons\* and seating force at outer supports.

(2) Negative tendons should be designed so that no tensile stress is developed across any joint during erection. Otherwise some temporary erection procedure must be required to keep the joint in compression until erection stresses change from tension to compression.

(3) When a designer calculates the internal ultimate moment in the positive moment region, he needs to consider the effects of the negative tendons which may be present at that section.

(4) Negative moment and shear capacity must be checked for both cantilever erection stages and for the completed structure under design and ultimate loads, as shown in the design of this bridge.<sup>16</sup>

---

\* Resultant reaction is zero for the positive tendons stressed during a determinate structure.

(5) If the outer support details provide no upward vertical restraint, the positive moment prestress design should consider this factor. Alternate solutions should be examined to decide whether the prestress should be increased or the vertical restraints provided at outer supports. The designer must be aware of the change of structure configuration if the side spans rise up from their supports under ultimate loading in the main span as shown in Sec. 8.3.3.1.

(6) The jacking forces required to adjust the end reaction or elevation of the bridge should be carefully calculated to prevent premature cracks at service load levels, as shown in Sec. 7.3.3.2.

(7) The sequence of positive moment tendon stressing operations should be specified to minimize or preferably eliminate tension in the top slab, especially at the closure segment.

(8) Although the model bridge was temporarily supported by bolts during cantilever erection, it would seem better to provide details so that compressive forces would be taken by temporary compression blocks and tensile forces would be taken by the bolts. This would prevent the high compressive stresses on the bolts in the unbalanced loading condition and stiffen the connection and thus reduce unbalanced deflections.

(9) Although the effects of creep and shrinkage were minimal in this study, Muller<sup>24</sup> points out for this class of structure:

The effect of steel and concrete creep must be considered with regard to moment distribution together with the possible effect of moment reversal. Final adjustment and compensation for shrinkage and concrete creep may help the structure to reach the optimum equilibrium.

#### 9.2.2 Construction Recommendations

(1) The pier segments should be carefully placed on the piers to close vertical and horizontal alignments, in order to minimize the final closure adjustments.

(2) Positive tendons in the main span should be inserted before casting the closure segment, in order to make sure that ducts are clear, since concrete may penetrate into the tendon duct during casting of the closure joint.

(3) Viscosity of epoxy resin and hardener should be similar for ease in mixing.

(4) If there is any small damage on the surface of the segment, it will be better to patch at the time of jointing.





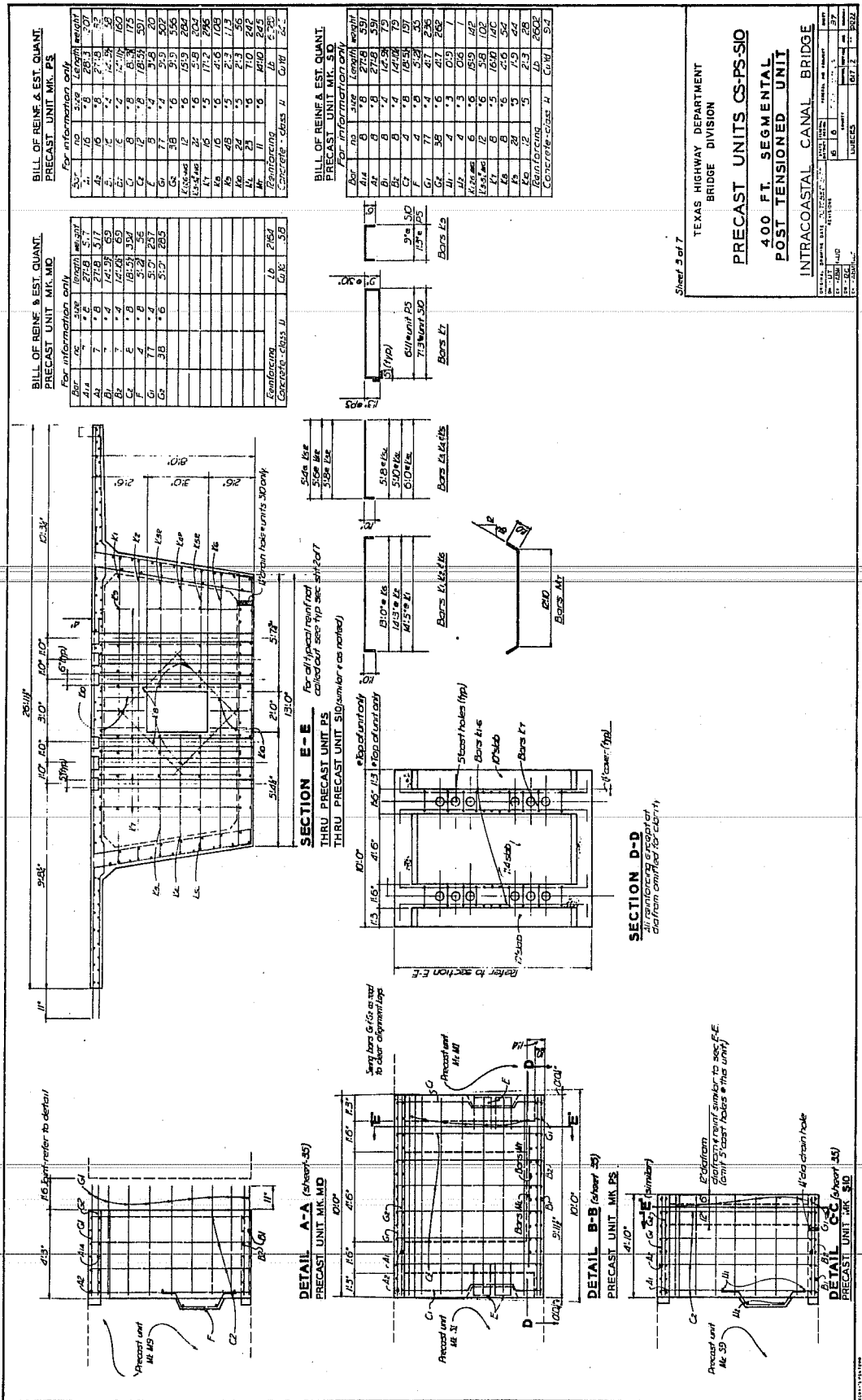












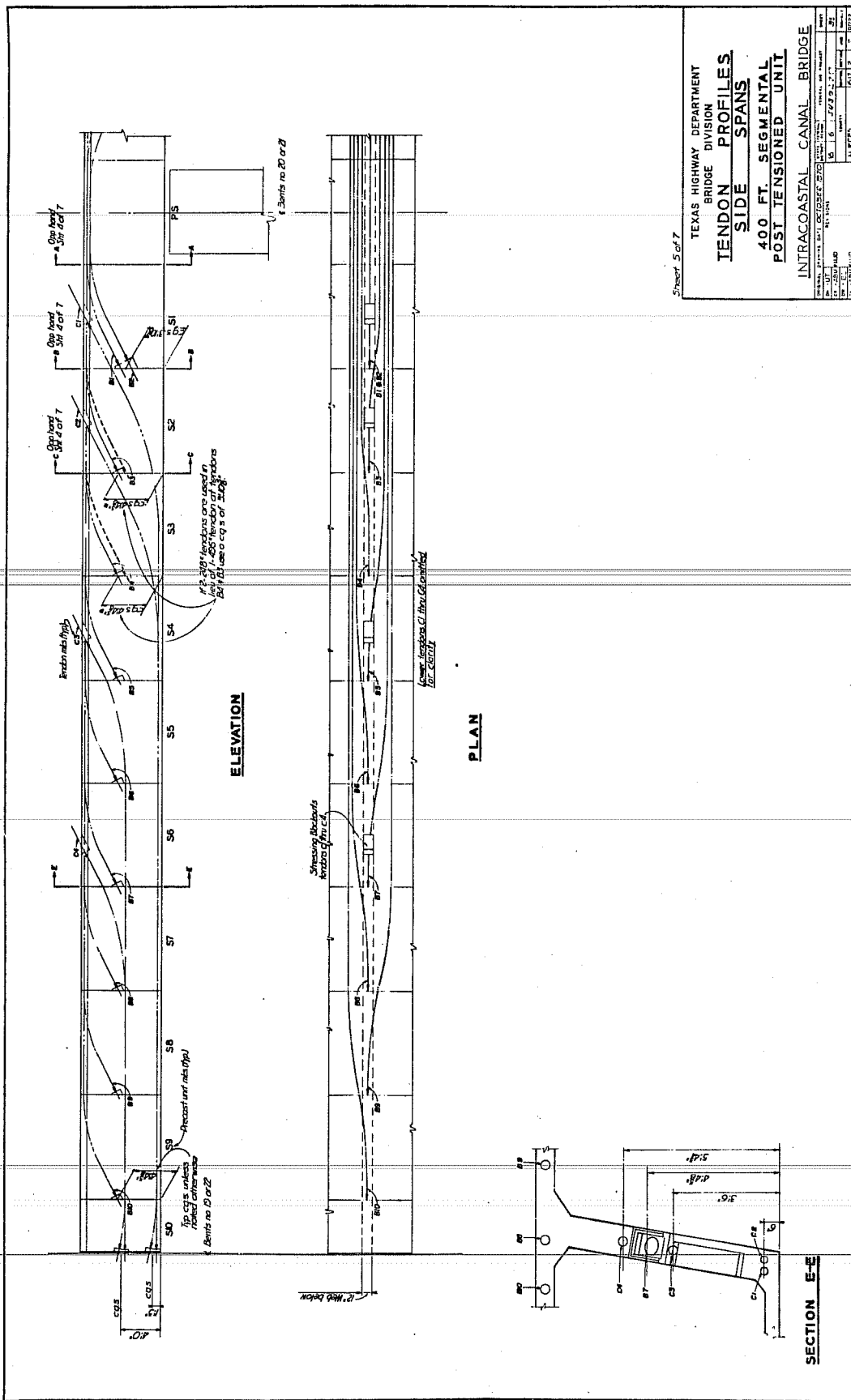
Sheet 3 of 7

TEXAS HIGHWAY DEPARTMENT  
BRIDGE DIVISION

**PRECAST UNITS CS-PS-SO**  
**400 FT. SEGMENTAL**  
**POST TENSIONED UNIT**  
**INTRACOASTAL CANAL BRIDGE**

DATE	NOV 19 1960
BY	...
CHECKED	...
APPROVED	...
SCALE	AS SHOWN
PROJECT	...
SHEET	...
TOTAL SHEETS	...
DESIGNED BY	...
DRAWN BY	...
IN CHARGE	...
DATE	...
BY	...
CHECKED	...
APPROVED	...
SCALE	...
PROJECT	...
SHEET	...
TOTAL SHEETS	...
DESIGNED BY	...
DRAWN BY	...
IN CHARGE	...
DATE	...
BY	...
CHECKED	...
APPROVED	...
SCALE	...
PROJECT	...
SHEET	...
TOTAL SHEETS	...
DESIGNED BY	...
DRAWN BY	...
IN CHARGE	...
DATE	...
BY	...
CHECKED	...
APPROVED	...
SCALE	...
PROJECT	...
SHEET	...
TOTAL SHEETS	...
DESIGNED BY	...
DRAWN BY	...
IN CHARGE	...
DATE	...
BY	...
CHECKED	...
APPROVED	...
SCALE	...
PROJECT	...
SHEET	...
TOTAL SHEETS	...
DESIGNED BY	...
DRAWN BY	...
IN CHARGE	...
DATE	...
BY	...
CHECKED	...
APPROVED	...
SCALE	...
PROJECT	...
SHEET	...
TOTAL SHEETS	...
DESIGNED BY	...
DRAWN BY	...
IN CHARGE	...
DATE	...
BY	...
CHECKED	...
APPROVED	...
SCALE	...
PROJECT	...
SHEET	...
TOTAL SHEETS	...
DESIGNED BY	...
DRAWN BY	...
IN CHARGE	...
DATE	...
BY	...
CHECKED	...
APPROVED	...
SCALE	...
PROJECT	...
SHEET	...
TOTAL SHEETS	...
DESIGNED BY	...
DRAWN BY	...
IN CHARGE	...
DATE	...
BY	...
CHECKED	...
APPROVED	...
SCALE	...
PROJECT	...
SHEET	...
TOTAL SHEETS	...
DESIGNED BY	...
DRAWN BY	...
IN CHARGE	...
DATE	...
BY	...
CHECKED	...
APPROVED	...
SCALE	...
PROJECT	...
SHEET	...
TOTAL SHEETS	...
DESIGNED BY	...
DRAWN BY	...
IN CHARGE	...
DATE	...
BY	...
CHECKED	...
APPROVED	...
SCALE	...
PROJECT	...
SHEET	...
TOTAL SHEETS	...
DESIGNED BY	...
DRAWN BY	...
IN CHARGE	...
DATE	...
BY	...
CHECKED	...
APPROVED	...
SCALE	...
PROJECT	...
SHEET	...
TOTAL SHEETS	...
DESIGNED BY	...
DRAWN BY	...
IN CHARGE	...
DATE	...
BY	...
CHECKED	...
APPROVED	...
SCALE	...
PROJECT	...
SHEET	...
TOTAL SHEETS	...
DESIGNED BY	...
DRAWN BY	...
IN CHARGE	...
DATE	...
BY	



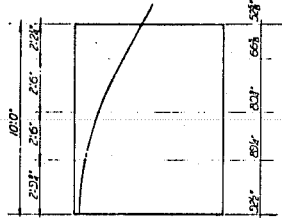


Sheet 5 of 7

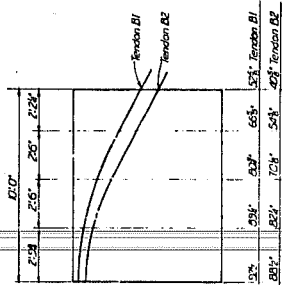
TEXAS HIGHWAY DEPARTMENT  
 BRIDGE DIVISION  
**TENDON PROFILES**  
**SIDE SPANS**  
 400 FT. SEGMENTAL  
 POST-TENSIONED UNIT  
 INTRACOASTAL CANAL BRIDGE

DESIGNED BY	DATE	SCALE	PROJECT NO.	CONTRACT NO.
CHKD BY	REVISED	AS SHOWN	100-1000	100-1000
APPROVED BY	DATE	BY	BY	BY

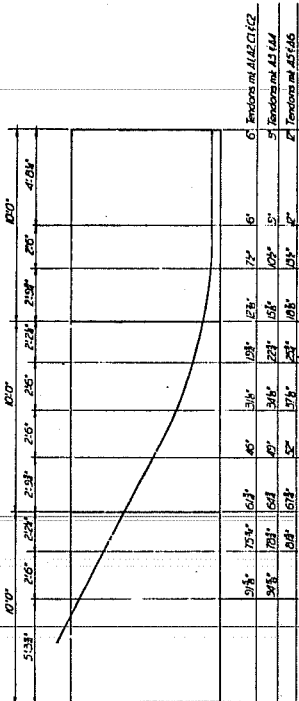
SECTION E-E



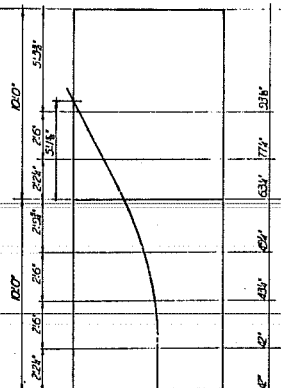
**TENDON PROFILES**  
TENDONS MK\_B3 THRU B10



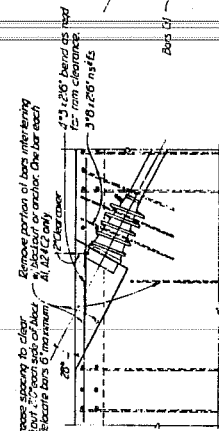
**TENDON PROFILES**  
TENDONS MK\_B1 & B2



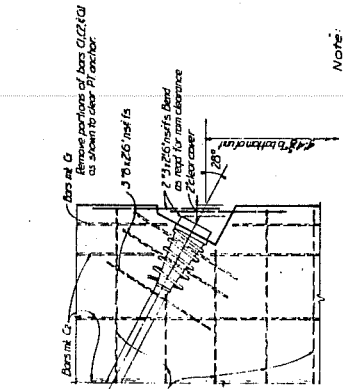
**TENDON PROFILES**  
TENDONS MK\_A1 THRU A6 - C1 & C2



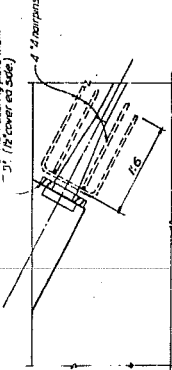
**TENDON PROFILES**  
TENDONS - MK\_C3 - C4 & B11



**TENDON ANCHORAGE**  
WEDGE TYPE ANCHOR  
TENDONS MK\_A1 THRU A6 & C1 THRU C4



**TENDON ANCHORAGE**  
WEDGE TYPE ANCHOR  
TENDONS MK\_B5 THRU B10



**TENDON ANCHORAGE**  
BEARING PLATE TYPE ANCHOR  
TYPICAL DETAIL

Note: Tendon anchorage details are not intended to limit types of strand systems used.

Sheet 6 of 7

TEXAS HIGHWAY DEPARTMENT  
BRIDGE DIVISION  
**TENDON PROFILES AND DETAILS**  
400 FT. SEGMENTAL  
POST-TENSIONED UNIT  
INTRACOASTAL CANAL BRIDGE

DATE	BY	CHECKED	DATE
10/1/00	J. L. ...	J. L. ...	10/1/00
10/1/00	J. L. ...	J. L. ...	10/1/00
10/1/00	J. L. ...	J. L. ...	10/1/00







TEXAS HIGHWAY DEPARTMENT

SPECIAL SPECIFICATION

ITEM 2131

EPOXY BONDING AGENT

1. DESCRIPTION. This item shall govern for the furnishing and application of epoxy material for use in the joint between precast concrete units, as required by the plans.

2. MATERIALS. The epoxy material shall be of two components, a resin and a hardener (1 to 1 ratio), meeting the following requirements:

- a. Pot Life Min. 90 minutes at 68 F (ASTM D1338)
- b. Compressive Strength 6,000 p.s.i. min.
- c. Tensile Strength (Direct or Bending) 2,000 p.s.i. min.
- d. Specific Gravity 70 to 120 lbs./cu.ft.
- e. Viscosity at 68 F 10,000 to 50,000 cps
- f. Coefficient of Thermal Expansion Within 10% of that for concrete

The material shall have a rate of absorption, rate of shrinkage, chemical resistance and weather resistance compatible with concrete and a consistency such that it will not flow appreciably when applied to a vertical concrete surface. The color shall be concrete gray.

The Contractor shall furnish the Engineer a sample of the material for testing, and a certification from a reputable laboratory indicating that the material complies with the above requirements.

The sample of the material submitted will be tested additionally for the following:

- a. Ability to join test specimen under the following conditions:

Temperature Range 50 F to 100 F  
 Surface Conditions Dry to Moist  
 (Moist is defined as 'one hour drying after complete saturation'.)

b. The joint material shall be able to develop 95 percent of the flexural tensile strength and 70 percent of the shear strength of a monolithic test specimen.

The test specimen shall be made of concrete having a minimum compressive strength of 6,000 p.s.i. The specimen will be tested with both dry and moist surface conditions.

3. CONSTRUCTION METHODS. Surfaces to which the epoxy material is to be applied shall be free from all oil, laitance or any other material that would prevent the material from bonding to the concrete surface. All laitance shall be removed by sanding or by washing and wire brushing.

Mixing of the resin and hardener components shall be in accordance with the manufacturer's instruction. Use of a proper sized mechanical mixer will be required.

The epoxy material shall be applied to all surfaces to be joined within the first half of the pot life as shown on the containers.

The coating shall be smooth and uniform and shall cover the entire surfaces to be joined with a maximum thickness of 1/16 inch. The units shall be joined within 45 minutes after application of the epoxy material.

No jointing operations shall be performed when the ambient temperature is below 50 F or above 100 F. When the temperature is above 85 F the epoxy coated surfaces shall be shaded from direct sunlight.

If the jointing is not completed within 45 minutes after application of the epoxy material the operation shall be stopped and the epoxy material shall be completely removed from the surfaces. Fresh material shall be applied to the surfaces before resuming jointing operations.

4. MEASUREMENT AND PAYMENT. No direct measurement or payment will be made for the materials, work to be done or equipment to be furnished under this item, but it shall be considered subsidiary to the particular items required by the plans and the contract.

2131.000  
3-71

2131.000  
3-71

## REFERENCES

1. Aldridge, W. W., and Breen, J. E., "Useful Techniques in Direct Modeling of Reinforced Concrete Structures," Model for Concrete Structures, ACI Publication No. 24, 1970, pp. 125-140.
2. American Concrete Institute, Building Code Requirements for Reinforced Concrete (ACI 318), Detroit, June 1963.
3. American Concrete Institute, Building Code Requirements for Reinforced Concrete (ACI 318), Detroit, 1971.
4. American Concrete Institute, "Guide for Use of Epoxy Compound with Concrete (ACI 403)," Journal of the American Concrete Institute, August 1962.
5. American Society for Testing and Materials, "Standard Method of Test for Working Life of Liquid or Paste by Consistency and Bond Strength (ASTM D 1338-56)," ASTM Standard, Part 16, June 1969, pp. 498-500.
6. American Association of State Highway Officials, Standard Specifications for Highway Bridges, Tenth Edition, American Association of State Highway Officials, Washington, D. C., 1969.
7. Bureau of Public Roads, Strength and Serviceability Criteria, Reinforced Concrete Bridge Members, Ultimate Design, Second Edition, Bureau of Public Roads, U. S. Department of Transportation, Washington, D. C., 1969.
8. Breen, J. E., and Orr, D. M. F., "A Rapid Data Acquisition and Process System for Structural Model Usage," Proceedings of Structural Model Symposium, Sydney, Australia, 1972.
9. Breen, J. E., and Burns, N. H., "Design Procedures for Long-Span Prestressed Concrete Bridges of Segmental Construction," Research Study Proposal, Center for Highway Research, The University of Texas at Austin, 1968.
10. Brown, R. C., "Computer Analysis of Segmentally Constructed Prestressed Box Girders," unpublished Ph.D. dissertation, The University of Texas, 1972.

11. Corley, W. G., Carpenter, J. E., Russell, H. G., Hanson, N. W., Cardenas, A. E., Helgaston, T., Hanson, J. M., and Hognestad, E., "Design Ultimate Load Test of 1/10-Scale Micro-Concrete Model of New Pontomac River Crossing, I-266," Journal of the Prestressed Concrete Institute, Vol. 16, No. 6, pp. 70-84.
12. Ferguson, P. M., Reinforced Concrete Fundamentals, Second Edition, John Wiley & Sons, Inc., New York, 1965.
13. Gallaway, T. M., "Industrialization and Modeling of Segmentally Precast Box Girder Bridges," unpublished Master's thesis, The University of Texas, 1971.
14. Ikeda, T., Precast Segmental Construction Method, Nikkan Kōgyō News Paper Inc. (JAPAN), 1969.
15. Kashima, S., "Experimental Study of Epoxy Resins as a Jointing Material for Precast Concrete Segments," unpublished Master's thesis, The University of Texas, 1971.
16. Lacey, G. C., "The Design and Optimization of Long Span, Segmentally Precast, Box Girder Bridges," unpublished Ph.D. dissertation, The University of Texas, 1970.
17. Lacey, G. C., and Breen, J. E., "State of the Art--Long Span Prestressed Concrete Bridges of Segmental Construction," Research Report 121-1, Center for Highway Research, The University of Texas at Austin, May 1969.
18. Leyendecker, E. V., and Breen, J. E., "Structural Modeling Techniques for Concrete Slab and Girder Bridges," Research Report 94-1, Center for Highway Research, The University of Texas at Austin, August 1968, pp. 26-28.
19. Leyendecker, E. V., "Behavior of Pan Formed Concrete Slab and Girder Bridges," unpublished Ph.D. dissertation, The University of Texas, 1969.
20. Lin, T. Y., Design of Prestressed Concrete Structures, Second Edition, John Wiley & Sons, Inc., New York, 1963.
21. Litle, W. A., Cohen, E., and Somerville, G., "Accuracy of Structural Models," Models for Concrete Structures, ACI Publication No. 24, 1970, pp. 65-124.
22. Matlock, H., and Haliburton, T. A., "A Program for Finite Element Solution of Beam-Columns on Nonlinear Supports," unpublished report, The University of Texas, June 1964.
23. Mattock, A. H., "Structural Model Testing--Theory and Applications," Journal of the PCA Research and Development Laboratories, Vol. 4, No. 3, September 1962, pp. 12-22.

24. Muller, J., "Long Span Precast Prestressed Concrete Bridge Built in Cantilever," Concrete Bridge Design, ACI Publication SP-23, 1969, pp. 705-740.
25. Neville, A. M., Properties of Concrete, John Wiley & Sons, Inc., New York, 1963.
26. Prestressed Concrete Institute (Japan), Construction Manual for Precast Concrete Segmental Construction, December 1968.
27. Prestressed Concrete Institute Post-Tensioning Committee, Recommended Practice for Grouting of Post-Tensioned Prestressed Concrete, PCI Specification Draft, 1970.
28. Scordelis, A. C., "Analysis of Simply Supported Box Girder Bridges," Report No. SESM 66-17, Department of Civil Engineering, University of California, Berkeley, October 1966.
29. Scordelis, A. C., Bouwkamp, J. G., and Wasti, S. T., "Structural Behavior of a Two-Span Reinforced Concrete Box Girder Bridge Model, Vol. II," Report No. US SESM 71-16, Department of Civil Engineering, University of California, Berkeley, October 1971.
30. Swann, R. A., "The Construction and Testing of a One-Sixteenth Scale Model for the Prestressed Concrete Superstructure of Section 5, Western Avenue Extension," Technical Report, Cement and Concrete Association, London, 1970.
31. VIDAR Corporation, "VIDAR 5404 D-DAS System Information," Technical Manual, California, May 1971.